CHAPTER 4. PERFORMANCE OF JET GROUT IMPROVEMENT DURING THE 1999 KOCAELI (TURKEY) EARTHQUAKE – CARREFOUR SHOPPING CENTER

1. INTRODUCTION

In many regions of the world, major urban centers have developed over low-lying areas of minimal local relief and in close proximity to waterfronts. In terms of geomorphology, these cities are typically situated atop marine and alluvial deposits that contain soft clays and/or loose, liquefiable sands. Of particular concern is the safety of infrastructure against earthquakes. Recent earthquakes in these settings have repeatedly demonstrated the high vulnerability of constructed facilities and lifelines to damage from liquefaction-related ground movements in sands and excessive strains in soft clays (Cooke and Mitchell 1999; Riemer et al. 1996). An increasingly common method of mitigating seismic hazards in these regions is through ground improvement. A variety of techniques have been developed in recent years, and experience has shown these methods to be generally effective in reducing earthquake-induced damages (Mitchell 1992; Mitchell et al. 1995; Yasuda et al. 1996). Although ground improvement is seeing increased acceptance and usage, there remains a critical lack of well-documented field case studies that would allow refinement of existing design methodologies, development of improved design guidelines, and a more rigorous assessment of our current capability to predict field performance (Mitchell and Wentz 1991; Mitchell et al. 1998; Mitchell and Wentz 1998).

The 1999 Kocaeli Earthquake (M=7.4) struck northwestern Turkey on August 17, 1999 and caused significant damage in urban areas located along Izmit Bay. Peak ground accelerations of 0.35g-0.40g were measured on rock at close distances to the fault rupture. Following the earthquake and significant aftershocks, the affected area was investigated to document geotechnical field performance. These studies focused on improved soil sites. The

observations showed that ground treatment was generally effective in mitigating earthquake-related damages, especially relative to nearby untreated sites (Martin et al. 2001).

This chapter presents the performance of a shopping complex in Turkey where the soils were improved with jet-grout columns and preload fills and subjected to the 1999 Kocaeli Earthquake (M7.4). Under construction at the time of the earthquake, the Carrefour Shopping Center covers an area of 55,000 m^2 and is founded on shallow footings, mats, and slabs-on-grade that rest on soft, saturated alluvial sediments consisting of clays, silts, and sands. High-modulus columns constructed by jet grouting were installed at close-to-moderate spacings to reduce anticipated static settlements in the clays and mitigate liquefaction in the sands. The site was subjected to a peak acceleration of approximately 0.2g during the earthquake. Grouting had been completed for about two-thirds of the site when the earthquake struck. Following the event, a field reconnaissance found stark contrast between the performance of the improved and unimproved sections. The jet-grout-treated areas suffered no apparent damage, whereas the unimproved sections of the complex, along with nearby untreated building sites, commonly suffered liquefaction-related settlements of up to 10 cm. This is the only case history known to the authors that documents the field performance of high-modulus columns used in this manner for liquefaction mitigation and direct instrumented measurement of liquefaction-induced settlements.

The Carrefour Shopping Center complex was of particular importance because the site was under construction at the time of the earthquake and contained both improved and unimproved soil sections that could be directly compared in seismic performance. The complex covers approximately 55,000 m^2 and is located along Izmit Bay as shown in Figure 4-1. The site lies 8 km northeast from the earthquake epicenter, and 5 km from the closest segment of the ruptured fault. Peak ground accelerations at the site were estimated at 0.24g. The soil profile consists of recent marine sediments with alternating strata of soft to medium clay, loose sands, and silts; the water table is found within 2 m of the ground surface. The soft clays and silts were improved using surcharge fills and wick drains, and small-diameter (0.6 m) high-modulus columns installed by jet-grouting were used to increase bearing support for shallow foundations and reduce liquefaction potential of a silty sand layer that was 1 to 3 m thick across the site.

Jet grouting had only been completed for about two-thirds of the site when the earthquake struck. Following the earthquake, a field reconnaissance was conducted and performance comparison made between the improved and unimproved sections. Stark contrasts were observed, as the treated areas suffered no damage, whereas the unimproved sections of the complex, along with untreated building sites located nearby, commonly suffered liquefaction-related settlements of up to 10 cm.

In-situ settlement measuring devices (settlement extensometers) installed at a non-jet-grouted section to monitor settlements under a surcharge fill made possible the unprecedented measurement of the earthquake-induced settlement at six elevations within the upper 25 m of the profile. As expected, significant settlements were attributed to silty sand strata, but it was surprising that comparable settlements also occurred in saturated silt/clay strata that were initially considered non-liquefiable, and for which the jet-grout columns were not designed to mitigate. Even so, the jet-grout columns were effective in mitigating liquefaction-related damages by apparently reducing cyclic shear strains and pore pressures, and minimizing post-earthquake reconsolidation settlements. This is the only performance case history known to the researchers in this study, documenting liquefaction mitigation using jet-grout columns installed in grids as opposed to columns installed contiguously in a pattern to form enclosed cells to contain liquefiable material (O'Tourke and Goh 1997).

Evidence of liquefaction type behavior of silts and clays was documented. Settlement measurements under the surcharge fill indicate that such soils that would traditionally classify as non-liquefiable were subjected to earthquake induced strength/stiffness loss. Plasticity and grain size characteristics of these soils were studied in relation to current design guidelines on the liquefaction susceptibility of soils with fines. There are important implications, as it may be shown that current guidelines are not reliable predictors of the seismic behavior of these materials.

Never before has liquefaction-type settlements induced by an earthquake been directly measured in the field, and more importantly, to the author's knowledge there has never been such clear demonstration of CL and CH soils suffering liquefaction-type strength loss and

softening. The data from this site could reveal previously unrecognized liquefaction behavior and potential vulnerabilities.

This chapter presents extensive information on soil conditions at the site and the ground improvement scheme implemented. Earthquake performance of improved and unimproved sections is summarized. Evaluations are given on the effectiveness of Cone Penetration Testing on the characterization and analysis of liquefaction susceptibility of such soils. Analyses have been performed to better understand the behavior of improved ground.

2. SOIL AND SITE CONDITIONS

The Carrefour Shopping Center complex is situated along Izmit Bay in a Quaternary marine setting of low ground elevation and minimal local relief. The relatively flat area was recently reclaimed from Izmit Bay using sandy fills. The site is underlain by a thick stack of soft alluvial sediments consisting of alternating strata of soft clays and silty sands. The depth to firm rock is not known for this site, but deep geological profiles from other sites in the vicinity suggest a depth of 80 to 100 m (DSI 1977). The water table is found within 2 m of the ground surface.

General site plan is shown in Figure 4-2. The site covers an area of about 55,000 m^2. A supermarket is located at the southeastern quadrant of the site, and a two-story parking garage is located at the southwestern quadrant. Both structures are supported on shallow foundations. Geotechnical field investigations for the facility included 108 Cone Penetration Tests (CPTs), 18 Standard Penetration Tests (SPTs), and four test pits (Zetas 1998). A suite of laboratory classification and index tests were performed as well. Collectively, data from these investigations were used for the geotechnical and seismic design of the facility, including the development of the soil improvement scheme. Majority of the subsoil investigations were performed during the design and construction phases of the project by the geotechnical consultant (102 CPT's, 17 Boreholes and 4 test pits). In addition to the investigations performed at design and construction phase, researchers from Virginia Tech conducted post-earthquake soil investigations at the site in the Fall of 2000. This work consisted of four seismic CPTs, two conventional CPTs, one SPT boring, and one

exploratory auger hole. Results of the subsoil investigations were made available to this study by the Zetas Earth Technology, the geotechnical consultant of the project.

Location of the subsoil investigations are shown in Figure 4-3. Coordinates of the subsoil investigations along a local coordinate system were available from the geotechnical consultant. Local coordinates were transformed into an AutoCad coordinate system from the relative orientation of the axis systems. Orientation of the axes for the local coordinate system and the AutoCad grid are shown in Figure 4-3.

The extensive array of CPT and SPT data indicated that the stratigraphy is highly variable with depth, but conditions are fairly uniform in lateral extent across the site. A typical profile and penetration test data from the site are presented in Figure 4-4. It can be seen that the CPT tip values are low, and with the exception of a 1 m-thick zone at a depth of 6 m, the values average about 1 MPa throughout the upper 20 to 25 m of the soil profile. SPT $N_{1,60}$ blow counts are less than 10 blows/ft. in most strata above 25 m. Shear wave velocities were measured by means of four post-earthquake seismic CPTs and indicated 110-140 m/sec for the top 10 m.

A composite soil profile for the site was established from the penetration tests and is shown in Figure 4-5 (see Section A-A' in Figure 4-2). This is the section through the Parking Lot and Shopping Center areas. The fill is thicker at the eastern end of the site where the shopping center is located. More will be mentioned in the following sections about the stratigraphy. The thicker fill material affected the shear strength and compressibility of the underlying clay and thus the selection of soil improvement scheme for this section of the site. Additionally, the silty sand layer (SP/SM) is thicker at the Parking Lot area (about 3-3.5 meters thick) than it is at the shopping center area.

A composite soil profile along Lot C and Parking Lot areas is shown in Figure 4-6 (see Section B-B' in Figure 4-2). The silty sand layer (SP/SM) is thicker at the Parking Lot area (about 3-3.5 meters thick) and gets thinner (about 1.0-1.5 meters thick) towards the Lot C area where the surcharge fill is located. The fill was in place at the time of the earthquake.

As can be seen in the figure, a medium dense clayey-gravel fill (GC) overlies the entire site, extending from the ground surface to an average depth of about 3 m. The fill was placed

decades prior to construction to reclaim the site from Izmit Bay. The fill varies from 2 to 4 m in thickness across the site and is thickest beneath the shopping center. The fill is located above the water table in most areas. The fill is highly variable in nature consisting of gravel, sand and clay mixtures.

A soft-to-medium silt/clay stratum that extends from a depth of 3 m to 6 m underlies the fill. Sand and gravel lenses up to 40 cm thick were encountered in this stratum in some areas. Average CPT tip resistances of 1 MPa were measured in this layer, along with shear wave velocities of 100 m/s. SPT $N_{1,60}$ values were 6 blows/ft., and the layer generally classifies as ML/CL. Initially, this layer was deemed "non-liquefiable" and only considered a problem from the standpoint of anticipated settlements and bearing capacity under static footing loads. As shown in Table 4-1, the soil contains an average of nearly 50% clay-sized particles (< 5μm) [although 2μm is usually considered the clay-size boundary, 5μm is used for the Chinese criteria as suggested by Seed and Idriss (1982)]. The CPTs indicated an average soil behavior type index, I_c, of nearly 3.0. Although such soils are not normally considered liquefiable, the soils meet two of the three Chinese criteria for being suspect (percent 5μm < 15%; LL < 35; and, water content > 0.9 x LL); the soil contains more than 15% clay-sized particles (5μm), but the water content is approximately equal to the liquid limit and the liquid limit is less than 35 (LL=33). Similar to findings in Adapazari as reported by Bray et al. (2001), this study shows that these materials are in fact susceptible to liquefaction-related effects (softening, loss of strength, settlement, etc.).

Below the clay and at an average depth of 6 m, a layer of loose-to-medium silty sand is encountered. Investigation of this layer was important because the soils were immediately identified as potentially liquefiable during the soil investigations before construction. Average CPT tip values are about 5 MPa, with friction ratios less than 1%. Typical SPT $N_{1,60}$ values are 13 blows/ft. Shear wave velocities in the stratum are in the range of 140 m/s. The stratum varies from 1.5 m to 4 m in thickness across the site; the stratum is 2.5 m thick beneath the supermarket building, about 4 m thick beneath the parking structure, and approximately 1.5 m thick beneath Lot C. The sand contains an average of 30% non-plastic fines and classifies primarily as an SM, although there are frequent SP and SC lenses. It should be also noted that the sand contains about 15% clay-sized particles (< 5μm) on

average, but the fines are still non-plastic. Collectively, the data indicate that the sandy soil stratum would be liquefiable under moderate levels of ground shaking.

Below the silty sand layer, a 1-m thick soft-to-medium silt/clay stratum is encountered. This stratum classifies as ML/CL and is similar to the ML/CL layer above the silty sand stratum. The soil contains 55% clay-sized particles (<5μm), and the water content was found to be 33%, close to its liquid limit (LL=35%). CPT tip resistances of about 1 MPa were measured, and SPT $N_{1,60}$ values were 3 blows/ft.

A stratum of medium-to-stiff clay of high plasticity (LL = 60 to 80 and classifies as CH) extends from a depth of 9 m to more than 35 m where the explorations were terminated. The stratum shows a gradual strength increase with depth, with CPT tip resistances increasing from 0.5 to 1.2 MPa between the depths of 9 m and 25 m. The clay becomes much stiffer below 25 m, with tip values approaching 5 MPa at a depth of 35 m. Sandy lenses were commonly encountered throughout this thick stratum.

In addition to the penetration data, four post-earthquake seismic CPTs were used to measure shear wave velocities at the site. The measurements were made in an unimproved soil area about 20 m outside the property boundary west of Lot C (see Figure 4-3). Figure 4-7 shows the shear wave velocity measurements performed by the Virginia Tech research team. It can be seen that the profile is nearly constant versus depth for the top 25 m, with an average value of about 120 m/s. From this depth, the velocities steadily increase from 120 m/s to nearly 250 m/s over the next 10 m. A more abrupt transition occurs at a depth of about 35 m where the values increase to approximately 400 m/s and where the exploration was terminated. Overall, the velocity profile indicates a soft site that classifies as a NEHRP Site Class “F” due to the presence of liquefiable sediments, otherwise the site would classify as “E” based on the V_s-30 value of 150 m/s (IBC 2000).

2.1. Subsoil Investigation Data

Geotechnical field investigations for the facility included 108 Cone Penetration Tests (CPTs), 18 Standard Penetration Tests (SPTs), and four test pits (Zetas 1998). These tests were performed at different phases of the project. All the investigation data were made available to this study by the geotechnical consultant to this project. Locations of the subsoil

investigations are shown in Figure 4-3. It is seen that the whole site is covered with extensive subsoil investigations. In this section subsoil investigation data are summarized for different sections of the site. Cross sections of soil layering depicted from the subsoil investigations are also presented.

A majority of the Cone Penetration Testing data were digitally available. Most of the CPT's extended to a depth of 20 meters. Several of the CPT's extended to more than 35 meters where the high plasticity clay gets stiffer.

Subsoil investigations were performed at different phases of the project. During the design phases it was brought up by the geotechnical consultant (Zetas 1998) to use CPT to assess the effectiveness of jet grout improvement. The idea behind this was to investigate the possible effect of cementation and densification of the foundation soils that were susceptible to liquefaction. This was brought up by the geotechnical consultant and was implemented in the quality control / quality assurance (QA/QC) specifications of the project. Tests were performed at pilot zones where before and after CPT's were compared for different jet-grout spacings and patterns. Cementation will not extend much outside the perimeter of the soil mixed column and therefore its effect will be limited. Furthermore jet-grout columns are installed by eroding the soil by air/water jetting. Therefore jet-grouting is basically a soil replacement technique. This is evidenced by the spoil that is carried out to the ground surface. Jet-grout columns act as stiff columns reduce the shearing on the subsoil during an earthquake. Jet-grout columns will act as Regardless of the seemingly faulty motivation and reasoning behind some of the subsoil investigations, this provided an extensive array of data.

2.2. Shopping Center

CPT locations at the Shopping Center area are shown in Figure 4-8. CPT soundings for several test locations are shown in Figure 4-9 through Figure 4-14. The first letter in the CPTs refer to the group name of the CPTs performed during a specific stage of subsoil investigations (i.e. pre-construction, QA/QC, post-earthquake etc.) It is seen that the soil layering is similar at these test locations. Layer thicknesses have been identified from each CPT location at this part of the site.

Plasticity and gradation characteristics of these layers were obtained from the boreholes and sampled soils. Average values are summarized in Table 4-1. Individual samples from each layer show some variability in soil properties. Therefore the names used to refer to these layers have been kept as general as possible. Soil classification is given for several samples obtained from boreholes in the following sections.

Soil behavior type index of the upper clay (mostly classifies as ML/CL) layer is higher than 2.6, sometimes as high as 3.0 on average. Penetration resistance of the silty sand layer varies from location to location. This layer is interbedded with silt/clay lenses as evidenced by sudden changes in penetration resistance, friction ratio and soil behavior type index with depth. Below the silty sand layer is the thin (1-2 meters thick) low plasticity silt/clay layer. Presence of this layer was confirmed with subsequent drilling and sampling. This layer is significant because it is of low plasticity in contrast to the high plasticity clay below. This layer is difficult to identify with the CPT but it has a lower soil behavior type index than the CH material below. Therefore the thickness of this layer was inferred from detailed analysis of the CPT soundings. This layer is soft with CPT penetration resistance values ranging between 0.5-1.0 MPa.

Penetration resistance of the high plasticity clay layer increases with depth. Penetration resistance value of this layer is close to 1.0 MPa in the upper levels and increase to 2 MPa at about 20 meters. This layer extends as deep as the extent of the subsoil investigations.

Layer thicknesses from the CPTs at this section of the site have been determined. Layer boundaries from these are shown Figure 4-15. Mean values are presented for layer interfaces along with the range of one standard deviation. Profile of soil behavior type index (I_c) is presented for median values and +/- one standard deviation range. As seen the I_c profile is also in agreement with the layer boundaries. Some interference of data is evident in between layer interfaces where I_c values change magnitude in between layers (i.e. from high I_c values in upper ML/CL to low I_c SP/SM interface).

Soil layering at North-South cross section (section A-A in Figure 4-8) is shown in Figure 4-16 with the CPT soundings along with this section. Similarly the West-East cross section

(Section B-B) is shown in Figure 4-17. It is seen that the fill layer is thicker towards the east section at this part of the site.

2.3. Parking Lot

CPT locations at the Parking Lot area are shown in Figure 4-18. CPT soundings for several test locations are shown in Figure 4-19 through Figure 4-22. It is seen that the soil layering is similar at these test locations.

Layer thicknesses from the CPTs at this section of the site have been determined. Layer boundaries from these are shown Figure 4-23. Mean values are presented for layer interfaces along with the range of one standard deviation. Profile of soil behavior type index (I_c) is presented for median values and +/- one standard deviation range. It is seen that the variability in layer boundaries is less than the variability at the Shopping Center area. This is particularly evident for the thickness of the fill layer. As discussed above thickness of the fill varies at Shopping Center area. Thickness of this layer is more uniform at the other sections, Parking Lot area and Lot C.

Soil layering at one cross section (section A-A in Figure 4-18) is shown in Figure 4-24 with the CPT soundings along with this section. Similarly the West-East cross section (Section B-B) is shown in Figure 4-25.

2.4. Lot C

In addition to the investigations performed at design and construction phase, researchers from Virginia Tech conducted post-earthquake soil investigations at the site in Fall 2000. This work consisted of four seismic CPTs, two conventional CPTs, one SPT boring, and one exploratory auger hole.

Because the shopping center had been completed and was operational at the time, these additional tests were performed along the perimeter of the property, as shown in Figure 4-26 (CPTs H1-H6). The SPT was performed adjacent to one of the CPTs (CPT-H4) and samples were obtained for index testing and classification / confirmation of the soils, especially for the silty and sandy layers associated with liquefaction. Also, a borehole was drilled adjacent

to the SPT and thin-walled Shelby tubes were used to obtain continuous samples of liquefiable silty sand found at a depth of 6 m to 9 m at this location.

CPT soundings for several test locations are shown in Figure 4-27 and Figure 4-28. These soundings are similar to the ones from other parts of the site. Layer boundaries from these are shown Figure 4-29. Mean values are presented for layer interfaces along with the range of one standard deviation. Profile of soil behavior type index (I_c) is presented for median values and +/- one standard deviation range.

Soil layering at the cross section along Virginia Tech test locations (section A-A in Figure 4-26) is shown in Figure 4-30 with the CPT soundings along with this section. Several of these CPTs are the deepest soundings at the site and extend as deep as 37 meters. It is seen that the penetration resistance at the top of the CH layer is about 1 MPa and increases to 2 MPa at about 20 meter depth. This layer gets stiffer at about 25 meters with penetration resistance as high as 3 MPa. Below this depth, penetration resistance ranges between 3-5 MPa along 25-35 meters, indicative of stiff to very stiff consistency. Higher shear wave velocities were also measured along this depth range of higher penetration resistance. Silty sand gets thinner and has lower penetration resistance towards the south direction along this section. Layering at cross section B-B is shown in Figure 4-31. Penetration resistance measurements of several soundings around 12-19 meters within CH show some variations indicative of some mixed soil conditions (i.e. probably some thin sand lens alterations). Another cross section towards West-East direction (section C-C) is shown in Figure 4-32. Soil layers are uniform in thickness at this section of the site. Similarly cross section D-D is shown in Figure 4-33.

3. FOUNDATION DESIGN AND SOIL IMPROVEMENT

The shopping center and two-story parking garage are founded on shallow footings, mats, and slabs-on-grade. Details of the foundation design and soil improvement are reported earlier by Emrem (2000). The primary foundation design issues were large anticipated settlements and bearing problems in the clay, along with potential liquefaction of the silty sand layer (SM) at an average depth of between 6 m and 9 m. Although not understood at the

time, the ML/CL strata above and below the SM layer were also a potential source of liquefaction-related damage. Surcharge fills and wick drains were used in some sections to improve the soft clays and silts, and jet-grout columns were installed beneath the footprints of the structures all areas to provide increased bearing support and reduced settlements in the clays and reduce liquefaction susceptibility of the sands. As discussed later, the surcharge fills probably over-consolidated the sands and silts and increased their liquefaction resistance, although this was not accounted for in the design.

The spacing and treatment depth for the jet-grout columns varied across the site due to differing soil conditions and foundation configurations. Grout column spacings, diameters, and depths for static design were selected mainly on the basis of footing size and location, and footing and slab-on-grade loads. To provide increased resistance against potential liquefaction, the designers incorporated blanket treatment beneath the building footprints using additional short jet grout columns through the sand layer. Grout column spacing details are provided in the following sections. When the earthquake occurred, jet grouting had been recently completed for the supermarket and was just beginning in the parking garage area. Thus, there were both improved and unimproved areas of the site subjected to strong ground shaking.

3.1. Shopping Center Area

The supermarket is a one-story structure covering an area of approximately 15,600 m^2; see Figure 4-34. Section A of the building is founded on isolated spread footings, while Section B is supported by a mat foundation. No surcharge fill was used for this structure because the original fill used to reclaim the site was thicker in this section and the underlying soft soils were already sufficiently strong and stiff. The only improvement was jet-grout columns, installed beneath both sections (A and B) to improve bearing support, reduce settlements of the clay, and to increase the liquefaction resistance of the underlying silty sand layer. As shown in Figure 4-35, primary and secondary grids of columns were installed in rectangular patterns to provide blanket treatment. The columns in the primary grid were 0.6 m in diameter with a center-to-center spacing of 4 m. These columns extended from the ground surface to a depth of 9.0 m. The secondary grid consisted of shorter, 2.5 m-long grouted

columns that were installed between the primary columns to further increase the liquefaction resistance of the silty sand stratum (about 2.5 m thick in this location). The secondary columns penetrated only the sand stratum, extending from a depth of 6.5 m to 9.0 m. In addition to the primary and secondary grids, 0.6 m-diameter 9 m-long columns were also installed at each spread footing location in Section A of the supermarket building. Groups of two and four jet- grout columns were installed directly beneath the exterior and interior footings, respectively. No treatment was performed outside the footprint of the building. Overall, the average area replacement ratio for the SM layer was 7.07%, and 1.77% for all other layers in the upper 9 m. Grouting had been finished and the building was being constructed (about 60% complete) at the time of the earthquake. Results of a load test on a 9-m long jet-grout column are shown Figure 4-36.

3.2. Parking Lot Area

The soils beneath the parking garage were improved using surcharge fills, wick drains, and jet-grout columns. As shown in Figure 4-34, the parking garage has a plan area of about 14,000 m^2, and the structure is founded on isolated footings with a slab-on-grade poured between the footings. The site was surcharged with a 3.3 m-high sand fill, and 20 m-long wick drains were installed at a 2.5-m spacing to speed up consolidation of the clay. Primary consolidation in the clay was complete and the surcharge had been removed a few weeks prior to the earthquake. The application and removal of the surcharge fill overconsolidated the near-surface silty and sandy layers to an overconsolidation ratio of 2 to 3, and increased the liquefaction resistance. Following fill removal, the area was to be blanket-treated using primary and secondary rectangular grids of jet-grout columns similar to the grouting plan for the supermarket. At the time of the earthquake, the surcharge fill had been removed and jet grouting was just beginning. Only 10% of the area had been treated, and construction of the parking garage had not yet begun.

3.3. Lot C Area

Lot C is located adjacent to the parking garage and encompasses an area of 4,160 m^2. The area is currently being used as an auxiliary parking lot. No structures were initially planned for this section, but the soils were being improved in anticipation of future development.

Similar to the Parking Garage section, Lot C was surcharged with a 3.3 m-high fill and 20 m-long wick drains were installed. Settlement extensometers were installed in three areas of Lot C to monitor settlements at several depths within the soil profile, including points located above and below the liquefiable sand layer. The surcharge fill was still in place at the time of the earthquake, and settlements were being monitored on a daily basis. Jet-grout column installation had not yet begun in this section. As discussed later in more detail, the settlement devices made possible the direct measurement of the earthquake-induced settlements of saturated strata in the upper 25 m.

3.4. Jet-Grout Column Construction

Jet-grout columns were installed at the Carrefour site using a single-fluid jet-grouting system with an injection pressure of 450 bars. Neat cement at a 1:1 water/cement ratio was used as the grouting agent. A summary of construction parameters used for the grouting operation is provided in Table 4-2. The column diameters are smaller and installation speeds faster (faster lift rates) than what is typically associated with most jet-grouting operations in the U.S. (Andrus and Chung 1995).

Quality assurance and quality control (QA/QC) tests on the completed columns included columns integrity tests, pullout tests, compression strength tests on core samples, and visual field inspection. Average 7- and 28-day unconfined compressive strengths from core samples were 2.0 MPa (280 psi) and 4.8 MPa (690 psi), respectively. These values are typical of single-fluid jet-grout columns in fine-grained soils.

4. FIELD PERFORMANCE DURING M7.4 KOCAELI EARTHQUAKE

As discussed earlier, peak ground accelerations during the Kocaeli Earthquake (M7.4) are estimated at 0.24g for the site. The morning following the event, the grouting contractor and site engineers conducted a site reconnaissance of the shopping complex that included a field inspection, with photographs and documentation, and reading of settlement monitoring devices that had been recently installed in Lot C (Zetas 1999). Virginia Tech personnel visited the site several days later and conducted follow-up inspections of the site, as well as

other building sites located nearby. The findings allowed the rare opportunity to make performance comparisons among sites that were in different stages of improvement.

4.1. Supermarket Building - (Jet grouting ⇒ no damage)

At the time of the earthquake, the foundations had been poured and steel framework erected for the supermarket building. It may be remembered that no preload was used in this section nor were wick drains installed. Post-earthquake field inspections found no structural damage in the building, and no sand boils or liquefaction-related effects, such as settlements, were found at the building or in the surrounding lot. The area was visibly unchanged by the event, and construction of the building continued as scheduled with no repairs necessary. As discussed earlier, liquefaction was predicted for this section if left unimproved (F.S. Liq'n ≈ 0.6), with the primary anticipated damage being liquefaction-induced settlements of approximately 6 to 10 cm. The lack of structural or liquefaction-related damage suggests the jet-grout columns effectively mitigated the anticipated effects.

It is believed that a main reason the columns were effective is that they introduced considerable shear stiffness and reduced earthquake-induced peak shear strains to levels below which significant pore pressures did not develop. To investigate this idea, the authors performed two simple one-dimensional site response analyses of the soil profile, one with and one without the estimated influence of the columns, and the results were compared. The Kocaeli time history recorded at the nearby IZT station was used as input into SHAKE91 (Idriss and Sun 1992) for these analyses. The first site response analysis was performed using the shear moduli of the untreated soil based on the measured shear wave velocities. For this case, the peak shear strains calculated for the strata in the upper 9 m of the profile were about 1%. Then, as a simple first-order approach, the influence of the stiff columns was simulated by assigning higher "equivalent shear moduli" to each improved layer based on the area and stiffness ratios (the columns were at least 50 to 60 times stiffer in shear than the soil). A second site response analysis was then run, and the calculated peak strains fell within the range of 0.01% to 0.02%, one order of magnitude lower than for the untreated case. The threshold shear strain required for initiation of pore pressure development was not determined for these soils, but this value is typically in the range of 0.01% for other sands

(Dobry et al. 1982). Thus, although the analysis was simple, the findings suggest that column stiffness may have played a major role in mitigating liquefaction damage by inhibiting pore pressure development in the upper 9 m during the Kocaeli event. Details of these analyses are reported in the following sections.

The possibility must also be considered that liquefaction, or at least significant pore pressure development, could have occurred in the soils beneath the shopping center, but the jet-grout columns provided sufficient support to prevent settlements. The absence of sand boils in this area does not necessarily indicate that liquefaction did not occur because the capping layer is too thick and the liquefiable layer too thin to cause surficial ground disruption. (Although the ML/CL and/or CH materials apparently suffered strength loss and softening beneath the fill in Lot C, it is not believed that these fine-grained materials would "liquefy" in a manner that would readily produce sand boils).

4.2. Parking Structure Area - (Surcharge fill, wick drains, no jet grouting ⇒ liquefaction-related settlements)

The parking structure had not yet been built and jet-grout column installation was just beginning in this section when the earthquake occurred. Wick drains had been installed and the area surcharged with a 3.3 m-high fill that had been removed a few weeks before the earthquake. In contrast to the supermarket area, significant settlements occurred in this section. Site personnel reported that the non-grouted portion of the parking structure area was inundated with 7 to 10 cm of water that ponded on the ground surface the morning after the earthquake, as shown in Figure 4-37. During field reconnaissance, it became apparent that the water originated from the underlying soil deposit via drainage through the wicks. The magnitude of the settlement should have equaled the depth of water ponding on the surface, as the amount of expelled water is expected to be reflective of the earthquake-induced volumetric change that occurred in the soil profile. The fairly uniform depth of water suggests the settlement was uniform. No sand boils were observed anywhere in the area.

In interpreting the observed behavior, it is important to consider the possible effects of the surcharge fills and the wick drains on the liquefaction behavior. The surcharge overconsolidated the sandy and silty layers to an overconsolidation ratio of 2 to 3. Some

increase is estimated in liquefaction resistance using the approach presented in Salgado et al. (1997). Only a modest increase in factor of safety is predicted, from 0.6 without the fill, to slightly more than 0.7 with the fill. Thus, the surcharge fills apparently played only a minor role in reducing the liquefaction susceptibility of the sand stratum. Detals of the liquefaction analyses are presented in the following sections.

It is not clear what role the wick drains played in the observed behavior. It was initially thought that the wick drains may have helped prevent liquefaction, as defined by r_u = 100%, by providing partial drainage during the event. But a preliminary analysis [as per the basic approach outlined in Seed and Booker (1977) and Mesri and Shahien (2001)] that considered the soil permeability, drain spacing (2.5 m), and flow capacity of the drains, indicates that the flow capacity of the wicks was many orders of magnitude too low to have been effective in preventing significant pore pressure build up during shaking in these low-permeability soils. It was also initially thought that the drains helped prevent surface disruption by providing a controlled drainage path during reconsolidation of the sand stratum (i.e., no sand boils formed although significant settlements occurred). Prevention of sand boils would have also kept the settlements more uniform. While the drains may have been effective in this regard, the level of effectiveness is somewhat moot because Ishihara's relationship predicted that soil boils were unlikely to occur in this section (Ishihara 1985).

4.3. Lot C Area – (wick drains, no jet grouting ⇒ liquefaction-related settlements)

Similar to the parking garage area, Lot C was surcharged with 3.3 m of fill and wick drains were installed. The fill was still in place at the time of the earthquake (see fill in background of photograph in Figure 4-37). To monitor settlements in the clayey soils due to the fill, settlement extensometers were installed at three locations in Lot C (SE1, SE2 and SE3 on Figure 4-38). The extensometers consisted of plastic guide pipes 5 cm in diameter with a set of magnetic rings that slid down along the outside of the fixed-in-place pipes as the soil profile settled. Settlement extensometers extended about 25 meter depth into the stiff bearing soil layer.

Settlement extensometers were installed during July 15-22 and the fill started being placed in July 27. The final height of the surcharge fill was reached within a week. The positions of the

magnetic rings were measured daily to determine the settlement at specific elevations within the soil profile. It is fortuitous that these devices were in place during the earthquake. Figure 4-39 shows the cross section of Lot C and the surcharge fill. As seen settlement extensometers 1 and 2 are closer to the edge of the surcharge fill whereas settlement extensometer is closer to the fill center.

Elevations of the six settlement rings installed at SE1 are shown in Figure 4-40 along with a nearby CPT sounding (F10). The profile was divided into five sections (Layers A though E) with six magnetic rings. Layer A is 4.99 m thick and consists of 2.30 m thick unsaturated fill layer and 2.69 m of the upper silt/clay (ML/CL) material. Layer B is 4.30 m thick and consists of 2.01 m of upper silt/clay material, 1.50 m of SP/SM material and 0.79 m of lower silt/clay (ML/CL) material. Layer C is 3.88 m thick with 0.21 m of ML/CL layer and 3.67 m of CH levels. Layers D and E are 7.22 m and 4.72 m thick respectively both consisting of CH material.

Settlement measurements of the SE1 rings are shown in Figure 4-41. Settlement of each ring is a measure of the cumulative vertical deformation of the soil layers below the ring. Vertical compression of each layer can be deduced from the relative movement of the rings above and below that layer. Vertical compressions of the layers from ring settlements are presented in Figure 4-42.

Of particular importance is the sudden offset in the curves following the Kocaeli Earthquake on 17 August 1999. By comparing pre- and post-earthquake readings, the settlements associated with the earthquake could be estimated for each ring location. And by subtracting the settlement of a given ring from that of the ring located immediately above, the settlement attributed to the portion of the soil profile situated between the two rings could be obtained. Earthquake-induced settlements occurred in less than 24 hours, the elapsed time between the reading of the instruments the day before and morning after the earthquake. As can be seen, the total earthquake-induced settlement of Lot C at this instrument location was 9.8 cm, and it was surprising that a significant percentage of the settlement was attributed to the clayey and silty strata. Layer A, which contains 2.3 m of medium dense unsaturated fill (GC) and 2.7 m of soft saturated ML/CL material, experienced a settlement of 3.1 cm. The gravelly fill

is not believed to have contributed significantly to the measured settlements. Layer B contains 1.5 m of cleaner SM material and 2.8 m of the ML/CL soil. The measured settlement in this layer was 3.4 cm. The average vertical strain in these upper layers was about 0.7%. Unexpectedly, the balance of the settlement, 3.3 cm, was associated with the underlying materials classified as CH (Layers C, D, and E) and reaching to a depth of more than 20 m, especially Layer C that underwent 2.6 cm of settlement (vertical strain of 0.7%). A definitive explanation as to how these fine-grained soils could have experienced such rapid settlements cannot be given at this time. It is suspected that the settlements are due to earthquake-induced strength loss/softening and subsequent constant-volume shearing distortions due to the overlying fill. Layering of the subsoil and the measured settlements within these layers are summarized in Table 4-3.

Earthquake induced deformation/settlement measurements were subtracted from the post-earthquake measurements. Therefore it was possible to observe the consolidation behavior of each layer under the surcharge fill. Compressibility and consolidation parameters were estimated from the vertical compression measurements of each layer. These include (1) expected the total settlement under the fill, (2) % consolidation at the time of the earthquake, (3) coefficient of consolidation ($c_{v\text{-}h}$), (4) constrained modulus (M) and (5) permeability.

The time rate of consolidation of the subsurface layer was determined using methods developed by Hansbo (1979). In this approach consolidation rate of a clay layer by the use of wick drains is modeled radial drainage. Drainage in the vertical direction is negligible compared to radial drainage and therefore it is not included in the analysis. The governing soil engineering property used in Hansbo theory is the horizontal coefficient of consolidation c_{vh}.

Time rate of consolidation using wick drains is evaluated using the following equation:

$$t = \frac{D^2 \mu}{8 c_{vh}} \cdot ln \frac{1}{1 - \overline{U}}$$

where :

t = time for a certain consolidation

D = diameter of dewatered soil cylinder (d_e)

c_{vh} = horizontal coefficient of consolidation

$\overline{U}$ = average percent of consolidation

The variable μ used in the above equation is found by:

$$\mu = \ln(n) - 0.75\,,\ n = \frac{d_e}{d_w}$$

Where d_w is the wick diameter determined through the width of the drain (b) and the thickness of the drain (t). The value of d_w is calculated by:

$$d_w = \frac{2(b \cdot t)}{\pi}$$

This approach was used to estimate the consolidation parameters of the soil layers from vertical compression data.

Vertical compression measurements of Layer A at SE1 are shown in Figure 4-43. Settlement measurements of this layer fit in a narrow range. Total settlement for this layer is estimated 16.0 cm. Coefficient of consolidation ($c_{v\text{-}h}$) is estimated 0.018-0.028 cm/s^2. Shaded region in the figure defines the range of settlements expected from the estimated total settlement and coefficient of consolidation range. These measurements and parameter estimates indicate that consolidation of this layer was 81% complete at the time of the earthquake.

Vertical compression measurements of Layer B at SE1 are shown in Figure 4-44. Settlement measurements of this layer fit in a narrow range. Total settlement for this layer is estimated 16.0 cm. Coefficient of consolidation ($c_{v\text{-}h}$) is estimated 0.011-0.016 cm/s^2. These

measurements and parameter estimates indicate that consolidation of this layer was 66% complete at the time of the earthquake.

Vertical compression measurements of Layer C at SE1 are shown in Figure 4-45. Settlement measurements of this layer fit in a fairly narrow range. Total settlement for this layer is estimated 4.7 cm. Coefficient of consolidation (c_{v-h}) is estimated 0.006-0.010 cm/s^2. These measurements and parameter estimates indicate that consolidation of this layer was 51% complete at the time of the earthquake.

Vertical compression measurements of Layer D at SE1 are shown in Figure 4-46. Total settlement for this layer is estimated 4.0 cm. Coefficient of consolidation (c_{v-h}) is estimated 0.005-0.011 cm/s^2. These measurements and parameter estimates indicate that consolidation of this layer was 48% complete at the time of the earthquake.

Vertical compression measurements of Layer E at SE1 are shown in Figure 4-47. Total settlement for this layer is estimated 2.0 cm. Coefficient of consolidation (c_{v-h}) is estimated 0.004-0.013 cm/s^2. These measurements and parameter estimates indicate that consolidation of this layer was 60% complete at the time of the earthquake. Estimated consolidation and compressibility parameters for the soils at this settlement extensometer location are summarized in Table 4-4.

Elevations of the six settlement rings installed at SE2 are shown in Figure 4-48 along with a nearby CPT sounding (F08). The profile was divided into five sections (Layers A though E) with six magnetic rings. Layer A is 5.00 m thick and consists of 2.00 m thick unsaturated fill layer and 3.00 m of the upper silt/clay (ML/CL) material. Layer B is 4.33 m thick and consists of 2.30 m of upper silt/clay material, 1.20 m of SP/SM material, 0.70 m of lower silt/clay (ML/CL) material and 0.13 m of CH material. Layers C, D and E are 3.89 m. 7.23 m and 4.72 m thick respectively, all consisting of CH material.

Settlement measurements of the SE2 rings are shown in Figure 4-49. Settlement of each ring is a measure of the cumulative vertical deformation of the soil layers below the ring. Vertical compression of each layer can be deduced from the relative movement of the rings above and below that layer. Vertical compressions of the layers from ring settlements are presented in Figure 4-50.

As can be seen, the total earthquake-induced settlement of Lot C was 11.8 cm, and it was surprising that a significant percentage of the settlement was attributed to the clayey and silty strata. Layer A, which contains 2 m of medium dense unsaturated fill (GC) and 3 m of soft saturated ML/CL material, experienced a settlement of 2.5 cm. The gravelly fill is not believed to have contributed significantly to the measured settlements. Layer B contains 1.2 m of cleaner SM material and 3 m of the ML/CL soil. The measured settlement in this layer was 4.6 cm. The average vertical strain in these upper layers was about 0.8%. Unexpectedly, the balance of the settlement, nearly 5 cm, was associated with the underlying materials classified as CH (Layers C, D, and E) and reaching to a depth of more than 20 m, especially Layer C that underwent 3.6 cm of settlement (vertical strain of 0.9%). A definitive explanation as to how these fine-grained soils could have experienced such rapid settlements cannot be given at this time. It is suspected that the settlements are due to earthquake-induced strength loss/softening and subsequent constant-volume shearing distortions due to the overlying fill. Layering of the subsoil and the measured settlements within these layers are summarized in Table 4-5.

Vertical compression measurements of Layer A at SE2 are shown in Figure 4-51. Settlement measurements of this layer fit in a narrow range. Total settlement for this layer is estimated 25.3 cm. Coefficient of consolidation ($c_{v\text{-}h}$) is estimated 0.020-0.030 cm/s^2. These measurements and parameter estimates indicate that consolidation of this layer was 89% complete at the time of the earthquake.

Vertical compression measurements of Layer B at SE2 are shown in Figure 4-52. Settlement measurements of this layer fit in a narrow range. Total settlement for this layer is estimated 20.4 cm. Coefficient of consolidation ($c_{v\text{-}h}$) is estimated 0.013-0.018 cm/s^2. These measurements and parameter estimates indicate that consolidation of this layer was 76% complete at the time of the earthquake.

Vertical compression measurements of Layer C at SE2 are shown in Figure 4-53. Settlement measurements of this layer fit in a fairly narrow range. Total settlement for this layer is estimated 8.6 cm. Coefficient of consolidation ($c_{v\text{-}h}$) is estimated 0.009-0.015 cm/s^2. These

measurements and parameter estimates indicate that consolidation of this layer was 60% complete at the time of the earthquake.

Vertical compression measurements of Layer D at SE2 are shown in Figure 4-54. Total settlement for this layer is estimated 5.3 cm. Coefficient of consolidation (c_{v-h}) is estimated 0.006-0.011 cm/s^2. These measurements and parameter estimates indicate that consolidation of this layer was 58% complete at the time of the earthquake.

Vertical compression measurements of Layer E at SE2 are shown in Figure 4-55. Total settlement for this layer is estimated 2.5 cm. Coefficient of consolidation (c_{v-h}) is estimated 0.0025-0.0055 cm/s^2. These measurements and parameter estimates indicate that consolidation of this layer was 36% complete at the time of the earthquake. Estimated consolidation and compressibility parameters for the soils at this settlement extensometer location are summarized in Table 4-6.

Elevations of the six settlement rings installed at SE3 are shown in Figure 4-56 along with a nearby CPT sounding (F07). The profile was divided into five sections (Layers A though E) with six magnetic rings. Layer A is 6.04 m thick and consists of 2.25 m thick unsaturated fill layer and 3.79 m of the upper silt/clay (ML/CL) material. Layer B is 2.09 m thick and consists of 0.16 m of upper silt/clay material, 1.50 m of SP/SM material, 0.43 m of lower silt/clay (ML/CL) material. Layer C is 4.99 m thick with 0.72 m of ML/CL layer and 4.27 m of CH levels. Layers D and E are 6.49 m and 4.99 m thick respectively both consisting of CH material.

Settlement measurements of the SE3 rings are shown in Figure 4-57. Settlement measurements of rings 3, 4, 5 and 6 were not possible for a period of time after the earthquake. Therefore it is not possible to estimate the earthquake induced settlements and consolidation settlements after the earthquake for some of the layers. It is not clear why readings could not be taken for a period of time. The guide pipe may have been bent slightly by the soil movements around. This may have possibly prevented the lowering of magnetic sensor through the guide pipe. It is still a question though if this was the case why it was possible to take readings at those elevations after a period of time. Vertical compressions of

the layers from ring settlements are presented in Figure 4-58. Layering of the subsoil and the measured settlements within these layers are summarized in Table 4-7.

Vertical compression measurements of Layer A at SE2 are shown in Figure 4-59. Settlement measurements of this layer fit in a narrow range. Total settlement for this layer is estimated 13.2 cm. Coefficient of consolidation ($c_{v\text{-}h}$) is estimated 0.018-0.028 cm/s^2. These measurements and parameter estimates indicate that consolidation of this layer was 80% complete at the time of the earthquake. Estimated consolidation and compressibility parameters for the soils at this settlement extensometer location are summarized in Table 4-8.

This type of earthquake-induced settlement measurement has not been possible previously, and provides a unique opportunity to better understand the behavior of these soils under strong ground shaking. The observations are also important, first, because apparent liquefaction-type behavior was demonstrated for an ML/CL material that was considered "non-liquefiable" by virtue of I_c values > 2.6 from the CPT and failure to meet the Chinese Criteria by virtue of a clay-sized fraction greater than 15%. Thus, clay-sized fraction and I_c values may not be appropriate indicators of liquefaction potential in some cases. And secondly, although further study is needed, it appears that the CH materials were also susceptible to at least some percentage of strength loss and softening under strong ground shaking – an unexpected and surprising possibility. ML/CL soils are thought to have undergone liquefaction-type behavior. However it is early at this stage to attribute liquefaction-type behavior to the CH soils without clearly understanding the behavior. Deformations at the CH soil can also be related to the collapse of the sensitive soil fabric due to disturbance. Sampling and testing of these soils are necessary to better understand their behavior under earthquake loading.

Comparison of pre- and post-earthquake settlements indicates that the subsoils under the fill have undergone earthquake induced deformations. The measurements are clearly associated with the soils at the top 9-10 meters of the soil profile. None of the layers at these depths except the SP/SM layer are permeable enough to drain in less than 24 hours. Wick drains definitely have decreased drainage times but this would still not be enough. This is clearly demonstrated by the time dependent settlements under the surcharge fill. In most cases 60-

70% consolidation is complete under the surcharge fill three weeks after fill placement (i.e. August 17). Therefore, even though it is thought that these deformations are induced by the earthquake it is not possible attribute these settlements/deformations to post-earthquake consolidation; at least in a time period shorter than a day. It is still possible though these deformations can be related to earthquake induced pore pressures, strength/stiffness loss and undrained deformations under this additional load. If this is the case these deformations should be shear distortions under the weight of the fill, rather than deformations associated with volume change.

Finite element analyses were performed using DYNAFLOW (Prevost 2002) to investigate this possibility. Elastic stiffness properties of the foundation soils were estimated from the compressibility parameters backcalculated from the settlement measurements described above. Finite element mesh used in the analyses is shown in Figure 4-60. Analyses were performed for axisymmetric conditions where the line of symmetry is through the center of the fill. Rectangular fill placement was modeled with an equivalent circle in this approach.

Several cases were analyzed where the fill was placed, the system brought to equilibrium under the weight of the fill, the displacements initialized to zero and the stiffnesses of the saturated foundation soils were reduced some percentage of the initial values. Poisson ratio of the foundation soils varied between 0.3-0.4 in modeling initial deformations under the fill. Following the initial analysis, Poisson ratio of the saturated soils was changed to a value so that the bulk modulus of the medium was kept equal to the bulk modulus of water (2.2×10^{10} Pa) and the shear modulus was reduced in comparison to the initial values. This makes sure that shear modulus is reduced while volume change is kept at incompressible levels. Values of Poisson ratio for these levels were greater than 0.49995 at this stage of the analyses. Stiffness reduction was only applied to the saturated soil layers where earthquake induced deformations were measured. Stiffness of the unsaturated fill was neither reduced nor was the Poisson ratio changed from the initial value. Stiffness of the SP/SM layer was reduced with the same amount as the other layers but the Poisson ratio of this layer was unchanged to simulate drained conditions.

Deformed shape of the mesh for one case (stiffness loss 70%) is shown in Figure 4-61. Deformations are exaggerated 20 times to make the deformation pattern visible. This shape corresponds to the additional deformations due to the applied stiffness loss, because initial deformations under the fill were cleared from the nodal displacement array. Deformation at the top of the fill is not uniform and shows some variation. Largest vertical deformations are observed near the edge of the embankment. It is seen that the deformations corresponds to a distortional deformation pattern. Some volume change is also present due to the SP/SM layer which was modeled compressible in the analyses. Displacement vectors are shown in Figure 4-62. A schematic of the deformations are shown in Figure 4-63. Settlement of the top of the original ground surface was calculated for each case. Mean of the ground settlement along with one standard deviation range is plotted in Figure 4-64.

It is seen that 65-75% of stiffness loss results in average vertical displacements close to the range measured by the settlement extensometers. Therefore it is possible to explain the measured deformations by constant volume deformations resulting from stiffness loss. This stiffness loss of course should be associated with some amount of pore pressure increase.

This simplified analysis show that an admissible deformation mode is available that can explain the measured deformations. It must be noted however this is a plane strain analysis of a cross section of the fill. Larger deformations should be expected for the three dimensional case. Therefore observed deformations may correspond to smaller magnitudes of stiffness loss.

Finally, the surcharge fill was still in place and would have masked any surficial ground disruption; however, no sand boils were found on the ground surface along the edges of the filled area. The wick drains are thought to have drained water from the underlying deposit due to earthquake-induced excess pore pressure development, similar to what occurred in the parking garage, but the fill prevented direct observation of expelled water.

4.4. Other Building Sites Nearby (no soil treatment ⇒ settlements and damage)

To provide additional performance comparisons between treated and untreated ground, properties adjacent to the shopping center site were reconnoitered following the earthquake.

Based on soil borings and CPTs in this general area, it is probable that the ML/CL and SM strata underlying the shopping center also underlie the surrounding sites. Liquefaction-related effects were common in unimproved soils in the immediate vicinity. Based on visual inspection by Virginia Tech personnel, the apartment buildings across the street commonly settled 5 to 10 cm, and the warehouses just outside the property boundary settled about 5 cm. No sand boils were observed at either of these locations. For the most part, the underlying soils appeared to develop pore pressures, soften, and settle beneath the structures, but did not exhibit the liquefaction behavior normally associated with cleaner sands.

4.5. Discussion of Soil Improvement Effectiveness

As shown in Table 4-9, the comparison of field behavior among the treated and untreated areas was used to gauge the effectiveness of soil treatment in mitigating earthquake–related damages. Although the presence of fine-grained soils and highly variable conditions complicated the liquefaction analysis, the behavior observed at the unimproved sections of the shopping complex and adjacent building sites was reasonably consistent with what was predicted for the Kocaeli Earthquake loading. More importantly, there was a clear distinction between the earthquake-related damage in the untreated areas and the lack of damage in the jet-grouted section. It is believed that the stiff close-to-moderately spaced columns reduced shear strains and restricted pore pressure development in the upper 9 m of the soil profile. In fact, the columns may have been more effective than initially credited because only the 3 m-thick SM stratum was considered liquefiable during design, and only this layer was treated during secondary grouting; however, measurements from Lot C indicate that all saturated strata in the upper 9 m of the profile contributed to earthquake-related settlements, especially the ML/CL strata. Even if significant pore pressures had developed in or migrated to the upper soils during the earthquake, as long as the jet-grout columns maintained structural integrity, their higher stiffness should have significantly reduced post-earthquake reconsolidation settlements.

As mentioned earlier, the jet-grout columns used for this project were of smaller diameter (0.6 m) and constructed using a faster installation procedure relative to most U.S. jet grouting operations. The replacement ratio was about 7% in the lower SM stratum, and 2% in the

ML/CL strata located above and below this layer. Also, the liquefaction mitigation approach used for this project is distinguished from the more common encapsulation approach of constructing rows of contiguous columns to form cells to contain liquefied material (i.e. O'Tourke and Goh 1997; Welsh and Burke 1991). The success of the ground treatment at this site suggests that similar applications of small-diameter high-modulus columns could prove useful at other sites where the soils are soft and mixed and liquefaction is of concern.

Of particular importance, the authors suspect that high-modulus columns may in some cases offer added benefits over stone columns in mixed and "dirty" soils that have low permeabilities (and do not drain rapidly) and are difficult to densify, especially in terms of reducing post-earthquake reconsolidation settlements. Also, jet-grout column installation does not densify the surrounding ground, as the improvement is solely from the strength and stiffness of the columns (and/or encapsulation of the liquefied material in cases where this approach is used). As a result, jet grouting can be used in situations where densification of the surrounding ground is not desirable owing to the need to avoid settlement during installation. It is also important to note that high-modulus columns of the type constructed using jet grouting can also be constructed using other installation techniques that might be more economical in some cases, such as wet soil mixing. Thus, the demonstrated effectiveness of the jet-grout columns at this site has relevance to other techniques whereby ground reinforcement via stiff columns can be achieved.

The application and removal of surcharge fills probably had only a minor effect on increasing the liquefaction resistance of the soils. Also, the wick drains probably did not play a significant role in reducing pore pressures during shaking, but may have helped prevent surficial ground disruption and/or contribute to settlements being more uniform. Finally, the surprising liquefaction-type behavior of the ML/CL soils, and apparently the CH materials, underscores the need for further research on these materials.

5. EXPECTED LIQUEFACTION BEHAVIOR OF UNIMPROVED GROUND DURING KOCAELI EARTHQUAKE AND EVAUALTION OF LIQUEFACTION RESISTANCE USING CPT

To better gauge the effectiveness of the ground improvement and to provide more insight into the liquefaction effects observed in unimproved ground, it was necessary to perform a liquefaction analysis of the site. The analysis was primarily concerned with determining whether the observed liquefaction behavior in unimproved ground was consistent with predicted behavior, and secondly, estimating what behavior would have occurred if ground improvement had not been implemented. Of particular benefit to the analysis were the measured liquefaction-related settlements at Lot C where the soils were unimproved. These data provided unique insight into the liquefaction behavior of the soils, especially the ML/CL strata.

Initial step in the evaluation of liquefaction potential involved the characterization of suspect soils by sampling and Cone Penetration Testing. Grain size and plasticity characteristics of the soils were determined. Effectiveness of Cone Penetration Testing in detecting and characterizing suspect liquefiable soils were investigated by comparing directly measured soil characteristics (i.e. fines content) and those estimated by CPT. Next step involved the estimation of earthquake induced stresses at the site with site response analyses. Finally penetration resistance results from CPT were used to assess the liquefaction resistance of these soils using current design guidelines. Therefore it was possible to assess the effectiveness of CPT and the current design methods in the assessment of liquefaction potential of soils with fines.

Ground motion recordings of the Kocaeli Earthquake (M7.4) and several aftershocks were available from the IZT recording station in Izmit approximately 8 km from the site. The IZT site is a rock site with a V_s-30 of 800 m/s and a NEHRP classification of B (Rathje et al. 2002). These motions were used to perform a site response analysis using the SHAKE91 computer code (Idriss and Sun 1992), and a peak ground acceleration of 0.24g was estimated for the site, close to the 0.23g peak value recorded at IZT. Cyclic stress ratio (CSR) was determined for the various soil strata from shear stresses calculated from site response analyses and the cyclic resistance ratio (CRR) values were estimated from the CPT

measurements as per Youd et al. (2001). In performing the liquefaction analysis, it was recognized that the majority of the suspect soils have low CPT tip resistances and high fines contents (I_c values > 2.6), a condition where the use of standard CPT liquefaction evaluation procedures can be unreliable (Seed et al. 2001). Therefore, caution and judgment were used in applying the CPT-based liquefaction procedure for these materials. Also, the highly variable and mixed conditions introduce considerable uncertainty in the prediction of field behavior. Because the liquefaction analysis was only intended to provide insight into the observed behavior and to establish general benchmarks for the effectiveness of the soil treatment toward mitigating damages, the analysis was considered appropriate for the purposes of this study.

As mentioned earlier, only the silty sand stratum (SM) that extends from a depth of 6 m to 9 m in most areas was initially assessed to be liquefiable. However, post-event measurements from Lot C indicated that significant liquefaction-related settlements occurred in the ML/CL strata, and thus all of the saturated strata in the upper 11.5 m of the profile are considered susceptible to liquefaction-type behavior.

Evidence of liquefaction was observed at the site and around the area. Detailed investigations have been performed concerning these soils. Fine grained soils that are not considered liquefiable by current design methods have been observed to liquefy at and around the site.

Finally, it was necessary to predict the liquefaction-induced settlements in unimproved ground across the site. Although the Ishihara and Yoshimine (1992) method could be used to predict settlements of the SM and SM/SP strata, this method is not directly applicable to the ML/CL soils prevalent at the site. Moreover, the measured settlements in Lot C (unimproved) allowed back-calculations of the apparent earthquake-induced volumetric strains associated with specific soil strata in the upper 25 m of the profile. These strain data, which averaged close to 1.0% in the upper 9 m, were used to predict the settlements of unimproved soil strata at other areas of the site and surrounding properties. Based on the range of thicknesses of the relevant strata, the predicted settlements in unimproved ground are on the order of 7 to 11 cm for the Parking Garage section, and 6 to 10 cm for the Supermarket area. These are probably upper-bound settlement predictions for non-loaded

areas because the measured settlements/strains in Lot C could have been due in part to constant-volume shearing distortions induced by the overlying surcharge fill, as opposed to pure volumetric straining.

Soil conditions beneath nearby vacant lots and building sites are thought to be similar to those at the shopping center complex. In particular, it is believed that the ML/CL and SM strata underlie much of the surrounding area. Three warehouses are located adjacent to the shopping center building and a set of six-story apartments is located approximately 100 m from the northern boundary of the site. Both facilities are founded on shallow footings and unimproved soil. The expected liquefaction and settlement potential at these untreated neighboring sites are assumed to be similar to those of the untreated areas at the shopping complex, and thus the expected factors of safety against liquefaction and settlements are assumed to fall somewhere in the range of 0.6 to 0.7, and 7 to 12 cm, respectively (the range of values estimated/observed for the Carrefour site). Although rough, these estimates still provide an additional benchmark for performance comparisons between treated and untreated ground. A summary of the expected liquefaction behavior of untreated soils is presented in Table 4-9.

In this section, current guidelines on the liquefaction of soils with fines are summarized. Description of the in-situ soils in terms of the characteristics pertinent to these guidelines is provided. Results of the liquefaction susceptibility analyses are summarized.

5.1. Characterization of Liquefiable Soils Using Cone Penetration Testing

Cone Penetration Testing is finding increased application in liquefaction analyses. Several papers have been published on the subject involving liquefaction case histories and relationships were developed to estimate liquefaction resistance to CPT measurements (Stark and Olson 1995; Suzuki et al. 1995). However there is still very limited information on the application of CPT for the liquefaction assessment of soils with fines.

Current liquefaction evaluation procedure recommends certain guidelines for the interpretations of CPT measurements in the evaluation of liquefaction resistance (Youd et al. 2001). These include normalizing CPT tip resistance for overburden pressure and fines content among others.

5.1.1. Normalization of q_c for Confining Pressure

Soil behavior type index (Ic) is calculated using the relationship below

$$I_c = \left[\left(\log Q - 3.47 \right)^2 + \left(\log F + 1.22 \right)^2 \right]^{0.5}$$

where Q is the normalized cone penetration resistance and F is the normalized friction ratio as defined below;

$$Q = \frac{q_c - \sigma_{vo}}{P_a} \left(\frac{P_a}{\sigma'_{vo}} \right)^n \text{ and } F = \frac{f_s}{q_c - \sigma_{vo}} \cdot 100\,\%$$

These parameters used in the equations are;

q_c : cone penetration resistance

f_s : sleeve friction

σ_{vo}, σ'_{vo} : total and effective vertical overburden stress respectively

P_a : atmospheric pressure in the same units as q_c, f_s, σ_{vo} and σ'_{vo}

n : stress exponent factor

The value of stress exponent n depends on the soil type and 1.0 is an appropriate value for clayey soils and 0.5 for clean sands. The selection of the stress exponent requires an iterative process because the procedure to determine the soil behavior type index (I_c) requires to assume a stress exponent which inherently is a function of soil type and therefore I_c. Robertson and Wride (1997) recommend using a stress exponent 1.0 to calculate I_c as the initial step. If the calculated $I_c > 2.6$ then it means the soil is a clayey and it is in agreement with the initial assumed value of stress exponent. However if the calculated $I_c < 2.6$, I_c should be recalculated using a stress exponent n = 0.5, a value that corresponds to clean granular soils. If the recalculated $I_c < 2.6$ then the soil is most likely granular. However if the recalculated Ic is > 2.6 then the soil is a sand-silt-clay mixture. In this case Ic should be once again be recalculated using a stress exponent 0.7.

Once a soil type consistent value of stress exponent n is determined, measured cone penetration resistance should be normalized for the effect of overburden pressure. Normalized cone penetration resistance is a dimensionless quantity and is defined as;

$$q_{c1N} = C_Q \cdot \frac{q_c}{P_a}$$

where q_c is the cone tip resistance; $C_q = (P_a/\sigma_{vo})^n$ correction for effective overburden stress; n is the stress exponent and P_a is the reference pressure level as discussed above.

5.1.2. Apparent Fines Content from CPT

Apparent fines content is defined in relation to soil behavior type index as;

Fines Content

= 0 % for $I_c < 1.26$

= 1.75 I_c3.25 – 3.7 x 100 (%) for $1.26 \leq I_c \leq 3.5$

= 100 % for $I_c > 3.5$

5.1.3. Normalization for Overconsolidation Effects

Surcharge fills were used to improve parts of the site. At one section the surcharge fill was removed when the earthquake struck. This section was overconsolidated due to the recently applied surcharge. Therefore the effects of this overconsolidation should be considered in evaluating of the liquefaction resistance of these soils. This is accounted in two steps (1) the effect of overconsolidation and therefore increased lateral stresses on the measured CPT resistance (2) the effect of overconsolidation on the resistance against liquefaction.

Effect of lateral stresses on penetration resistance was first recognized by Durgunoglu and Mitchell (1975a; 1975b). Based on a series of tests performed at the calibration chamber Salgado et al. (1997) have suggested a procedure where they introduce a normalization factor (C_{NH}) to account for the effect of overconsolidation on the measured tip resistance and a separate normalization factor to account for the effect of overconsolidation on the liquefaction resistance.

For normally consolidated deposits the effect of confining pressure is accounted for using C_Q as discussed above. Salgado et al. (1997) propose the following normalization where the effect of vertical effective stress and overconsolidation are normalized separately;

$$q_{c1,Ko,NC} = C_Q \cdot C_{NH} \cdot \frac{q_c}{P_a}$$

where $q_{c1,Ko,NC}$ is the normalized cone penetration resistance, q_c is the measured cone penetration resistance, P_a the reference pressure, C_Q is the normalization factor for normally consolidated resistance (denoted as C_{NV} in their terminology) and C_{NH} is the normalization factor for the overconsolidated stress state. The relation between the at-rest earth pressure coefficients at normally consolidated and overconsolidated states is;

$$C_{NH} = \left(\frac{K_o}{K_{o,OC}} \right)^{0.5}$$

This recommendation is based on calibration chamber tests run using clean silica sands. Selection of the exponential factor 0.5 in the above equation is based on the observations that q_c is related to the square-root of lateral stress (Salgado et al. 1997). A different exponential factor (i.e. 0.7 for intermediate soils, 1.0 for clayey soils) may be more appropriate as in the case of C_Q. However these will have a minor effect on this already approximate relationship.

Normalized penetration resistance ($q_{c1,Ko,NC}$) should be converted to a clean sand equivalent and the cyclic resistance ratio (CRR) estimated.

$$CRR_{OC} = CRR \frac{1 + 2K_{o,OC}}{1 + 2K_o}$$

5.2. Current Guidelines to Assess the Liquefaction Susceptibility of Soils with Fines

Based on sites where liquefaction was and was not observed after earthquakes in China, Wang (1979) established that silty/clayey soils containing less than 15-20% particles finer than 5 μm and with in-situ water content (w_n) close to liquid limit (LL) are susceptible to liquefaction. Based on these observations, Seed and Idriss (1982) stated that clayey soils (i.e.

soils that plot above the A-line on the plasticity chart) could be susceptible to liquefaction if all three of the following conditions are met;

(1) Material finer than 5 micron (0.005 mm) < 15 %

(2) Liquid limit < 35%

(3) Water content > 0.9 x Liquid limit

Due to its origin, this standard is known in the literature as the "Chinese Criteria". Current procedures recommend the use of Chinese Criteria to assess the liquefaction susceptibility of soils with fines. If all the above criteria are met the soil is considered susceptible to liquefaction and it is recommended to retrieve undisturbed samples and test to assess behavior and strength under dynamic loading. The soil is considered "safe" against liquefaction when any one these requirements are not met.

Koester (1992) investigated the difference of liquid limit determined from tests with the fall cone method the procedure commonly used in China (i.e. in Wang's liquefaction study) and the Casagrande percussion device. Based on the results of this comparative study he noted that the determination of LL by means of the fall cone used in China produced values that are about 4 points higher than those values determined by means of the Casagrande percussion device. Koester recommended a slight reduction of the Liquid Limit condition of the Chinese Criteria before using it as a screening tool when the Casagrande method has been used. Similarly, Andrews and Martin (2000) reduced the Liquid Limit condition for liquefaction susceptibility to LL < 32. Andrews and Martin then used 2μm as the limit between silt-size and clay-size particles, with < 10% clay-size particles being necessary for a silty or clayey soil to be liquefiable. Moreover, Andrews and Martin recommend the omission of the w_n/LL ratio criterion as a condition in the liquefaction susceptibility of silty soils.

Boulanger et al. (1997; 1998) report a case history of liquefaction at the Moss Landing site during the 1989 Loma Prieta Earthquake. It is indicated that that a deposit of clayey soil might have contributed to the observed surface deformations/disruptions. They concluded that indiscriminate use of the Chinese Criteria as a substitute for detailed laboratory and in-

situ testing should be avoided. They recommend undisturbed sampling and testing of the suspect soils for behavior under cyclic loading.

The location of a soil on the Casagrande plasticity chart and, or in combination with, the use of the "C" descriptor of the Unified Soil Classification System (USCS) have also been introduced as a tool to identify potentially liquefiable soils. Youd (1998) follows a series of assumptions to state that natural soil deposits that have a "C" descriptor (soils with "clay" descriptor, i.e. CH, CL, SC, and GC) are screened as non-liquefiable. Potentially liquefiable fine-grained soils should have LL < 35 and plot below the A-line or have PI < 7.

Seed et al. (2001) indicate that soils that have LL < 30 and PI < 10 are liquefiable, and those with 30 < LL < 40 and 10 < PI < 12 fall into an "uncertain range". Undisturbed samples of soils that plot in that region of the plasticity chart should be obtained for laboratory testing. Polito (2000) used a wider range of the plasticity chart, and according to his criteria, soils with LL < 25 and PI < 7 are liquefiable. Soils that have 25 < LL < 35 and 7 < PI < 10 are potentially liquefiable, and finally soils with 35 < LL < 50 and 10 < PI < 15 are susceptible to cyclic mobility.

The current state-of-the-art and state-of-the-practice for liquefaction study is established in the summary report from the 1996 NCEER and 1998 NCEER/NSF workshops on evaluation of liquefaction resistance of soils (Youd et al. 2001). The use of Chinese Criteria is recommended to confirm the liquefaction susceptibility of silts and clays in this consensus document.

Most of the soils that liquefied at the site were considered non-liquefiable during the design and construction phases, shortly before the 1999 earthquake. Only a small fraction of the soils at the site that classify as SP and SM were considered liquefiable and ground improvement works have been carried out to mitigate the liquefaction potential of these specific soils ignoring any potential related to soils with significant fines. Soils that liquefied, contained particles finer than 5μ as high as 50% by weight compared to the 15% limit specified by Chinese Criteria. These observations are consistent with previous studies that indicate that it is not the amount of fines but the plasticity that control liquefaction behavior

(Polito 2000). These soils have low liquid limits generally lower than 40 even though they plot above the A-line.

The use of Cone Penetration Testing (CPT) has been investigated to assess the liquefaction susceptibility of these soils. Assessment of liquefaction susceptibility with CPT requires to indirectly estimate the fines content and therefore a clean sand equivalent tip resistance $q_{c1,cs}$ which in turn is used to estimate the cyclic strength of the soil. Applicability of CPT in liquefaction analysis is limited to soils with soil behavior index I_c less than 2.6 corresponding to soils with little fines (Lunne et al. 1997). Majority of the soils that liquefied at the site have shown to have $I_c > 2.6$ as expected from the high levels of fines content.

5.3. Grain Size and Plasticity Characteristics

Two boreholes were drilled within a meter of CPT-H4 (shown in Figure 4-26). At one of the drilling points, standard penetration tests were performed and soils were sampled with the split spoon. Index properties of the soil samples retrieved at 1 meter intervals are shown in Figure 4-65. It should be noted that the data is obtained from conventional SPT samples that span a 45 cm (36 inches) thick zone. It is seen that the soils at the top 8 meters have considerably lower plasticity (both liquid limy and plasticity index) than the soils below that depth. High plasticity clay is present below about 9 meters at this location. Soil samples retrieved from this layer indicate that the soil have high water content, close to its liquid limit in most cases.

Following figures show how the soil samples from the liquefied depths compare with the Chinese Criteria. Natural water content of the soil samples are shown in Figure 4-66 in relation to the liquid limit. Plasticity characteristics are shown in Figure 4-67. Grain size characteristics are shown in Figure 4-68.

Measured fines content (defined as material passing #200 sieve) along with ratio of material finer than 5 and 2 microns are given in Table 4-10. The levels above the CH layer have low plasticity and natural water content close to the liquid limit. These soils have fines content as high as 80% and material finer than 5μ as high as 54%.

The soils at the top 8-9 meters at this section are the soils that exhibited liquefaction-type behavior during the earthquake. These soils belong to the SP/SM and ML/CL levels described in the previous sections. Individual soil samples at these depths may vary by plasticity and gradation characteristics resulting in soil classification of other categories (i.e. CL/ML, SC/GC etc.). Naming convention followed in the previous section is a generalization to capture the general characteristics of the soils at these depths. Local variations in soil properties exist at the site.

Previous investigations indicate that layering is highly variable in the vertical direction below the fill material and above the CH material at 8.5 meters depth at this location. For this purpose a second borehole was auger-drilled on the opposite side of CPT-H4. Three tube samples, each 50 cm thick were obtained from the zone 6.0 meters to 7.5 meters from ground surface. These tubes were divided into 10 cm thick segments and the soil in each segment was tested for index properties. Visual inspection of the soils during slicing of the tube samples confirmed this variability. Results of the lab tests on these samples are summarized in Table 4-11. Measured properties are variable for the samples. It is apparent that the SPT samples obtained have not been able to capture this variability. Not only they missed some bypassed/unsampled levels between the split spoon samples, they also averaged out thin levels into one bulk unit.

For example the split-spoon sample between depths 6.0-6.45 classifies as CL/SC with 50.8% fines and with liquid and plastic limits of 25 and 20. We have used dual symbols as specified by ASTM because the measured fines content is very close to 50% boundary which separates low plasticity clay (CL) and clayey sand (SC) groups. Four of the five thin-slice samples from these elevations are non-plastic and have fines content ranging between 9.1%-43.2%. The fact that the bulk sample has fines content higher than all of the thin-slice samples indicate that there is also lateral variability at very close distances. This shows how the bulk sample can average out local variations in soil characteristics.

A similar observation holds when we compare the soil from 7.0-7.45 meters sampled split-spoon with the thin slice samples from depths 7.0-7.5 meters. The split-spoon sample again classifies as CL/SC with 50.9% fines and with liquid and plastic limits of 26 and 19. Two of

the thin slice samples are non-plastic and classify as silty sand (SM) where the other three samples classify as low plasticity clay (CL). These samples have fines content ranging between 31.9%-70.0%.

Measured gradation and plasticity characteristics of these two split-spoon samples are strikingly similar. However this should not indicate the lack of soil variability along depth where the high degree of variability is evidenced by the thin slice samples. It is evident that the split spoon samples are just averages of highly variable soil conditions and they exhibit similar values.

These results show how standard procedures of sampling can skip thin layers that may be important for the project. Split spoon sampling was performed at every 1 meters at one of the boreholes. In general practice SPT is performed at 1.5 meter (5 ft) intervals. This procedure can skip important factors in mixed ground conditions. This demonstrates how conventional sampling can skip some important information regarding soil characteristics. However it would not be easy to justify more thorough investigations. Detailed sampling was performed at this site after the post-earthquake observations and measurements.

These results clearly indicate that current guidelines fail to assess the liquefaction susceptibility of soils with fines. Three of the criteria presented above should be satisfied to for a soil to be considered susceptible to liquefaction. The criterion in terms of clay content (denoted by material fines than 5μ) does not identify liquefaction susceptibility correctly. Most of the sampled soils have much more than 15% clay content. This observation is in agreement with the recent studies performed at Virginia Tech (Polito 2000) which indicate that the amount of fines is not the key factor for liquefaction susceptibility of soils with fines. Plasticity characteristics of the fine grained soils are more important in terms of liquefaction-type behavior rather than clay content or material finer than 5μ. Similar observations have been made in studies regarding liquefaction events at other sites of Kocaeli Earthquake (Bray et al. 2001; Sancio et al. 2003).

Cone Penetration Testing is finding wider application in subsoil investigations and also assessment of liquefaction susceptibility. Applicability of CPT to soils with fines is not tested yet. Current guidelines recommend sampling and testing of the soils to assess liquefaction

susceptibility. Such soils are identified by soil behavior index (I_c) greater than 2.6. Therefore CPT is not directly applicable to soils with considerable fines.

The boreholes discussed above were drilled adjacent to CPT-H4. Therefore it is possible to test how well CPT performed in characterization of these soils. Results are shown in Figure 4-69 for CPT measurements, estimated soil behavior index (I_c) and estimated fines content from I_c. This is compared with measured fines content of the samples from the adjacent boreholes. Shown in the figure is the apparent fines content estimated from CPT along with the fines content from borehole samples. Solid circles are from the split spoon SPT samples and the hollow circles represent the 10 cm thick slices from the shellby tube samples. The extent of the tick marks represent the depth range the sample is drawn from. Split spoon samples cover a 45 cm thick soil zone whereas the sliced samples cover a 10 cm thick zone.

Low plasticity silt/clay layer at the top has low penetration resistance an indication of its soft consistency. Soil behavior index throughout this layer is about 3.0 which is an indication of the high fines content. Observations during drilling revealed the presence of some coarse sand-fine gravel levels. No soil samples are retrieved from this depth. Given description is based on the visual observation of material transported to the ground surface with the drilling mud. This thin level is detected by the CPT at about 4.8 meter depth with a slight increase in penetration resistance, decreases in friction ratio and soil behavior index. Such thin layers sandwiched between soft Therefore the penetration resistance may as well be a low value than the actual penetration resistance of this thin sandy/gravel layer. This could also have affected the sleeve friction measurements therefore the estimates of soil behavior index and fines content.

Visual inspection of the drilling fluid and also the retrieved samples reveal that there is a difference in color between the top 1 meter and the rest of this layer. Material at the top one meter is manly a reddish brown in color whereas the lower levels of this layer exhibit a dark gray color with no noticeable odor.

Fines content for this layer was measured to be around 45%-80%. Three of the four samples have about 80% fines. Estimates of fines content from CPT measurements range between 40%-70%. Variation of estimated fines content is fairly uniform except the thin sand/gravel

layer that was not detected with the borehole samples. Fines content for this level is estimated to be about 20% using CPT data. However as discussed above, thin layer effect on measured tip resistance may have caused an overestimation of the fines content.

Below this is the sandy level composed of silty sand and sand mixture. Visual observations during drilling indicate that this layer is highly variable in nature. Penetration resistance, soil behavior index and fines content vary considerably in the vertical direction. Measured fines content varies between 10%-80%.

Fines content from thin slice samples are in very good agreement with the estimated fines content. Quick changes are captured by CPT estimates of fines content. On the other hand split spoon samples seem to average out the fines content that is variable with the zones they sample from.

Peak penetration resistance of in this layer reaches 9.1 MPa between 6.5-7.0 meter depth. Normalized cone penetration resistance (q_{c1N}) is 10.6, for this peak value for the level of effective vertical stress at this depth (σ_{vo}' = 72 kPa). This comparably higher penetration resistance zone is the relatively cleaner section of this layer. This level has about 10% fines as obtained from the four thin slice samples and classifies as SP/SM. Cone penetration testing predict the same amount of fines for this level.

Soil behavior index for this 2.5 meter thick layer is above 2.6 except the higher penetration resistance zone (SP/SM) and some occasional thin levels within this layer. The soils at this layer are dark grey in color. Most of the samples from this level are non-plastic. There are some samples that exhibit low plasticity.

It is seen that both split spoon samples from this level measure about 50% fines. Split spoon samples miss the SP/SM level. Such could cause a misrepresentation of soil layering and cold lead to erroneous characterization of critical layers. In this case the SP/SM layer was detected by CPT and was classified as liquefiable and the soil improvement scheme was designed to mitigate liquefaction susceptibility of this layer. Truncated columns were built in between the grid of jet grout columns at the level of this layer. Other layers (i.e. low plasticity silt/clay layers) were not considered liquefiable because of their high clay content in accordance with the Chinese criteria. The only liquefiable layer at the site was the SP/SM

according to the liquefaction design guidelines of the time. Thickness of this formation varies across the site. Jet-grout columns were proposed to also reduce the settlements from the soft clayey levels. ML/CL levels were not identified as liquefiable by the geotechnical consultant during the design phase of the project. Therefore missing the SP/SM level during subsoil investigations would have omitted the liquefaction susceptibility at this site.

Below is the low plasticity silt/clay layer which is about 1 meter thick at this location. This layer is soft as evidenced by the low penetration resistance (q_c ~ 1 MPa). Soil behavior index for this layer is about 3.2. Estimated fines content for this layer ranges between 80%-90% compared to the measured fines content of 95%. This layer is dark grey in color.

Below is the high plasticity clay that extends as deep as 35 meters. Liquid limit for this layer ranges between 55-77. Material finer than 5m is consistently above 70%. Fines content for this layer is 98% Fines content is consistently higher than 98% for deeper samples. CPT estimate of fines content is about 75%-80%.

Above results indicate that CPT is able to detect variations in soil conditions. It is possible to detect layers that may be critical that would possibly go undetected with borehole sampling. CPT works very well in estimating fines content using current correlations (Lunne et al. 1997). Fines content is predicted at about 40-60% where the actual measurements indicated fines content as high as 80%. In such cases, most of the time it is not the actual fines content but the ball-park value to distinguish silty/clayey levels.

Grain size and plasticity characteristics of these layers indicate that these layers are not susceptible to liquefaction according to current design guidelines. This is mainly because of the high clay content (percent finer than 5μ) of the silt/clay layers above the CH layer. Additionally these levels consistently have high values of soil behavior index. Current guidelines recommend the soil to be initially sampled to test for I_c values larger than 2.6. It is suggested to sample to soil and test for grain size and plasticity ad to see how the material stands with respect to Chinese criteria. Further sampling and cyclic testing is recommended if Chinese criteria suggest the material has liquefaction potential. Therefore CPT is not applicable by itself for most materials with fines, which will most likely have I_c values greater than 2.6.

5.4. Site Response Analyses to Estimate Earthquake Induced Stresses

Procedures to assess liquefaction potential of a site involve the estimation of the two quantities (1) the demand induced by the earthquake and (2) the capacity of the soil with respect to cyclic loading. Demand induced on the soil is measured by a cyclic stress ratio which is related to the of the average shear stress acting on the soil. Average shear stress is estimated using peak ground acceleration at the soil surface and earthquake magnitude (Youd et al. 2001). Capacity of the soil is estimated from the curves that are developed from a large database of from numerous earthquakes since 1966. These capacity curves make use of the penetration resistance of the soil (either Standard Penetration Resistance or Cone Penetration Resistance) to estimate the cyclic resistance ratio of the soil.

In this study cyclic stress acting on the soil is estimated with simplified one dimensional site response analysis. It is not always possible to perform site response analysis in practice because shear wave velocity profile is not always readily available for most projects. In most cases hazard level consistent peak ground acceleration is used rather than a design acceleration history. Using peak ground acceleration at ground surface earthquake induced shear stresses are estimated for the soil profile using the simplified procedure.

Shear wave velocity is measured at four test locations along the site boundary. Measurements are performed with a downhole setup where the cone is equipped with two geophones placed with 1.0 meters separation. Separation time of waves to the upper and lower geophones was evaluated by a cross correlation technique and thus shear wave velocity of the profile is estimated. Shear wave velocity measurements are shown in Figure 4-7. It is seen that the shear wave velocity is about 100-150 m/s at the top 25 meters of the profile and gets stiffer beyond this depth reaching 400 m/s at 37 meters depth where the exploration was terminated.

Velocity measurements near the surface show some variability within the irregularly placed fill. As seen the top 25 meters of the profile have a fairly constant velocity varying between 100 to 140 meters/s. Below this depth velocity increases to values 250 m/s at a depth of about 30 meters and then to about 400 m/s at 37 meters depth where the exploration was terminated. The velocity model used in site response analysis is selected to capture the range and trends of measurements as shown in the figure. It is not possible to capture the thin

ML/CL layer (about 1 meter thick) located below the SP/SM layer with the measurement intervals. Therefore SP/SM levels along with the ML/CL layer below are merged into one layer for site response analysis.

Site response analyses were performed using the commonly used program SHAKE91 (Idriss and Sun 1992) which is the updated version of the program SHAKE (Schnabel et al. 1972). This program models horizontally polarized vertically propagating shear waves in horizontally layered soil media. Wave propagation equation is used with the equivalent nonlinear method where iterations are performed to estimate the strain compatible values of shear modulus and damping. This procedure requires the use of shear modulus and damping values for a range of strain values. Calculations are performed in the frequency domain using the strain compatible equivalent linear shear modulus and damping ratio values of the soil layers.

Shear wave velocity model used of the site is shown in Figure 4-70. This model is developed using the shear wave velocity measurements performed after the earthquake near the perimeter of Lot C (Figure 4-26). Therefore the thickness of the layers in the model may be different than the layering at other locations. The same layering sequence exists throughout the site as evidenced from extensive array of site investigations.

Site response analysis is performed for the soil profile at each CPT location. Thickness of layers at such test locations is derived from the results of the penetration test. Thicknesses of the layers at the given velocity model are modified to match the layering of the investigated CPT. Velocity of the specific layer is kept unaltered as the layer thicknesses are adjusted. Therefore an augmented profile is generated for each CPT location using the results of the CPT and shear wave velocity model. Site response analyses are performed for about 100 points where soil layering data is available (i.e. CPT test locations).

Strain dependency of shear modulus and damping was utilized using the relationships developed by Ishibashi and Zhang (1993). This formulation expresses shear modulus degradation and strain dependent damping ration in terms of mean effective confining pressure (σ'_m) and soil plasticity (PI). Soils were grouped into three categories for site

response analyses. Characteristic curves were developed for the fill, low plasticity sand/silt/clay mixtures and high plasticity clay.

Fill layer is highly variable throughout the site. Gradation characteristics and plasticity of the clayey portion changes both horizontally and vertically for this layer. A low value of plasticity index was assigned to account for the granular characteristic of this layer. This low value plasticity index (PI=10) generates shear modulus degradation and damping curves in between those for medium plasticity clay and granular material.

Below the fill are the 7-8 meter thick low plasticity silt/clay layers and the silty sand levels. These layers are grouped into one common stack for site response analyses. Curves are generated for PI = 10 and mean effective confining pressure σ'_m = 50 kPa. Such plasticity is representative of average properties for these layers and the mean confining pressure is selected to correspond to stress level at mid-depth of this stack.

High plasticity clay at the lower levels is characterized by plasticity index PI = 40. Level of confining stress does not affect the shape of the curves at such high plasticity levels in Ishibashi and Zhang curves.

Shear modulus degradation curves are shown in Figure 4-71 for the fill, low plasticity silt/clay/sand mixture and high plasticity clay. Similarly strain dependent damping curves for these three soil groups are shown in Figure 4-72.

Peak shear stress at each layer is calculated using the results of site response analyses and the cyclic stress ratio is calculated. Cyclic stress ratio (CSR) is a measure of the demand imparted on the soil by the earthquake.

$$CSR = \frac{\tau_{average}}{\sigma'_{vo}} \frac{1}{MSF} = 0.65 \frac{\tau_{peak}}{\sigma'_{vo}} \frac{1}{MSF}$$

Two sets of site response analysis were performed to estimate the earthquake induced shear stresses (1) for the M=7.4 earthquake at August 17, 1999 and (2) M=5.8 aftershock at September 13, 1999. Recordings of these motions were available from a nearby recording station.

As discussed in the following sections, the same procedure is used to estimate earthquake induced stresses and strains on the soil at sections of the site improved with jet-grout columns.

5.4.1. Recorded Ground Motions

Kocaeli Earthquake of August 17, 1999 was a magnitude M_w=7.4 event. The earthquake is associated with the right lateral strike slip North Anatolian Fault that extends along the east west direction. Carrefour site is located 8 km from the epicenter and 5 km from the observed fault rupture. Ground motion recordings of the Kocaeli Earthquake (M7.4) were available from the IZT recording station in Izmit approximately 8 km from the site.

Availability of shear wave velocity data from the recording station site and Carrefour site were used to estimate the ground motions and earthquake induced shear stresses. Site response analyses were performed and the level of expected acceleration throughout the profile estimated for the earthquake (M7.4 August 17 1999) and one aftershock (M5.8 September 13 1999). Results of these analyses were used to investigate the conditions of liquefaction at the site.

Shear wave velocity measurements were performed at the IZT recording station site with SASW testing (Rathje et al. 2002). As seen in Figure 4-73 there is a 3 meter thick layer at the surface which has a shear wave velocity of 250 m/s. Under this layer is a 6.5 meters of soft rock with Vs = 700 m/s which lies above a competent layer of Vs = 1500 m/s. Lithological descriptions of these units are not available. This is a very stiff site and classifies as “Class B” according to NEHRP provisions and as “Rock” according to IBC (IBC 2000). Extending the velocity profile to 30 m, average shear wave velocity of the top 30 meters for this site is 800 m/s, making it also a rock site (S_B) in the UBC classification system.

Baseline corrected ground acceleration time histories of main earthquake ground motion recorded at IZT station is shown in Figure 4-74. The mean and the trend in the recorded motion is removed to baseline correct the recording. The longitudinal component (East-West) is aligned near-parallel to the fault and it is larger in peak amplitude than the transversal (North-South) component. Values of peak ground acceleration for the longitudinal and

transversal components are 0.226g and 0.169g respectively. Longitudinal component of ground motion was used in site response analyses.

One significant event following the Kocaeli Earthquake was the M_w=5.8 aftershock of September 13, 1999. Epicenter of this earthquake was about 20 km from the site. Baseline corrected ground acceleration time histories of ground motion recorded at recorded at IZT station is shown in Figure 4-75. Though it has a higher peak ground acceleration than the mainshock of August 17 this was a significantly smaller event as evidenced by the short duration.

One interesting observation with this aftershock is the considerable difference in the two components of motions. Peak ground acceleration for the E-W component is about 0.3g, a larger value than the peak acceleration of the main shock of August 17. On the other hand peak ground acceleration is about 0.08g. This dichotomy between both horizontal components is an unusual situation. There are several possible explanations (1) there may be a problem with the recording device where one of the channels may have malfunctioned during analog-to-digital conversion giving an over-amplified or under-amplified signal in any of the horizontal directions (2) the device may be tilted (possibly from the main earthquake a few weeks before) causing a miscalibration of the device and a possible directional bias in the recording (3) polarization of shear waves along E-W direction due to the relative location of the recording station, i.e. shear wave radiation pattern where shear waves are polarized in one specific direction (4) the building that houses the recording device may have an effect on the recorded motion; the effect of the building may be along a specific direction simply due to geometry (5) a local feature unique to the site or to the path between the source or the recording station. Relative locations of the site, recording station and the aftershock epicenter are shown in Figure 4-76.

Brief examination of the three different components of motions indicates that the strong component of motion is a shear wave (as opposed to a surface wave). Pseudo-acceleration response spectra of both components are compared. They both peak at about the same period. There is not an odd peak in either of the spectra. It is not likely to have a problem with the

recording device (digital conversion, tilting) where the recorded motions do not indicate any obvious problem like an irregular noise signal etc.

The building definitely has an effect such as every other recording station not at the free field. However in most cases this effect is negligible. Possibility of some other building effect is possible, but comparison of the spectra of the aftershock the mainshock recordings does not reveal any structural effects that would be common in both recordings.

Amplitudes of ground motion associated with P waves during the first 2 seconds of motion are similar in magnitude in both directions. Shear waves which cause the larger shaking amplitudes arrive at about 2.5 seconds and amplitude of motion in both direction are strikingly different. This suggests that the location of the recording station with respect to the earthquake source is oriented such that the S waves are strongly polarized in one direction (i.e. EW direction). The event is small enough to be characterized as a point. It is possible that the recording station site is located such that S wave radiation pattern of this event resulted in drastically different S wave motion in these orthogonal directions.

On the other hand ground motion recordings at YPT station for the same event are shown in Figure 4-77. Angular orientation of this site is slightly different than IZT station and the station is farther away from the earthquake source. S waves arrive at about 4.5 seconds and are similar in amplitude in both directions. Amplitude of strong motion in both horizontal directions is similar, typical of most earthquake recordings. The angular orientation of the two recording sites with respect to the source is not different enough to cause a big change. The azimuth angle for both stations is only about 15 degrees different. Given such a slight change in angular orientation it should be expected that the radiation pattern of the shear waves be similar for both sites. Therefore this rules out the possibility of a radiation pattern effect that would cause such a dichotomy in ground motions in both horizontal directions.

Therefore is it most likely some feature specific to the path between the earthquake source and the recording station site caused this irregularity in the recorded motion. Some path effect caused the earthquake motions to be strongly polarized in one direction. However it is not possible to bring more explanation to this phenomenon.

Is it possible to have strikingly different motion amplitudes in two horizontal directions at Carrefour site similar to IZT recording station site? How does this directional variability in soil motions affect liquefaction analysis at the site for the M=5.8 event?

It is strongly possible that the recording of the September 13 aftershock is the actual ground motion at the site. The main task is to estimate the ground motions at Carrefour site. It should be noted that Carrefour site has almost the same azimuth as the YPT station with respect to the epicenter of the aftershock. However the site conditions at Carrefour site and YPT site are different. YPT site is a deep soil site. Site conditions below the softer sediments (30-35 meters) Carrefour site are similar to the near surface conditions at IZT recording station site. This is evidence by the increasing shear wave velocity at the base of the Carrefour profile and the measured near surface velocity (i.e. Vs ~ 600 m/s) at IZT station. Given the proximity of the site and the recording station, the rock outcrop at the near IZT station dips down towards the Izmit Bay and is overlain by soft bay sediments at Carrefour site.

Above arguments suggest that the motions at IZT station during the aftershock are specific to that region and direction between the aftershock epicenter and IZT station. The fact that the YPT station has similar amplitudes of motion in both horizontal direction indicates that such a feature is not present between the aftershock and the YPT station. As seen in Figure 4-76 Carrefour site is located along the path between the aftershock and the YPT station. It is very likely that ground motions at Carrefour site had similar amplitudes in both horizontal directions. However the amplitude should not be as high as the EW component.

The best approach in this case is to use the EW component but to reduce it some amount to simulate motions at Carrefour site. This way we still can use a recording to perform site response analysis. Therefore, EW component of the aftershock recording at IZT station is used in the site response analyses to estimate earthquake induced shear stresses during the M5.8 aftershock. However the shear stresses were reduced some amount to represent the average magnitude of the two recorded components.

5.4.2. Estimated Ground Motions and Earthquake Induced Stresses at Carrefour Site – August 17, 1999 Kocaeli Earthquake M7.4 and September 13, 1999 Aftershock M5.8

These motions were used to perform a site response analysis using the SHAKE91 computer code (Idriss and Sun 1992), and a peak ground acceleration of 0.24g was estimated for the site, close to the 0.23g peak value recorded at IZT. Site response analyses were performed using the E-W component of the recorded IZT motion to estimate the ground motion at Carrefour site. Velocity profiles at the recording station site and Carrefour site were used in these analyses. One-dimensional site response analyses were performed with SHAKE91. Recorded motion was deconvoluted down to the top of the soft rock layer (V_s = 700 m/s) at the station site and this motion was input at the base of the Carrefour velocity model.

Outcrop motion at the top of the soft rock layer was estimated by deconvoluting the recorded motion down to the soft rock layer. The thin surficial deposit was assumed to behave linearly elastic in these transformations using flat shear modulus degradation and constant damping (damping ratio = 1%) in the analyses. In any case this transformation does not bring significant changes to the spectral content of the motion. This procedure is performed for consistency in the site response analyses even though it is an insignificant process in terms of site response analysis.

Acceleration response spectra of recorded and deconvoluted motions (IZT EW) for 5% oscillator damping are plotted in Figure 4-78. There is only a slight difference between spectral response of both motions only in high frequency response (i.e. periods less than 0.2 seconds).

Site response analyses were performed for the profiles generated from CPT test locations. It is necessary to specify a coefficient in SHAKE to convert peak shear strains at each iteration to uniform equivalent shear strain. Uniform strain is used to calculate shear strain dependent shear modulus and damping. Values of 0.65 and 0.50 are used for this purpose for the M7.4 earthquake and M5.8 aftershock respectively. These parameters are consistent with the general recommendations (Idriss and Sun 1992).

Peak shear stresses at each level were available as part of the results from the program. Peak shear stresses were reduced by the coefficient 0.65 in calculating CSR. Additionally magnitude scaling factor (MSF) was applied to estimate the CSR of M7.5 which the design

charts are based on. Magnitude scaling factor for the M7.4 earthquake and M5.8 aftershock are 1.035 and 1.930 respectively as recommended by current design guidelines. CSR from M5.8 aftershock was further multiplied by 0.625 to convert the CSR from 0.299g EW component to a CSR of the average amplitude of both components (0.187g).

Results of site response analyses are grouped into different parts of the site (i.e. shopping center, parking lot area and lot c). Variability in site response and therefore earthquake induced stresses occurs due to variability in thickness of soil layers. Calculated CSR values for the mainshock and the aftershock are for each section of the site are grouped and the median value is estimated for each part of the site. Median relationship is estimated using the data from all the analyses and multiple segments of polynomials were fit to the data. 95% confidence intervals were also estimated for the regression analyses.

Variability is solely due to variation of soil thicknesses. Shear wave velocity was inferred from measured velocities at the perimeter of Lot C. It is possible that the magnitude of shear wave velocity changes from point to point for the same layer but this was not accounted for at the site.

Results of site response analyses are shown in Figure 4-79 for two locations (CPT's A13 and D10) at Shopping Center area along with soil layering. Thickness of the top fill shows some variation at this part of the site, mainly getting thicker towards the eastern end of the site. Estimated median curve and the 95% confidence interval for CSR are shown in Figure 4-80 both for the mainshock and the aftershock. It is seen that there is some variability in the estimated interval. As noted above this variability in site response is due to variability in soil layering across this section of the site.

Results of site response analyses are shown in Figure 4-81 for two locations (CPT's A2 and E12) at Parking Lot area along with soil layering. Estimated median curve and the 95% confidence interval for CSR are shown in Figure 4-82 both for the mainshock and the aftershock.

Results of site response analyses are shown in Figure 4-83 for two locations (CPT's F2 and F4) at Lot C along with soil layering. It must again be noted that the site response analyses was performed with the 3.3 meters present on top of the soil profile. Cyclic stress ratio was

estimated from the site response analyses with fill present and the effective stress was calculated using the weight of overburden, 3.3. meter fill and hydrostatic water pressures. This basically assumes that consolidation settlements under the fill were complete at the time of the earthquake. We know from the measurements of the settlement extensometers in place, that some portion of the consolidation settlement was complete at the time of the earthquake. Estimated median curve and the 95% confidence interval for CSR are shown in Figure 4-84 both for the mainshock and the aftershock. It is seen that there is considerably less variability in estimated CSR in comparison to the two other sections of the site. This is mainly because the soil layering is much more uniform at Lot C, causing a more uniform site response.

5.5. Cyclic Resistance Ratio (CRR) from CPT

Comparison of a CPT sounding with nearby boreholes shows that CPT works well in characterizing the soil profile. It works as a good tool to identify the soil type and to estimate fines content. Therefore clean sand equivalent penetration resistance ($q_{c1,cs}$) is estimated using general guidelines.

It must be recognized however most soils at the site would be assessed non-liquefiable based on plasticity and grain size characteristics. Furthermore CPT is not directly applicable in the liquefaction analysis of the soils where soil behavior index is greater than 2.6. ML/CL layers above and below the SP/SM layer belong to this category based on their I_c values.

Furthermore it was concluded that the soils at the site; low plasticity silt/clay layers (ML/CL) layers and the poorly graded sand – silty sand layer (SP/SM) have undergone liquefaction type behavior during the Kocaeli Earthquake. This was evidenced by the expelled water at Parking Lot area and also the earthquake induced deformations measured with the settlement extensometers at Lot C. It is very likely that expelled water came up through the wick drains originated from the SP/SM layer because none of the layers in the profile even though they may have liquefied are permeable enough to drain out the waters so quickly. At least the expelled water cannot be used to justify or rule out any liquefaction type behavior at the ML/CL layers. However on the other hand vertical deformation measurements at Lot C under the surcharge fill strongly suggest that SP/SM layer and ML/CL layers as well were subjected to some amount of earthquake induced strength/stiffness loss as a result of pore

pressure rise. It is not possible to support this at the time with any lab testing but this is the only explanation other than instrument malfunctioning. On the other hand even though

Therefore the main basis of the liquefaction analyses is that these soils liquefied at the M7.4 earthquake and did not liquefy during the M5.8 aftershock. Cyclic resistance ratio is estimated from the clean sand equivalent penetration resistance using the CRR design curve shown in Figure 4-85.

5.5.1. Shopping Center Area

Variation of soil behavior type index (I_c) along the suspect liquefiable soils for CPT-A6 is shown in Figure 4-86. This CPT is located within the Shopping Center area. Additionally shown are the estimated CSR profiles for the mainshock and the aftershock and the CRR estimated from the cone penetration data. CRR results presented in this figure and the following figures are obtained by averaging the original data over a 20 cm thick moving average window. It is seen that the I_c for the upper ML/CL layer is about 2.7. I_c for the SP/SM layer is low, except for some levels with fines, where it exceeds 2.6. I_c for the lower ML/CL layer is about 2.9. Estimated cyclic resistance is consistently lower than the estimated cyclic stresses for the M7.4 Kocaeli Earthquake except for some lever of the SP/SM layer with higher penetration resistance. Estimated cyclic resistance is consistently higher than the cyclic stresses estimated for the M5.8 aftershock.

Profiles of soil behavior type index (I_c) and cyclic stresses along the suspect liquefiable soils for CPT-A15 are shown in Figure 4-87. It is seen that the I_c for the upper ML/CL layer ranges between 2.7-3.1. I_c for the SP/SM layer is low, except for some levels with fines where it exceeds 2.6. I_c for the lower ML/CL layer is about 3.3. Estimated cyclic resistance is consistently lower than the estimated cyclic stresses for the M7.4 Kocaeli Earthquake and higher than the cyclic stresses estimated for the M5.8 aftershock.

Profiles of soil behavior type index (I_c) and cyclic stresses along the suspect liquefiable soils for CPT-D1 are shown in Figure 4-88. It is seen that the I_c for the upper ML/CL layer ranges between 2.7-3.2. I_c for the SP/SM layer is low, except for some levels with fines, where it exceeds 2.6. I_c for the lower ML/CL layer is about 3.2. Estimated cyclic resistance is

consistently lower than the estimated cyclic stresses for the M7.4 Kocaeli Earthquake and higher than the cyclic stresses estimated for the M5.8 aftershock.

Profiles of soil behavior type index (I_c) and cyclic stresses along the suspect liquefiable soils for CPT-D2 are shown in Figure 4-89. It is seen that the I_c for the upper ML/CL layer ranges between 2.7-3.2. I_c for the SP/SM layer is low, except for some levels with fines, where it exceeds 2.6. I_c for the lower ML/CL layer is about 3.1. Estimated cyclic resistance is consistently lower than the estimated cyclic stresses for the M7.4 Kocaeli Earthquake and higher than the cyclic stresses estimated for the M5.8 aftershock.

Profiles of soil behavior type index (I_c) and cyclic stresses along the suspect liquefiable soils for CPT-D3 are shown in Figure 4-90. It is seen that the I_c for the upper ML/CL layer ranges between 2.7-3.5. I_c for the SP/SM layer is low, except for some levels with fines, where it exceeds 2.6. I_c for the lower ML/CL layer is about 3.1. Estimated cyclic resistance is consistently lower than the estimated cyclic stresses for the M7.4 Kocaeli Earthquake and higher than the cyclic stresses estimated for the M5.8 aftershock.

Profiles of soil behavior type index (I_c) and cyclic stresses along the suspect liquefiable soils for CPT-D4 are shown in Figure 4-91. It is seen that the I_c for the upper ML/CL layer ranges between 2.6-3.4. I_c for the SP/SM layer is low, except for some levels with fines, where it exceeds 2.6. I_c for the lower ML/CL layer is about 3.3. Estimated cyclic resistance is consistently lower than the estimated cyclic stresses for the M7.4 Kocaeli Earthquake and higher than the cyclic stresses estimated for the M5.8 aftershock.

Profiles of estimated cyclic resistance ratio from the CPTs at this section have been compiled. Median profile of CRR from the collective data is presented Figure 4-92 along with +/- one standard deviation range. It is seen that the cyclic resistance ratio varies between 0.10-0.15 for the layers thought to have liquefied during the Kocaeli Earthquake.

5.5.2. Parking Structure Area

Parking structure section of the site was surcharged with a 3.3 m-high surcharge fill and 20 m-long wick drains were installed at a 2.5 m spacing to speed up consolidation of the clay. The surcharge was removed after consolidation was complete and was not in place at the

time of the earthquake. Therefore soils in the parking structure area were overconsolidated due to the placement and removal of the surcharge fill.

It is important to consider the possible effects of the surcharge fills and the wick drains on the liquefaction behavior. The surcharge overconsolidated the sandy and silty layers to an overconsolidation ratio of 2 to 3. The effect of increased lateral stresses on liquefaction resistance is estimated using the approach presented in Salgado et al. (1997).

Profiles of soil behavior type index (I_c) and cyclic stresses along the suspect liquefiable soils for CPT-A1 are shown in Figure 4-93. This CPT was performed before any surcharge fill placement. It is seen that the I_c for the upper ML/CL layer ranges between 2.6-3.1. I_c for the SP/SM layer is low, except for some levels with fines, where it exceeds 2.6. I_c for the lower ML/CL layer is about 2.8. Cyclic resistance profiles for the site before and after surcharge are presented. Estimate of cyclic resistance ratio (CRR) at the time of the earthquake is shown by the line higher magnitude CRR curve. CRR for the case if the surcharge fill had not been placed at all is shown for comparison. Estimated cyclic resistance is consistently lower than the estimated cyclic stresses for the M7.4 Kocaeli Earthquake except some levels of higher resistance. Estimated cyclic resistance is consistently higher than the cyclic stresses estimated for the M5.8 aftershock.

Profiles of soil behavior type index (I_c) and cyclic stresses along the suspect liquefiable soils for CPT-E10 are shown in Figure 4-94. This CPT was performed after placement and removal of the 3 meter thick surcharge fill. It is seen that the I_c for the upper ML/CL layer ranges between 2.7-3.3. I_c for the SP/SM layer is low, except for some levels with fines, where it exceeds 2.6. I_c for the lower ML/CL layer is about 3.1. Cyclic resistance profiles for the site before and after surcharge are presented. Estimated cyclic resistance is consistently lower than the estimated cyclic stresses for the M7.4 Kocaeli Earthquake except some levels of higher resistance. Estimated cyclic resistance is consistently higher than the cyclic stresses estimated for the M5.8 aftershock.

Profiles of soil behavior type index (I_c) and cyclic stresses along the suspect liquefiable soils for CPT-E16 are shown in Figure 4-95. This CPT was performed after placement and removal of the 3 meter thick surcharge fill. It is seen that the I_c for the upper ML/CL layer

ranges between 2.7-3.1. I_c for the SP/SM layer is low, except for some levels with fines, where it exceeds 2.6. I_c for the lower ML/CL layer is about 3.2. Cyclic resistance profiles for the site before and after surcharge are presented. Estimated cyclic resistance is consistently lower than the estimated cyclic stresses for the M7.4 Kocaeli Earthquake except some levels of higher resistance. Estimated cyclic resistance is consistently higher than the cyclic stresses estimated for the M5.8 aftershock.

Profiles of soil behavior type index (I_c) and cyclic stresses along the suspect liquefiable soils for CPT-E19 are shown in Figure 4-96. This CPT was performed after placement and removal of the 3 meter thick surcharge fill. It is seen that the I_c for the upper ML/CL layer ranges between 3.0-3.3. Some thin sandy pockets are present with in this layer as evidenced by low I_c values. I_c for the SP/SM layer is low, except for some levels with fines, where it exceeds 2.6. I_c for the lower ML/CL layer is about 3.4. Cyclic resistance profiles for the site before and after surcharge are presented. Estimated cyclic resistance is consistently lower than the estimated cyclic stresses for the M7.4 Kocaeli Earthquake except some levels of higher resistance. Estimated cyclic resistance is consistently higher than the cyclic stresses estimated for the M5.8 aftershock.

Profiles of estimated cyclic resistance ratio from the CPTs at this section have been compiled. Median profile of CRR from the collective data is presented Figure 4-97 along with +/- one standard deviation range. It is seen that the cyclic resistance ratio varies between 0.10-0.14 for the layers thought to have liquefied during the Kocaeli Earthquake.

5.5.3. Lot C Area

Lot C is located adjacent to the Parking Structure and encompasses an area of 4,160 m^2. Lot C was surcharged with a 3.3 m-high fill at the time of the earthquake. The fill was included in the one-dimensional site response analyses.

Profiles of soil behavior type index (I_c) and cyclic stresses along the suspect liquefiable soils for CPT-A1 are shown in Figure 4-98. This CPT was performed before any surcharge fill placement. It is seen that the I_c for the upper ML/CL layer ranges between 2.6-3.1. I_c for the SP/SM layer is low, except for some levels with fines, where it exceeds 2.6. I_c for the lower ML/CL layer is about 2.8. Cyclic resistance profiles for the site before and after surcharge

are presented. Estimate of cyclic resistance ratio (CRR) at the time of the earthquake is shown by the line higher magnitude CRR curve. CRR for the case if the surcharge fill had not been placed at all is shown for comparison. Estimated cyclic resistance is consistently lower than the estimated cyclic stresses for the M7.4 Kocaeli Earthquake except some levels of higher resistance. Estimated cyclic resistance is consistently higher than the cyclic stresses estimated for the M5.8 aftershock.

Profiles of soil behavior type index (I_c) and cyclic stresses along the suspect liquefiable soils for CPT-E10 are shown in Figure 4-99. This CPT was performed after placement and removal of the 3 meter thick surcharge fill. It is seen that the I_c for the upper ML/CL layer ranges between 2.7-3.3. I_c for the SP/SM layer is low, except for some levels with fines, where it exceeds 2.6. I_c for the lower ML/CL layer is about 3.1. Cyclic resistance profiles for the site before and after surcharge are presented. Estimated cyclic resistance is consistently lower than the estimated cyclic stresses for the M7.4 Kocaeli Earthquake except some levels of higher resistance. Estimated cyclic resistance is consistently higher than the cyclic stresses estimated for the M5.8 aftershock.

Profiles of soil behavior type index (I_c) and cyclic stresses along the suspect liquefiable soils for CPT-E16 are shown in Figure 4-100. This CPT was performed after placement and removal of the 3 meter thick surcharge fill. It is seen that the I_c for the upper ML/CL layer ranges between 2.7-3.1. I_c for the SP/SM layer is low, except for some levels with fines, where it exceeds 2.6. I_c for the lower ML/CL layer is about 3.2. Cyclic resistance profiles for the site before and after surcharge are presented. Estimated cyclic resistance is consistently lower than the estimated cyclic stresses for the M7.4 Kocaeli Earthquake except some levels of higher resistance. Estimated cyclic resistance is consistently higher than the cyclic stresses estimated for the M5.8 aftershock.

Profiles of soil behavior type index (I_c) and cyclic stresses along the suspect liquefiable soils for CPT-E19 are shown in Figure 4-101. This CPT was performed after placement and removal of the 3 meter thick surcharge fill. It is seen that the I_c for the upper ML/CL layer ranges between 3.0-3.3. Some thin sandy pockets are present with in this layer as evidenced by low I_c values. I_c for the SP/SM layer is low, except for some levels with fines, where it

exceeds 2.6. I_c for the lower ML/CL layer is about 3.4. Cyclic resistance profiles for the site before and after surcharge are presented. Estimated cyclic resistance is consistently lower than the estimated cyclic stresses for the M7.4 Kocaeli Earthquake except some levels of higher resistance. Estimated cyclic resistance is consistently higher than the cyclic stresses estimated for the M5.8 aftershock.

Profiles of estimated cyclic resistance ratio from the CPTs at this section have been compiled. Median profile of CRR from the collective data is presented Figure 4-102 along with +/- one standard deviation range. It is seen that the cyclic resistance ratio varies between 0.10-0.14 for the layers thought to have liquefied during the Kocaeli Earthquake.

5.6. Liquefaction Analyses – Summary

Evidence of liquefaction was observed at Carrefour site. Subsoil investigations reveal that the soils that exhibited liquefaction type behavior were fine grained and would classify as nonliquefable according to current design guidelines. Furthermore current design guidelines recommend CPT unsuitable for assessing the liquefaction potential of such soils. This provided a unique opportunity to document this unusual behavior and to test the effectiveness of CPT in predicting liquefaction potential of these soils.

Liquefaction resistance was estimated from the extensive array of CPTs at the site. Cyclic stress ratio for each CPT location was estimated with site response analysis.

The most critical CRR-CSR match for each CPT profile was found two earthquake scenarios; M7.4 Kocaeli Earthquake and M5.8 September 13 Aftershock. Two sets of lowest CRR/CSR ratios were selected for with Ic lower than and greater than 2.6. These data points were selected using the CRR curves that were averaged over a 20 cm moving average window.

Compiled results for sandy soils ($I_c < 2.6$) are plotted in Figure 4-103. It is seen that the liquefaction occurrence data associated with the M7.4 event fall into the liquefaction zone defined by the cyclic resistance ratio boundary. Data points for the M5.8 event where no liquefaction occurrence was observed at the site generally fall into the non-liquefaction zone.

Compiled results for silty/clayey soils ($I_c > 2.6$) are plotted in Figure 4-104. It is seen that the liquefaction occurrence data associated with the M7.4 event fall into the liquefaction zone

defined by the cyclic resistance ratio boundary. Data points for the M5.8 event where no liquefaction occurrence was observed at the site generally fall into the non-liquefaction zone.

Liquefaction evaluation procedure predicts similar behavior for silty/clayey soils and sandy soils. It also successfully separates occurrence and non-occurrence of liquefaction events successfully for both types of soils.

6. EFFECT OF STIFF COLUMNS – EVALUATION WITH HOMOGENIZATION

Densification techniques such as vibro-densification have been used extensively to mitigate liquefaction of sandy soils. Dense and stiff soil columns are formed with vibro-densification. In most cases crushed gravel is poured in the zone that is being densified to account for the volume change due to densification of the native soil. In many cases the effects of densification extends from the densified column as far as a few diameters of the column. In many vibro-densification projects, a minimum penetration resistance (q_c, $N_{1,60}$) is specified that has to be achieved midway between the columns. Spacing of the columns is selected based on experience and test sections densification of the sandy soils is achieved (Mitchell 1981).

It has been recognized by previous researchers that these stiff columns carry part of the shear stresses induced by the earthquake and reduce cyclic stresses on the native soil (Baez and Martin 1992, Baez 1995). Shear stresses are shared among the stiff columns and the soil in proportion to their stiffnesses. The basic assumption behind this simplification is that the soil and the stiffer zones (densified soil, stone column, jet grout column etc.) deform compatibly. Soil and the columns undergo the same shear deformations as the induced stresses in each component are shared in proportion of their shear modulus. Interaction of the stiff reinforcements and the soil around may be more complicated, however this is a reasonable simplification.

Jet- grout columns are installed by eroding the soil with high pressure water and/or air as the grout is injected. Alternatively deep mixing columns are installed by mixing the grout with continuous flight augers. These techniques are replacement methods. In contrast to vibro-

densification methods these methods do not cause volume change and densification to the native soil.

The effect of stiff elements is twofold, the first one being the reduction of shear stresses on the native soil. On the other hand the same stiffening effect reduces induced strains. Even though we define liquefaction resistance using a stress based approach, strain is more fundamentally related to pore pressure increases and therefore triggering of liquefaction.

This analysis has limitations because (1) it is a total stress analysis and cyclic induced pore pressures are not considered in the site response analysis (2) there is an averaging process which inherently assumes that the effects of nonlinearity apply to the soil, stiff columns and also the homogenized system in the same manner.

6.1. Analysis of Soil-Jet Grout System with Homogenization

Soil-column system is homogenized into an equivalent system. Lateral variability is averaged out so that the overall system represents a soil-column system deforming compatibly. In the end the homogenized system can be analyzed as a one-dimensional system using simple site response analysis procedures. Shear stresses and shear strains can be estimated to gain insight into liquefaction susceptibility of the improved soils.

Several assumptions in this process include

(1) Strain compatibility between the soil and the columns. Stiff columns move and deform with the surrounding soil.

(2) Shear stress is shared in proportion to the stiffness of the columns and the soil. Shear stress on the homogenized system is decomposed into its components (those acting on the soil and column) based on the proportion of the stiffnesses of these elements.

(3) Strain dependence of stiffness and damping is utilized to impose nonlinearity. Furthermore it is assumed that the same nonlinearity effects (i.e. shear modulus degradation and damping) apply to both, soil and columns as well as the homogenized mass. This adds great simplicity because the same stiffness ratio exists at small strain levels (ratio of the small strain moduli). It is possible to produce a “hybrid” strain dependent properties by averaging

out two sets of modulus degradation and strain dependent curves. However at this point it would diminish the simplicity introduced here without significant benefits.

Assuming strain compatibility between the soil and the column and thus the homogenized soil-column system;

$$\frac{\tau_c}{G_c} = \frac{\tau_s}{G_s} = \gamma_c = \gamma_s = \gamma_{eq}$$

Where τ_c is the shear stress on the columns and G_c is the shear modulus of the columns and γ_c the shear strain. Alternatively τ_s, G_s and γ_s refer to the shear stress, modulus and strain in the soil. Compatible strains in the soil and the columns indicate that the shear stress on the soil and the column will be proportional to the shear moduli of the soil and the column.

Equivalency of the discrete soil-column system and the homogenized system suggests that there exist an equivalent shear stress τ_{eq} along with an equivalent shear strain γ_{eq}.

$$\frac{\tau_{eq} A_{total}}{G_s A_s + G_c A_c} = \gamma_{eq} = \gamma_c = \gamma_s$$

Shear modulus of the homogenized composite mass is calculated

$$G_{eq} = a_c G_c + (1 - a_c) G_s$$

where a_c is the area ratio of the columns (i.e. replacement ratio) given by A_c/A_{total} and a_s is the area ratio of the soil mass given by A_s/A_{total}.

Shear stress on the soil is related to the shear stress on the homogenized mass in relation to the ratio of the respective shear moduli;

$$\tau_s = \frac{G_s}{G_{eq}} \tau_{eq}$$

Therefore ratio of the shear stress on the homogenized mass to that on the soil is given by;

$$\frac{\tau_{eq}}{\tau_s} = \frac{G_{eq}}{G_s} = a_c\left(\frac{G_c}{G_s} + \left(\frac{1-a_c}{a_c}\right)\right)$$

An equivalent formulation was developed by Baez (1995) where the above ratio is recognized as the stress reduction factor K_G. Cyclic stress ratio (CSR) of the improved soil is defined as CSR x K_G; CSR being the unimproved cyclic stress ratio on the native soil.

This averaging process overlooks the subtleties in the interaction of the soil surrounding the columns. One issue that needs more clarification is the assumption of compatible deformations. Compatible deformations do not necessarily result in sharing of stresses as discussed in the above sections. Jet grout column deforms compatibly with the surrounding soil as long as structural integrity is maintained. However such stiffness contrast may cause strain gradients in the horizontal direction. In other words, the stiff column may deform compatibly with the immediate soil around but the stiff mass may deform within the soft soil (or the soil mass may flow around the stiff column). This may cause nun-uniform strain Therefore strain compatibility does not necessarily warrant uniform strains. Once uniform strains do not exist we cannot talk about the sharing of stresses in proportion to stiffness of the elements. In such a condition stress concentrations will also exist. Strain is compatible at a point or at a small zone but the strains are not uniform in the horizontal direction Uniform strain distribution may not be a reasonable assumption when the columns are not closely spaced. The condition where the interaction with the soil and the columns is not equivalent to a uniform strain distribution remains to be further investigated. Therefore homogenization may not be a realistic representation of soil column interaction in modeling improved ground performance during earthquakes.

6.2. Application of Homogenization Technique to Improved Ground Performance at Carrefour Site

Series of site response analyses have been performed both on the unimproved soil and the homogenized profile. Shear stress reduction estimated from the unimproved and improved

soil has been estimated. In addition to the shear stress reduction the effect of the stiff columns on the expected shear strains have also been compared. It has been recognized that pore pressures start developing when shear strain level exceeds a threshold value (Dobry et al. 1982).

Ground motion recorded at Izmit station (IZT) during the August 17, 1999 Kocaeli Earthquake has been used in the analysis. This recording has been scaled to various peak ground accelerations (0.01g, 0.025g, 0.05g, 0.075g, 0.1g, 0.125g, 0.15g, 0.175g, 0.2g, 0.225g, 0.25g, 0.275g and 0.3g).

Magnitude and distance will affect the ground motions in a way that we cannot account for by simply scaling the peak ground acceleration. What we have done here by scaling the pga by unreasonably high scaling factors. However the main purpose of this series of site response analysis is to compare the shear stresses under different acceleration levels keeping everything else (i.e. earthquake magnitude, distance effects).

Shear modulus of the unimproved soil and modulus ratio of the jet-grout columns along with replacement ratio have been used to estimate an equivalent modulus for the homogenized section representing the improved soil mass. Stiffness of the jet grout columns is estimated from several relationships and available data.

Jet grout columns are brittle elements. Unconfined compression test results indicate that axially loaded cylindrical samples of concrete fail at 0.1% axial strain (concrete book). We may expect a more ductile behavior in case of shear loading and especially when the columns are confined with the surrounding soil. Average 7- and 28-day unconfined compressive strengths from core samples were 2.0 MPa (280 psi) and 4.8 MPa (690 psi), respectively. These tests are performed on samples that are retrieved during construction from jet grout column at ground surface. Grab samples are poured in cylindrical molds and tested in the lab after curing. Therefore sample strength may not be a direct representation of the variability of the in-situ jet grout column.

Secant Young's modulus can be estimated from the axial compressive strength and assuming the sample fails at 0.1% axial strain. Alternatively Young's modulus can be estimated from

compressive strength as $E = 4733(\text{compressive strength})^{0.5}$ (units in MPa). These relationships yield Young's modulus values 4,760 MPa and 10,330 MPa respectively.

Pile integrity tests were performed to ensure the length and continuity of the installed jet grout columns (Zetas 1998). This test is commonly used for quality control and assurance purposes where the head of the pile is struck with a hammer and the traveling wave is monitored with an accelerometer. Travel time of the wave reflected from the base of the column is used to estimate the length. These tests suggest that wave velocity in jet grout columns is 2750 m/s. Young's modulus (E) is related to wave velocity (V) with $E = \rho V^2$, where ρ is the jet-grout column mass density. This modulus is estimated from wave velocity which is a small strains parameter. Small strain stiffness is expected to be higher than the stiffness under working load levels. Using the measured/estimated wave velocity Young's modulus is estimated 15,900 MPa (2306 ksi).

Young's modulus of jet-grout column is estimated as 5,000 MPa based on these values. It is on the lower end of the estimated values to represent the overall variability of the material properties along the column. Shear modulus is estimated 2,083 MPa using a Poisson ratio of 0.2.

Shear wave velocity model presented in Figure 4-70 is used in the homogenized site response analyses. Jet grout column extends 9 meters deep into the base of the SP/SM layer. Truncated jet-grout columns are installed along the thickness of the SP/SM layer in between the full length columns. As discussed in the previous sections this results in an area replacement ratios of 1.77% for the upper layers and 7.07% for the SP/SM layer.

Shear wave velocity of the improved layers range between 110-130 m/s. Shear modulus for these layers range between 21.8-30.4 MPa (assuming a mass density = 1.80 g/cm^3 for the soils). As seen, the jet grout column is estimated 164-229 times stiffer than the soils that were improved.

Composite stiffness of the homogenized model is estimated using the values of stiffness and replacement ratios for different soil layers.

Soil layering in this model is taken from one of the CPTs at the Parking Lot section (CPT-A07). Thickness of the layers (fill, upper ML/CL, SP/SM and lower ML/CL) are 1.45 m, 4.55 m, 3.1 m and 2.6 m respectively at this section. Jet grout column extends to the base of the SP/SM layer. Soil layering, corresponding shear wave velocity model and the placement of jet grout columns are presented in Figure 4-105.

Composite shear modulus is estimated for the profile using the values of shear modulus for the soil and the jet grout columns along with the replacement ratio. Composite shear modulus of the zones with 1.77% replacement ratio ranges between 58.2-62.3 MPa. The variability in the range results from the thin layer of 120 m/s within ML/CL as opposed to the remaining sections with shear wave velocity of 110 m/s. due to the variability of the soil shear modulus along this depth range. Composite shear modulus of the zone with 7.07% replacement ratio is 175.5 MPa.

Shear stress reduction ratio (K_G) is estimated from the ratio of the shear modulus of the native soil to the composite shear modulus. Therefore shear stress reduction factor ranges between 0.374-0.416. The higher end of the range is for the thin section within ML/CL with shear wave velocity of 120 m/s. Shear stress reduction factor is 0.173 for the SP/SM layer which has a 7.07% replacement ratio.

It is seen that the homogenization technique predicts a 63% and 83% stress reduction for the levels with replacement ratios 1.77% and 7.07% respectively.

It is assumed that the effects of nonlinearity apply equally to both the soil and the stiff columns. Therefore a common degradation curve is utilized for the homogenized soil-column mass. Shear modulus degradation curves and strain dependent damping curves that were used in site response analyses (Figure 4-71 and Figure 4-72) were implemented for the homogenized composite soil-column system.

Site response analyses are performed for different levels of shaking. Of particular interest is the shear stress on the soil for unimproved and unimproved cases. Peak shear stress for the unimproved soil is directly taken from the results of the analyses of the unimproved soil profile. Peak shear stress from the improved composite soil profile is decomposed into two

components; the shear stress on the soil and the shear stress on the jet grout columns in proportion to the respective values of shear modulus.

Peak shear stresses induced on the unimproved soil for different levels of base shaking are shown in Figure 4-106. It is seen that the base shaking levels range between 0.01g-0.30g and the level of shear stress increases with depth and shaking level.

Peak shear stresses induced on the unimproved soil for different levels of base shaking are shown in Figure 4-107. It is seen that the shear stress on the improved soil is significantly reduced for all shaking levels.

Similarly cyclic stress ratio for the unimproved case is presented in Figure 4-108. As seen the cyclic stress ratio within the suspect liquefiable layers ranges between 0.20-0.32 for peak base acceleration level of 0.3g. Cyclic stress ratio for the improved case is shown in Figure 4-109. CSR for this case reduces to about 0.05-0.11 for the suspect liquefiable layers. The reduction is larger for the SP/SM layer with higher replacement ratio. This is a significant reduction demonstrating the effect of stiff columns.

Peak shear strain for the unimproved soil profile is shown Figure 4-110. Peak shear strain for the improved soil profile is shown in Figure 4-111. It is seen that shear strains of the improved profile is greatly reduced for all shaking levels.

Calculated ratio of the peak shear stress on the improved soil to the peak shear stress on the unimproved soil for shaking level 0.01g is presented in Figure 4-112. Reduction ratio of the peak shear stresses are close to the value of the shear stress reduction ratio (K_G). Improvement of the top 9 meter with jet grout columns causes a slight increase is in the shear stresses on the levels below the improved zone. Shear strain ratio for the improved and unimproved cases are shown in Figure 4-113. Peak shear strains are reduced similar to the ratios predicted by the shear stress reduction factor.

Calculated ratio of the peak shear stress on the improved soil to the peak shear stress on the unimproved soil for shaking level 0.025g is presented in Figure 4-114. Reduction ratio of the peak shear stresses are close to the value of the shear stress reduction ratio (K_G). Shear strain ratio for the improved and unimproved cases are shown in Figure 4-115. Peak shear strains are reduced similar to the ratios predicted by the shear stress reduction factor.

Calculated ratio of the peak shear stress on the improved soil to the peak shear stress on the unimproved soil for shaking level 0.05g is presented in Figure 4-116. Reduction ratio of the peak shear stresses are close to the value of the shear stress reduction ratio (K_G). Shear strain ratio for the improved and unimproved cases are shown Figure 4-117. Peak shear strains are reduced similar to the ratios predicted by the shear stress reduction factor.

Calculated ratio of the peak shear stress on the improved soil to the peak shear stress on the unimproved soil for shaking level 0.10g is presented in Figure 4-118. Reduction ratio of the peak shear stresses are close to the value of the shear stress reduction ratio (K_G). Shear strain ratio for the improved and unimproved cases are shown Figure 4-119. Peak shear strains are reduced to smaller values than the ratios predicted by the shear stress reduction factor.

Calculated ratio of the peak shear stress on the improved soil to the peak shear stress on the unimproved soil for shaking level 0.15g is presented in Figure 4-120. Reduction ratio of the peak shear stresses are close to the value of the shear stress reduction ratio (K_G). Shear strain ratio for the improved and unimproved cases are shown Figure 4-121. Peak shear strains are reduced similar to the ratios predicted by the shear stress reduction factor. Peak shear strains are reduced to smaller values than the ratios predicted by the shear stress reduction factor.

Calculated ratio of the peak shear stress on the improved soil to the peak shear stress on the unimproved soil for shaking level 0.20g is presented in Figure 4-122. Reduction ratio of the peak shear stresses are close to the value of the shear stress reduction ratio (K_G). Shear strain ratio for the improved and unimproved cases are shown Figure 4-123. Peak shear strains are reduced similar to the ratios predicted by the shear stress reduction factor. Peak shear strains are reduced to smaller values than the ratios predicted by the shear stress reduction factor.

Analyses with homogenization indicate that shear stresses are reduced in accordance with the estimates of shear stress reduction ratio (K_G). This is not an unexpected finding because the major assumptions behind the shear stress reduction factor (K_G) and the homogenization technique are the same; strain compatible deformations. Shear stresses at the improved zones are reduced based on the assumption that the soil and the stiff columns deform compatibly and the stresses are shared based on stiffness of each unit.

Interestingly, shear strains are reduced to lower values than the strain levels from the shear stress reduction factor. Difference between the shear stress reduction ratio and the calculated shear strains reduction increases with increasing shaking level.

Values of calculated peak shear stress on the unimproved soil are plotted with respect to the peak shear stress on the improved soil are plotted in Figure 4-126. Data is from the improved levels (i.e. top 9 meters) for all the analysis cases. Plotted values are grouped into two different replacement ratios of 1.77% and 7.07%. Improved to unimproved shear stress relationships that correspond to the two improvement ratio are provided as well (K_G = 0.17 and 0.37). It is seen that the as observed in the previous figures.

Maximum values of peak shear stress from each improved layer (Fill, ML/CL and SP/SM) are plotted in for improved and unimproved cases. Maximum value for each layer is plotted for all the analysis cases. Again it is seen that the calculated stress ratio aligns with the shear stress reduction ratio. Average values of the peak shear stresses for each layer are selected for improved and unimproved cases and the results are plotted in Figure 4-128.

Site response analyses were performed to estimate the earthquake induced stresses and strains at sections of the site that were improved at the time of the earthquake (i.e. Supermarket Building Area and parts of Parking Structure Area). Effect of the stiff columns was investigated only for the main event.

7. EFFECT OF STIFF COLUMNS – MODELING STRESS AND STRAIN REDUCTION WITH FINITE ELEMENT ANALYSES

Effect of stiff column reinforcement has been studied for the soil conditions and ground improvement scheme at Carrefour site. Dynamic behavior of a soil column improved with stiff columns is modeled. Finite element program DYNAFLOW (Prevost 2002) was used in the analyses.

The analyses included three sets with different column spacings. One segment of soil-column system was modeled in the analyses. Finite element mesh for one of the models is shown in Figure 4-135. Locations of the nodes selected for output are also shown in the figure. This mesh represents the jet grout column configuration at Carrefour site with the exception of the

additional secondary columns within the SP/SM layer. Jet grout column is 0.6 meters in diameter and spaced 4 meters center-to-center. Two other models included the same diameter column spaced 3 and 5 meters center-to-center. Jet grout column is located at the centerline of the model. Sides of the model are truncated at each side in the middle of the soil in between adjacent columns. Node pairs at each elevation on each side of the finite element mesh were assigned to be equivalent. Therefore node pairs along the grid boundaries share the same equations and they undergo equivalent dynamic behavior. This provides a repetitive symmetry along each side of the mesh.

One additional case with no jet grout column was analyzed for comparison.

Base of the model was fixed in the vertical direction and the base acceleration was applied in the horizontal direction. EW component of the Kocaeli Earthquake from IZT recording station is used in the analyses. Selection of the ground motion is arbitrary because the main purpose of the analyses is to evaluate the general pattern of the behavior and to compare the effect of stiff columns with the unimproved case.

The soil profile and the shear wave velocity model used in the homogenized site response analyses (Figure 4-105) were used for the geometry and the material properties of the model.

This stiffness value is obtained by averaging out the shear modulus of the jet grout column by the area ratio in the in plane direction. This made it possible to reduce the three-dimensional system to plane strain geometry. Shear modulus of the jet grout column is estimated 2.083×10^6 kPa as discussed in the previous section. This value vas reduced to 2.454×10^5 kPa to distribute the effect of 0.6 m diameter column over the 4 meter column spacing. Similar averaging was performed and an equivalent jet grout column modulus was determined for other column spacings. Equivalent stiffness for 3 and 5 meter column spacing is estimated 3.272×10^5 kPa and 1.963×10^5 kPa respectively.

Dynamic analyses were performed in the time domain using elastic properties. Time integration parameters of $\alpha = 0.50$ and $\beta = 0.25$ were used in the analyses. This pair of coefficients corresponds to the trapezoidal algorithm in Newmark family of finite difference integration schemes (Newmark 1959).

Of particular importance was the effect of the stiff column reinforcement on the shear stresses and shear strains in the soil in comparison to the unimproved case.

Shear strain histories at selected nodal points within the unimproved soil are plotted in Figure 4-136. It is seen that the peak strain levels within the soil reach as high as 0.3%. Shear stresses are plotted in Figure 4-137 for the same case.

Shear strain histories at selected nodal points within the soil are plotted in Figure 4-138 for Case 1 where the column spacing is 3 meters. It is seen that the strain levels within the soil are considerably smaller compared to the unimproved case.

Shear strain histories at selected nodal points along the centerline of the mesh are plotted in Figure 4-139 for the same case. Several of these nodes are within the jet grout column (at top 9 meters) and the others are within the soft clay layers below. It is seen that the shear strains within the jet grout column are very similar in amplitude to the shear strains within the soil. This shows that the shear strains within the soil and the columns are compatible.

Histories of shear stress at selected nodal points within the soil are plotted in Figure 4-140 for the same case. Similarly shear stresses at the nodal points within mesh centerline are plotted in Figure 4-141. It is seen that the shear stresses within the jet grout column are much larger in amplitude than the shear stresses on the soil at the same elevation. Compatible shear deformations warrant the sharing of the stresses in proportion to the stiffnesses of the soil and the jet grout column.

Shear strain histories at selected nodal points within the soil are plotted in Figure 4-142 for Case 2 where the column spacing is 4 meters. Shear strain histories at selected nodal points along the centerline of the mesh are plotted in Figure 4-143 for the same case. It is seen that the shear strains within the jet grout column are very similar in amplitude to the shear strains within the soil as in Case 1.

Variation of shear strain over finite element mesh at an analysis step (at t = 7.8 seconds) is plotted in Figure 4-144. This shows the distribution of shear strains over the jet grout column at the top 9 meters, the soil around the jet grout column and the soil below the treated depth. It is seen that the magnitude of shear strain within the improved zone is uniform in the horizontal direction at any given depth. Some uneven distribution is noticed near the top and

bottom elevations of the improved section. Strains within the jet grout column are slightly larger than the strains in the soil at the top 2 meters. Similarly the strains within the soil are slightly higher within the soil around 7-9 meters depth compared to the strains within the jet grout column and the soil further away at the same elevations. These are boundary effects. Jet grout column is not restrained and it is free to move laterally along the edges. This causes uneven deformations at these zones.

Histories of shear stress at selected nodal points within the soil are plotted in Figure 4-145 for the same case. Similarly shear stresses at the nodal points within mesh centerline are plotted in Figure 4-146. It is seen that the shear stresses within the jet grout column are much larger in amplitude than the shear stresses on the soil at the same elevation as in Case 1.

Variation of shear stress ratio (shear stress / total vertical stress) over finite element mesh at an analysis step (at t = 7.8 seconds) is plotted in Figure 4-147. It is seen that the stresses are concentrated along the jet grout column in comparison to the soil around.

Shear strain histories at selected nodal points within the soil are plotted in Figure 4-148 for Case 3 where the column spacing is 5 meters. Shear strain histories at selected nodal points along the centerline of the mesh are plotted in Figure 4-149 for the same case. It is seen that the shear strains within the jet grout column are very similar in amplitude to the shear strains within the soil as in previous improved cases.

Histories of shear stress at selected nodal points within the soil are plotted in Figure 4-150 for the same case. Similarly shear stresses at the nodal points within mesh centerline are plotted in Figure 4-151. It is seen that the shear stresses within the jet grout column are much larger in amplitude than the shear stresses on the soil at the same elevation as in previous improved cases.

These analyses show that the jet grout columns and surrounding soils deform compatibly and therefore shear stresses within the soil are reduced in comparison to the unimproved case. Jet grout columns work as stiff members and carry most of the load.

8. EFFECT OF STIFF COLUMNS – MODELING PORE PRESSURE GENERATION WITH FINITE ELEMENT ANALYSES

One more approach to understand the effect of jet grout reinforcement included a coupled analysis where the pore pressure generation was modeled for unimproved and improved cases. These analyses again were performed using DYNAFLOW (Prevost 2002). Multi-yield soil model developed by Prevost (1985) was used in the analyses.

The multi-yield soil model is a kinematic hardening plasticity model. Kinematic hardening is capable to models cyclic loading can be modeled as opposed to isotropic hardening. The model is applicable to both cohesive and cohesionless soils. Model parameters can be estimated from conventional laboratory tests (i.e. triaxial, simple shear) and field test (i.e. CPT, SPT). The model utilizes a family of yield surfaces of varying sizes that are bounded by the outermost yield surface (i.e. failure surface). No pure elastic domain exists in the model where the first yield surface is chosen as a yield surface of size zero which coincides with the initial stress point. As the stress point moves, it translates the current yield surface which is called the "active yield surface". Therefore as plastic flow takes place the yield surface changes both its position and size. As the active yield surface translates and/or expands it touches the next outlying yield surface and makes it the active yield surface. Plastic deformations and plastic modulus characteristics are determined from the current stress state and the relative position of the stress point with respect to the "active" yield surface. The model is described by Prevost (1985) in detail. Procedures to estimate model parameters are outlined by Popescu and Prevost (1993).

Dynamic analyses were performed in the time domain using elastic properties. Time integration parameters of $\alpha = 0.50$ and $\beta = 0.25$ were used in the analyses. This pair of coefficients corresponds to the trapezoidal algorithm in Newmark family of finite difference integration schemes (Newmark 1959).

Base of the model was fixed in the vertical direction and the base acceleration was applied in the horizontal direction. EW component of the Kocaeli Earthquake from IZT recording station is used in the analyses.

Development of pore pressures is modeled in the saturated soils that were improved. Soil profile and the finite element mesh from the previous section is used in the analyses (Case 2, 0.6 m diameter jet grout columns with 4 m center-to-center spacing). The only difference between the elastic model in the previous section and the model herein is the presence of the secondary jet-grout columns within the SP/SM layer. Secondary columns were not included in the elastic analyses in the previous section. In this set of analyses secondary columns are defined within the SP/SM layer.

Shear strength of the soil is defined by cohesion and friction angle. Yield condition is defined by Mohr-Coulomb criterion in this analysis. Other yield criteria such as von Mises and Drucker-Prager are also available for this model. Initial stiffness of the soil layers was estimated from soil profile and the shear wave velocity model in the previous sections (Figure 4-105). Poison ratio of the soil skeleton was assumed 0.3 for the analyses. This is not particularly important because of the saturated nature of the soils. Volumetric compressibility will be very high regardless of the Poisson ratio of the solid skeleton because of the low soil permeability and nearly undrained conditions. Compressibility of water is taken as 2.2×10^7 kPa.

Basic shear strength and stiffness parameters of the multi-yield model are estimated for the soils in the model. Plasticity parameters can be approximated by running element tests. Element tests were performed to estimate the plasticity parameters associated with the model. Results of one cyclic triaxial test are shown in Figure 4-152. As seen the soil has a friction angle $\phi' = 30$ degress and is initially consolidated to a cell pressure of 100 kPa. Plasticity parameter Xpp = 0.15 for this case. Cyclic axial load is applied with undrained conditions. This loading corresponds to a cyclic stress ratio 0.12. It is seen that pore pressures increase gradually with each cycle and the soil response gets softer. The sample liquefies at 9^{th} cycle.

Similarly another element test is shown in Figure 4-153. The soil in this slement teat has the same properties except the plasticity parameter is 0.05. It is seen than even though the level of loading is larger in amplitude than the previous example (CSR = 0.15) it takes more cycles to liquefy. This shows how the plasticity parameter controls the pore pressure generation.

Several element tests were performed with different plasticity parameter and the results are shown in Figure 4-154. It is seen that each data set groups into a unique curve of CSR vs number of cycles to liquefaction. Based on these results plasticity parameter for the model was selected as 0.05.

One analysis was performed for the unimproved soil profile. Shear stress is plotted against shear strain in Figure 4-155 through Figure 4-162 for the course of shaking for soil between 3.8 – 8.7 m. It is seen that soil behavior is highly nonlinear with large strains. Pore pressures at these depths are shown in Figure 4-163. It is seen that pore pressures increase significantly at the initial stage of shaking.

Analyses were performed for the soil profile improved with jet grouting. Shear strain is plotted against shear strain in Figure 4-164 and Figure 4-165 for the course of shaking for soil at 6.2 m and 8.2 m respectively. It is seen that the strains are significantly limited in the soil compared to the unimproved case. Stress strain behavior is more linear in this case. Pore pressures along the soil profile are shown in Figure 4-166. It is seen that pore pressures do not increase for this case.

This case confirms the findings reported in the previous section. As seen the shear strains are limited and pore pressure development is mitigated with the help of jet grout columns.

9. SUMMARY AND CONCLUSIONS

The Carrefour Shopping Center, a 55,000-m^2 complex in Izmit, Turkey was being built at the time of the M7.4 Kocaeli Earthquake on August 17, 1999. Estimated peak ground accelerations during the earthquake were 0.24g. Soft and liquefiable saturated alluvial sediments underlie the site, and the structures are supported on shallow footings and mats. Soft clays and silts had been improved using surcharge fills and wick drains, and small-diameter (0.6 m) high-modulus jet-grout columns were used to increase bearing support for shallow foundations and reduce the liquefaction potential of a 3 m-thick silty sand layer. The main shopping center building was partially built, and only the area beneath the footprint of the building and a small portion of the parking garage had been jet-grouted when the earthquake struck. Post-earthquake field reconnaissance, along with settlement monitoring

devices installed in adjacent Lot C, made possible the performance comparison between jet-grouted sections and adjacent untreated areas. The jet-grout-treated sections showed no damage, but the untreated areas of the site, along with other nearby untreated sites, commonly experienced settlements of 10 to 12 cm. The jet-grout columns were effective in reducing liquefaction-related damages in the treated areas.

A number of important points are summarized:

1. The jet-grout columns used at this site were of smaller diameter (0.6 m) and installed using a faster lift rate (50 cm/min.) relative to what is typical in the US. The replacement ratio was 7% in the silty sand, and 2% in all other strata within the top 9 m. Also, the approach of using close-to-moderately spaced high-modulus columns to mitigate liquefaction at this site is distinguished from the more common approach of constructing rows of contiguous columns to form cells to contain liquefied material.

2. The application and removal of a 3.3-m thick surcharge fill in the parking garage area only moderately reduced liquefaction potential, increasing the factory of safety against liquefaction from about 0.6 to 0.7.

3. Wick drains installed in the parking garage area and Lot C (non-jet-grouted sections) did not reduce pore pressures during shaking in these low-permeability soils, but may have helped prevent surficial disruption and kept settlements more uniform during post-earthquake reconsolidation.

4. Liquefaction-type behavior occurred in ML/CL soils that were initially assessed as "non-liquefiable" based on I_c (Soil Behavior Type Index) values from CPTs approaching 3.0, and failure to meet one of the three Chinese criteria [the soil contained an average of 50% clay-sized particles (< 5μm)]. The soils appear to be similar to those also associated with documented liquefaction-type behavior in Adapazari during the Kocaeli Earthquake. The findings suggest that the Chinese criterion of percentage of clay-sized particles exceeding 15% may not be a reliable indicator of liquefaction potential in some cases. Further research is needed to better understand the behavior of such soils.

5. Subsoil conditions were investigated with an extensive array of in-situ testing. Most of the data consisted of CPT soundings. Evaluation of these soundings revealed that CPT was effective in characterizing the soil conditions. CPT results were further used to evaluate the liquefaction potential at the site for the Kocaeli Earthquake (M7.4) and a M5.8 aftershock. Current guidelines were used in assessing the liquefaction resistance. These guidelines recommend CPT unsuitable for soils with considerable fines ($I_c > 2.6$). However it was shown that CPT was effective in predicting liquefaction-type behavior of these soils as well as soils with $I_c < 2.6$.

6. A definitive explanation for significant earthquake-induced settlements measured in a high-plasticity clay stratum (CH) in Lot C has not yet been found. It is suspected that the settlements are related to earthquake-induced strength loss and softening in these materials followed by shearing distortions due to the overlying fill. It appears unlikely that the settlements can be explained by instrument malfunction. If the suspected behavior is indeed real, then this study could indicate a previously unrecognized vulnerability of these soils.

7. Preliminary site-response analyses using higher "equivalent soil moduli" to simulate the influence of the stiffer columns (at least 100 to 200 times stiffer than the soil at this site) suggest that the high shear stiffness may have led to greatly decreased cyclic shear strains that were kept near threshold levels such that significant earthquake-induced pore pressures did not develop in the upper 9 m of the profile. Peak cyclic shear strains were estimated to have been in the range of 0.5-1% without the columns, and in the range of 0.02-0.05% with the columns.

8. Even if significant pore pressures had developed in or migrated to soils in the upper 9 m during the earthquake, as long as the jet-grout columns maintained structural integrity, their higher stiffness in vertical compression should have significantly reduced post-earthquake reconsolidation settlements relative to untreated soil.

9. The demonstrated success of the ground treatment at this site suggests that similar applications of small-diameter high-modulus columns could prove effective in cases where the soils are soft and mixed and liquefaction is of concern. Because of their high

stiffness, such columns may in some cases offer added benefits over stone columns in mixed and "dirty" soils (that have low permeabilities, do not drain rapidly and are difficult to densify), especially in terms of reducing post-earthquake reconsolidation settlements. Also, high-modulus columns of the type constructed using jet grouting can be constructed using other installation techniques, such as wet soil mixing, that might be more economical in some cases. Thus, the findings from this study are relevant to other techniques whereby ground reinforcement using stiff columns can be achieved.

10. Finite element analyses were performed to investigate the effect of stiff column reinforcements. These analyses reveal that the soil and the stiff columns deform compatibly. Shear strains are reduced in comparison to the unimproved case and most of the shear stresses are carried by the stiff columns. This may bring an insight into the seismic behavior of soils improved with stiff columns.
11. Finite element analyses were performed to model the pore pressures for unimproved and improved ground conditions. It is seen that pore pressure development is prevented with the aid of stiff columns.

Table 4-1. Average grain size and index test data for soil strata at Carrefour site.

Depth of Stratum (m)	USCS	LL (%)	PL (%)	W (%)	> #4 sieve (%)	< #200 sieve (%)	< 5 μm (%)	< 2 μm (%)	I_c Value from CPT*
0 to 3	Fill (GC)	-	-	-	-	-	-	-	-
3 to 6.5	ML/CL	33	23	32	0	88	47	38	3.0
6.5 to 9	SM w/ SP, SC lenses	NP	NP	24	6	30	16	14	2.2
9 to 10	ML/CL	35	24	35	0	95	55	42	2.9
10 to 35	CH w/ SM, ML lenses	66	29	55	0	100	74	61	3.3

* I_c = soil behavior type index (Lunne et al. 1997)

Table 4-2. Construction parameters used for jet-grout column construction at Carrefour

Jet-grout system	Jet-1
Column diameter	60 cm
Number of nozzles	2
Nozzle size	2 mm
Rods lifting speed	50 cm/min
Rods rotation speed	20 rev/min
Injection pressure	450 bars
Water/cement ratio	1/1

Table 4-3. Layer thicknesses, earthquake induced settlement and estimated total settlement – Settlement Column 1

Layer	Initial Thickness (m)	Contained Layers	Earthquake induced vertical deformation (cm)	Estimated total static deformation (cm)
A	4.99	GC (2.30 m) Upper ML/CL (2.69 m)	3.1	16.0
B	4.30	Upper ML/CL (2.01 m) SM/SM (1.50 m) Lower ML/CL (0.79 m)	3.4	16.0
C	3.88	Lower ML/CL (0.21 m) CH (3.67 m)	2.6	4.7
D	7.22	CH (7.22 m)	0.5	4.0
E	4.72	CH (4.72 m)	0.2	2.0

Table 4-4. Estimated consolidation and compressibility parameters – Settlement Column 1

Layer	Estimated % consolidation		M (kPa)	c_{vh} (cm^2/s)	k (10^{-6} cm/s)
	at the time of the earthquake	at the end of monitoring			
A	81	88	2237	0.018-0.028	0.79-1.23
B	66	86	1747	0.011-0.016	0.62-0.90
C	51	76	5366	0.0060-0.010	0.11-0.18
D	48	67	11733	0.0050-0.011	0.042-0.092
E	60	71	15340	0.0040-0.013	0.026-0.083

Table 4-5. Layer thicknesses, earthquake induced settlement and estimated total settlement – Settlement Column 2

Layer	Initial Thickness (m)	Contained Layers	Earthquake induced vertical deformation (cm)	Estimated total static deformation (cm)
A	5.00	GC (2.0 m) ML/CL (3.0 m)	2.5	25.3
B	4.33	Upper ML/CL (2.30 m) SM/SM (1.20 m) Lower ML/CL (0.70 m) CH (0.13 m)	4.6	20.4
C	3.89	CH (3.89 m)	3.6	8.6
D	7.23	CH (7.23 m)	1.1	5.3
E	4.72	CH (4.72 m)	-	2.5

Table 4-6. Estimated consolidation and compressibility parameters – Settlement Column 2

Layer	Estimated % consolidation		M (kPa)	c_{vh} (cm^2/s)	k (10^{-6} cm/s)
	at the time of the earthquake	at the end of monitoring			
A	89	98	1275	0.020-0.030	1.54-2.31
B	76	94	1380	0.013-0.018	0.92-1.28
C	60	88	2940	0.0090-0.015	0.30-0.50
D	58	84	8544	0.0060-0.011	0.069-0.13
E	36	68	12272	0.0025-0.0055	0.020-0.044

Table 4-7. Layer thicknesses, earthquake induced settlement and estimated total settlement – Settlement Column 3

Layer	Initial Thickness (m)	Contained Layers	Earthquake induced vertical deformation (cm)	Estimated total static deformation (cm)
A	6.04	GC (2.25 m) Upper ML/CL (3.79 m)	1.9	13.2
B	2.09	Upper ML/CL (0.16 m) SM/SM (1.50 m) Lower ML/CL (0.43 m)		
C	4.99	Lower ML/CL (0.72 m) CH (4.27 m)		
D	6.49	CH (6.49 m)		
E	4.99	CH (4.99 m)		

Table 4-8. Estimated consolidation and compressibility parameters – Settlement Column 3

Layer	Estimated % consolidation		M (kPa)	c_{vh} (cm^2/s)	k (10^{-6} cm/s)
	at the time of the earthquake	at the end of monitoring			
A	80	93	2804	0.018-0.028	0.63-0.98
B					
C					
D					
E					

Table 4-9. Summary of apparent effectiveness of soil treatment during earthquake

Section	Treatment Used*	Predicted Behavior w/out Treatment	Observed Behavior	Apparent Effectiveness of Treatment
Supermarket Building (60% complete)	Jet-grout columns with replacement ratio of 7% in silty sand and 2% in other layers.	F.S. $_{Liq'n}$ ~ 0.6 Sand boils not likely. Δ H ≈ 6 to 10 cm	No structural or ground damage. No sand boils or settlements.	Prevented liquefaction-related damages; reduced cyclic shear strains, prevented pore pressure build up.
Parking Garage	Surcharge fill 3.3-m thick applied and removed. Wick drains installed. Only 10% of area jet-grouted.	F.S. $_{Liq'n}$ ~ 0.7 Sand boils not likely. Δ H ≈ 7 to 10 cm	Settlements of 7 to 10 cm (estimated). No sand boils.	Surcharge fills slightly increased liquefaction resistance. Wicks did not reduce pore pressures during shaking, but may have helped prevent sand boils.
Lot C	Wick drains installed. Surcharge fill 3.3-m thick in place during earthquake. No jet grouting.	F.S. $_{Liq'n}$ ~ 0.75 (beneath fill) Sand boils not likely. Δ H measured, prediction not needed	Settlements of 10 to 12 cm measured. No sand boils.	Wicks may have helped prevent sand boils and non-uniform settlements during post-earthquake reconsolidation.
Adjacent Warehouses and Apartment Buildings	None.	F.S. $_{Liq'n}$ ~ 0.6 - 0.7** Δ H ≈ 7 to 12 cm** (assumed)	Settlements of 5 to 10 cm common beneath structures. No sand boils.	--

* At time of Kocaeli Earthquake; ** Assuming soil conditions are similar to those beneath Carrefour site.

Table 4-10. Index properties of SPT samples

Sample depth (m)	USCS	LL (%)	PL (%)	> #4 sieve (%)	< #200 sieve (%)	< 5 μ (%)	< 2 μ (%)
2-2.45	CL	45	24	1.5	79.8	51.5	40.2
3-3.45	SC/GC	52	28	25.9	48.0	27.5	25.2
4-4.45	CL/ML	33	23	0.0	83.2	44.1	38.6
5-5.45	CL/ML	34	23	0.0	85.0	41.5	33.0
6-6.45	CL/SC	25	20	2.3	50.8	32.6	27.6
7-7.45	CL/SC	26	19	9.2	50.9	28.5	24.0
8-8.45	CL/ML	34	24	0.0	95.2	54.1	42.3
9-9.45	CH	55	25	0.0	98.3	74.3	60.3
10-10.45	CH	56	25	0.0	99.7	75.0	61.5
11-11.45	CH	61	27	0.0	99.9	74.3	60.7
12-12.45	CH	68	29	0.0	99.8	73.7	59.3
13-13.45	CH	65	28	0.0	99.4	71.2	55.7
14-14.45	CH	72	30	0.0	99.9	75.1	60.4
15-15.45	CH	72	30	0.0	99.6	75.6	61.7
16-16.45	CH	70	32	0.0	98.4	74.8	62.6
17-17.45	CH	77	34	0.0	98.6	74.9	63.4
18-18.45	CH	68	30	0.0	98.2	73.4	61.6
19-19.45	CH	66	29	0.0	98.0	74.0	62.7

Table 4-11. Index properties of sliced Shellby tube samples

Sample depth (m)	USCS	LL (%)	PL (%)	> #4 sieve (%)	< #200 sieve (%)	< 5 μ (%)	< 2 μ (%)
6.0-6.1	SC	31	18	2.7	43.2	33.3	27.0
6.1-6.2	SM	NP	NP	1.0	28.6	15.3	13.1
6.2-6.3	SM	NP	NP	3.3	40.3	20.7	17.6
6.3-6.4	SM	NP	NP	21.1	21.3	16.7	14.7
6.4-6.5	SM-SP	NP	NP	0.0	9.1	4.3	3.6
6.5-6.6	SM-SP	NP	NP	0.0	9.5	4.2	3.8
6.6-6.7	SM-SP	NP	NP	0.0	10.0	4.7	3.7
6.7-6.8	SM-SP	NP	NP	0.0	10.1	4.6	3.7
6.8-6.9	SM	NP	NP	0.0	22.2	16.8	14.2
6.9-7.0	CL/ML	35	24	0.0	86.9	47.5	37.8
7.0-7.1	CL	27	19	0.0	61.7	37.6	30.2
7.1-7.2	SM	NP	NP	11.1	31.9	15.4	12.9
7.2-7.3	CL	38	24	0.0	67.8	42.0	36.0
7.3-7.4	CL	38	25	0.0	70.0	42.5	36.3
7.4-7.5	SM	NP	NP	2.5	46.6	24.1	22.0

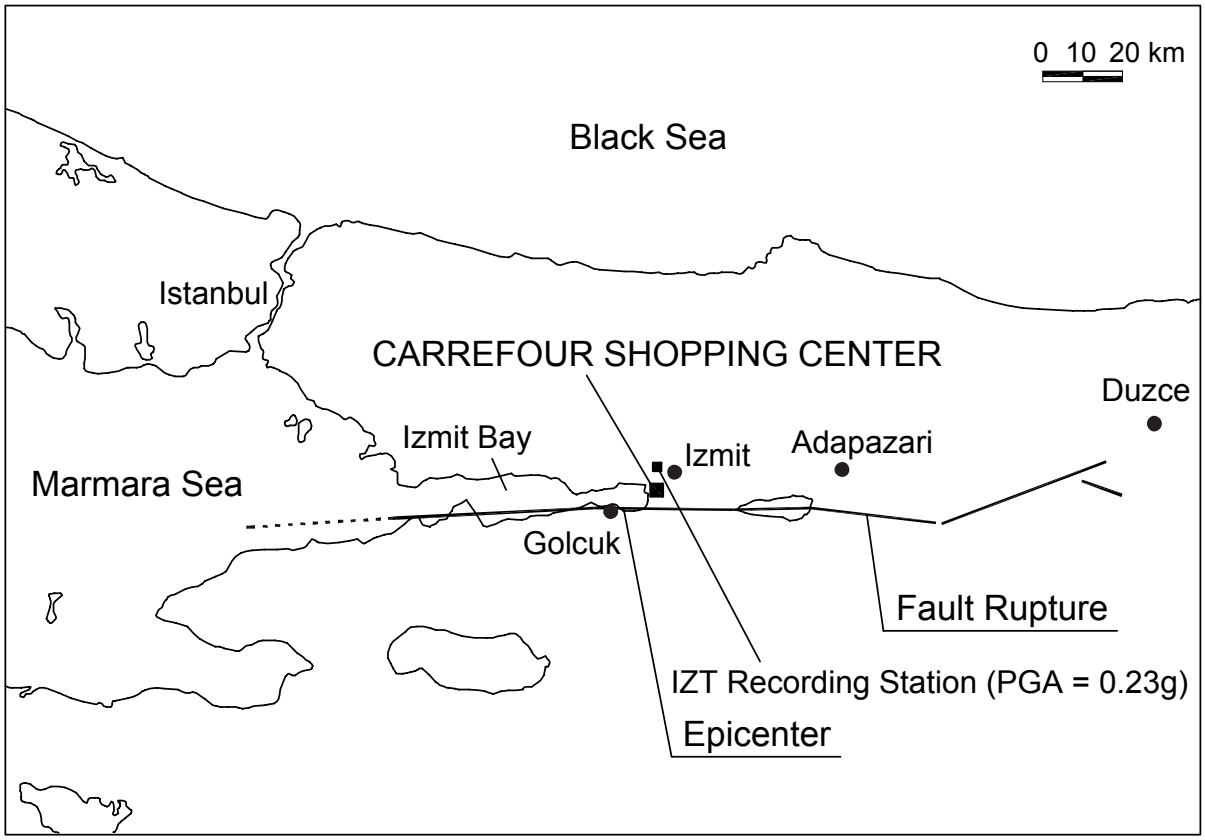

Figure 4-1. Map of affected area of 1999 Kocaeli Earthquake (M7.4) and location of Carrefour Shopping Center along Izmit Bay. Note close proximity to ruptured fault and IZT seismic recording station.

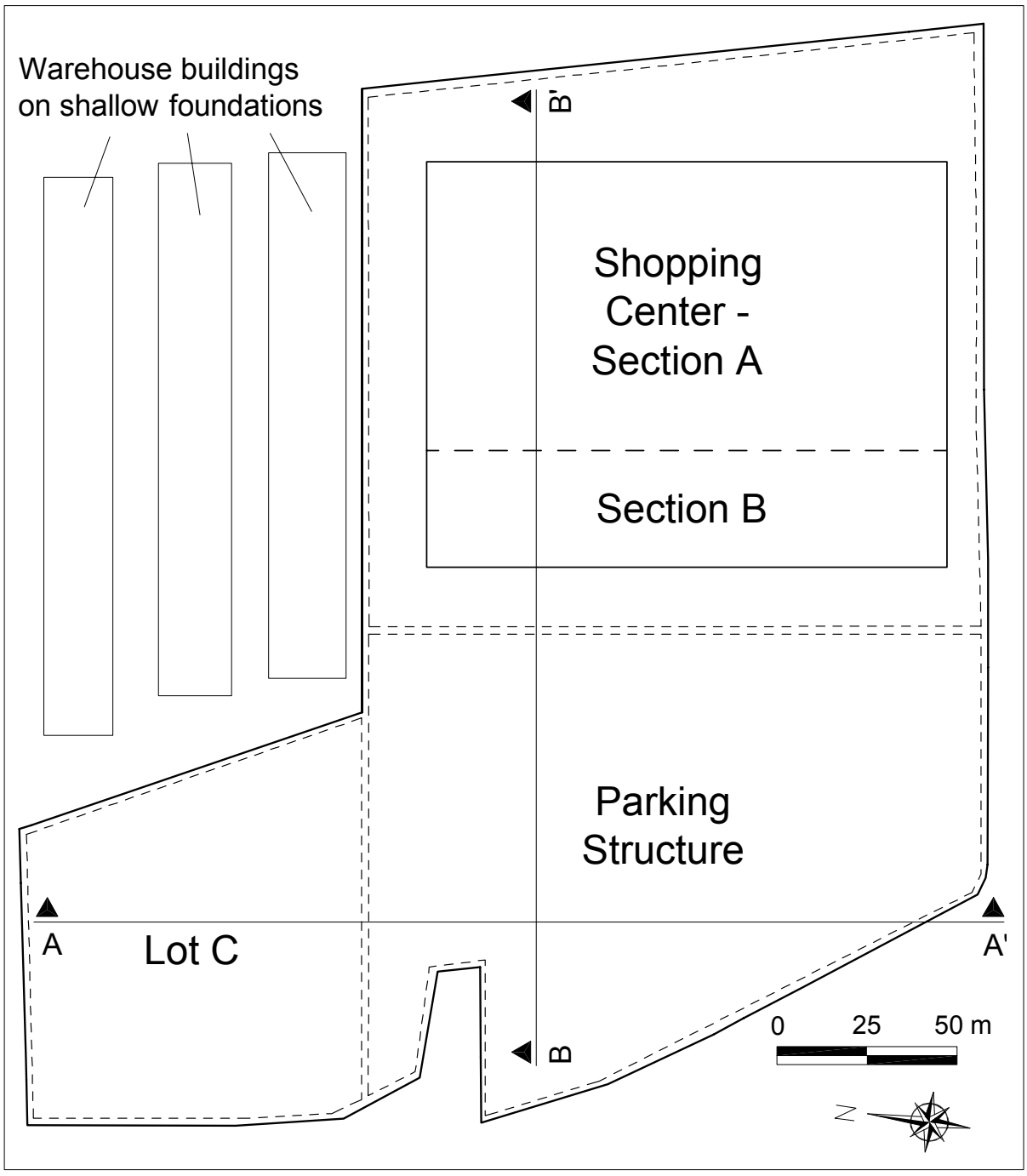

Figure 4-2. Carrefour Shopping Center – Site Plan

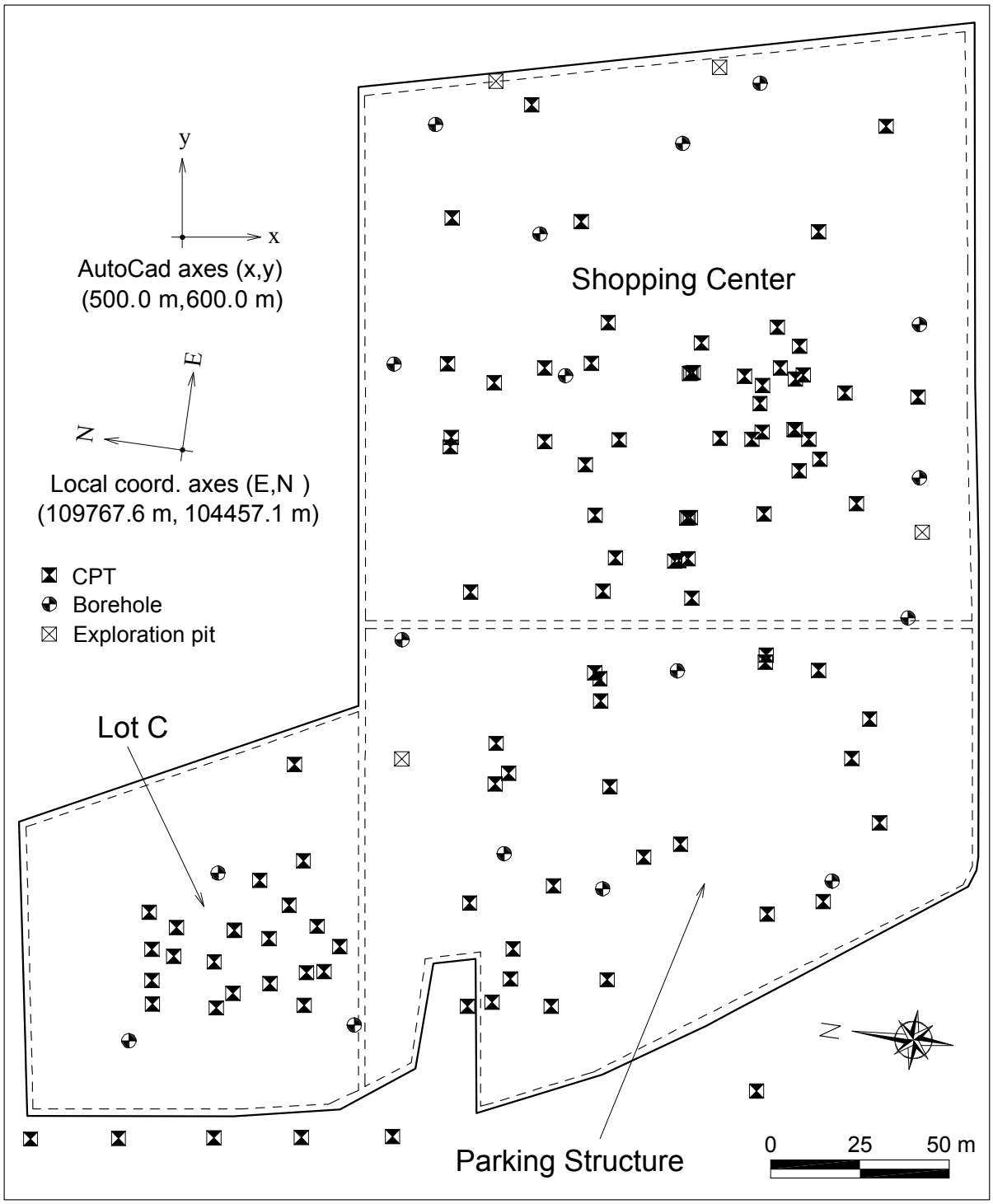

Figure 4-3. Site plan and location of site investigations

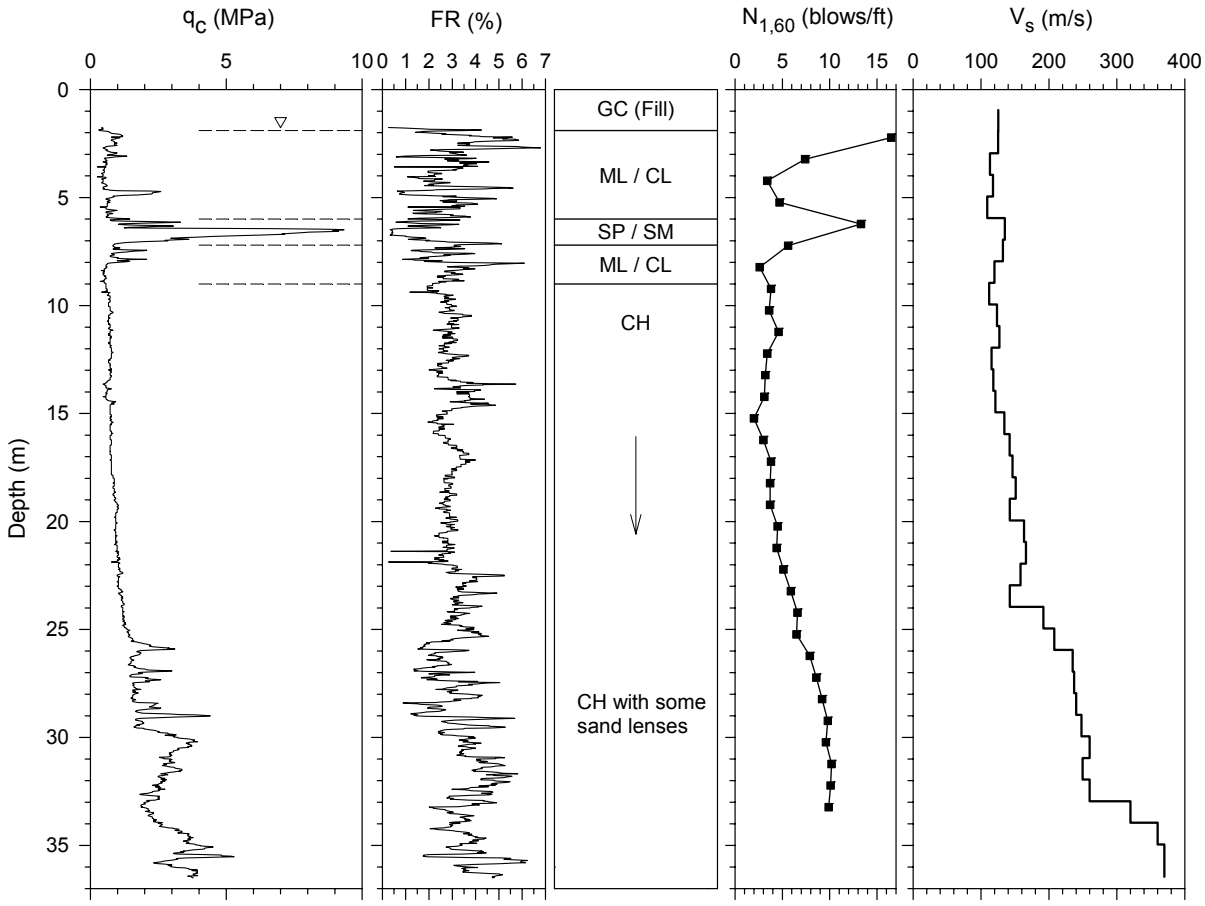

Figure 4-4. Typical pre-improvement geotechnical parameters from Carrefour site.

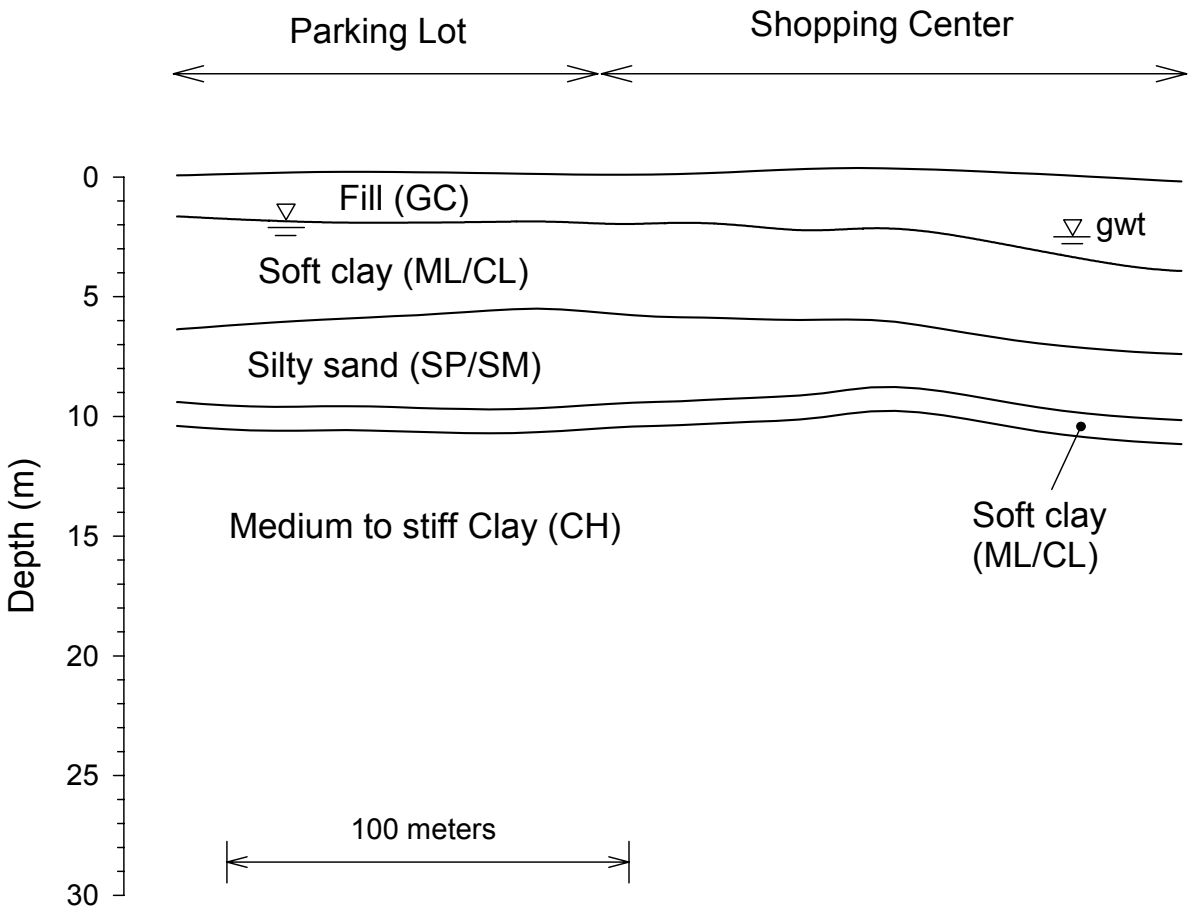

Figure 4-5. Cross section of soil layering through the Parking Lot and Shopping Center areas (Section A-A in Figure 4-2)

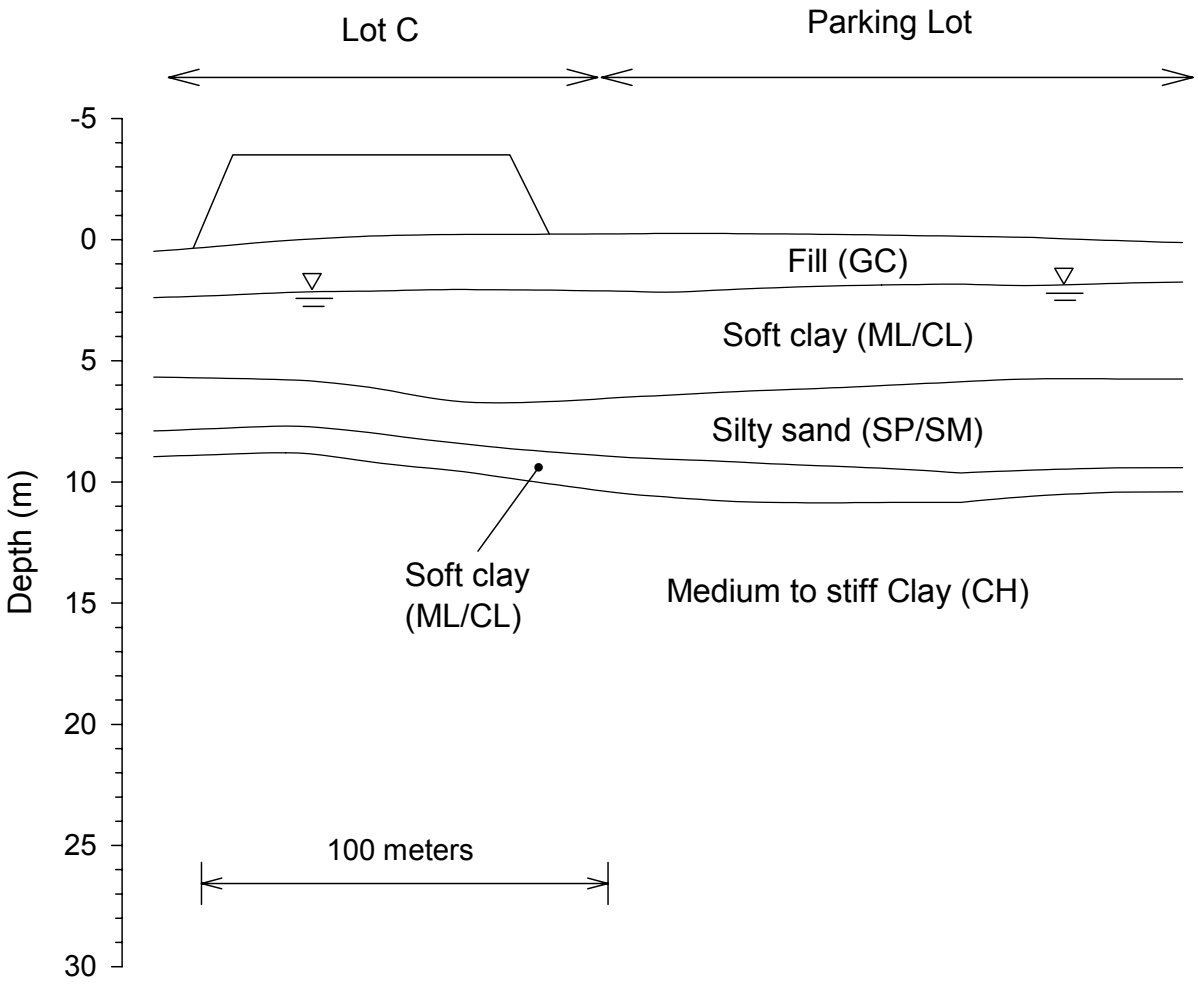

Figure 4-6. Cross section of soil layering through Lot C and Parking Lot areas (Section B-B in Figure 4-2)

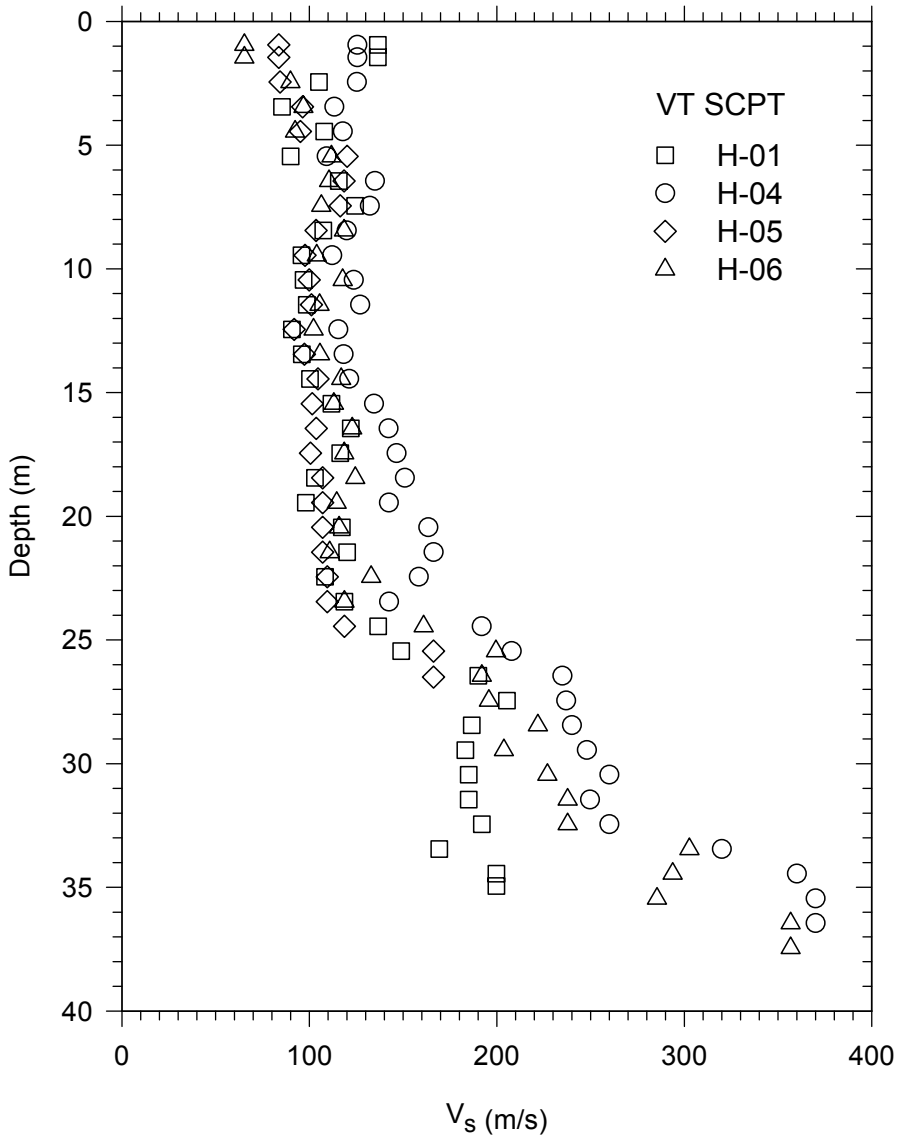

Figure 4-7. Shear wave velocity measurement performed at the site boundary

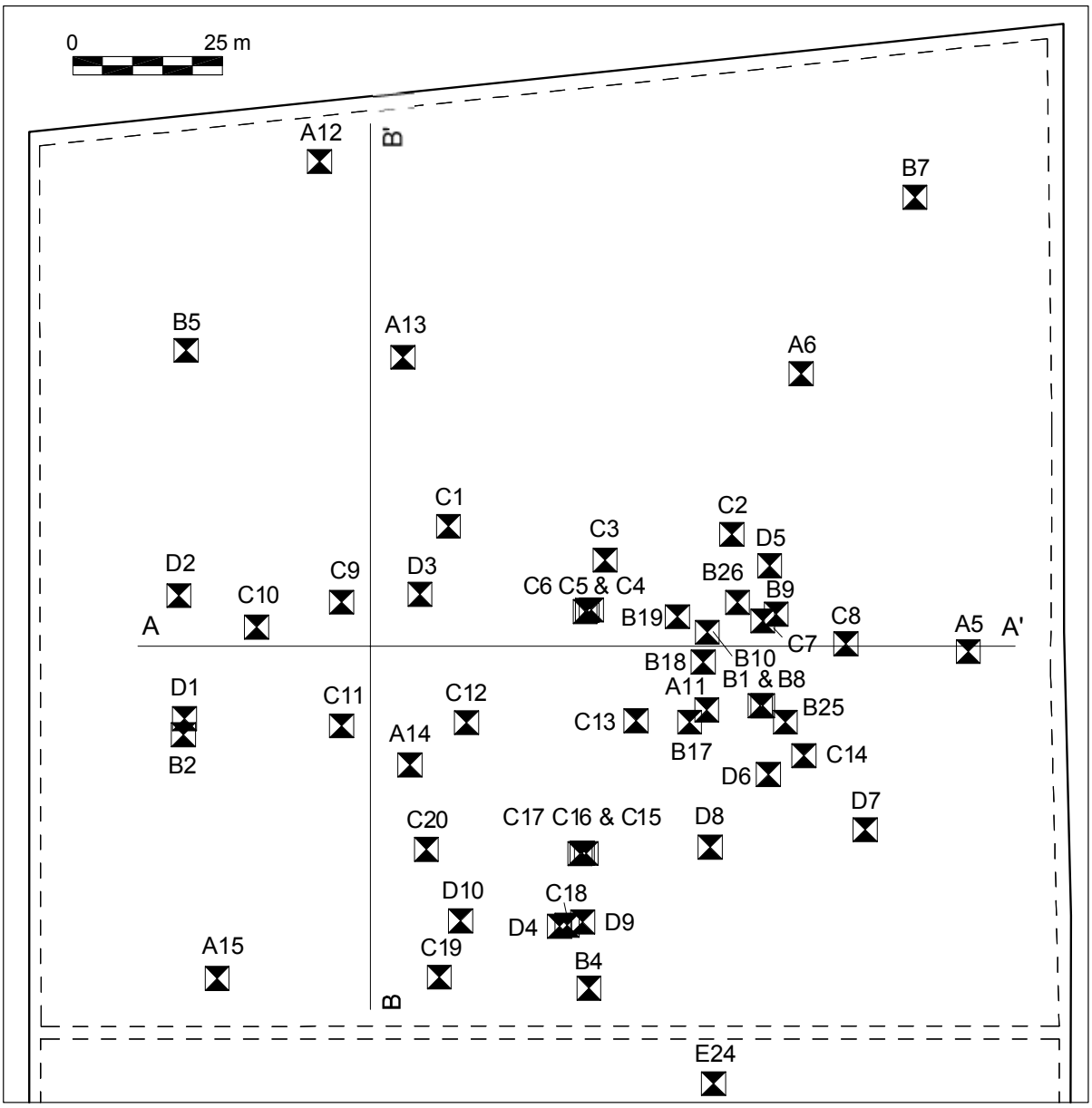

Figure 4-8. Shopping Center area – CPT locations

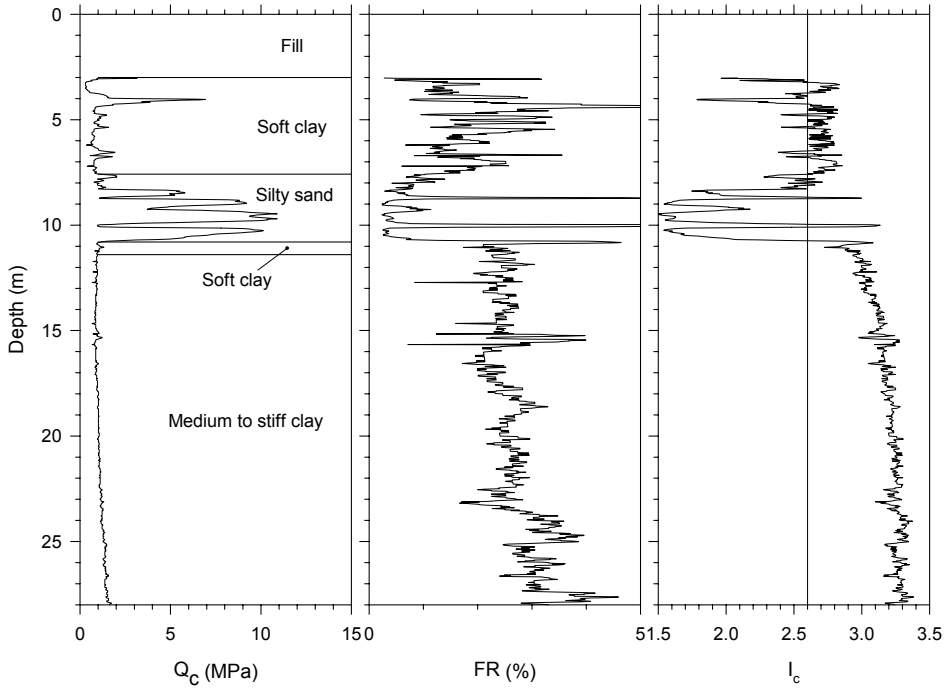

Figure 4-9. CPT sounding from Shopping Center area – A6

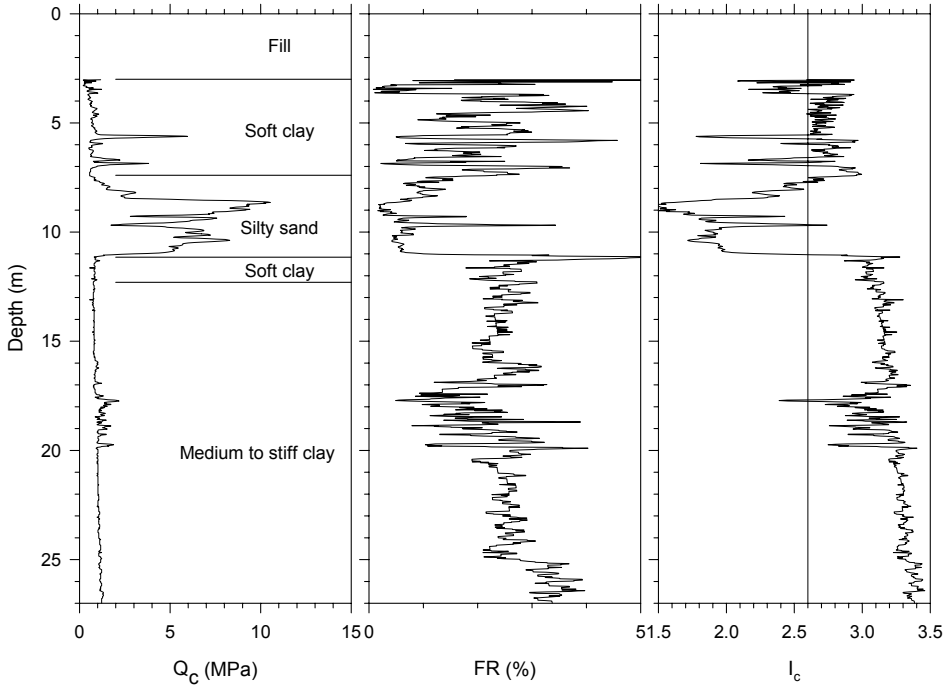

Figure 4-10. CPT sounding from Shopping Center area – A11

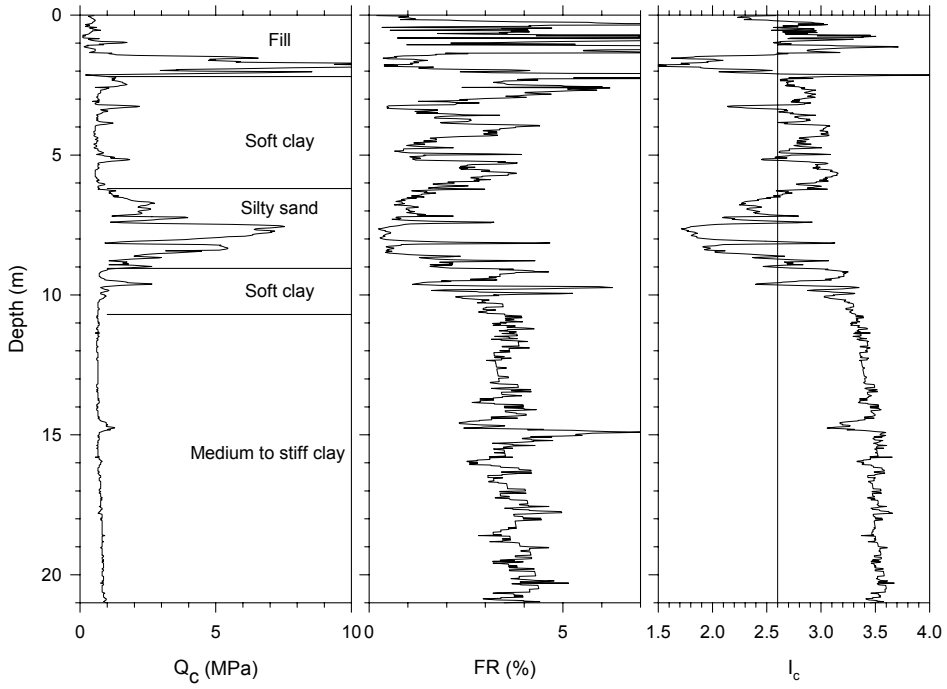

Figure 4-11. CPT sounding from Shopping Center area – A15

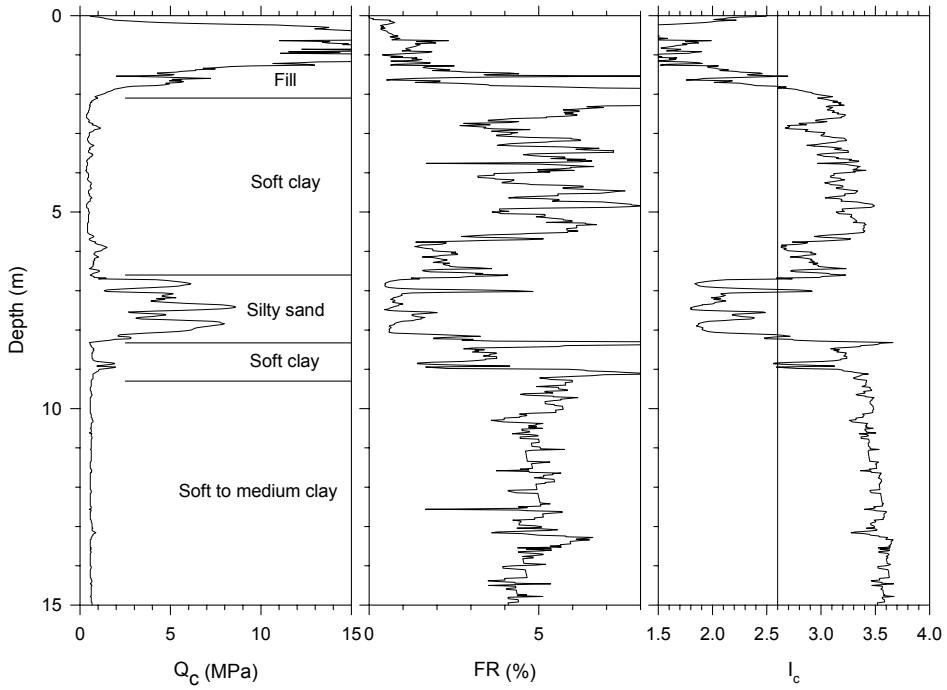

Figure 4-12. CPT sounding from Shopping Center area – C1

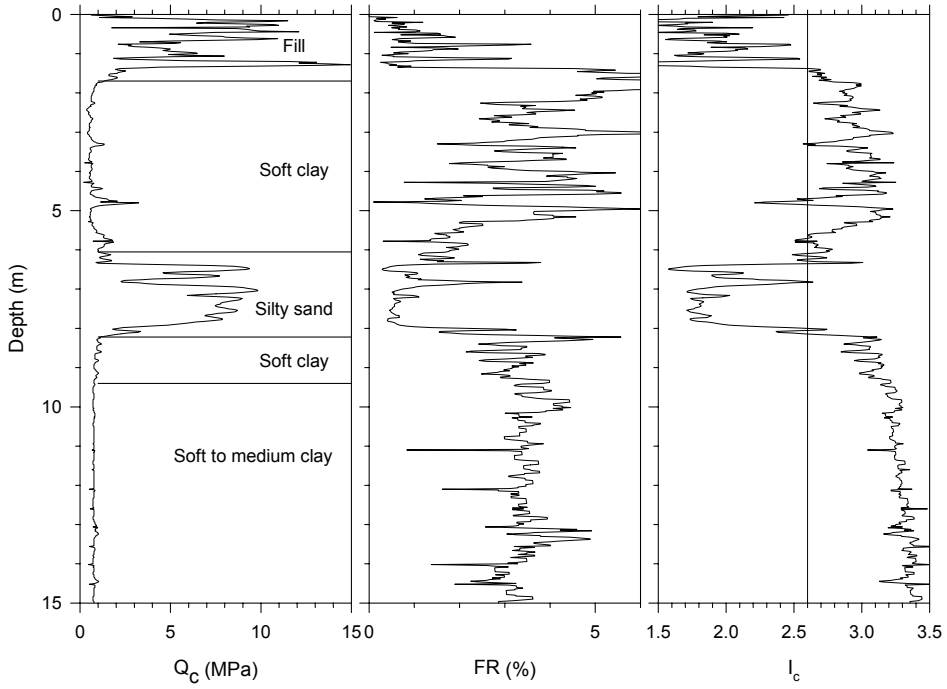

Figure 4-13. CPT sounding from Shopping Center area – C2

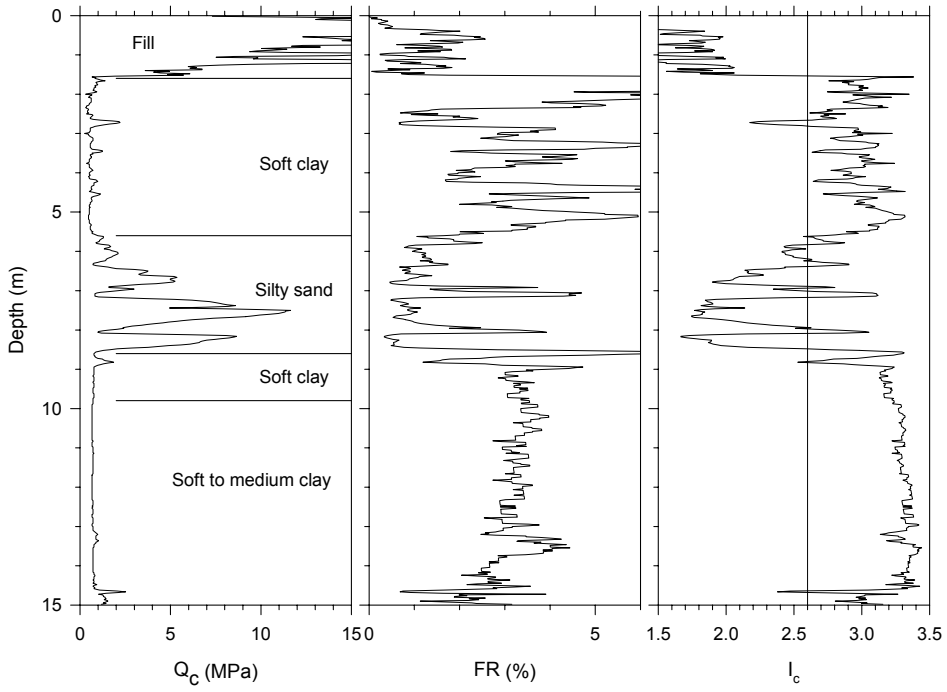

Figure 4-14. CPT sounding from Shopping Center area – C20

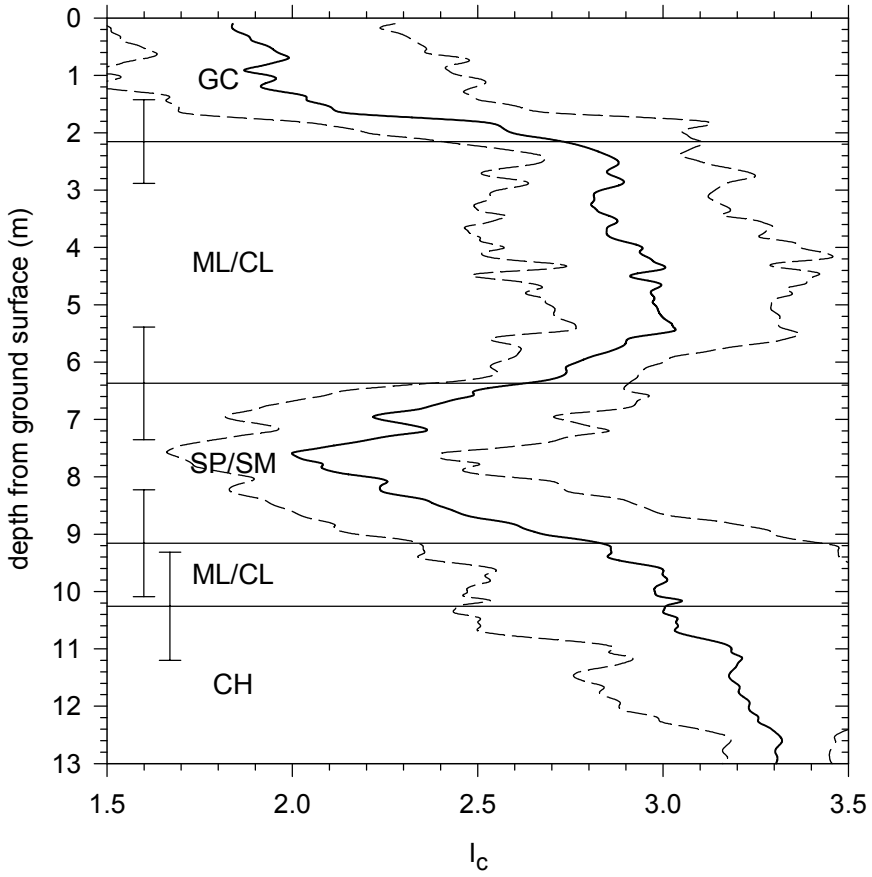

Figure 4-15. Soil behavior index (I_c) for the Shopping Center area. Median values and one standard deviation range from the CPT's at this section of the site. Layer boundaries inferred from these CPT's with mean values with plus/minus one standard deviation range.

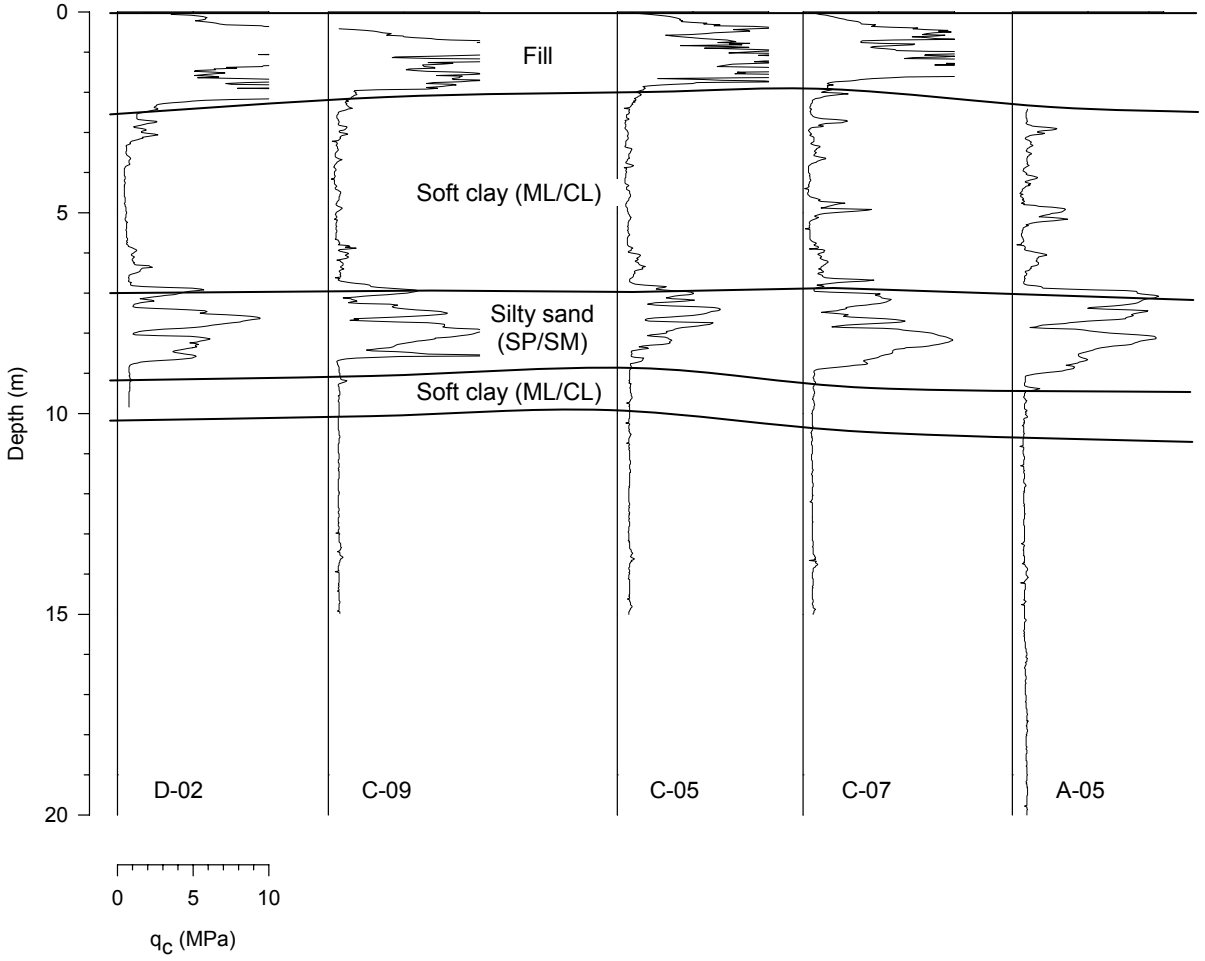

Figure 4-16. Cross section of soil layering - Shopping Center (section A-A)

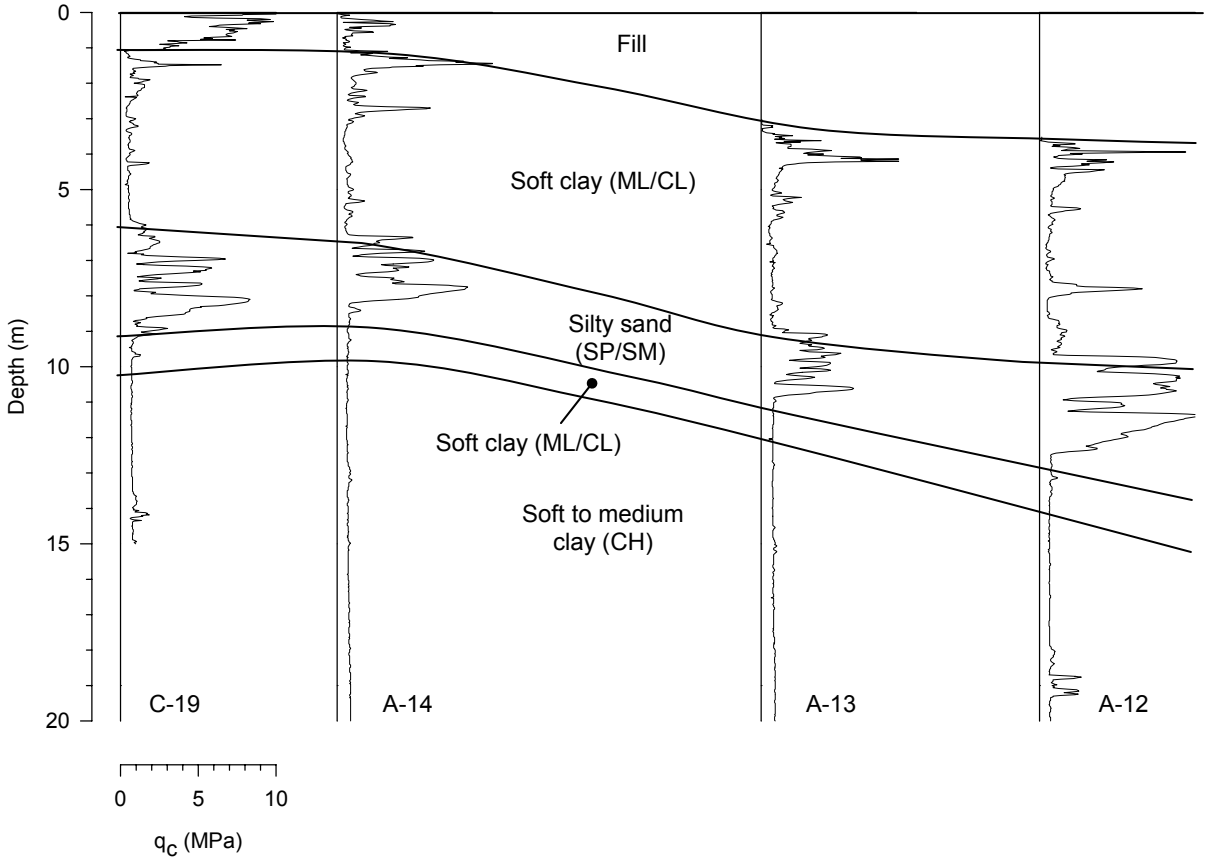

Figure 4-17. Cross section of soil layering - Shopping Center (section B-B)

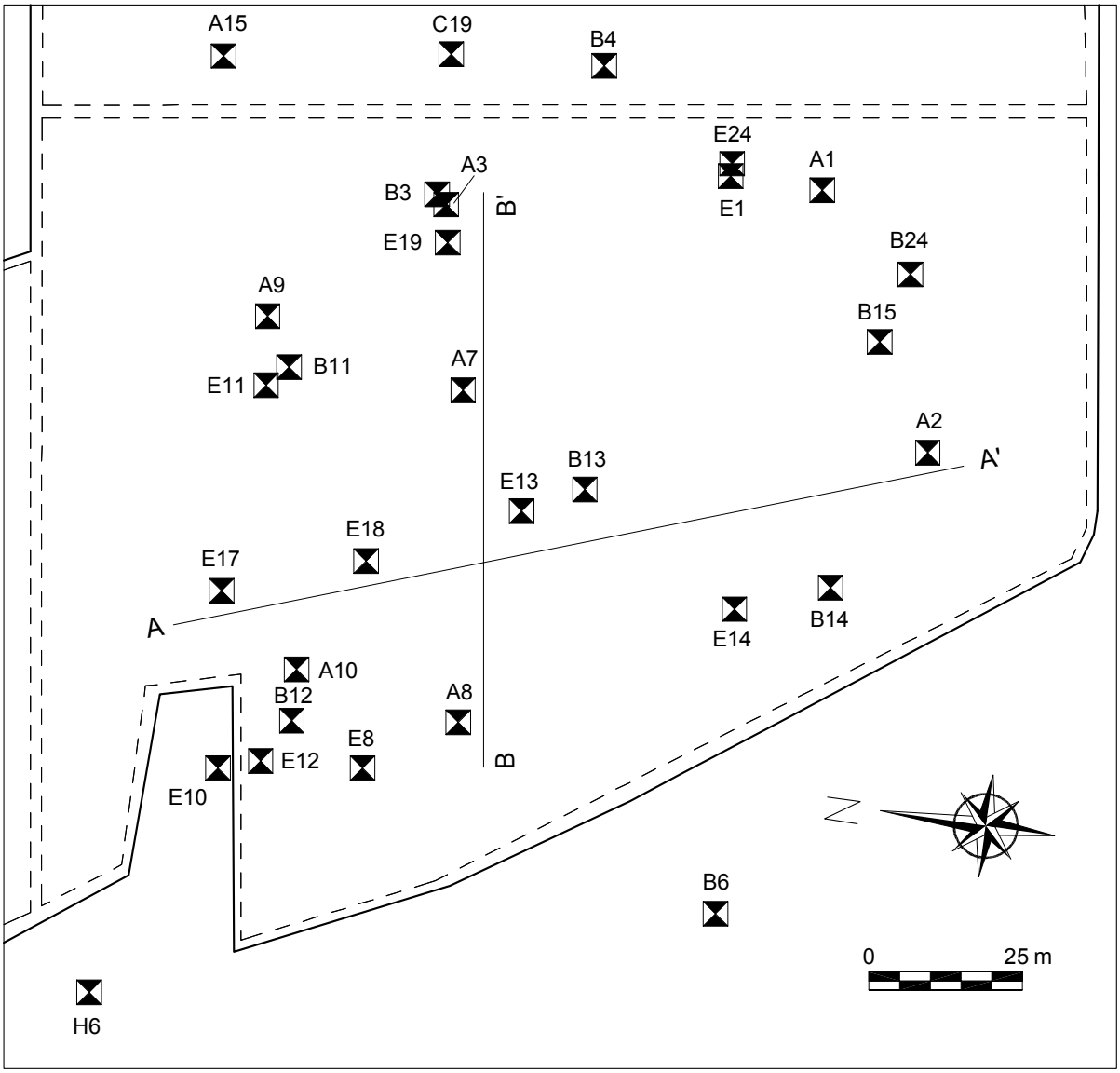

Figure 4-18. Parking Lot area – CPT locations

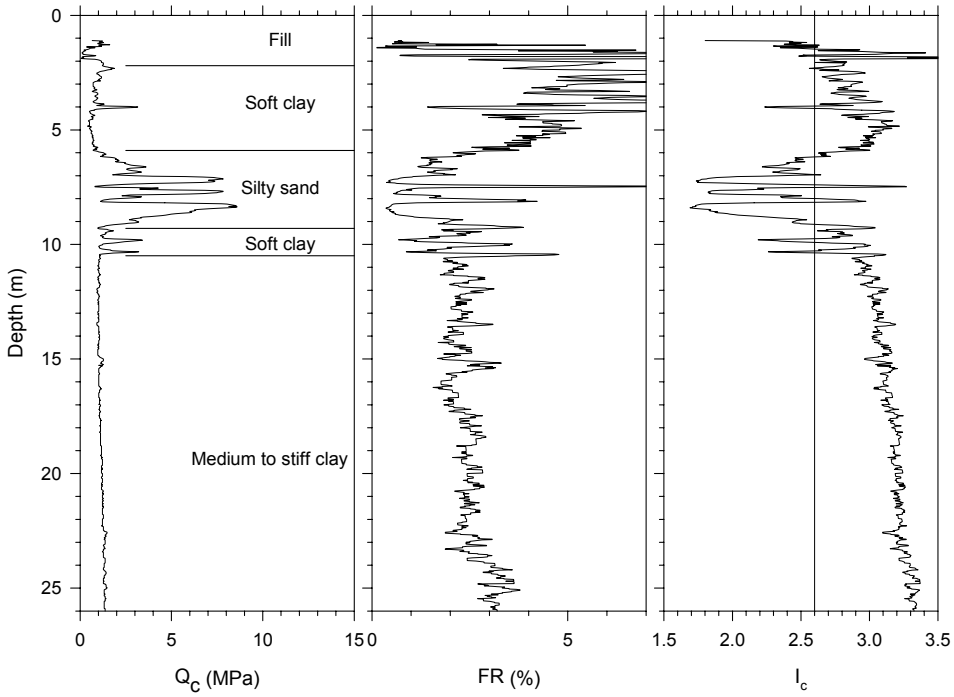

Figure 4-19. CPT sounding from Parking Lot area – A1

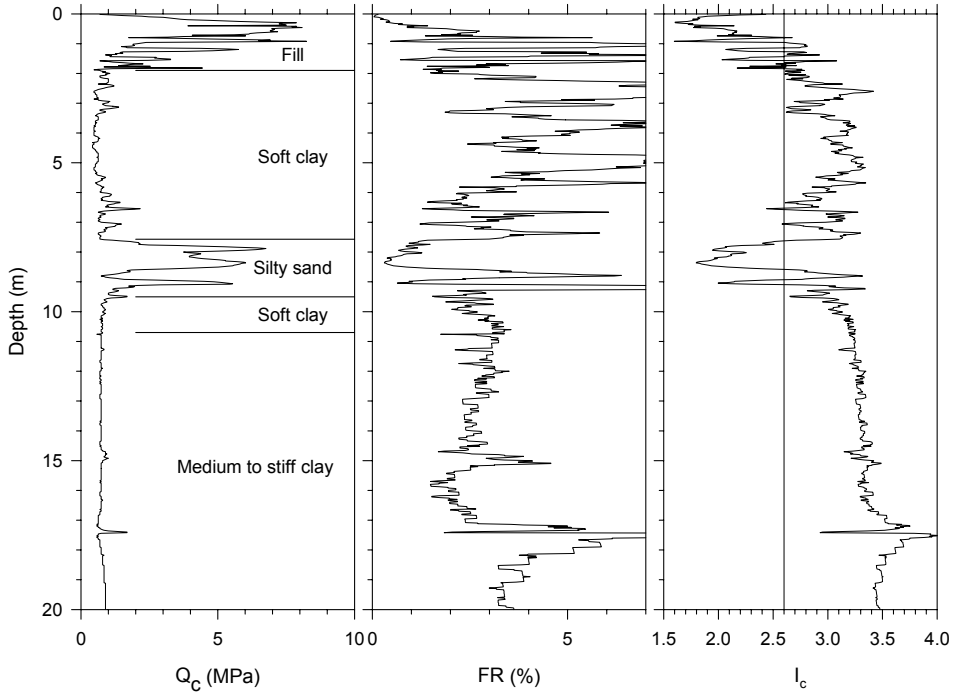

Figure 4-20. CPT sounding from Parking Lot area – E10

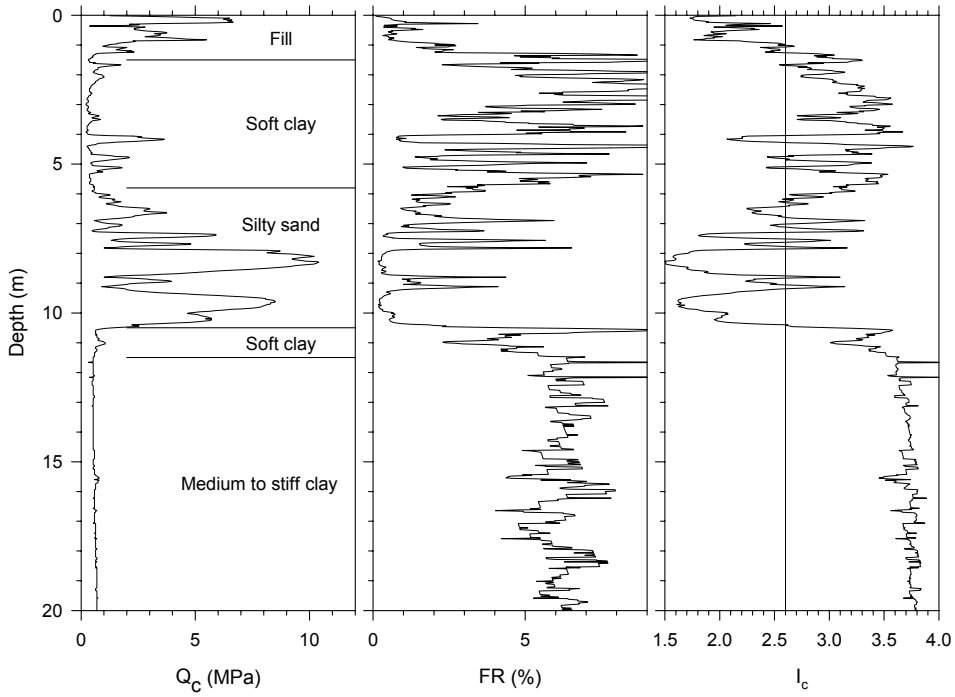

Figure 4-21. CPT sounding from Parking Lot area – E14

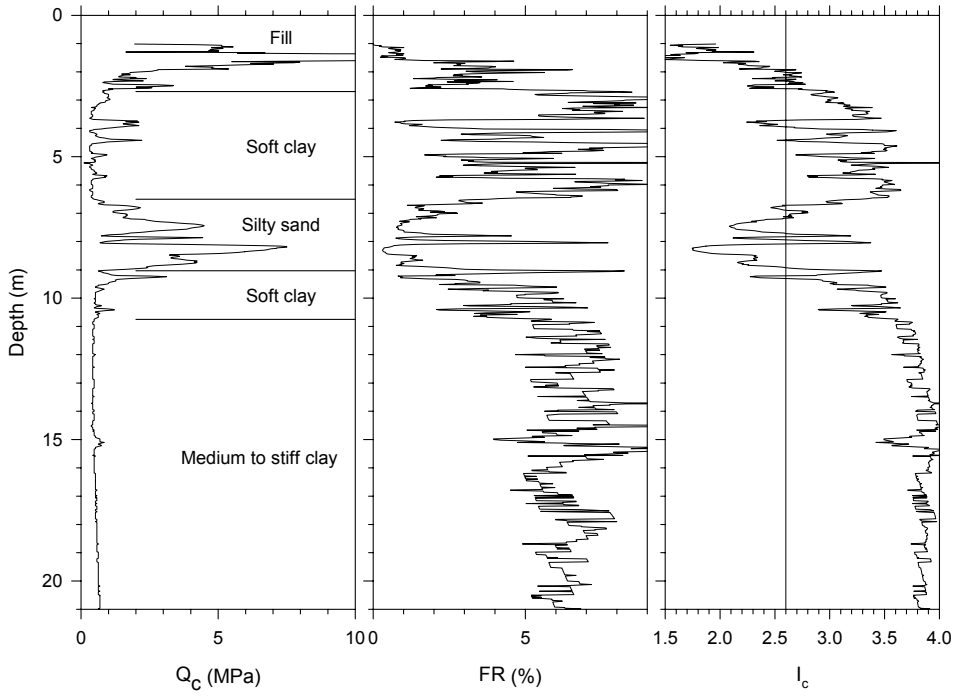

Figure 4-22. CPT sounding from Parking Lot area – E19

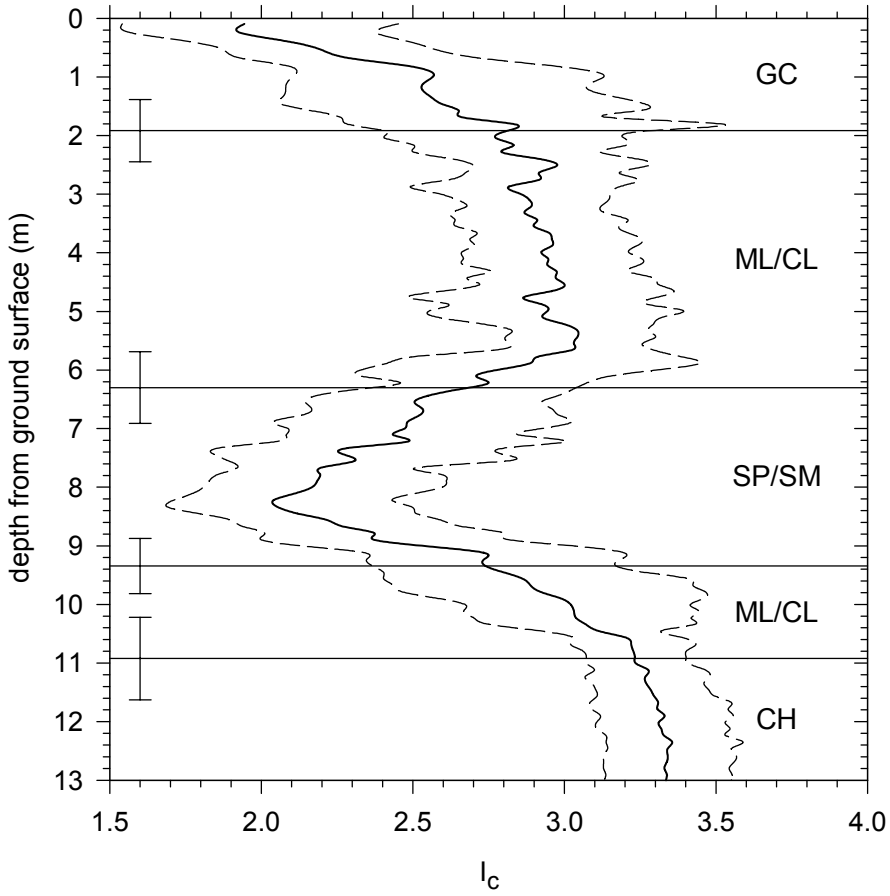

Figure 4-23. Soil behavior index (I_c) for the Parking Lot area. Median values and the 95% confidence interval (based on a log-normal distribution) from the CPT's at this section of the site. Layer boundaries inferred from these CPT's; mean values with plus/minus one standard deviation range.

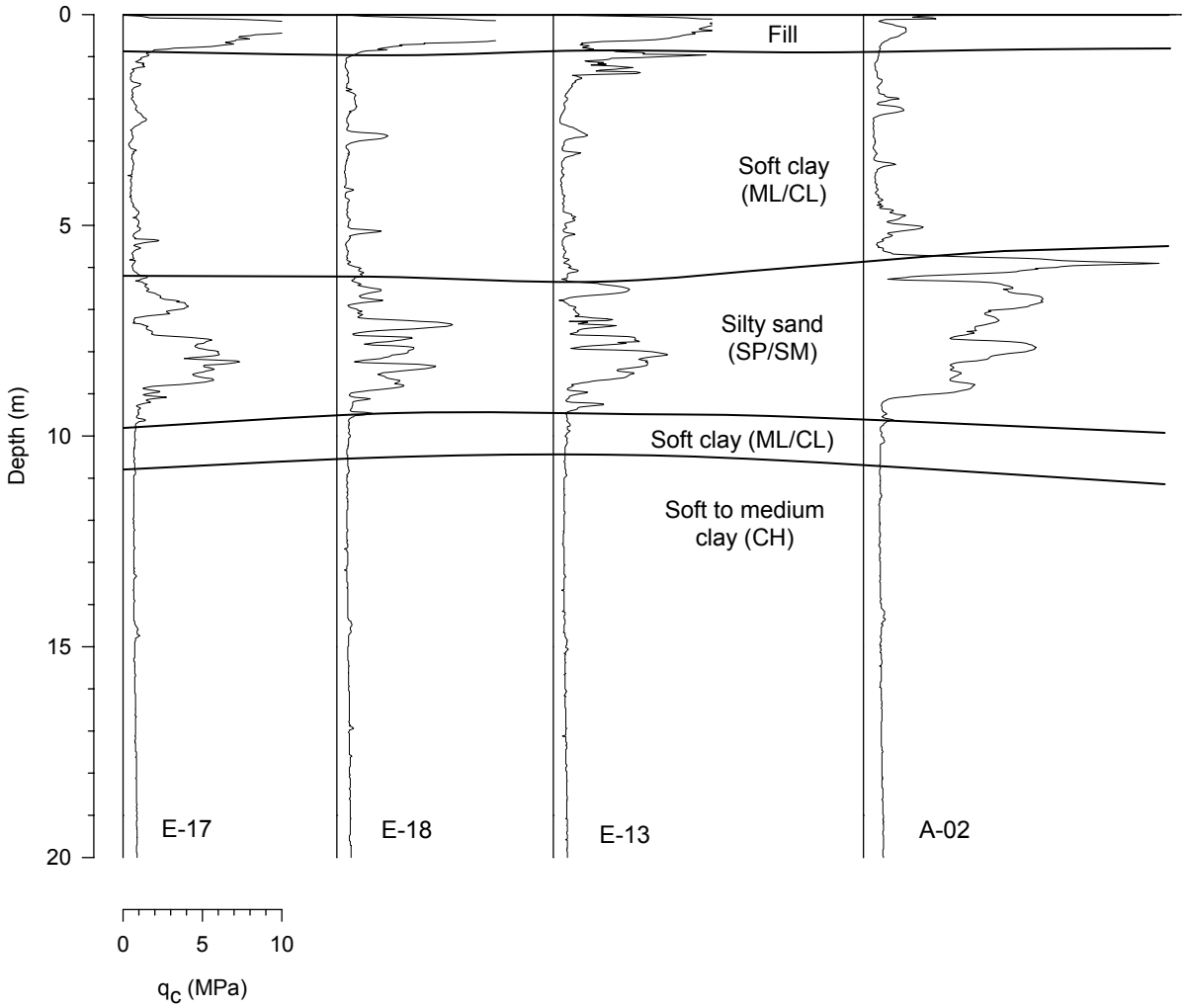

Figure 4-24. Cross section of soil layering – Parking Lot (section A-A)

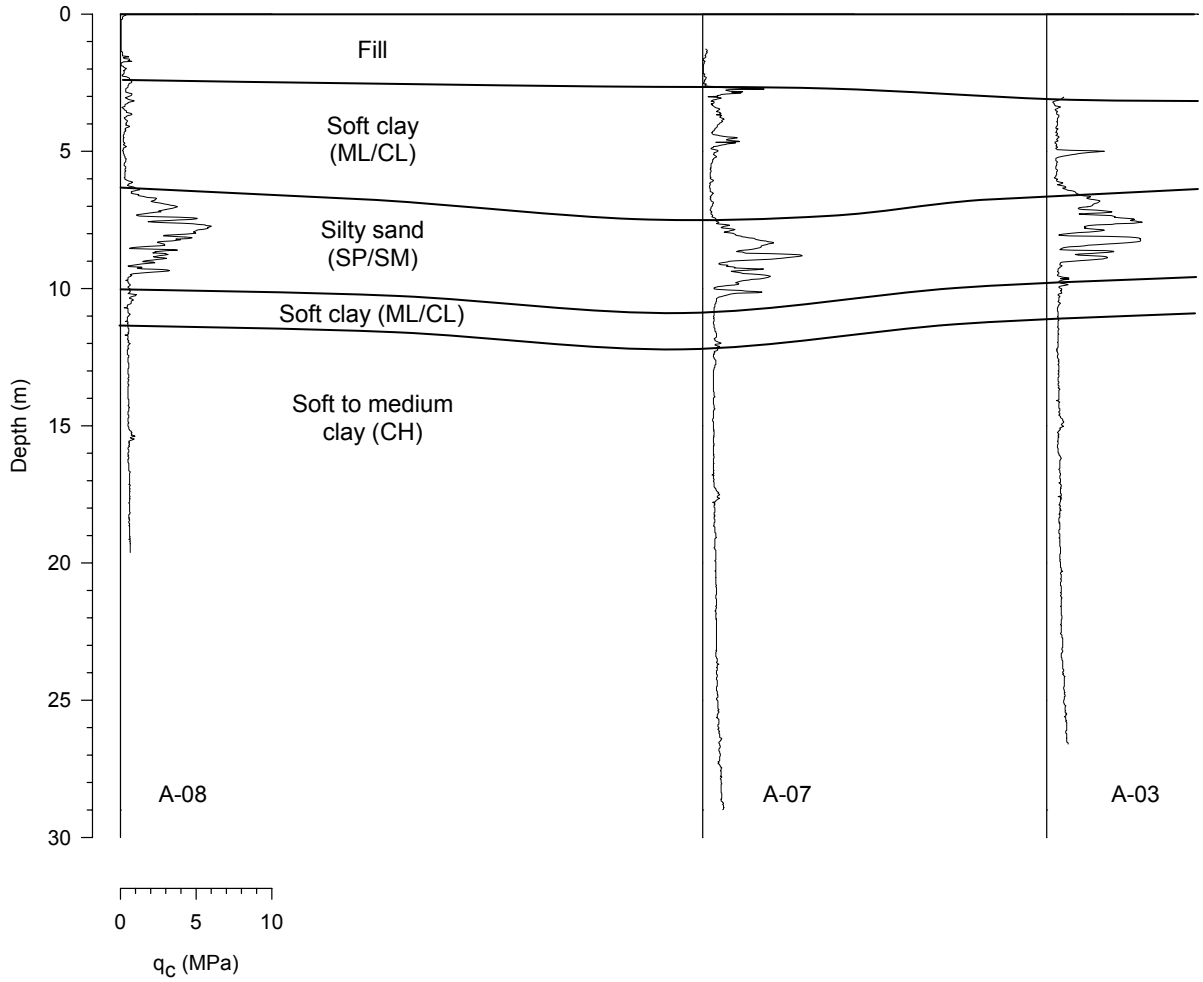

Figure 4-25. Cross section of soil layering – Parking Lot (section B-B)

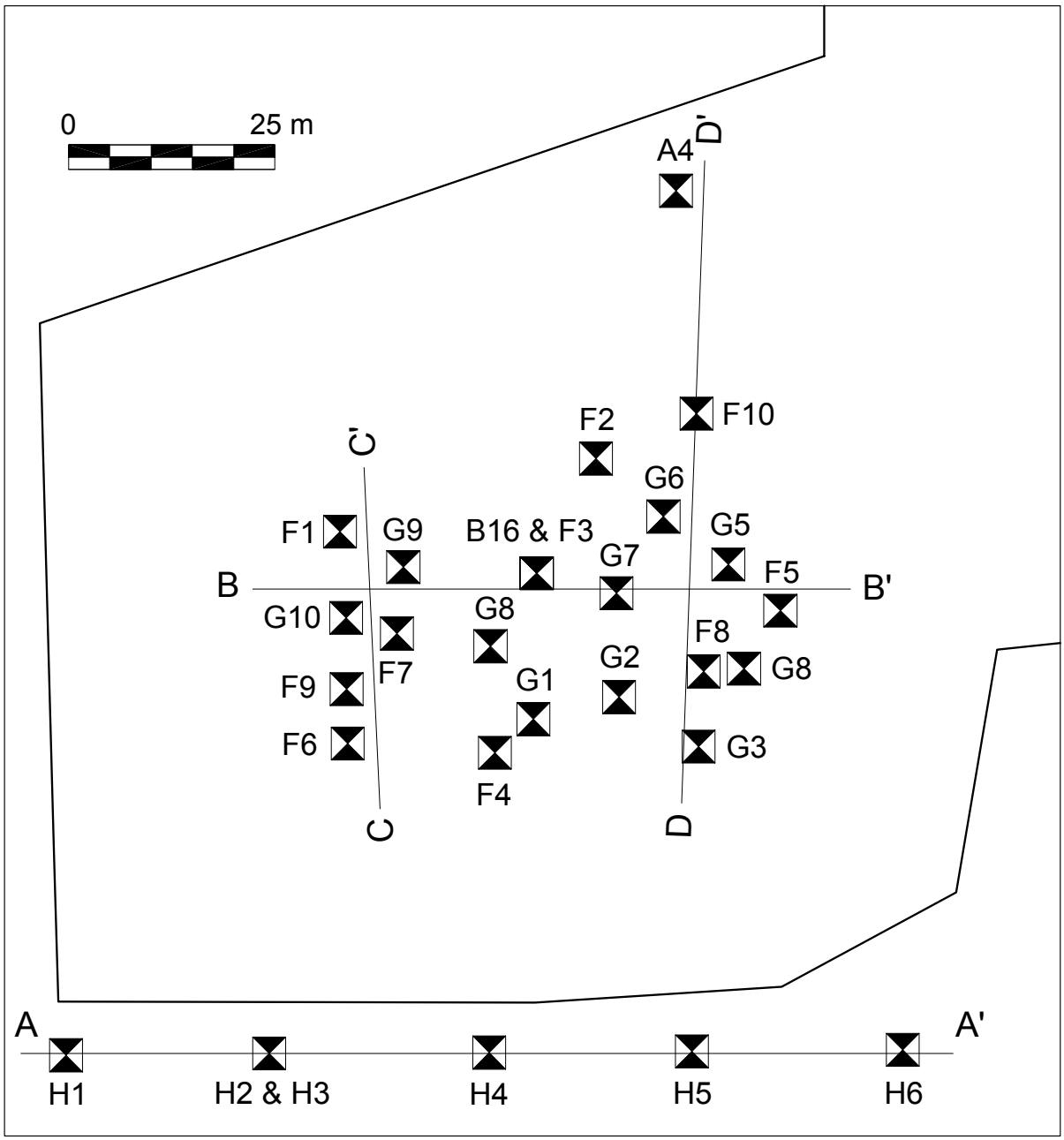

Figure 4-26. Lot C area – CPT locations

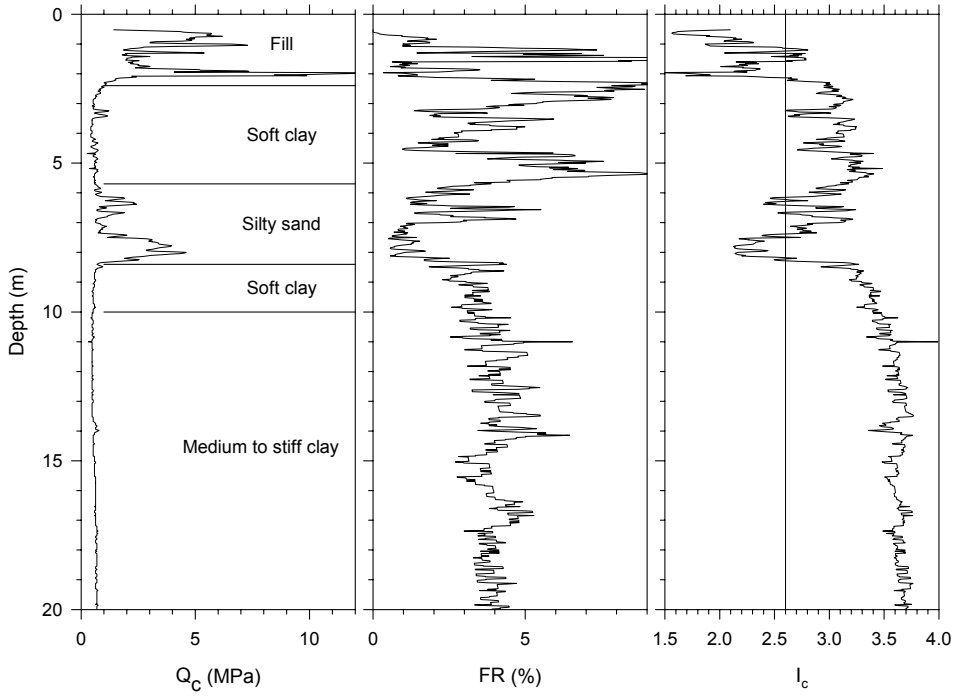

Figure 4-27. CPT sounding from Lot C area – F2

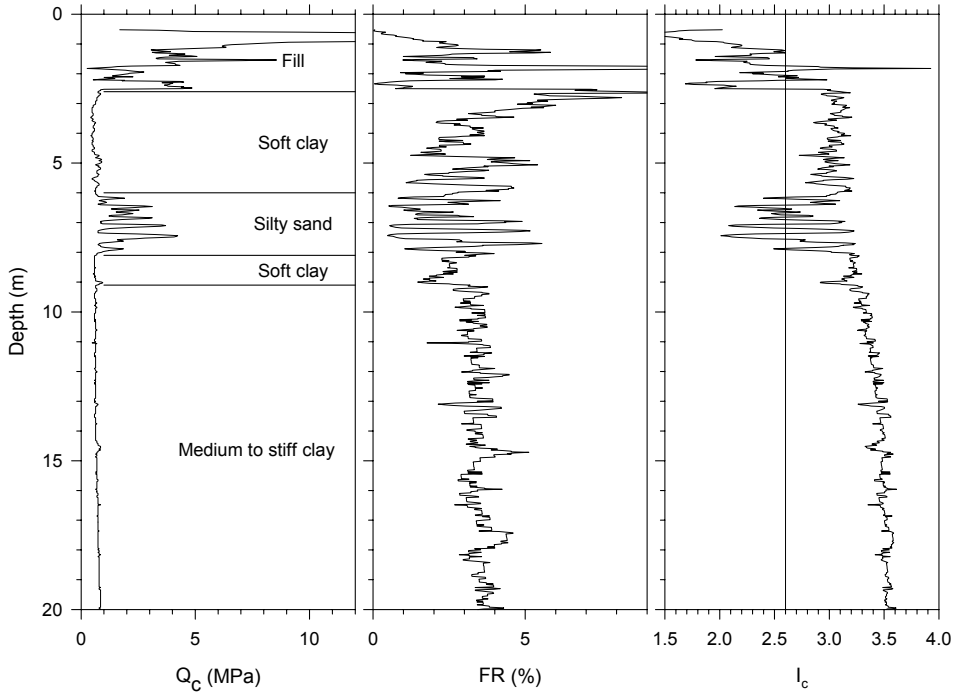

Figure 4-28. CPT sounding from Lot C area – F4

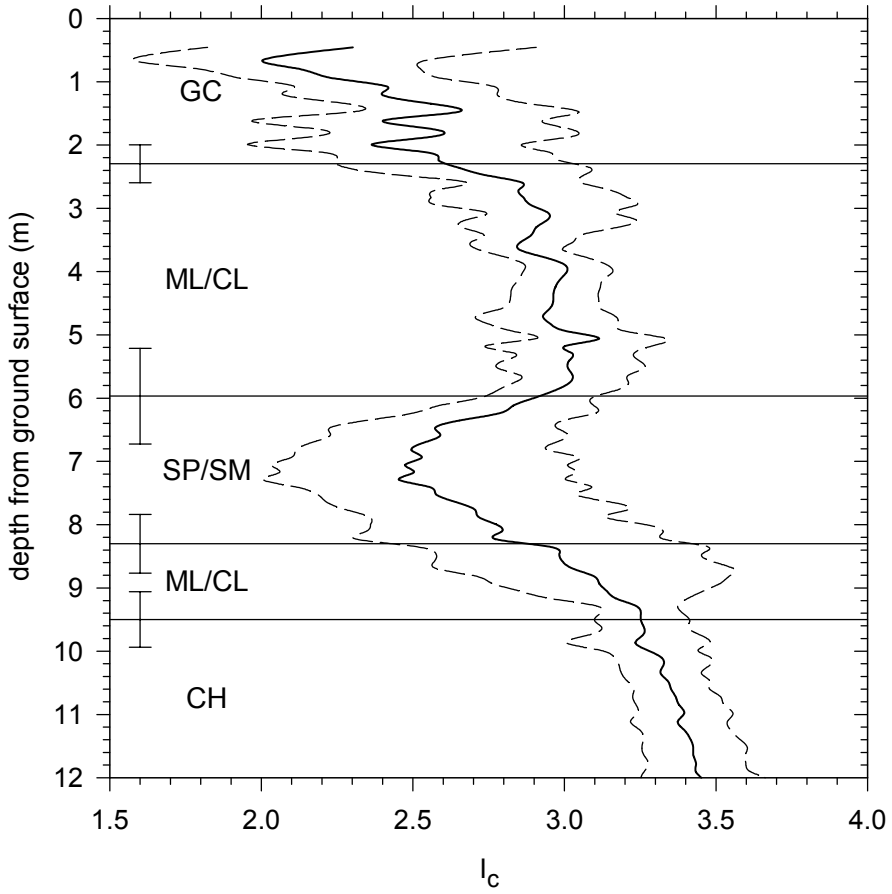

Figure 4-29. Soil behavior index (I_c) for the Lot C area. Median values and the 95% confidence interval (based on a log-normal distribution) from the CPT's at this section of the site. Layer boundaries inferred from these CPT's; mean values with plus/minus one standard deviation range.

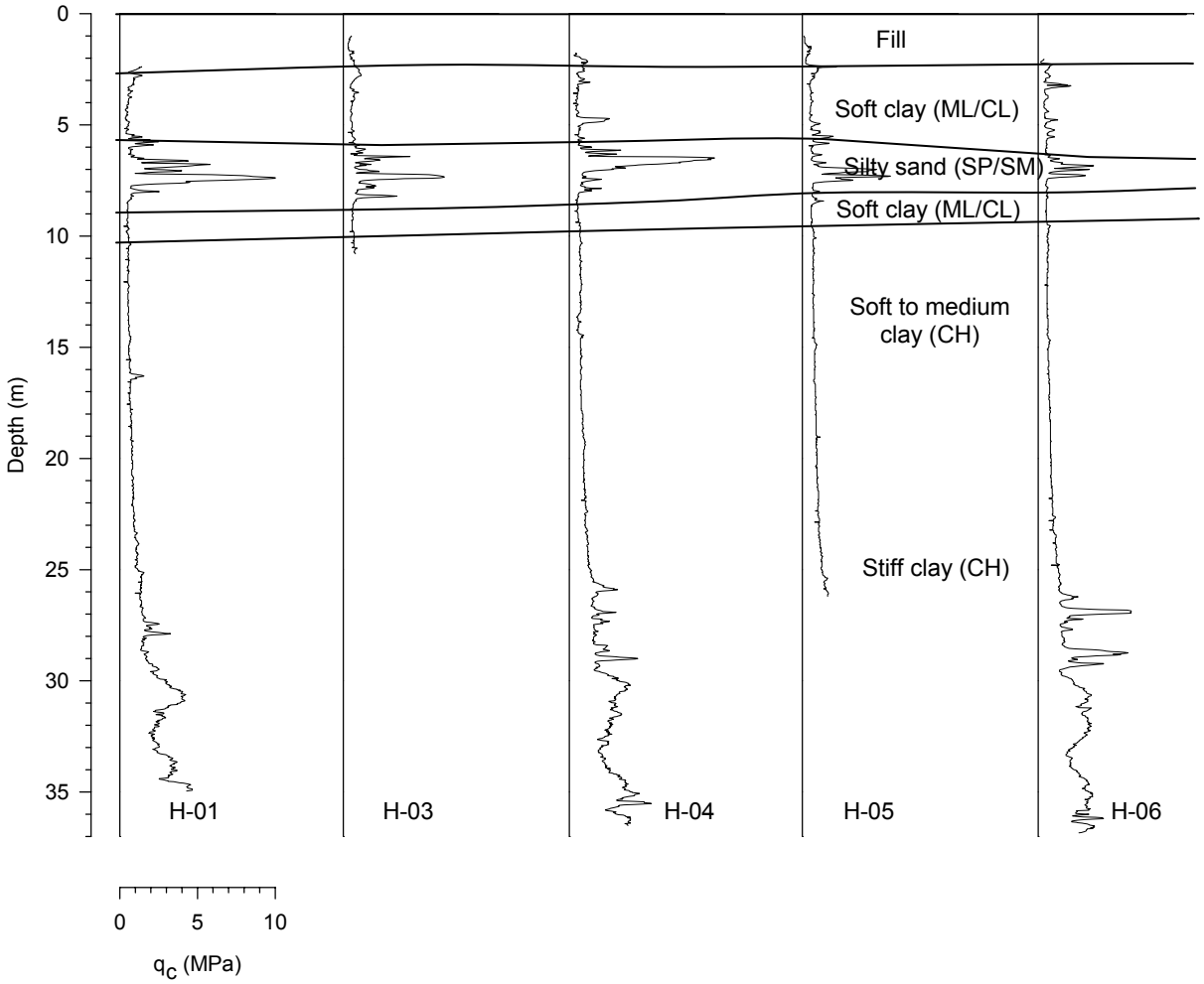

Figure 4-30. Cross section of soil layering – Lot C (section A-A)

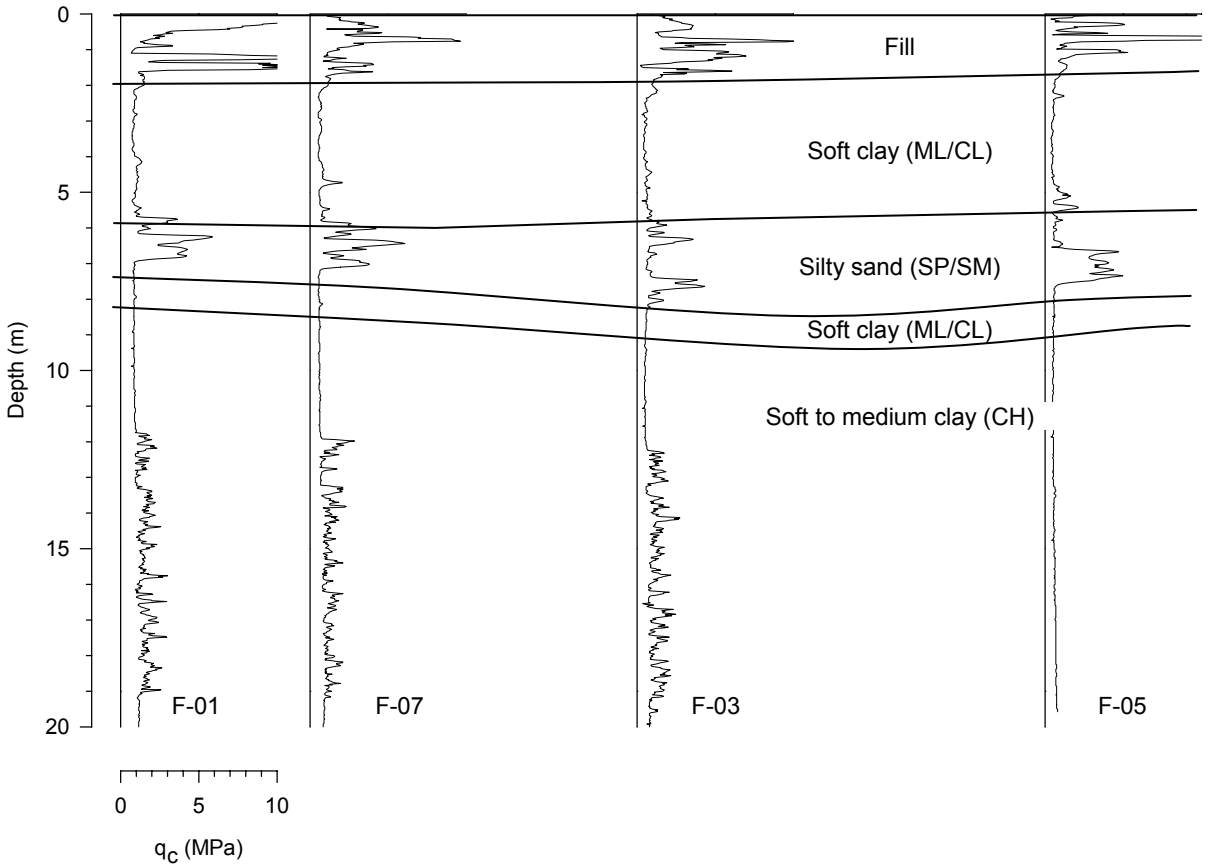

Figure 4-31. Cross section of soil layering – Lot C (section B-B)

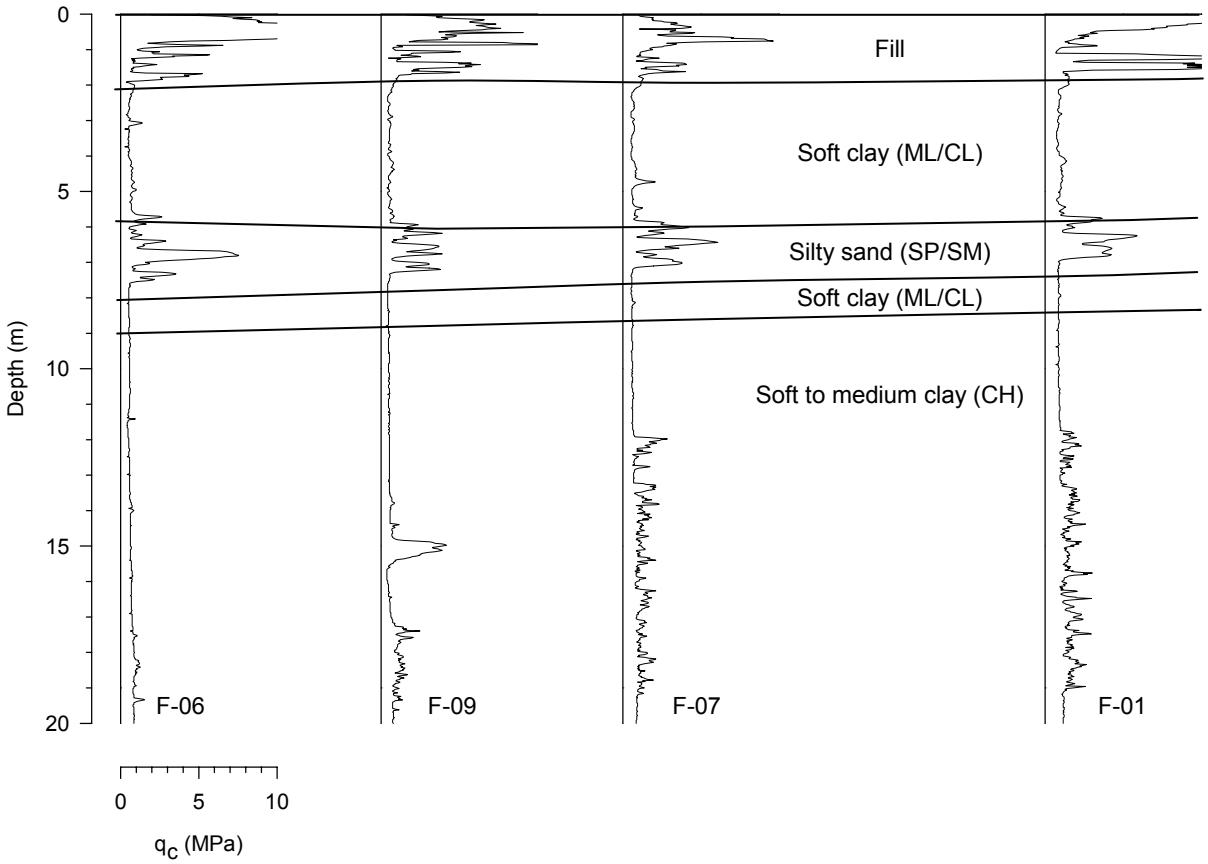

Figure 4-32. Cross section of soil layering – Lot C (section C-C)

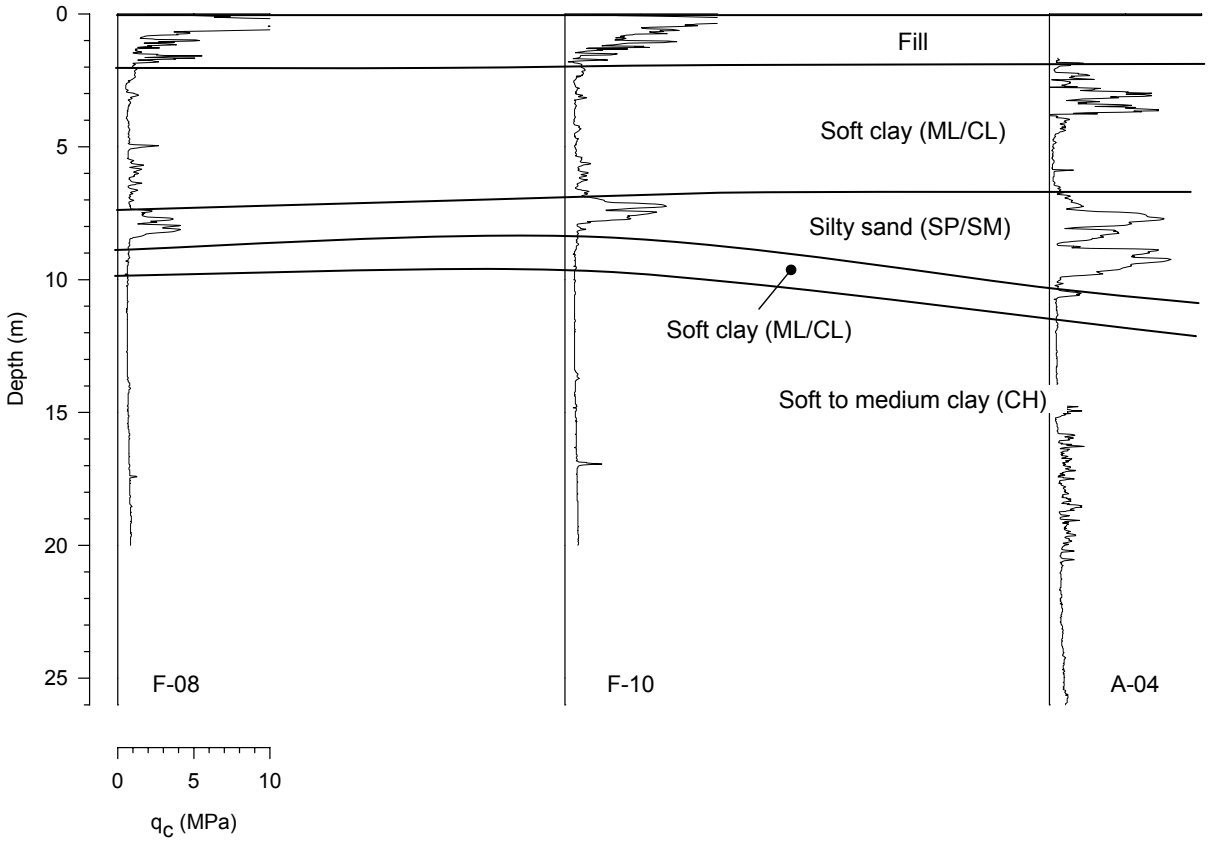

Figure 4-33. Cross section of soil layering – Lot C (section D-D)

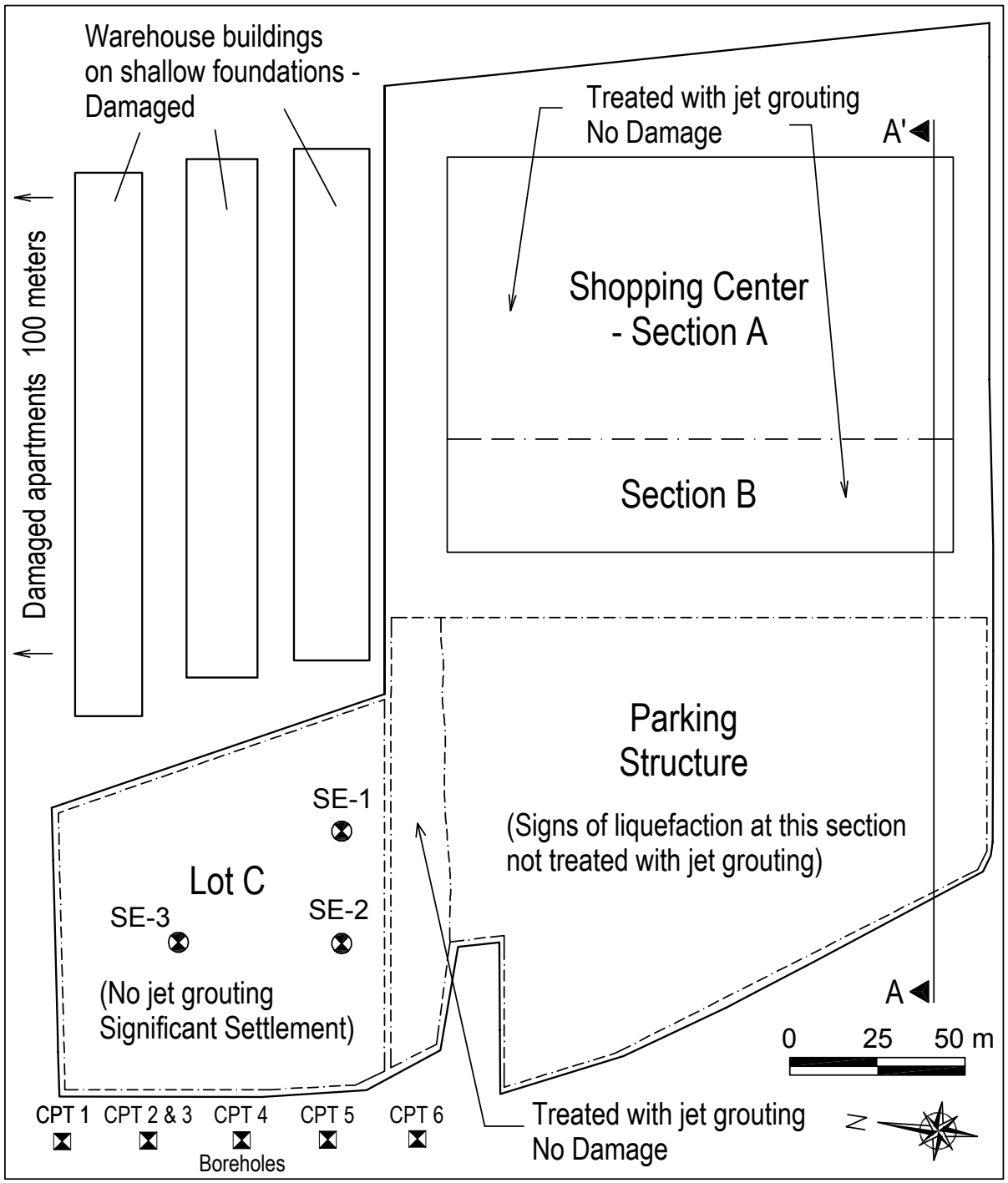

Figure 4-34. Site plan of Carrefour Shopping Center showing improved area and unimproved areas along with observed earthquake damages. Locations of post-earthquake soil investigations are also indicated.

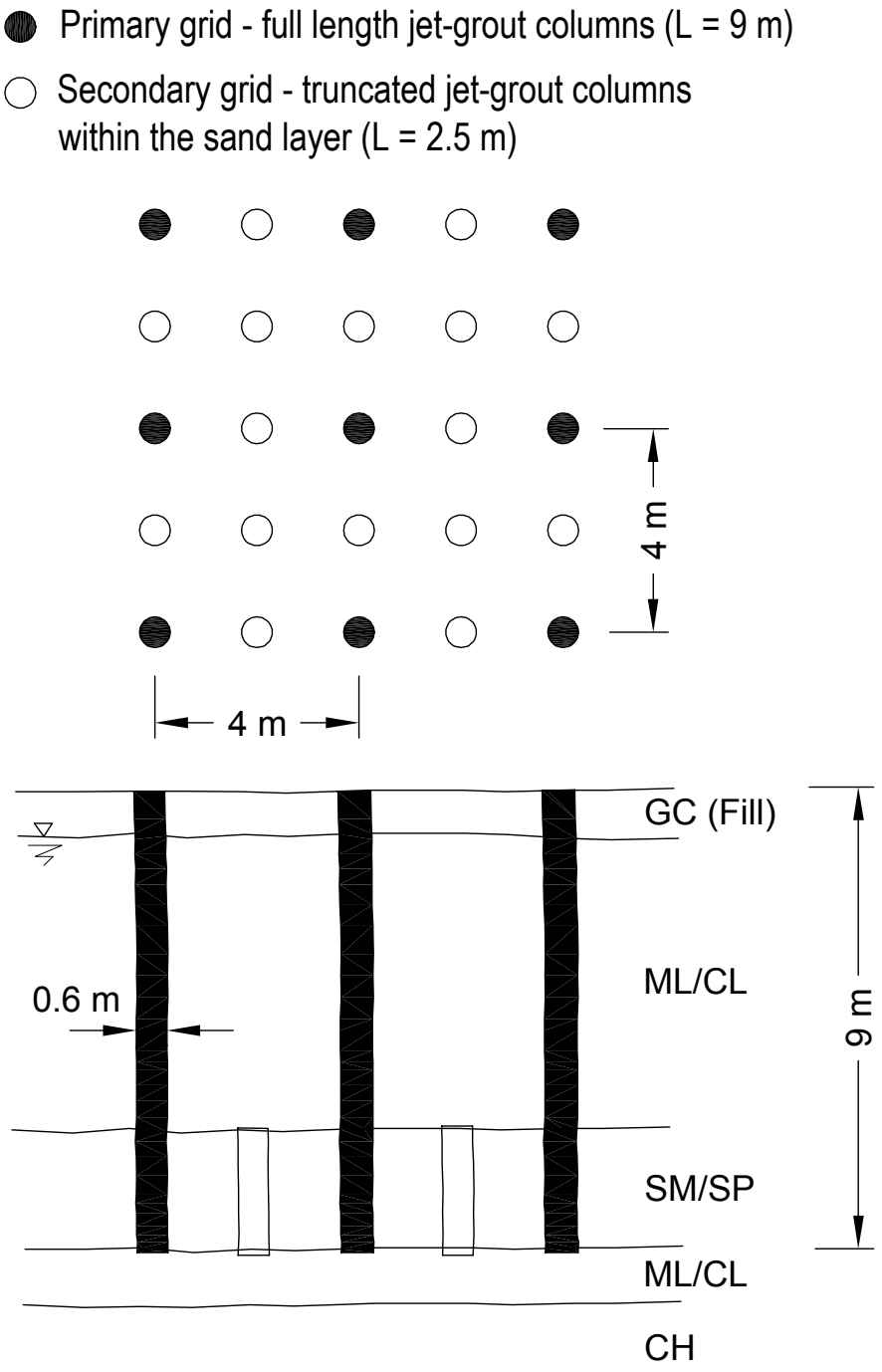

Figure 4-35. Layout of jet-grout columns used for blanket treatment beneath Shopping Center building at Carrefour site. Additional columns were used at footing locations to provide additional bearing support. Average replacement ratio beneath building was about 7% in the SM layer and 2% in overlying strata.

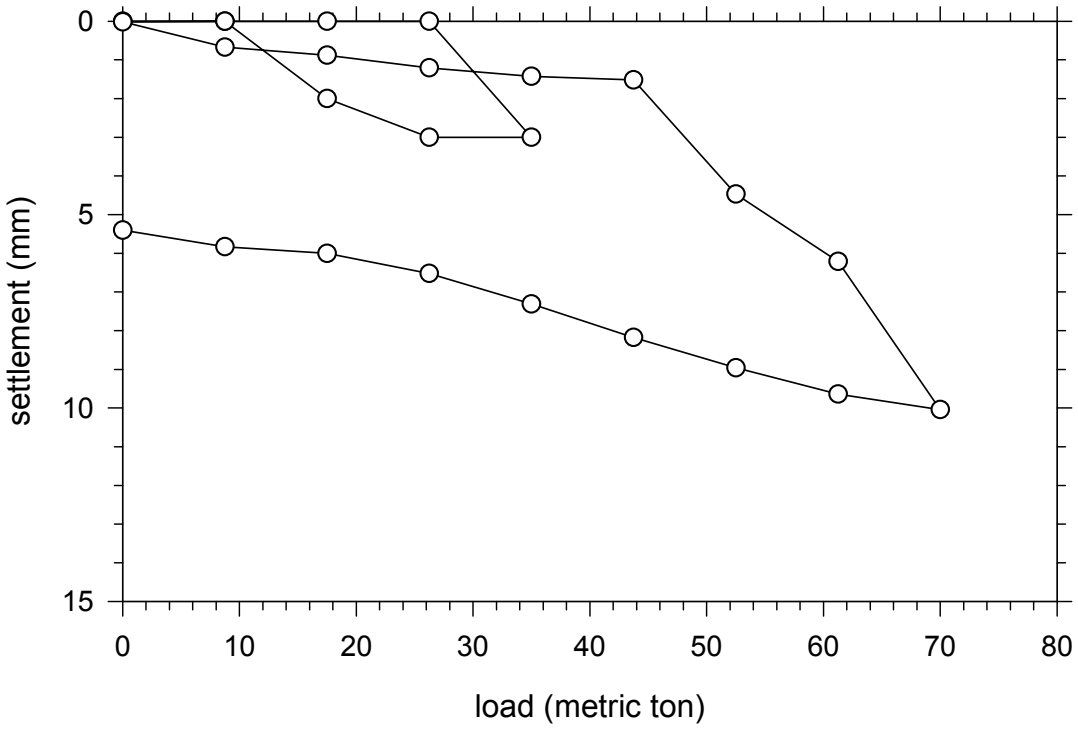

Figure 4-36. Jet grout load test performed during construction as part of the QA/QC program

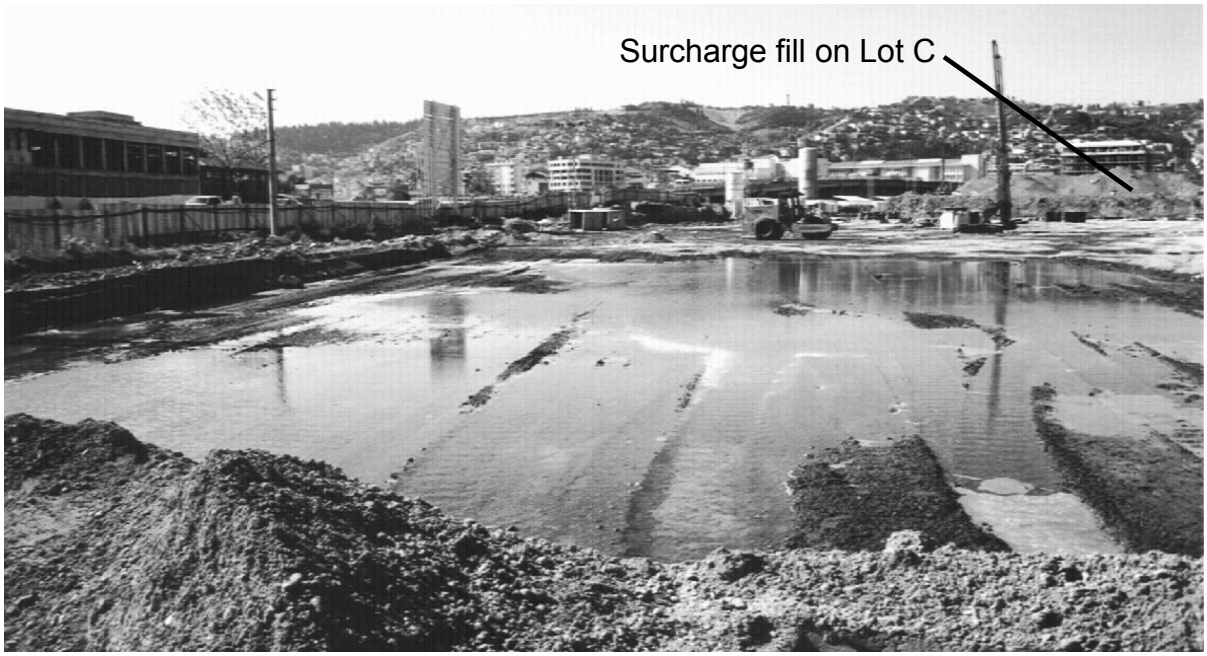

Figure 4-37. Ponding of water (7 to 10 cm deep) at untreated portions of the parking structure that was expelled through wick drains following the M7.4 Kocaeli Earthquake. Lot C, under surcharge fill, is visible at the right rear of the inundated area. Photograph taken the morning after the event.

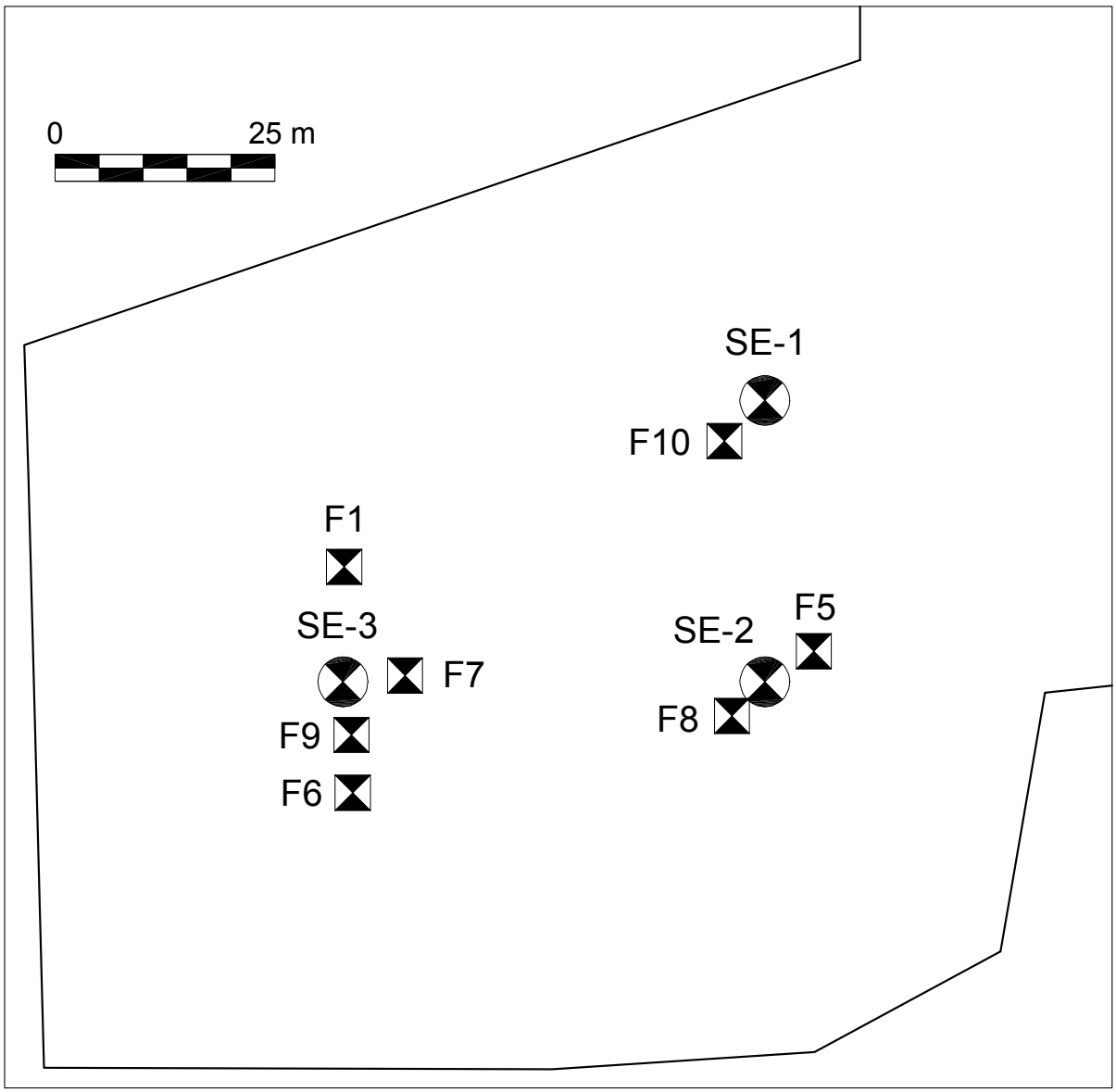

Figure 4-38. Lot C area – location of settlement extensometers and the nearby CPTs

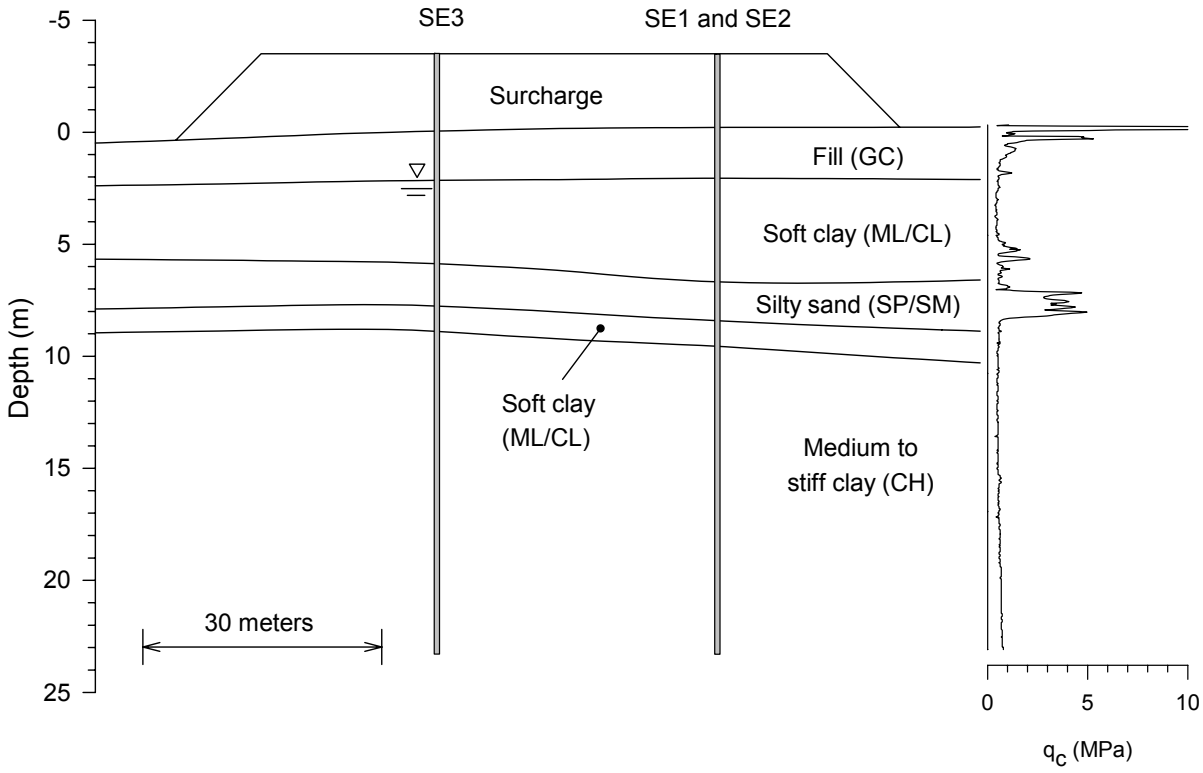

Figure 4-39. Soil layering and surcharge fill at Lot C

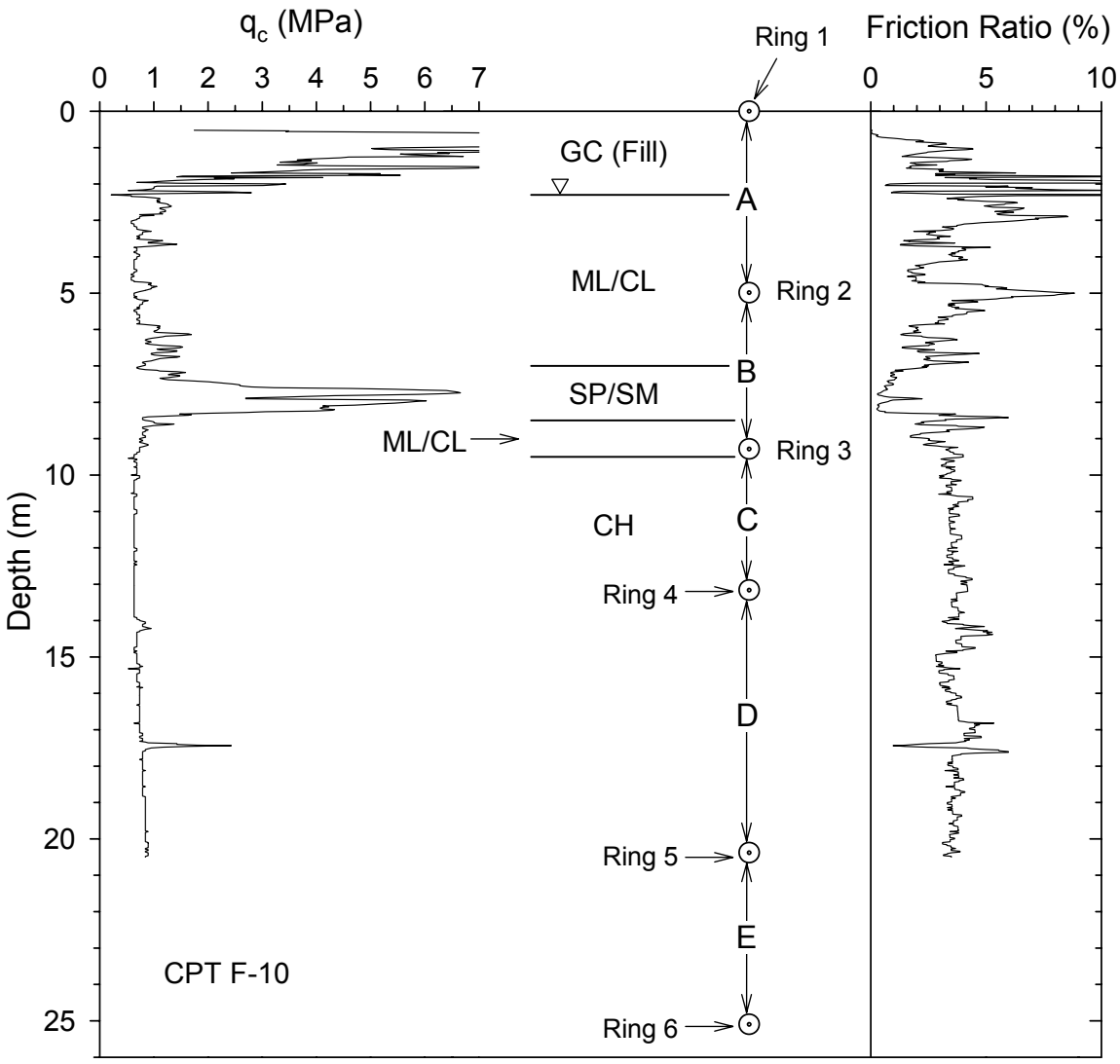

Figure 4-40. Soil conditions near SE1 in Lot C (unimproved soils) where settlements were measured. Figure shows positions of settlement rings, soil layers A – E, and CPT results.

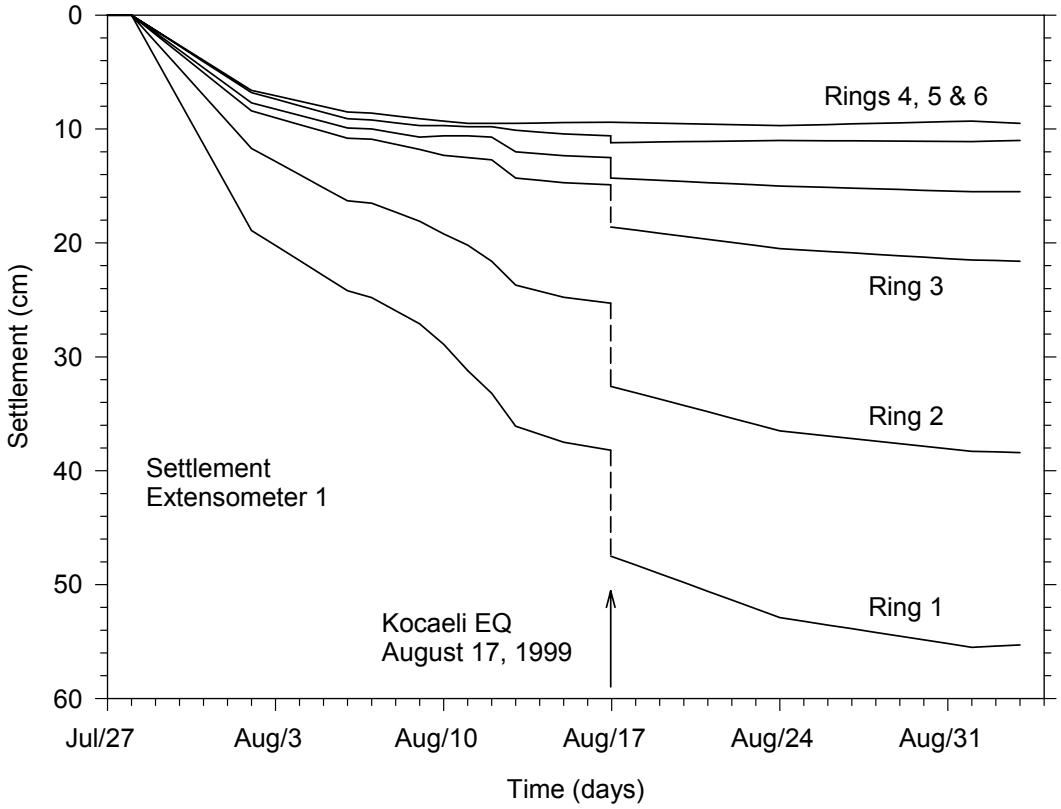

Figure 4-41. Settlement of magnetic rings – Settlement extensometer 1

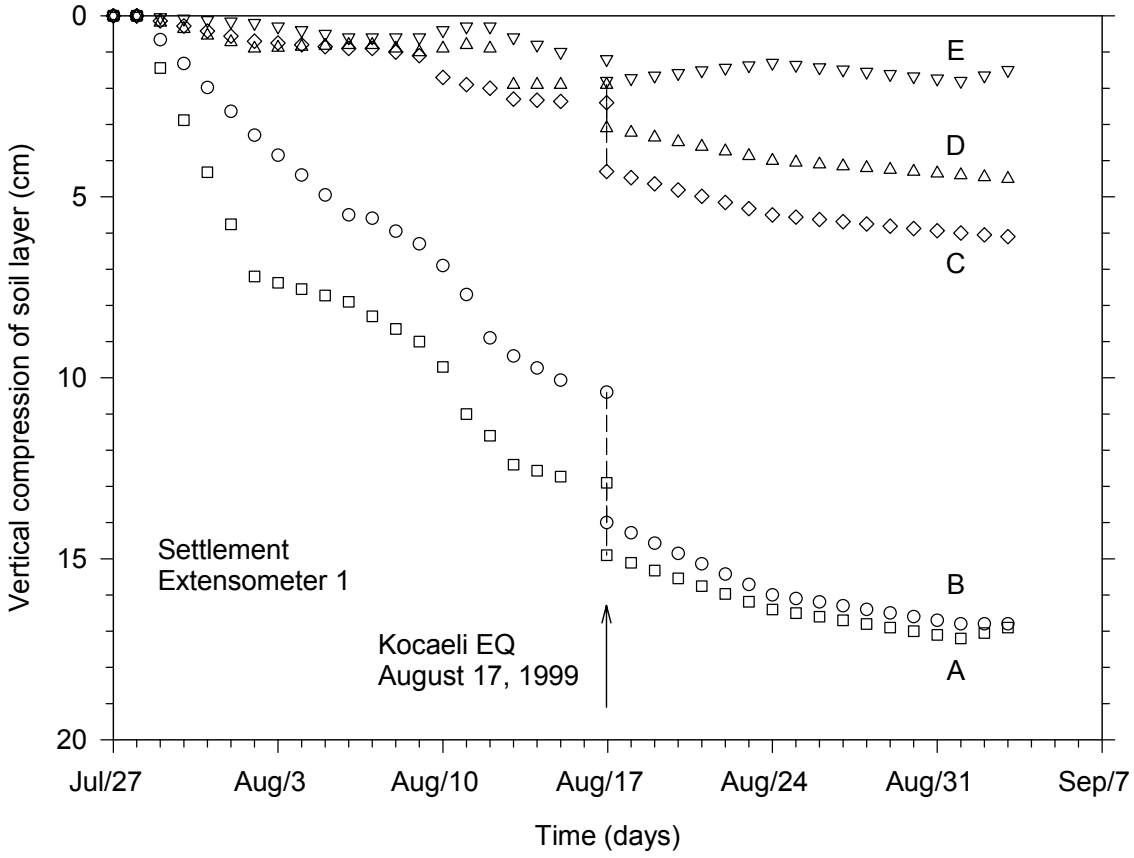

Figure 4-42. Vertical deformation of soil layers – Settlement extensometer 1

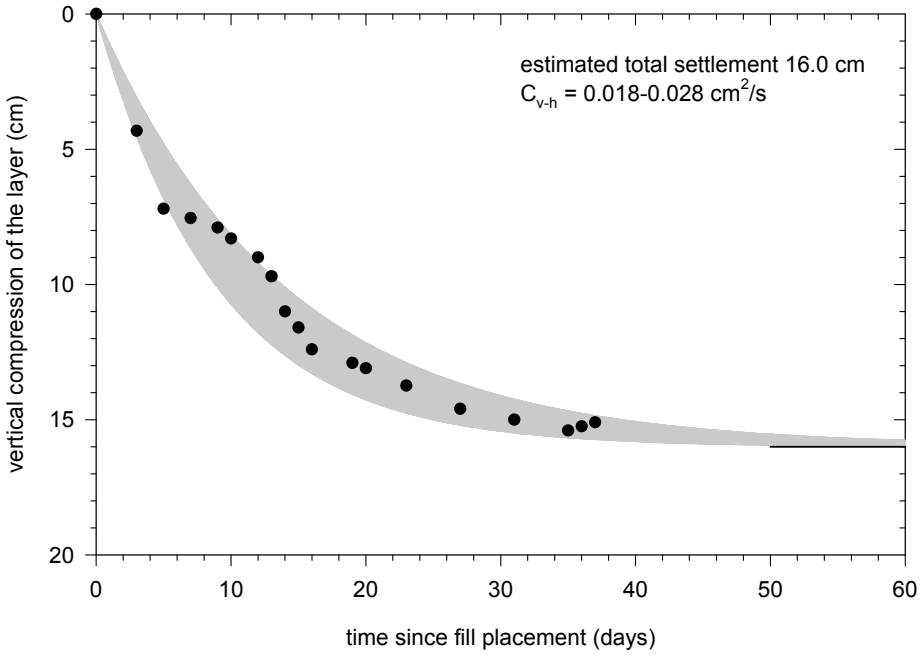

Figure 4-43. Settlement extensometer 1 – Layer A : measured settlements, estimated coefficient of consolidation and estimated total consolidation settlement

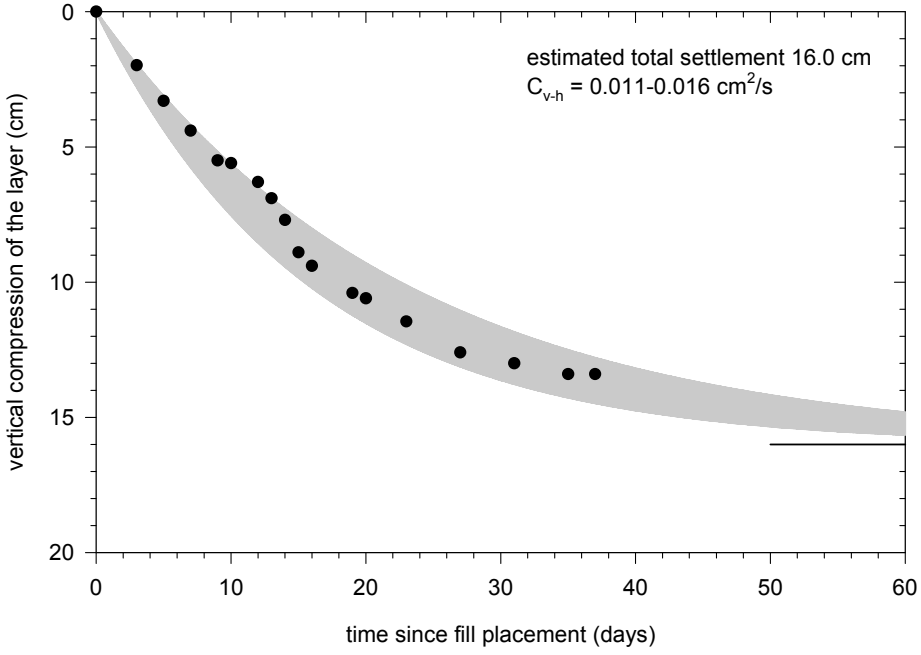

Figure 4-44. Settlement extensometer 1 – Layer B : measured settlements, estimated coefficient of consolidation and estimated total consolidation settlement

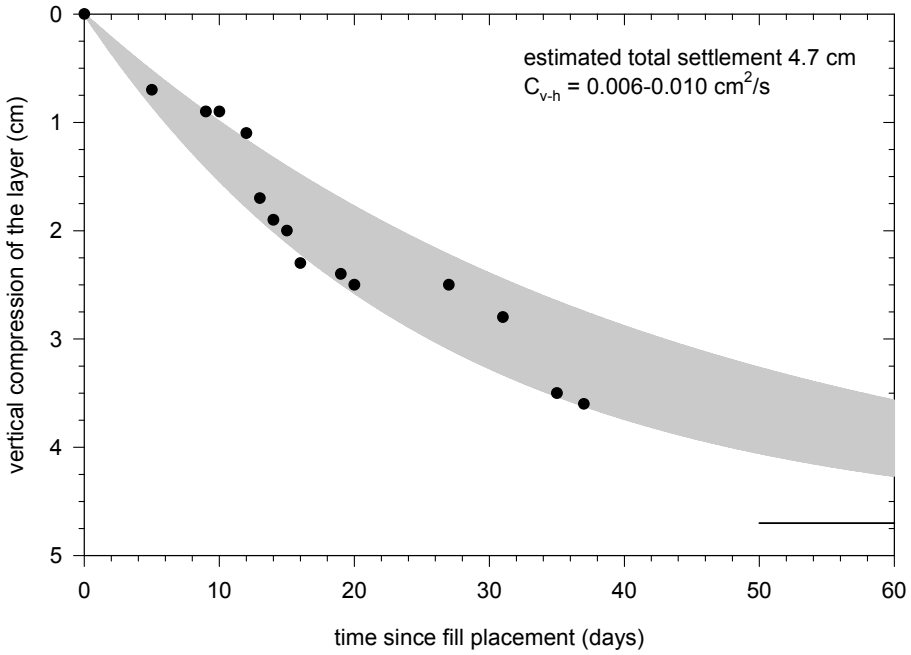

Figure 4-45. Settlement extensometer 1 – Layer C : measured settlements, estimated coefficient of consolidation and estimated total consolidation settlement

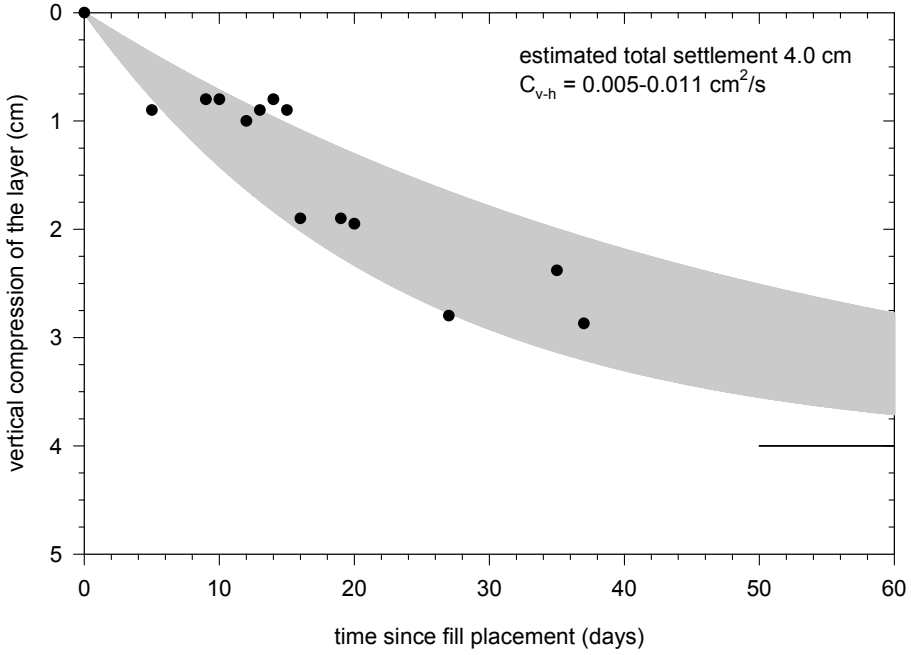

Figure 4-46. Settlement extensometer 1 – Layer D : measured settlements, estimated coefficient of consolidation and estimated total consolidation settlement

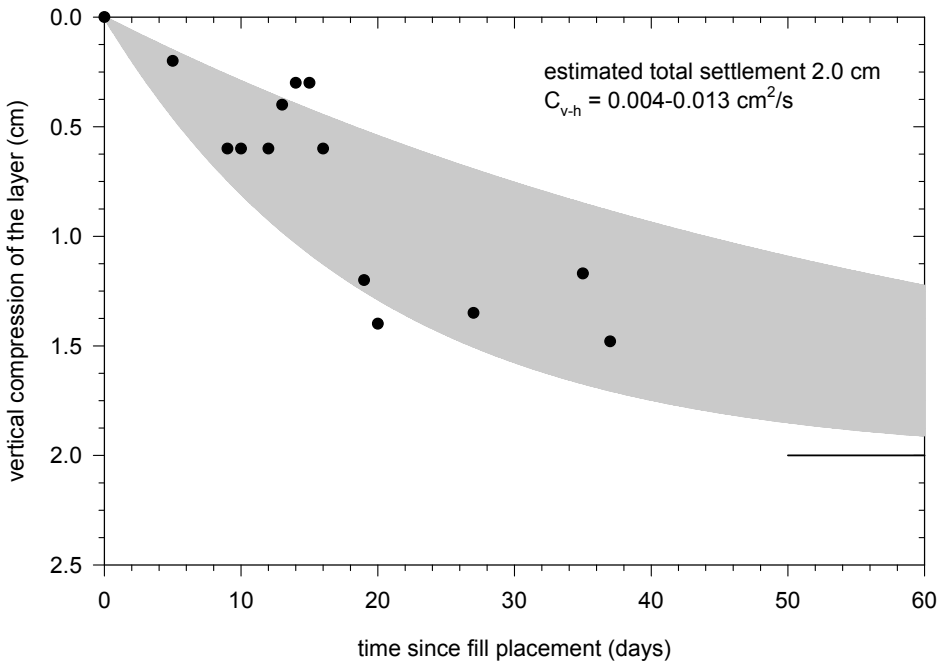

Figure 4-47. Settlement extensometer 1 – Layer E : measured settlements, estimated coefficient of consolidation and estimated total consolidation settlement

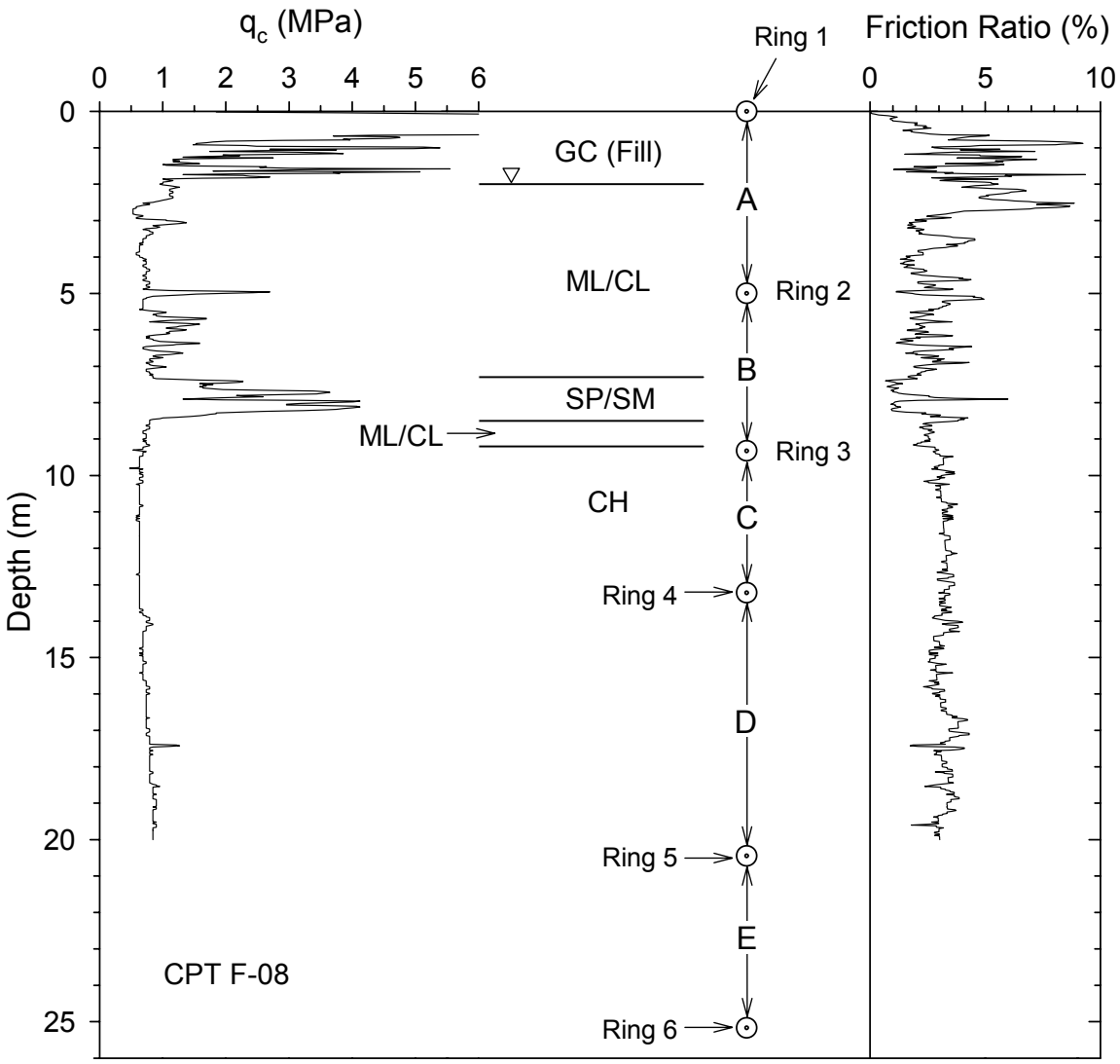

Figure 4-48. Soil conditions near SE2 in Lot C (unimproved soils) where settlements were measured. Figure shows positions of settlement rings, soil layers A – E, and CPT results.

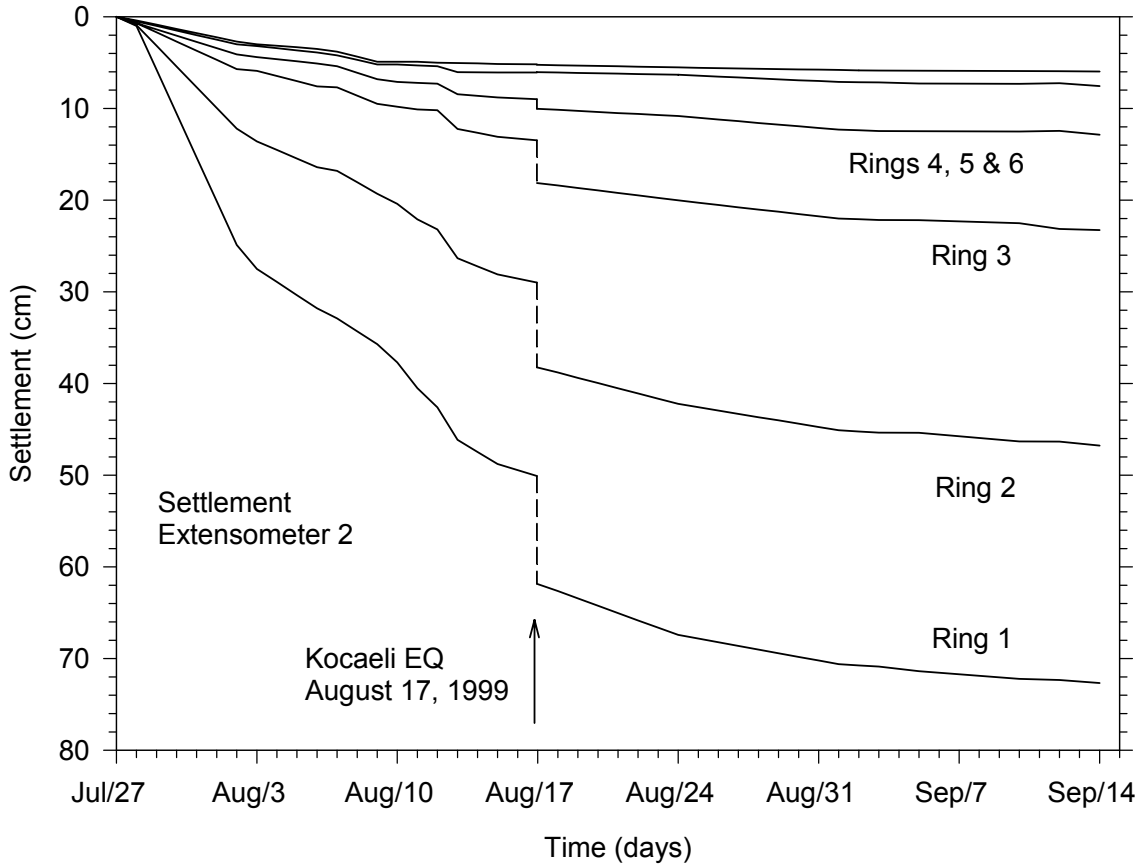

Figure 4-49. Settlement of magnetic rings – Settlement extensometer 2

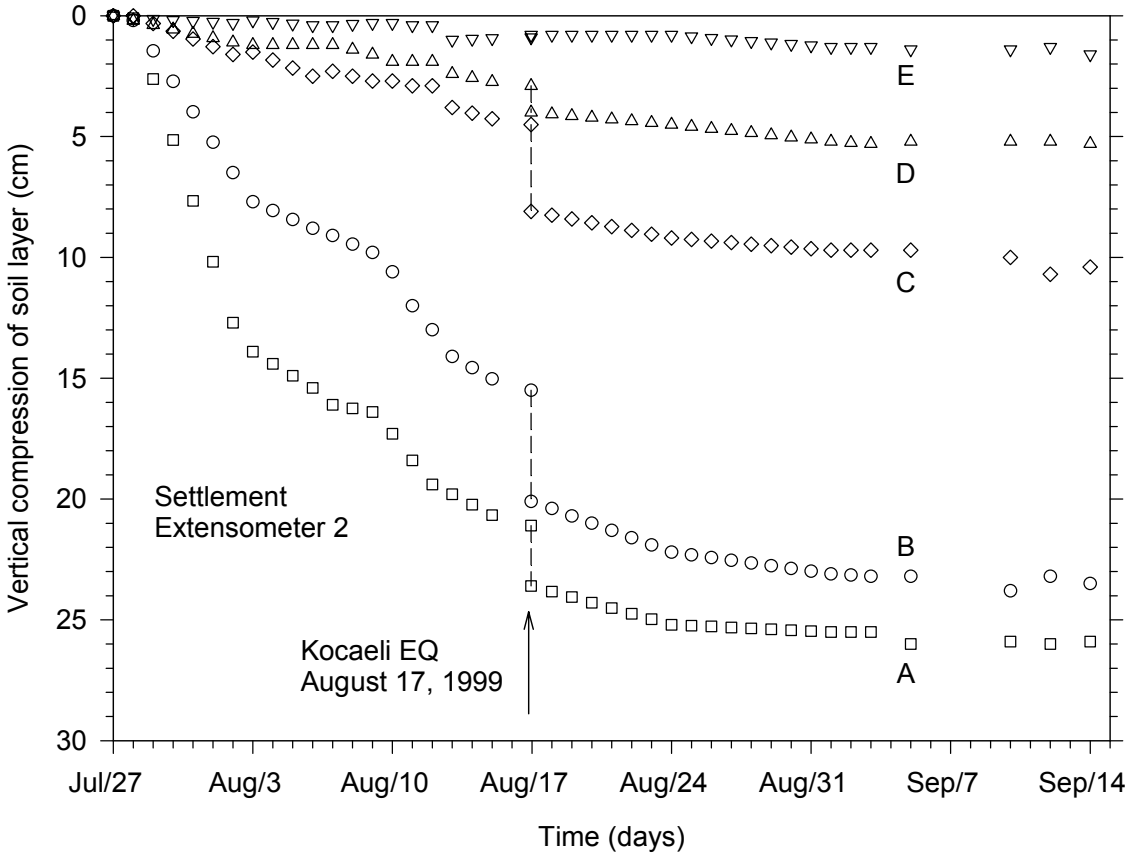

Figure 4-50. Vertical deformation of soil layers – Settlement extensometer 2

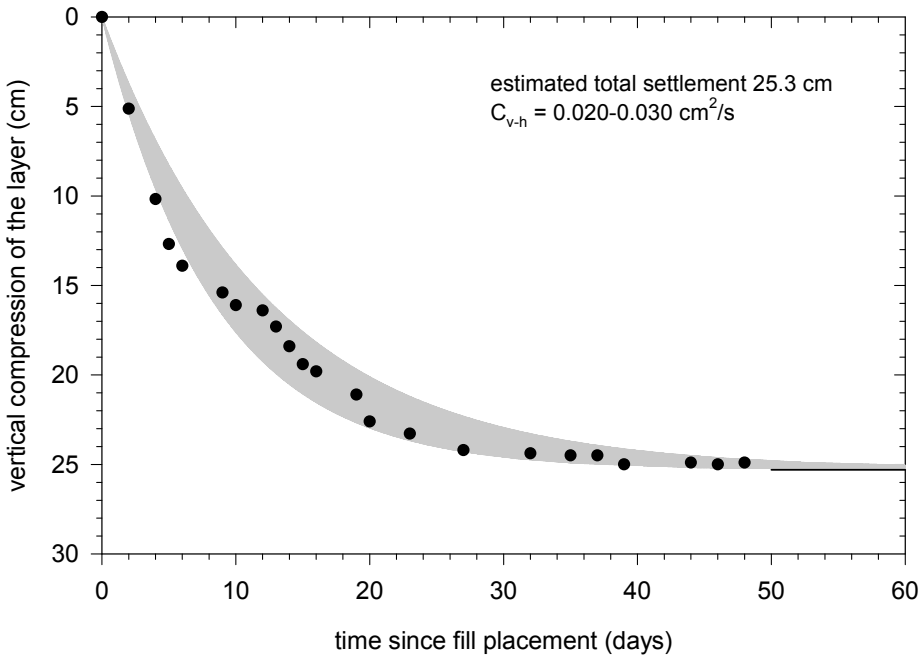

Figure 4-51. Settlement extensometer 2 – Layer A : measured settlements, estimated coefficient of consolidation and estimated total consolidation settlement

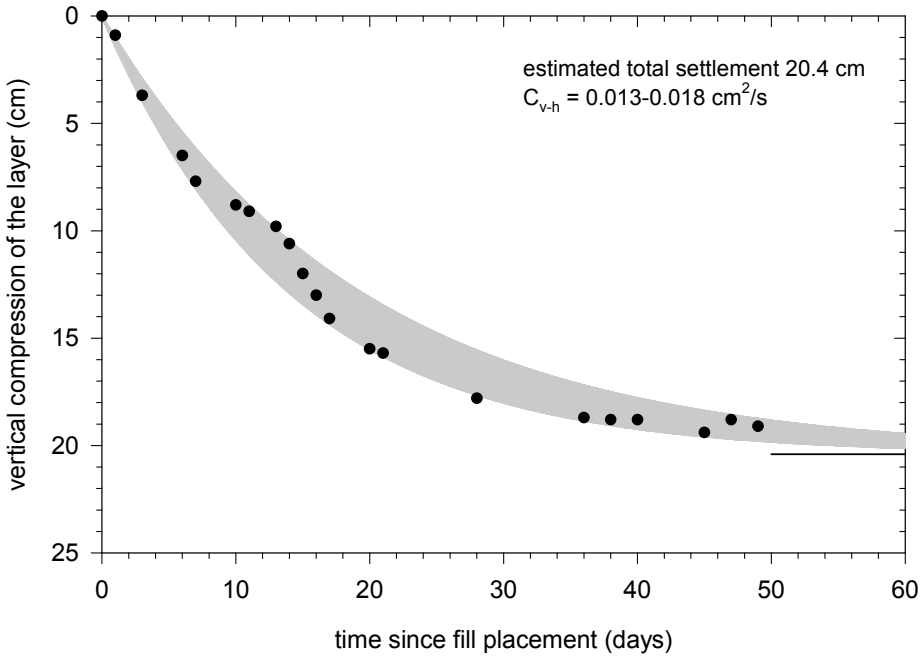

Figure 4-52. Settlement extensometer 2 – Layer B : measured settlements, estimated coefficient of consolidation and estimated total consolidation settlement

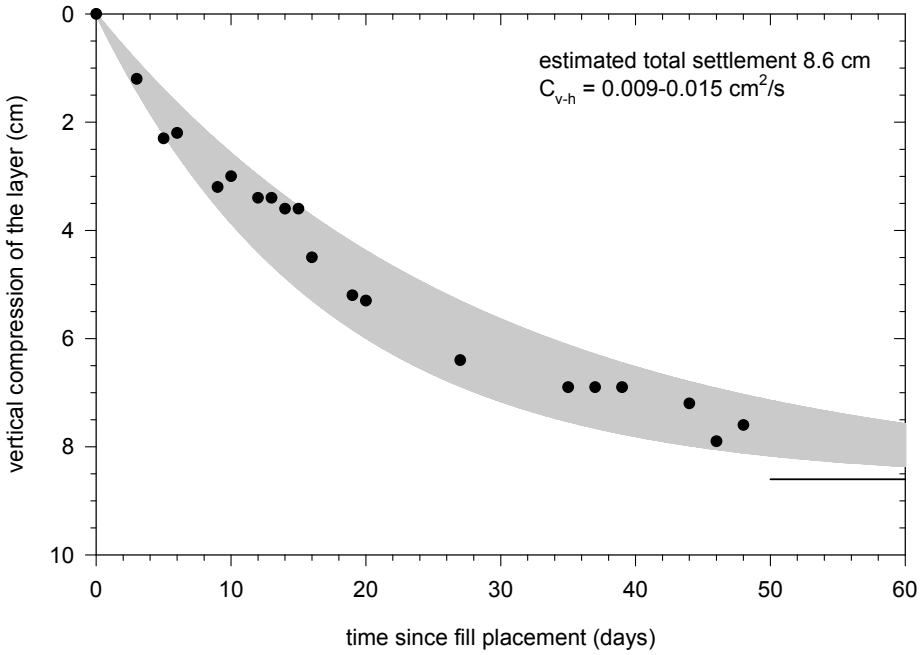

Figure 4-53. Settlement extensometer 2 – Layer C : measured settlements, estimated coefficient of consolidation and estimated total consolidation settlement

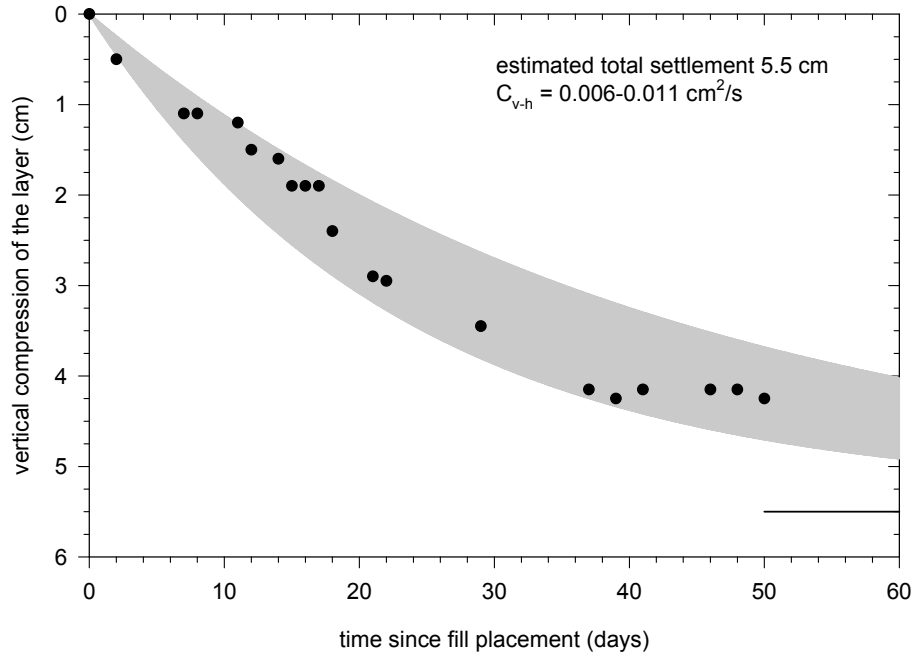

Figure 4-54. Settlement extensometer 2 – Layer D : measured settlements, estimated coefficient of consolidation and estimated total consolidation settlement

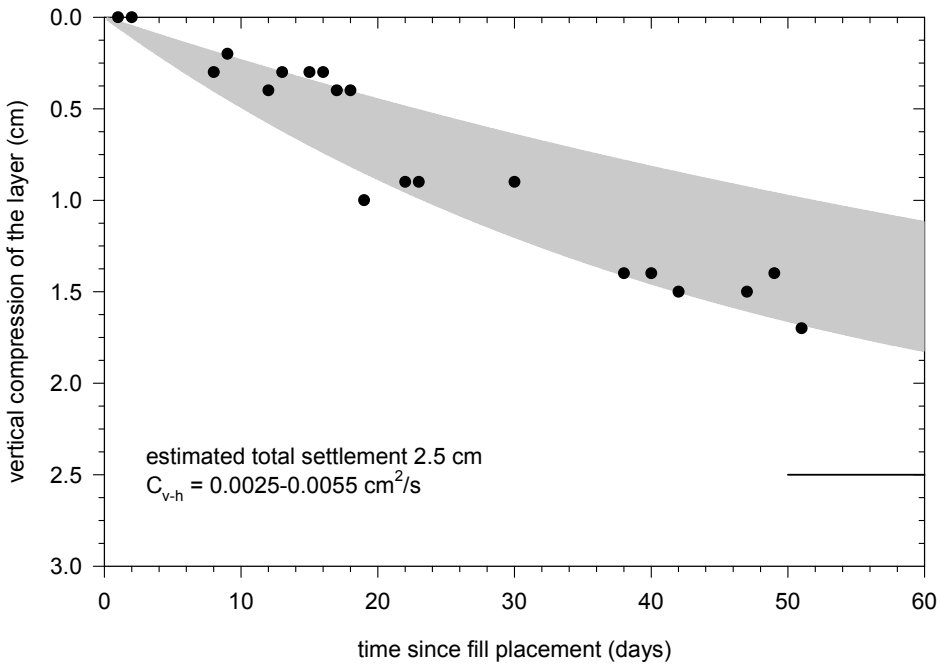

Figure 4-55. Settlement extensometer 2 – Layer E : measured settlements, estimated coefficient of consolidation and estimated total consolidation settlement

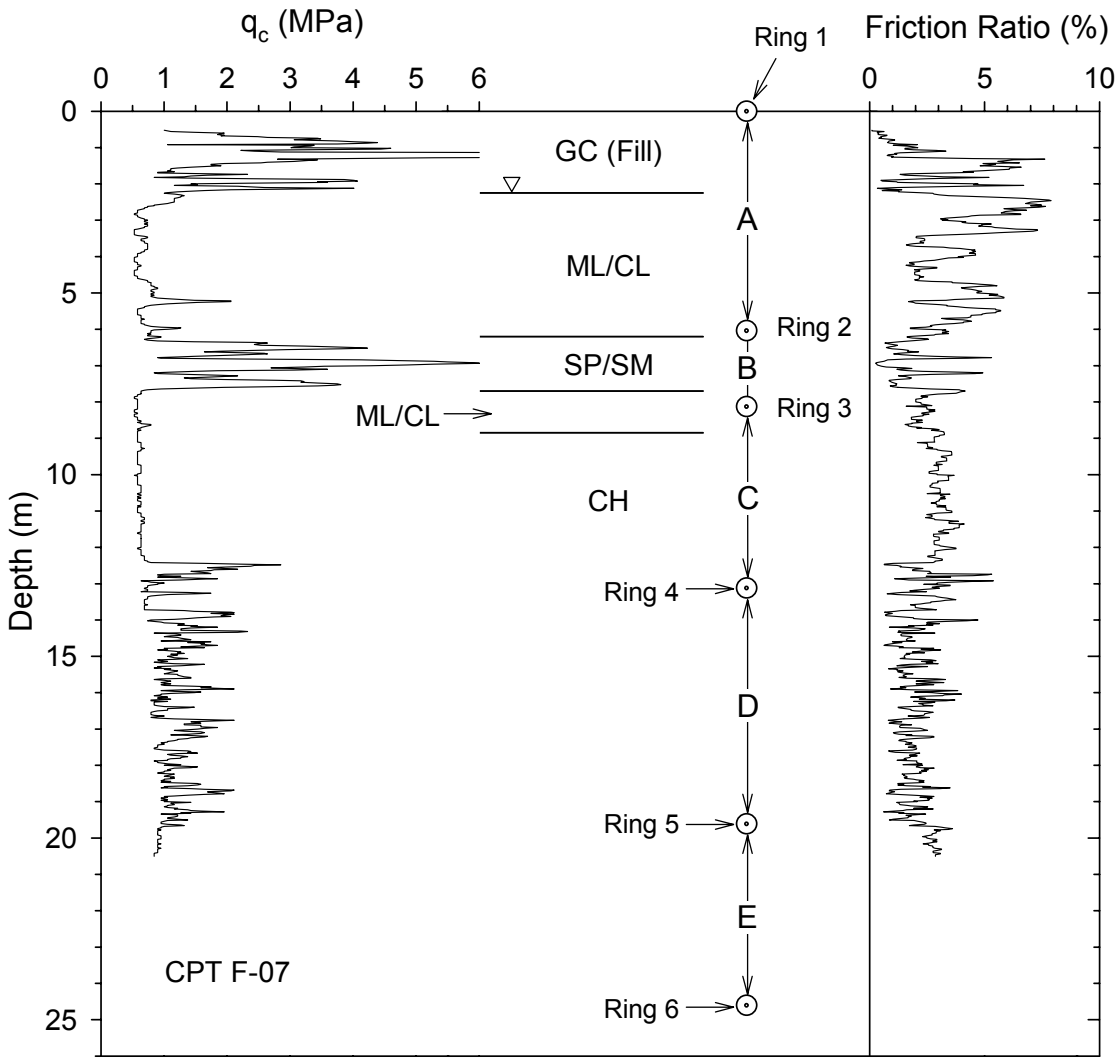

Figure 4-56. Soil conditions near SE3 in Lot C (unimproved soils) where settlements were measured. Figure shows positions of settlement rings, soil layers A – E, and CPT results

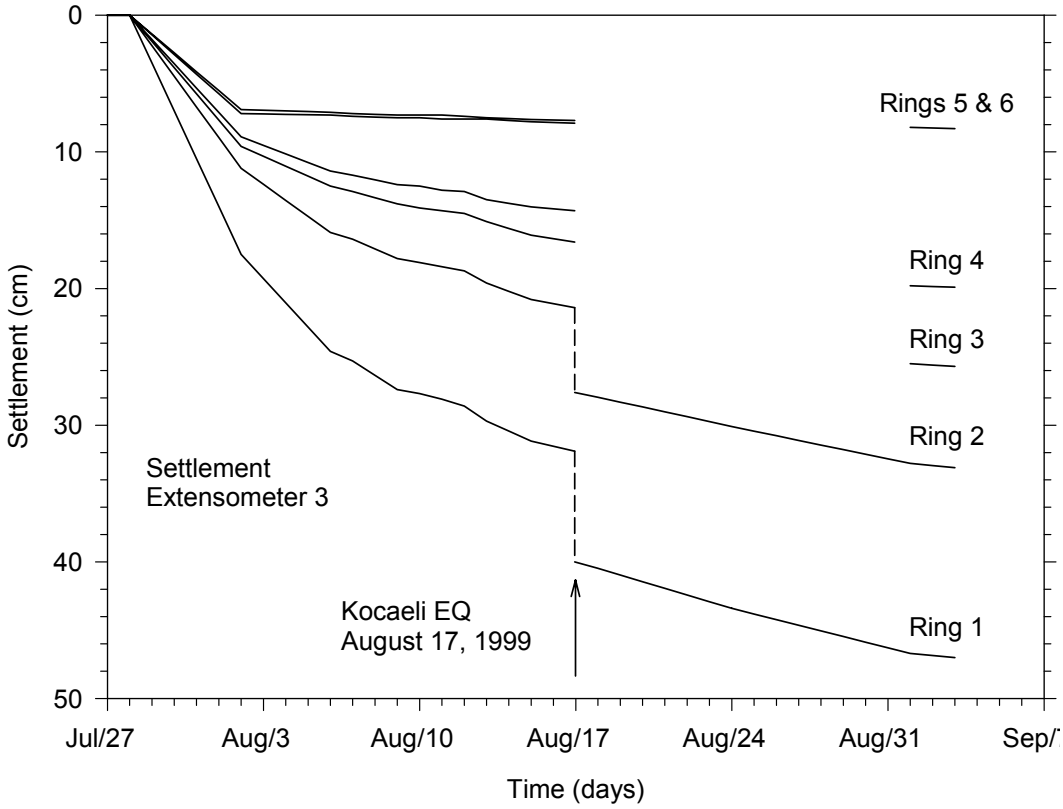

Figure 4-57. Settlement of magnetic rings – Settlement extensometer 3

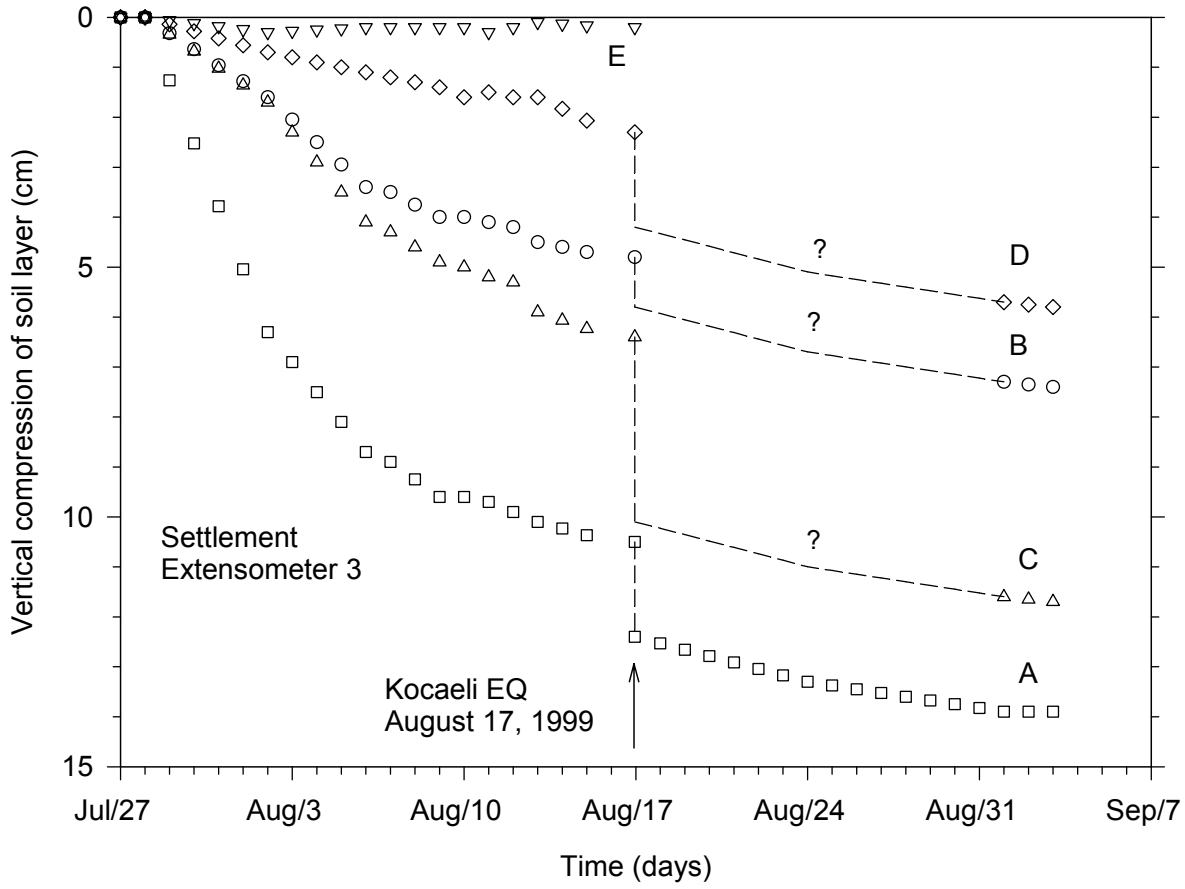

Figure 4-58. Vertical deformation of soil layers – Settlement extensometer 3

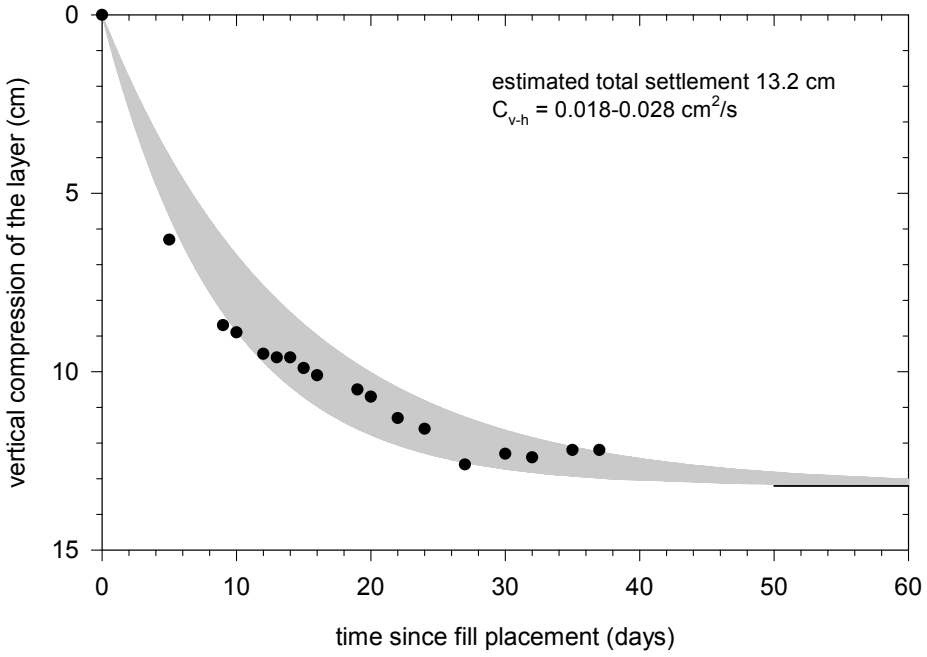

Figure 4-59. Settlement extensometer 3 – Layer A : measured settlements, estimated coefficient of consolidation and estimated total consolidation settlement

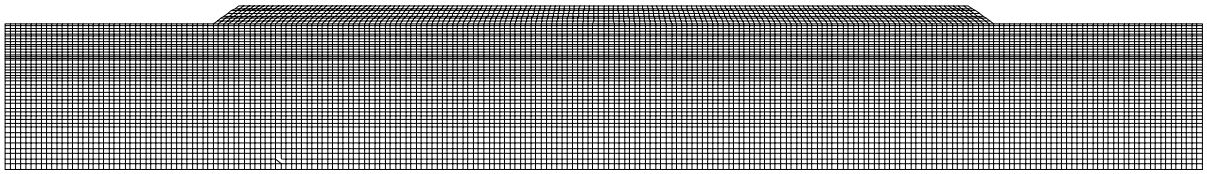

Figure 4-60. Finite element mesh used in the analysis of post-earthquake deformations at Lot C

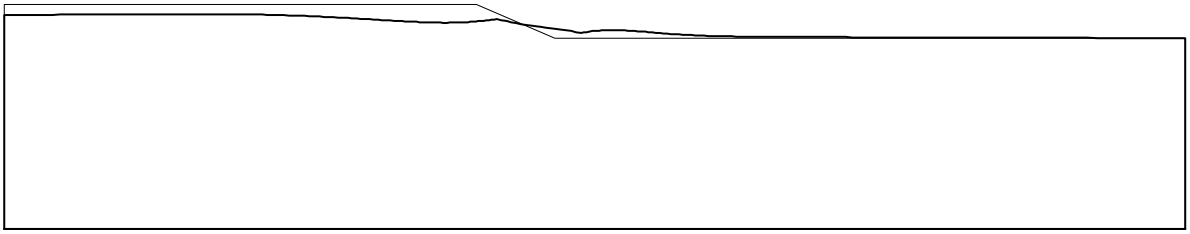

Figure 4-61. Deformed shape (deformation exaggeration 20 x)

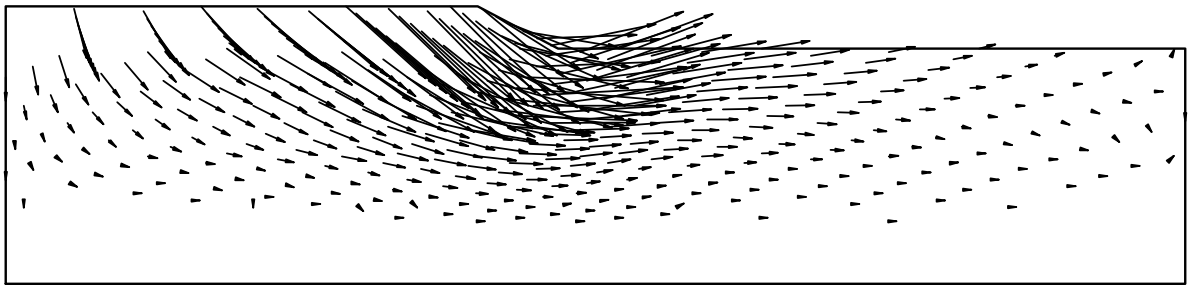

Figure 4-62. Displacement vectors (exaggeration 60x)

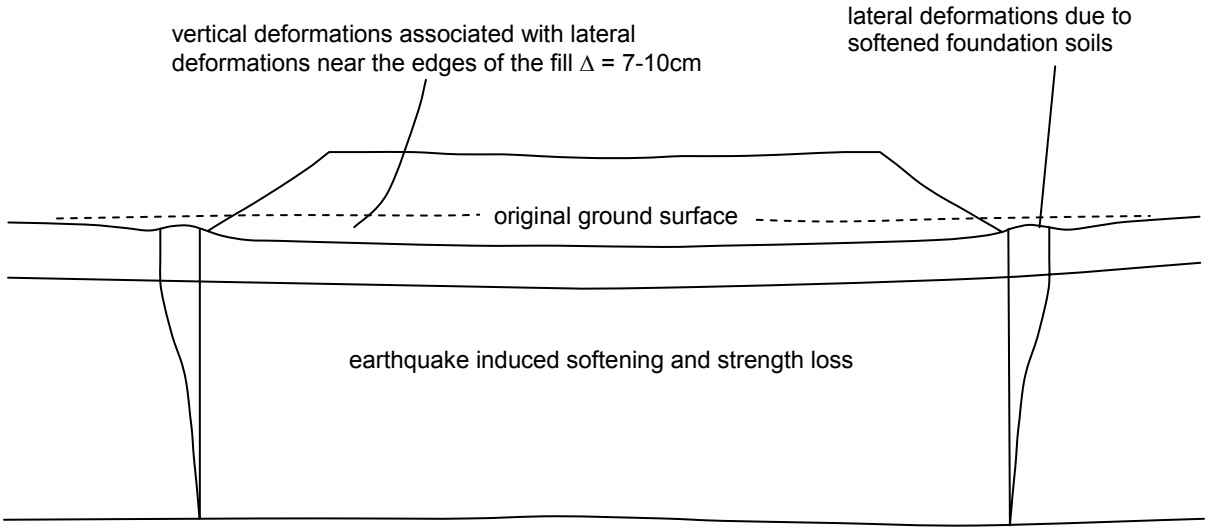

Figure 4-63. Schematic of deformations due to softened foundation soils

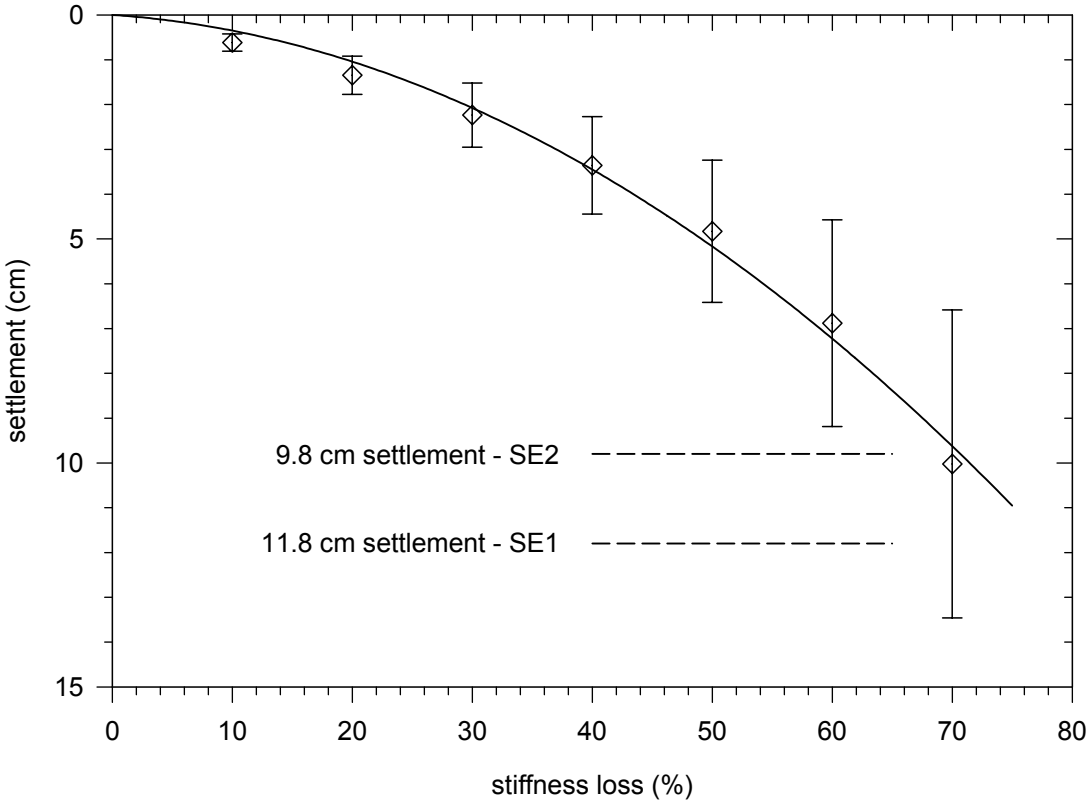

Figure 4-64. Results of finite element analyses – earthquake induced settlements in relation to stiffness loss of the foundation soils.

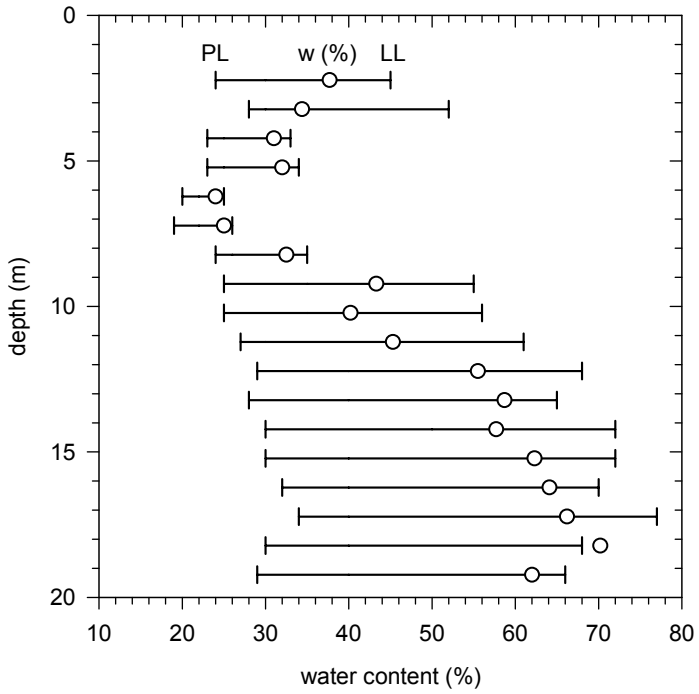

Figure 4-65. Plasticity properties and natural water content of split spoon samples

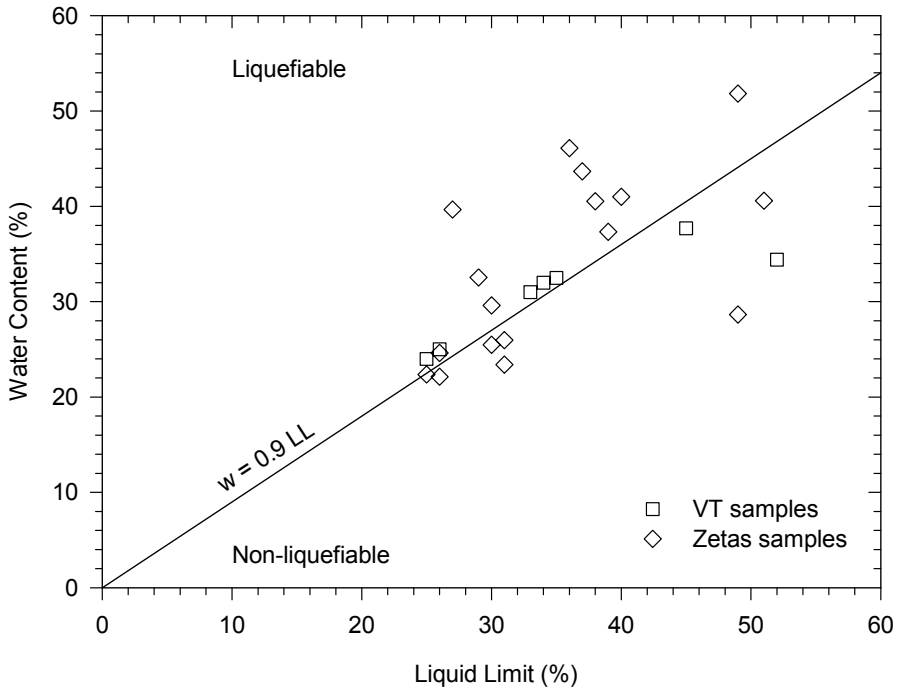

Figure 4-66. Natural water content of the liquefied soils in comparison to liquid limit

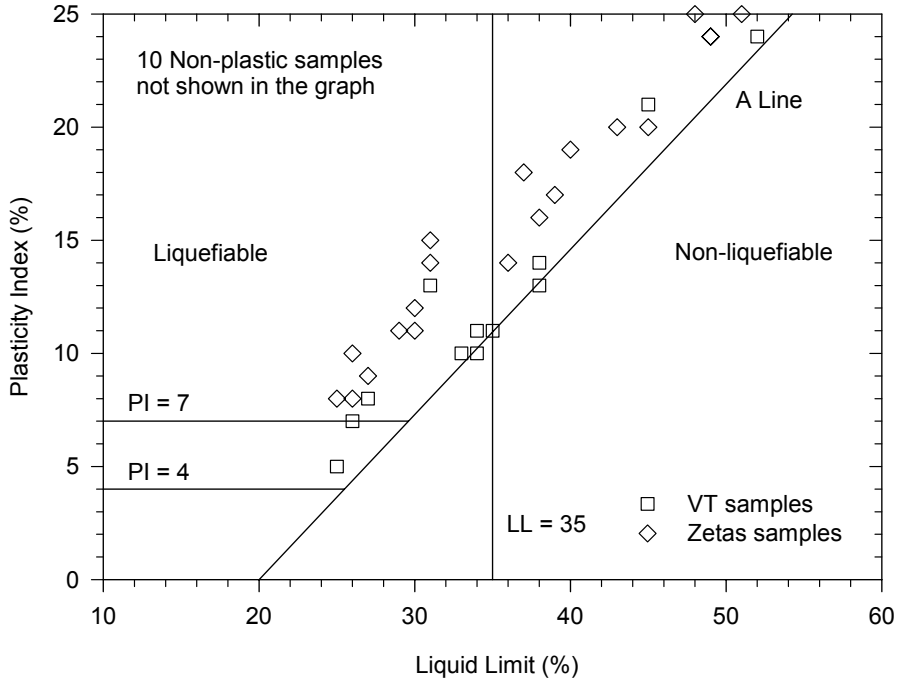

Figure 4-67. Plasticity characteristics of the liquefied soils

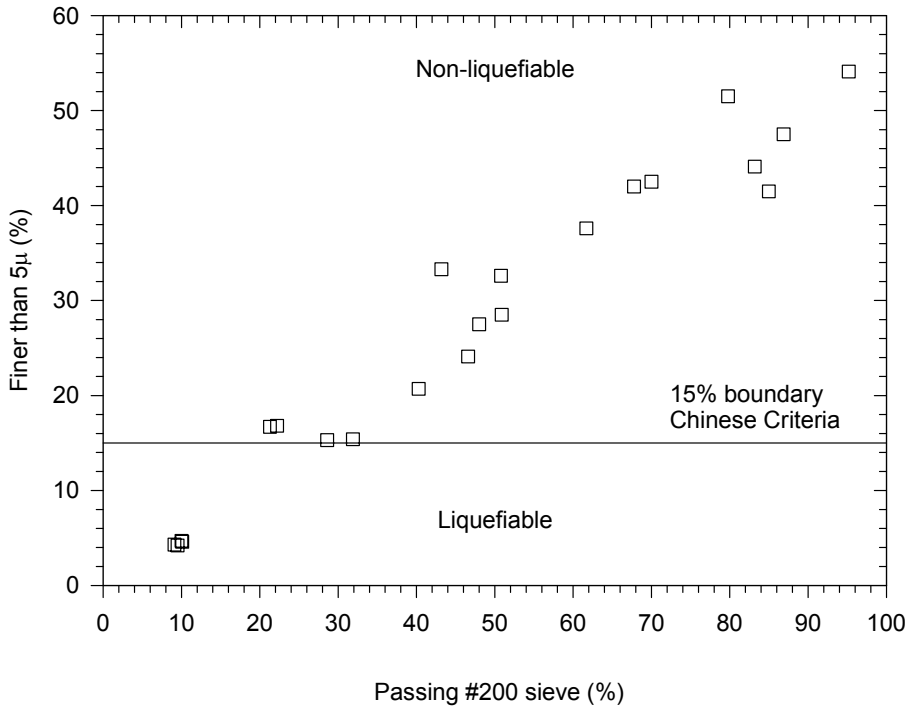

Figure 4-68. Gradation characteristics and clay content of the liquefied soils

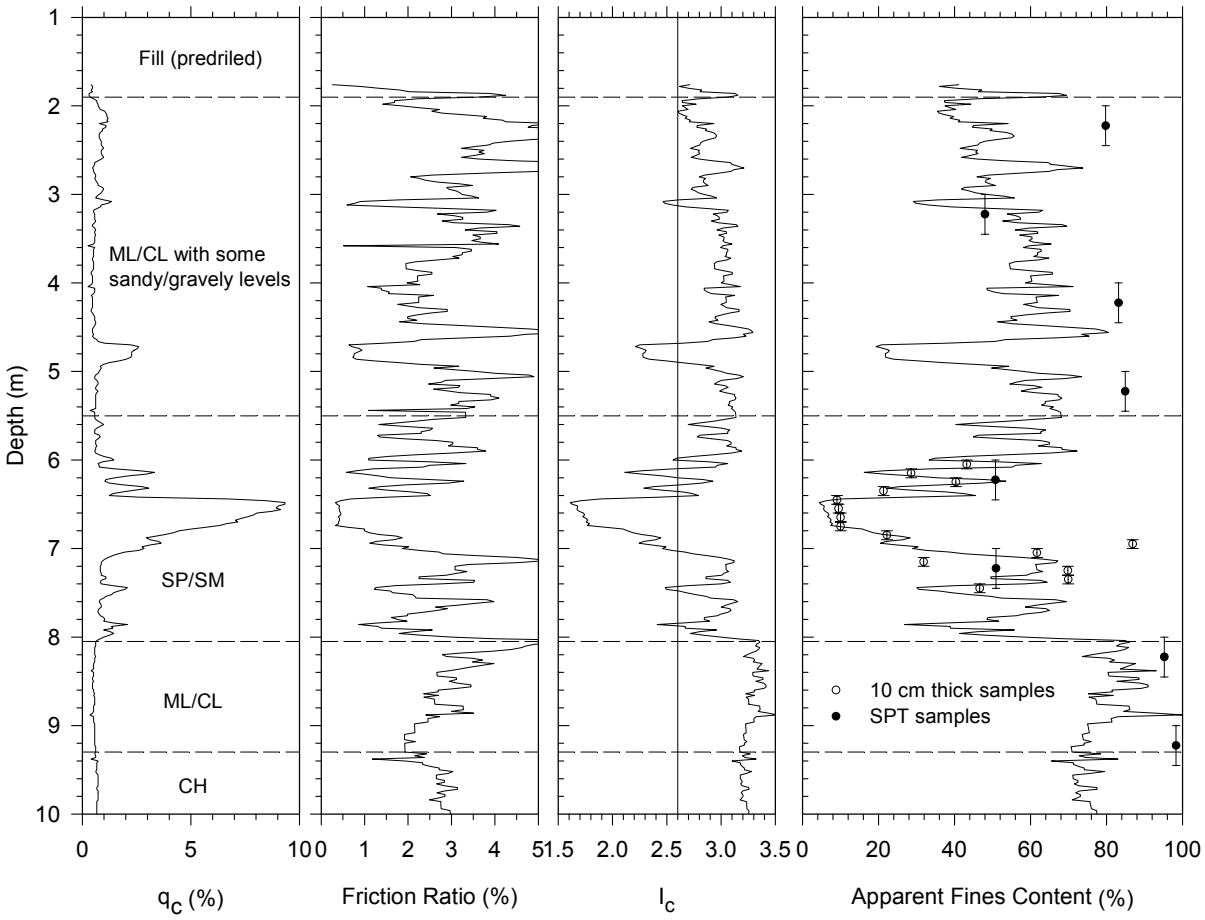

Figure 4-69. Estimated fines content using CPT and measured values from adjacent boreholes (SPT samples and sliced Shellby tube samples) – CPT-H4. Solid circles represent the SPT samples and hollow circles represent 10 cm thick samples sliced from the Shelly tubes. Extent of the tick bar indicates the depth range the sample is retrieved from.

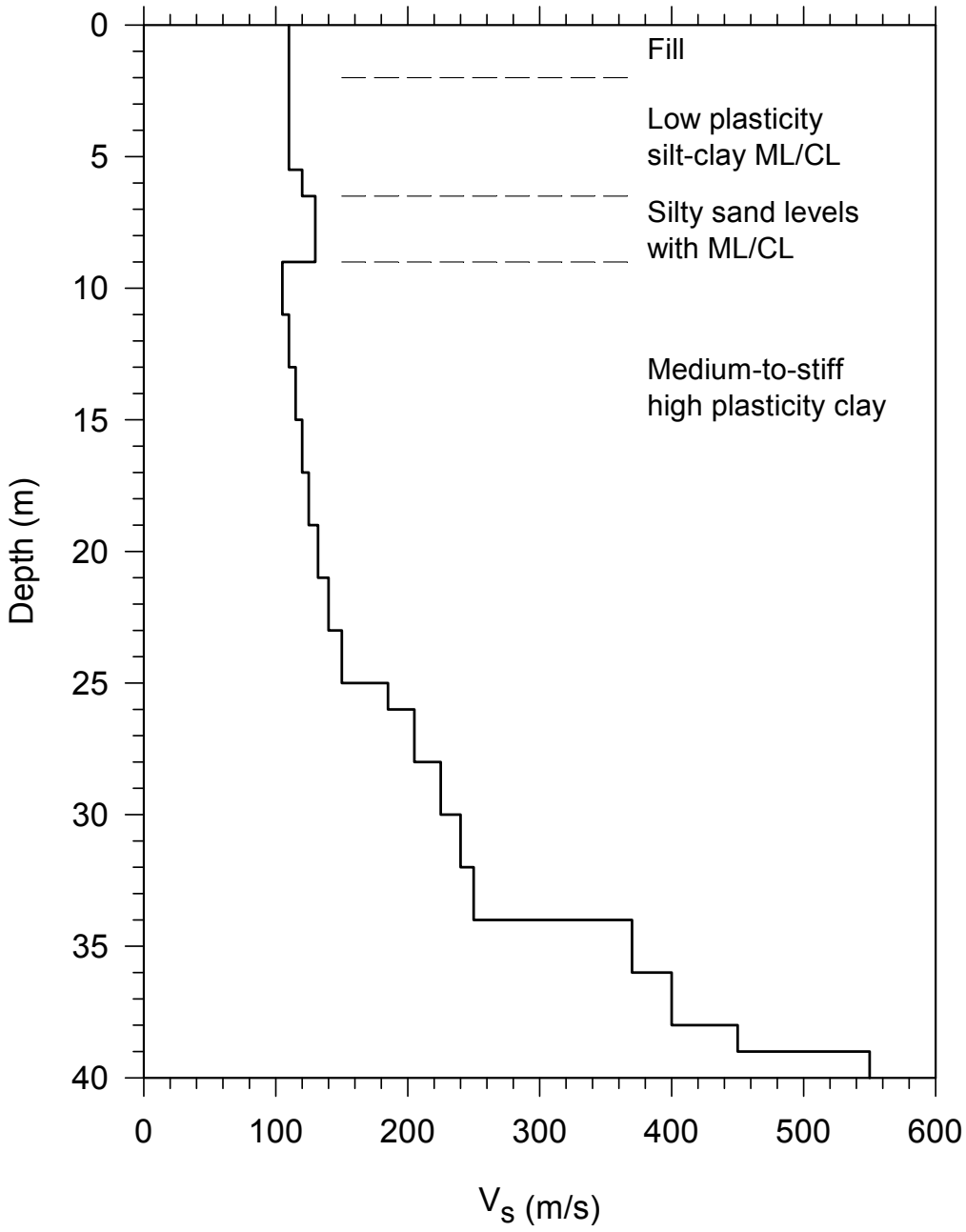

Figure 4-70. Shear wave velocity model of the site used in site response analyses

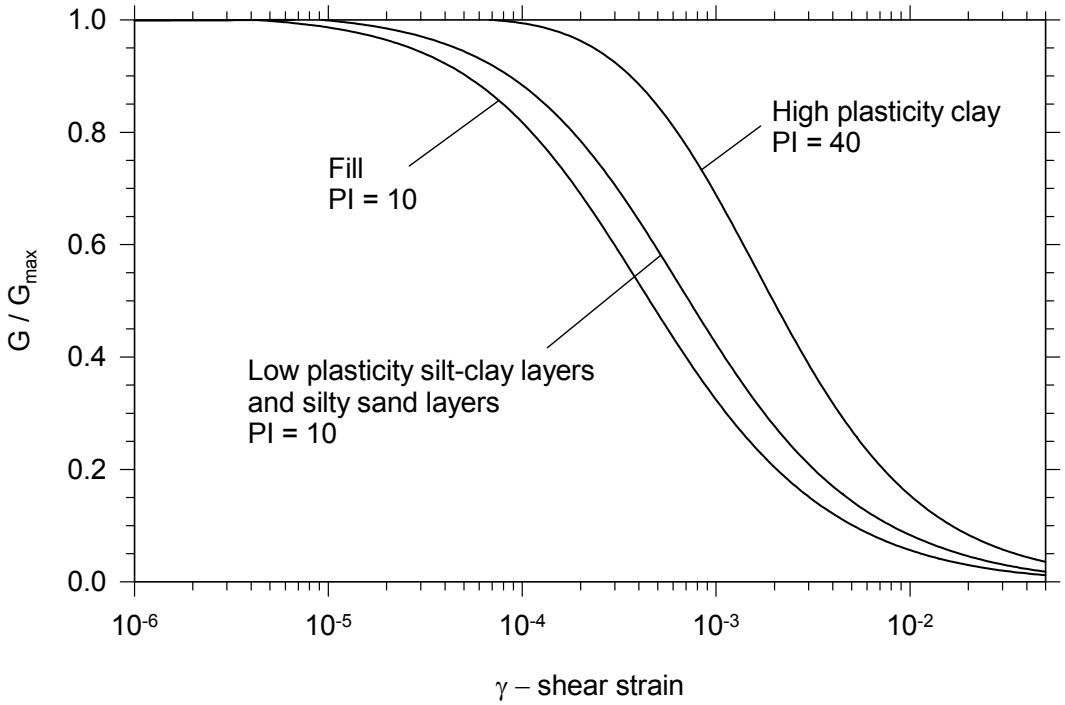

Figure 4-71. Shear modulus degradation curves used in the site response analyses

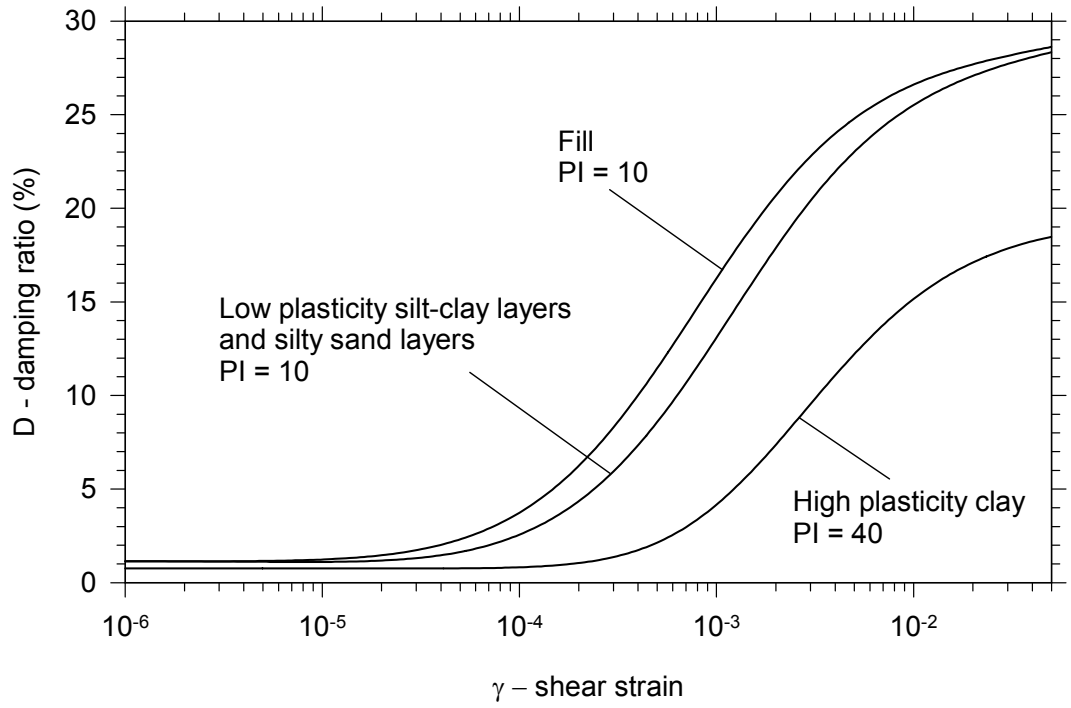

Figure 4-72. Strain dependent damping curves used in the site response analyses

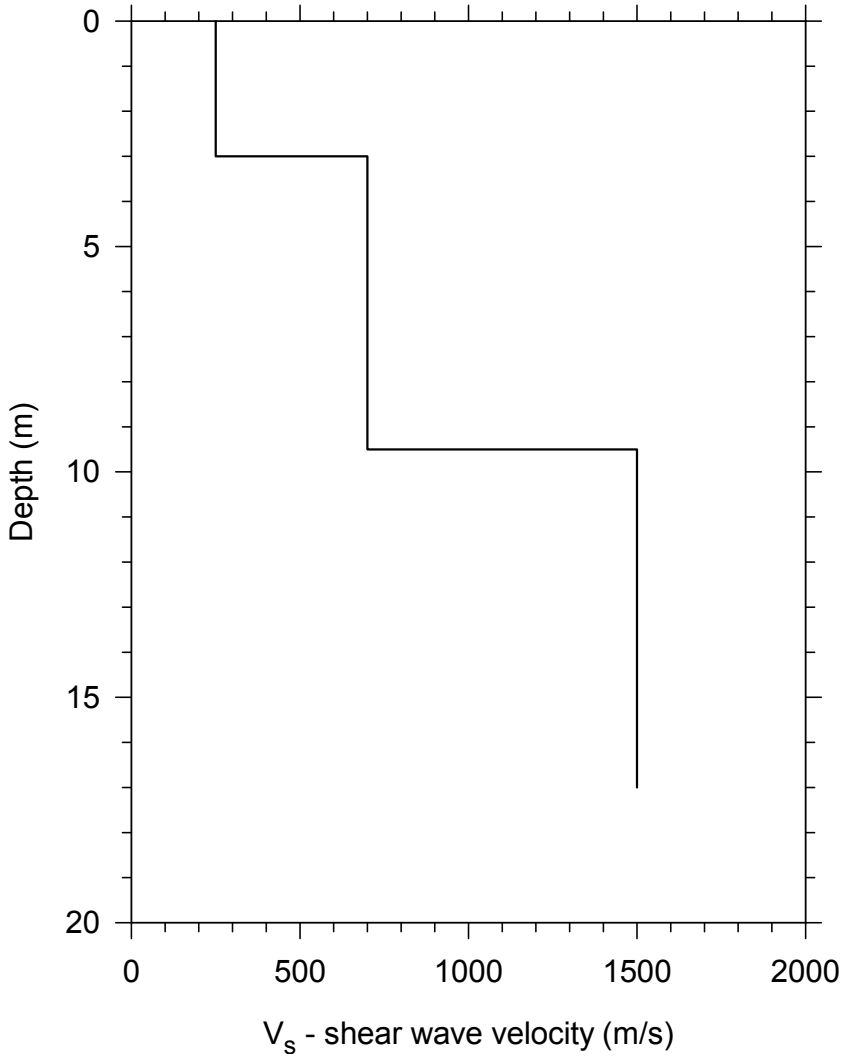

Figure 4-73. Shear wave velocity at IZT recording station site

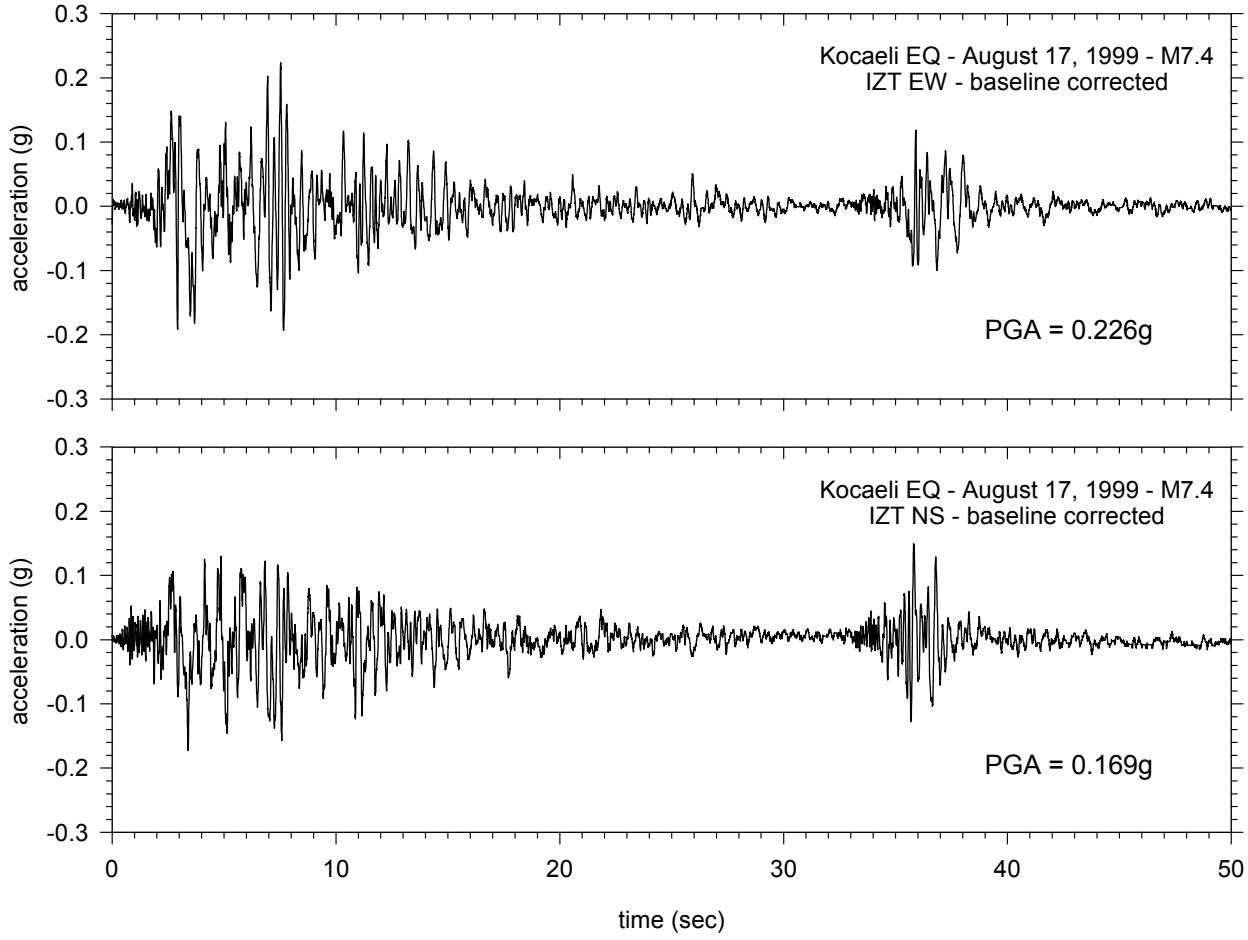

Figure 4-74. Baseline corrected acceleration time history recorded at Izmit (IZT) station

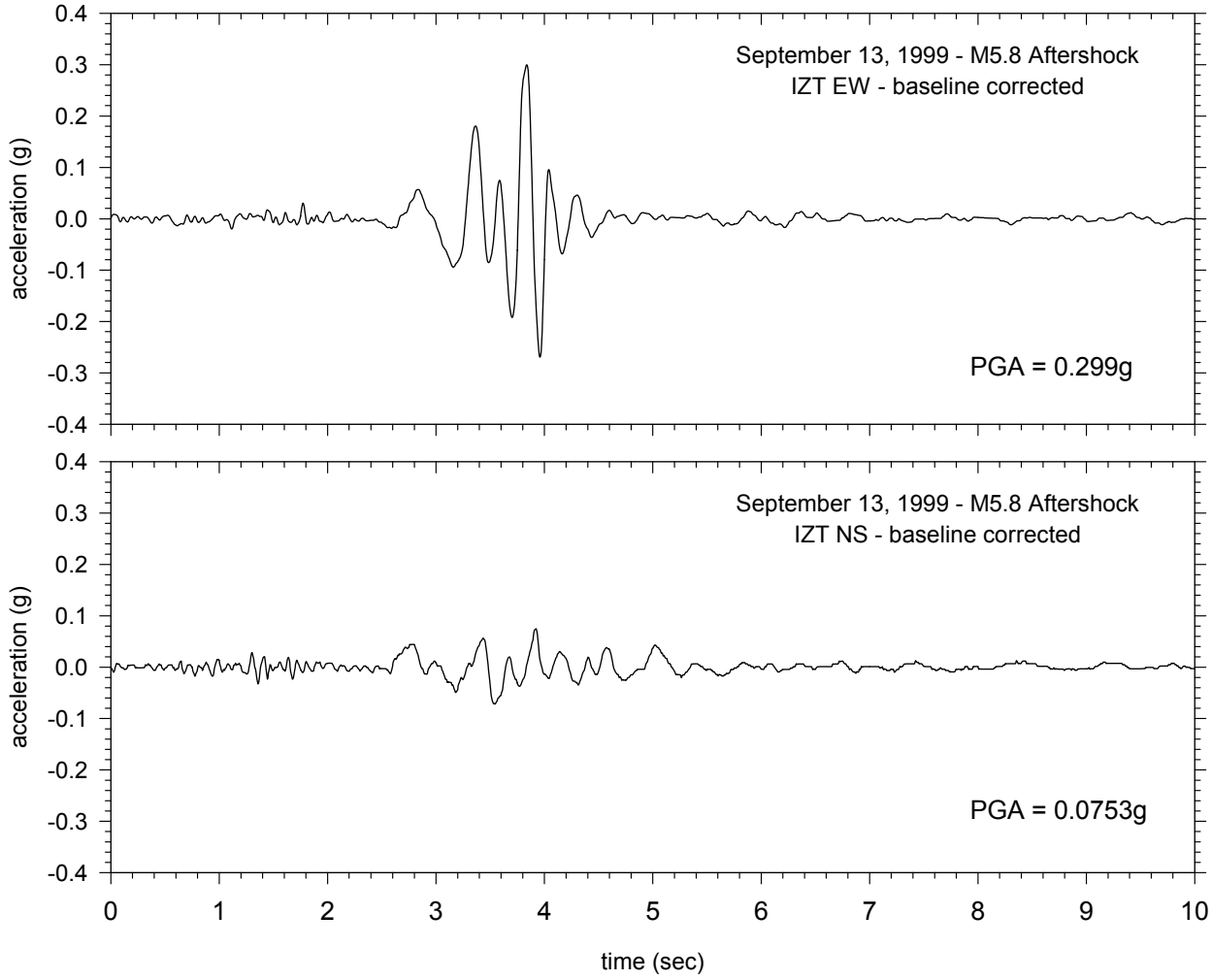

Figure 4-75. Baseline corrected acceleration time history recorded at Izmit (IZT) station – M5.8 aftershock of September 13, 1999

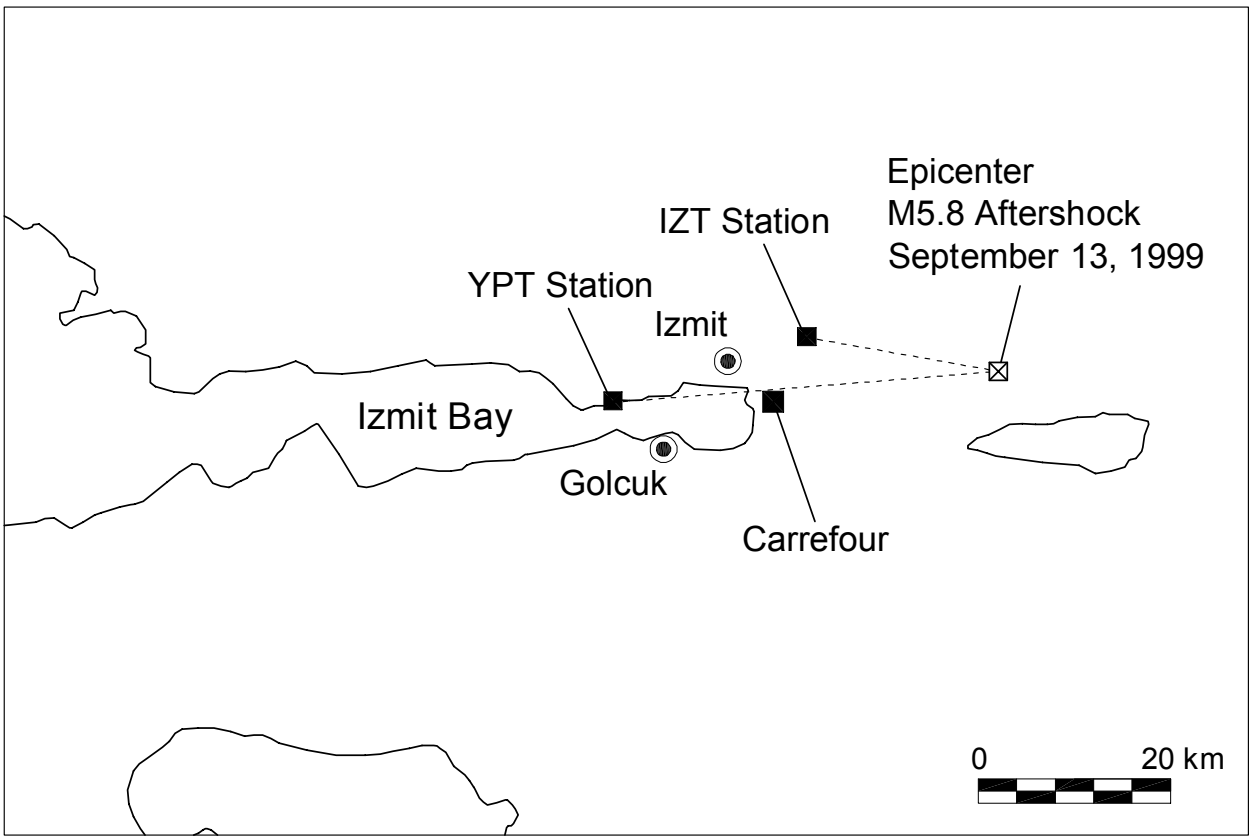

Figure 4-76. Relative locations of Carrefour site, M5.8 aftershock of September 13, 1999 and Izmit (IZT) and Yarimca Petkim (YPT) recording stations.

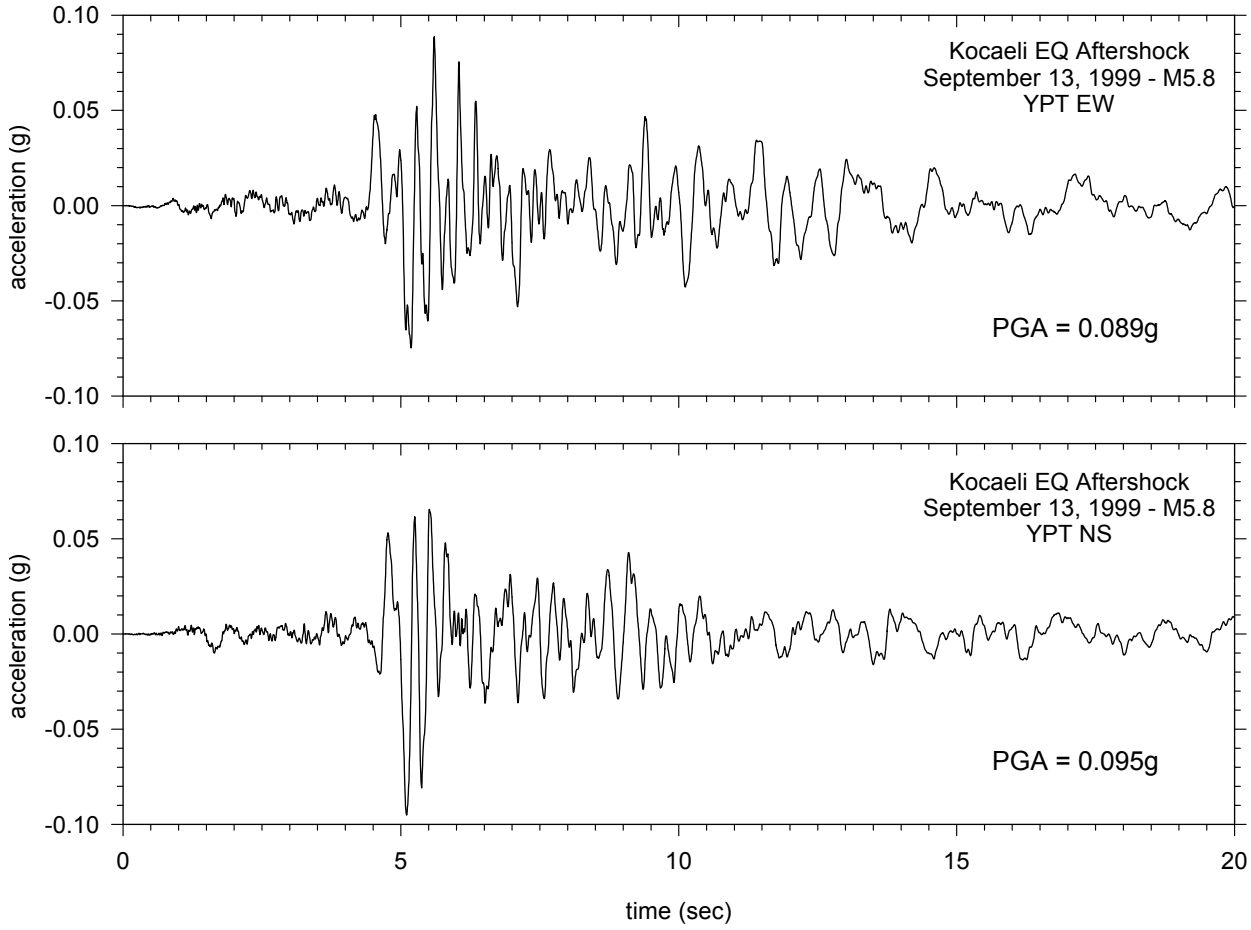

Figure 4-77. Ground motion recorded at YPT station – M5.8 aftershock of September 13, 1999

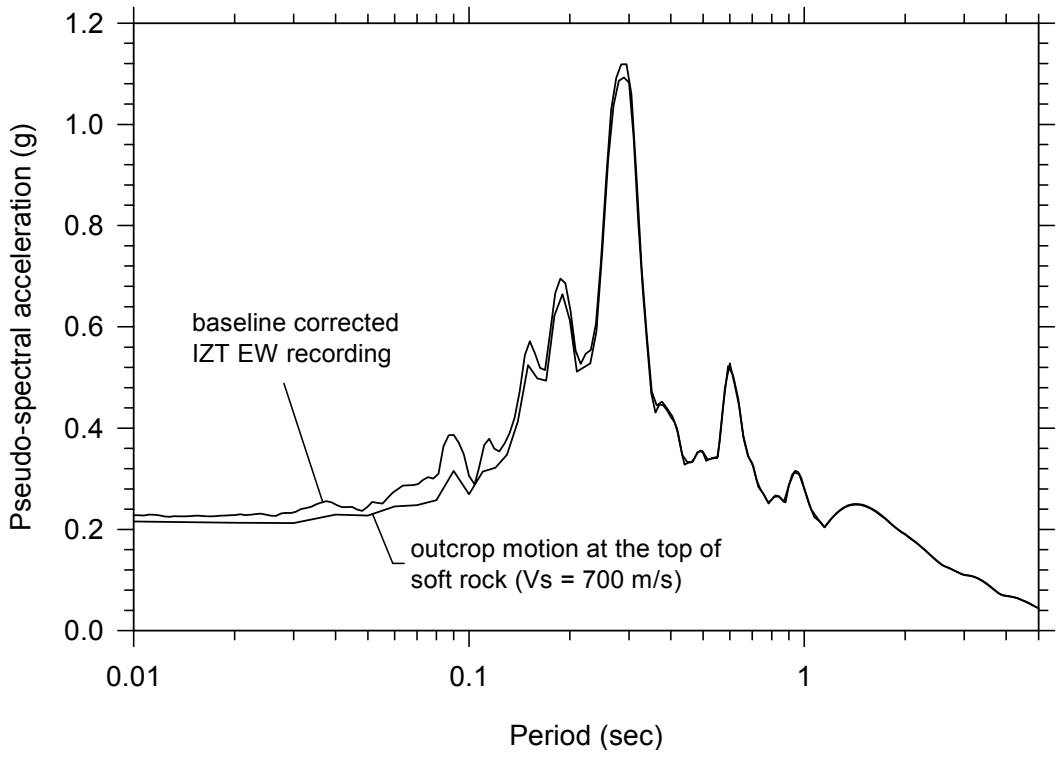

Figure 4-78. Comparison of response spectra – baseline corrected motion and deconvoluted softrock outcrop motion

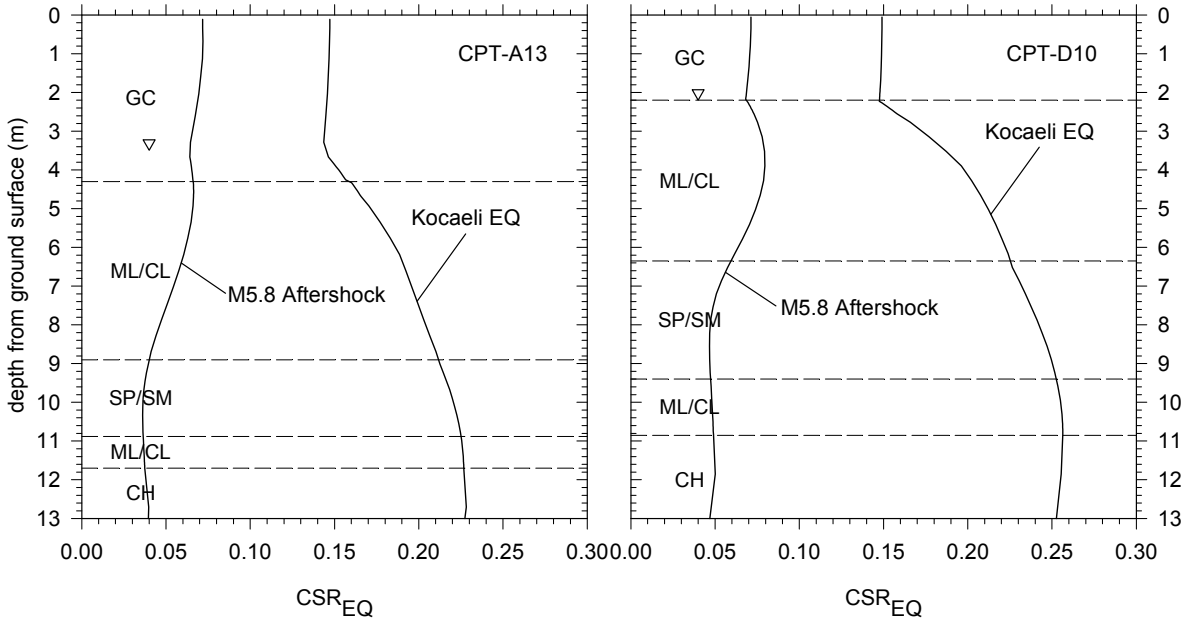

Figure 4-79. Estimated cyclic stress ratio for two CPT locations at Shopping Center area

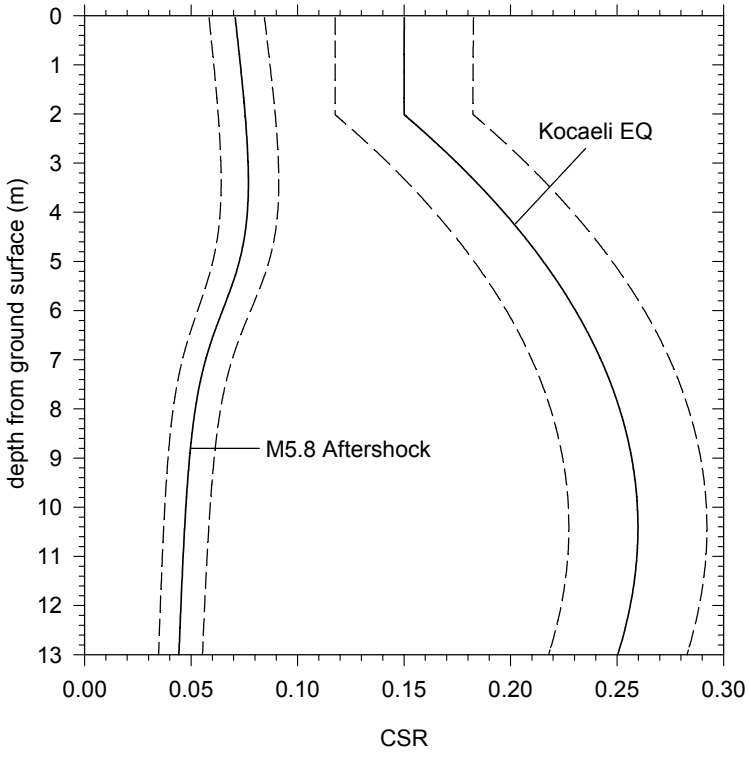

Figure 4-80. CSR for Shopping Center area – median curve and 95% confidence interval

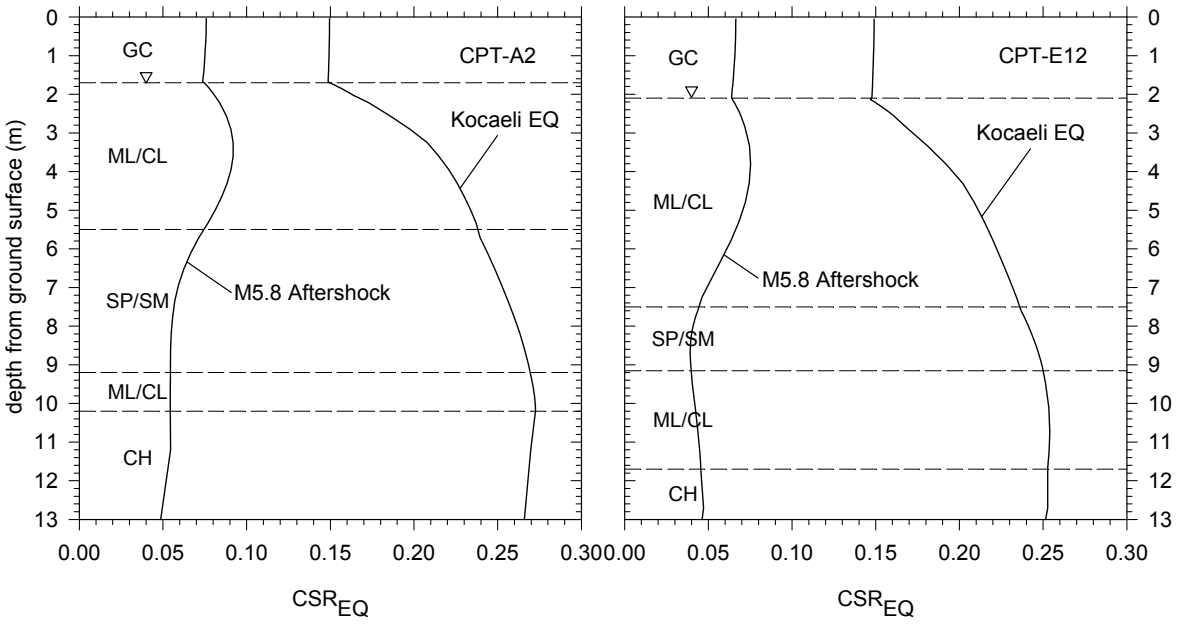

Figure 4-81. Estimated cyclic stress ratio for two CPT locations at Parking Lot area

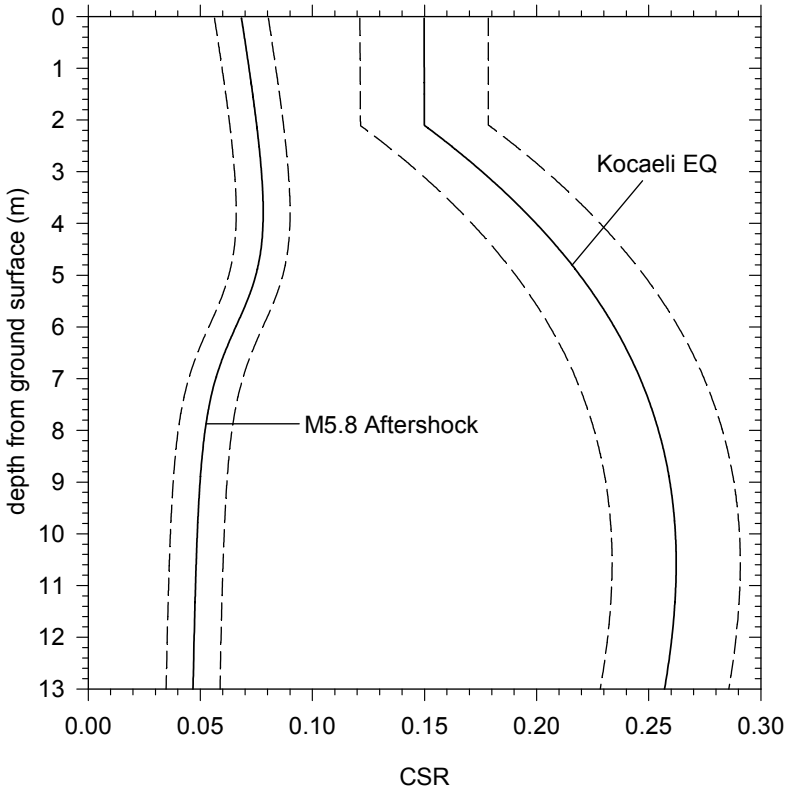

Figure 4-82. CSR for Parking Lot area – median curve and 95% confidence interval

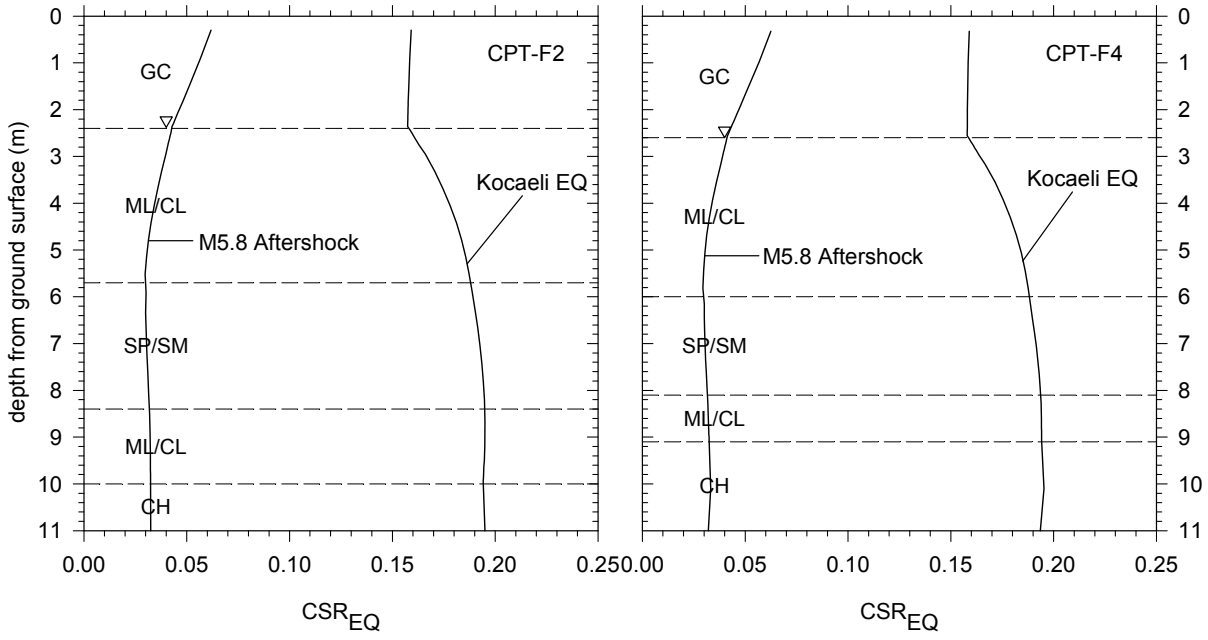

Figure 4-83. Estimated cyclic stress ratio for two CPT locations at Lot C

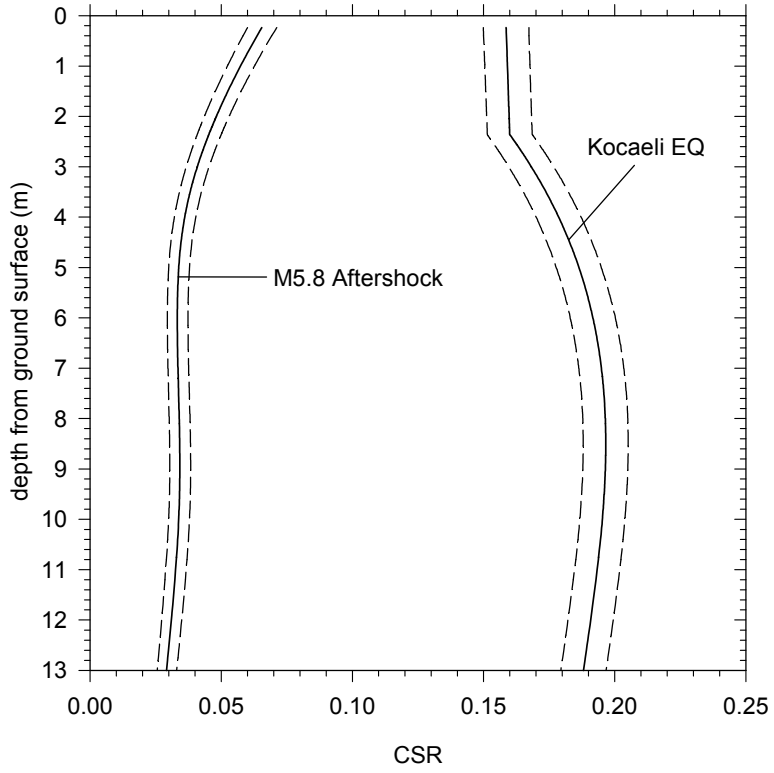

Figure 4-84. CSR for Lot C (fill present) – median curve and 95% confidence interval

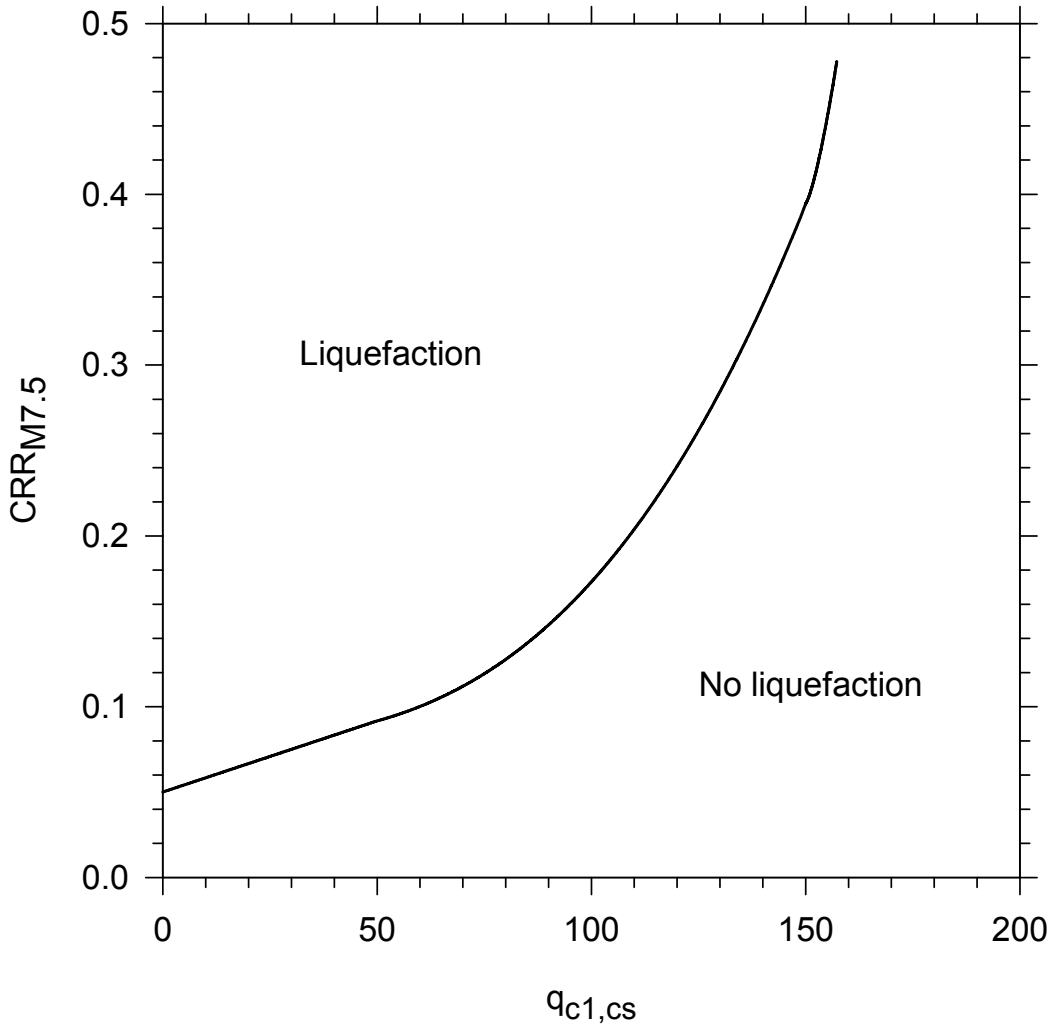

Figure 4-85. Cyclic resistance ratio boundary for CPT based design

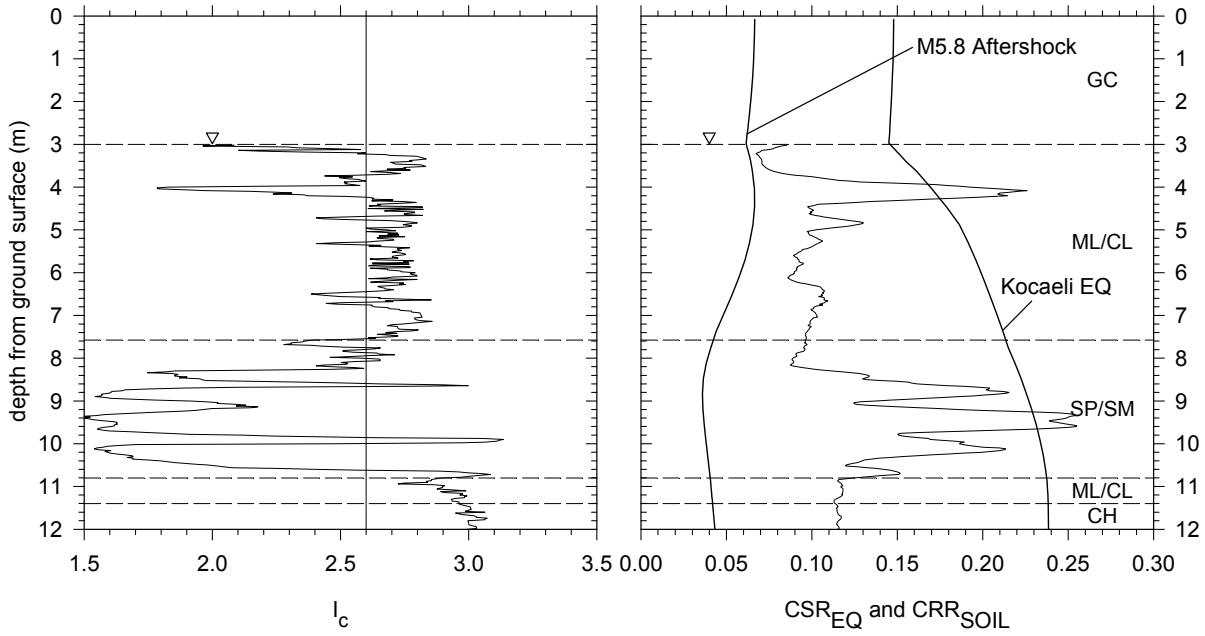

Figure 4-86. Soil behavior type index and cyclic stresses – A6 (Shopping Center)

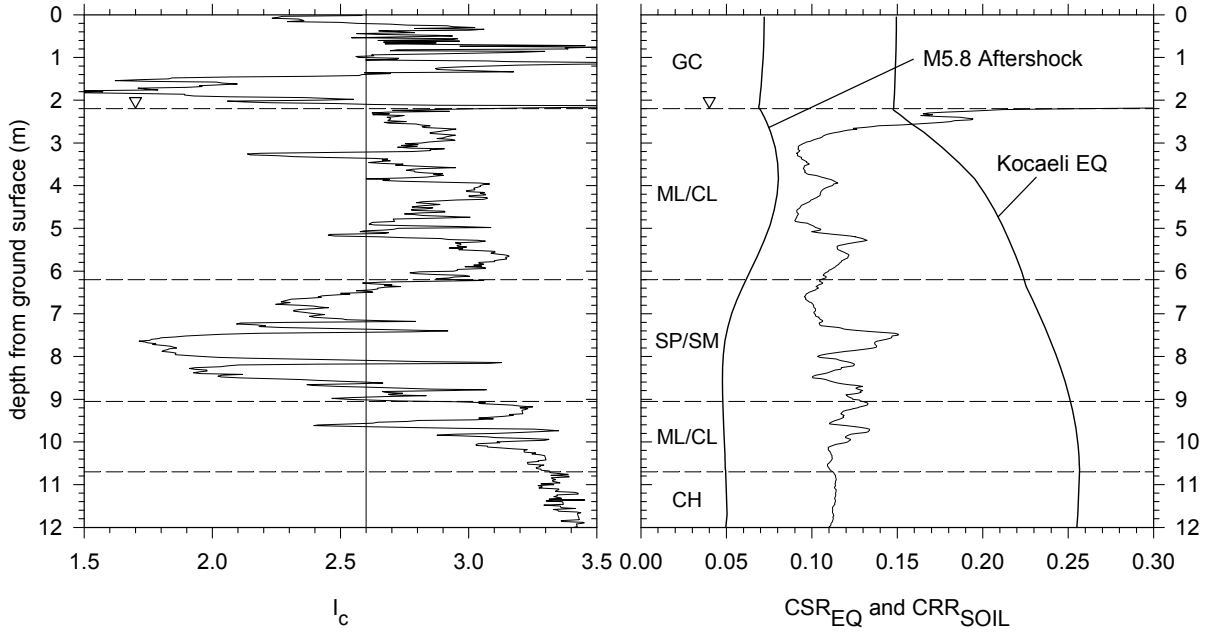

Figure 4-87. Soil behavior type index and cyclic stresses – A15 (Shopping Center)

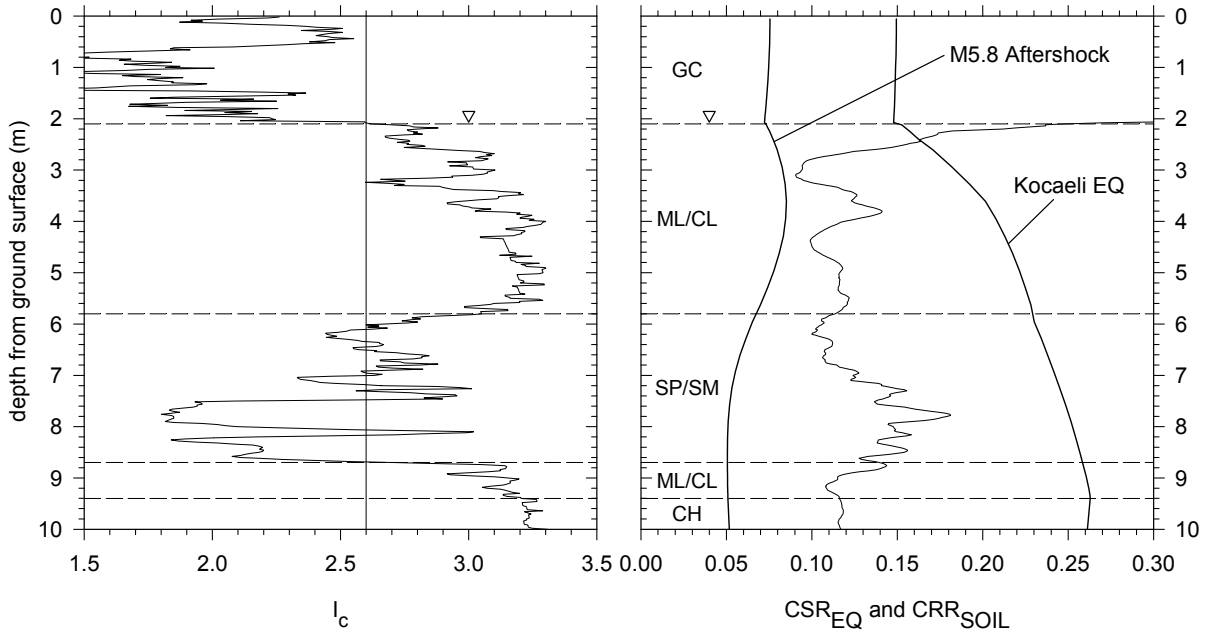

Figure 4-88. Soil behavior type index and cyclic stresses – D1 (Shopping Center)

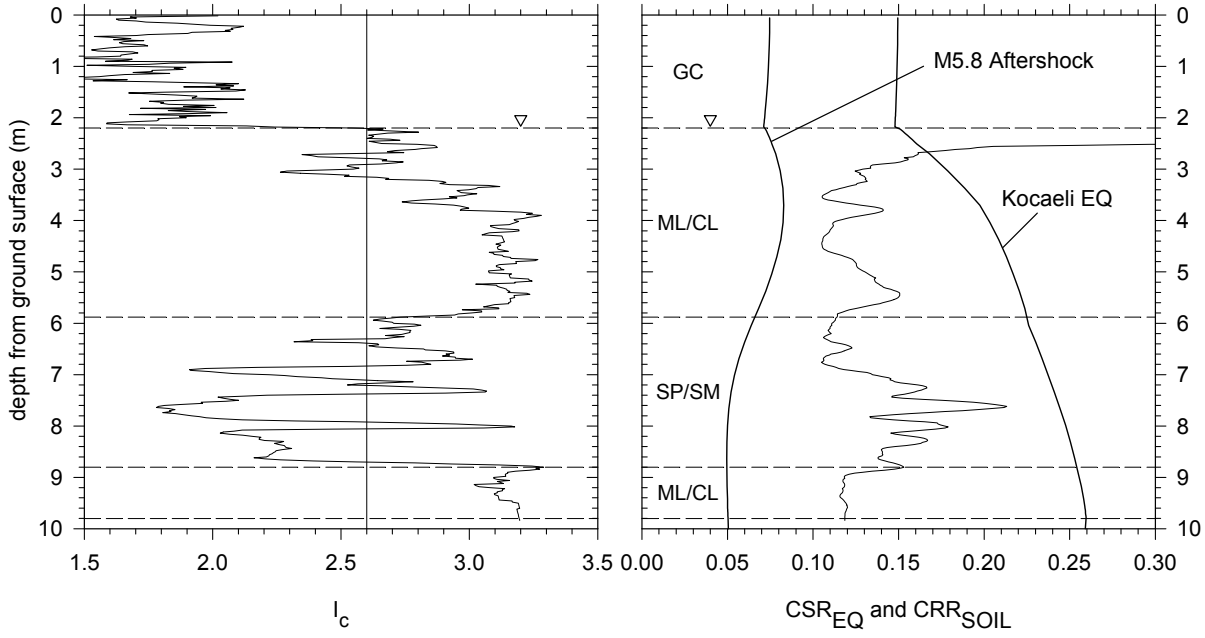

Figure 4-89. Soil behavior type index and cyclic stresses – D2 (Shopping Center)

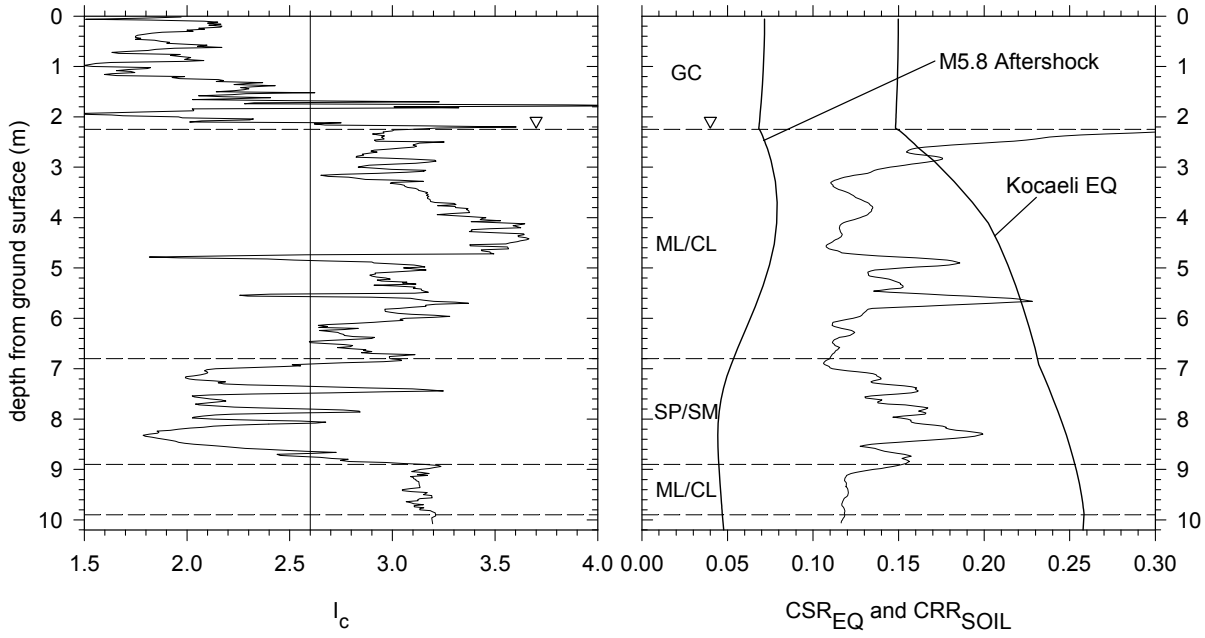

Figure 4-90. Soil behavior type index and cyclic stresses – D3 (Shopping Center)

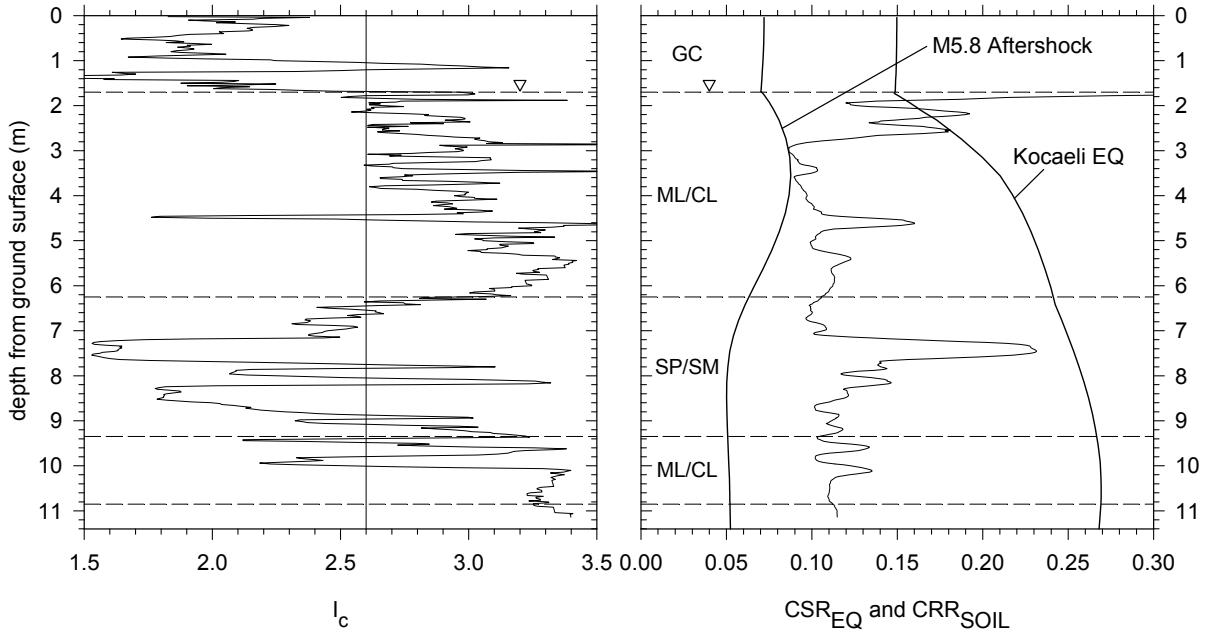

Figure 4-91. Soil behavior type index and cyclic stresses – D4 (Shopping Center)

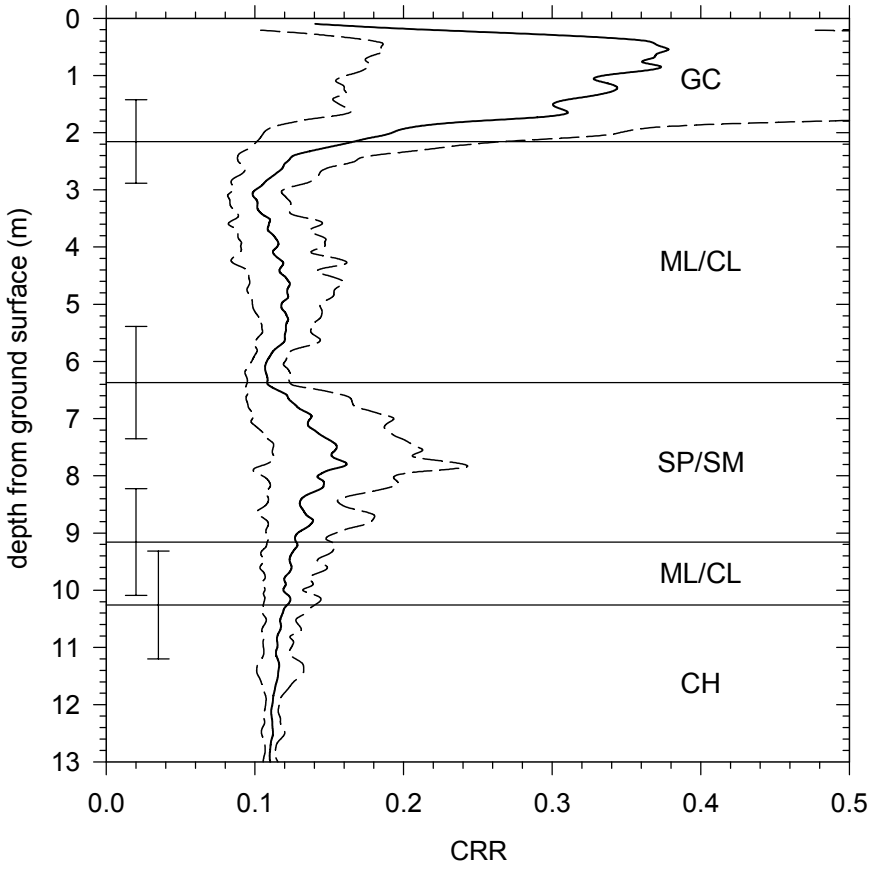

Figure 4-92. Estimated cyclic resistance ratio (CRR) for the Shopping Center area. Median values and the 95% confidence interval (based on a log-normal distribution) from the CPT's at this section of the site. Layer boundaries inferred from these CPT's; mean values with plus/minus one standard deviation range.

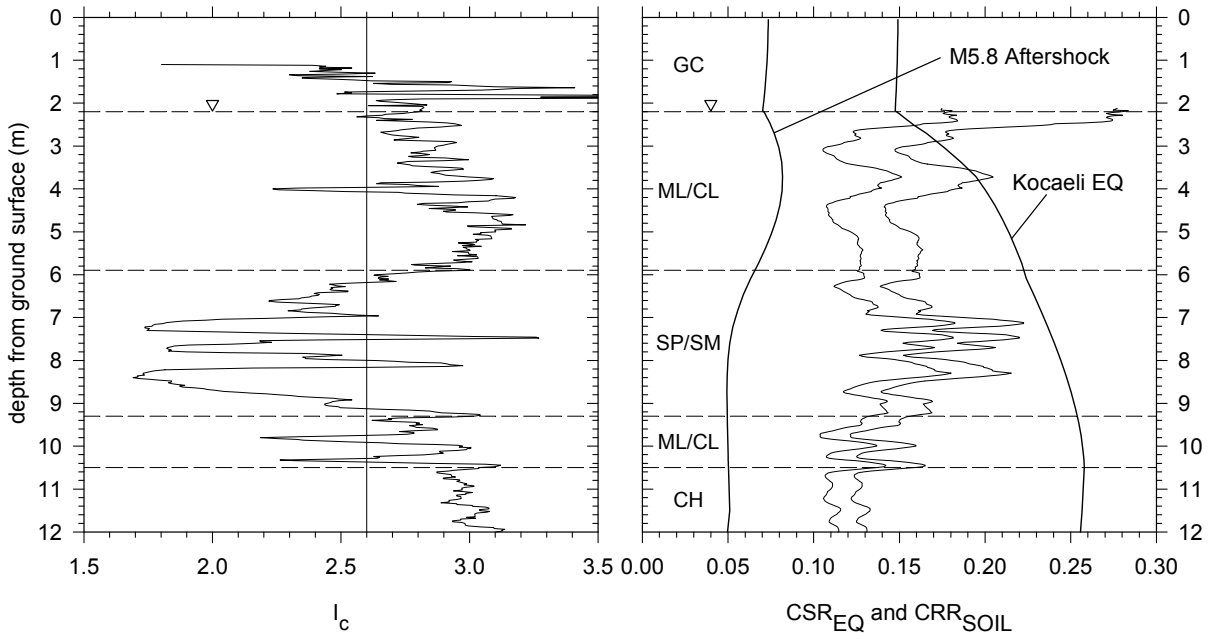

Figure 4-93. Soil behavior type index and cyclic stresses – A1 (Parking Lot)

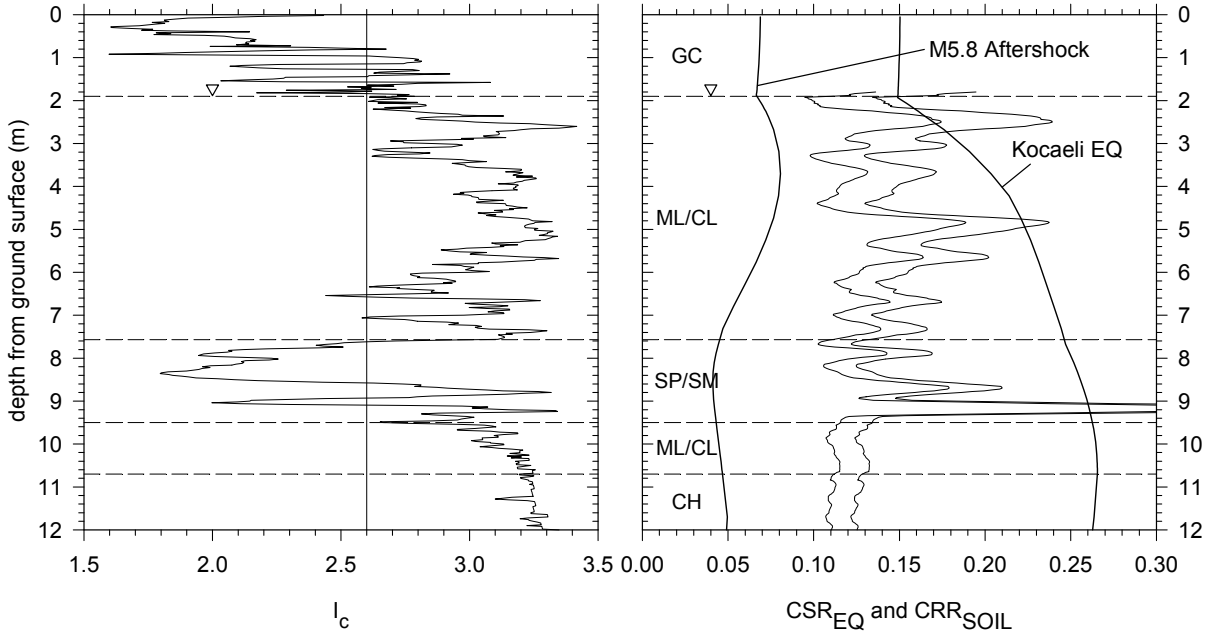

Figure 4-94. Soil behavior type index and cyclic stresses – E10 (Parking Lot)

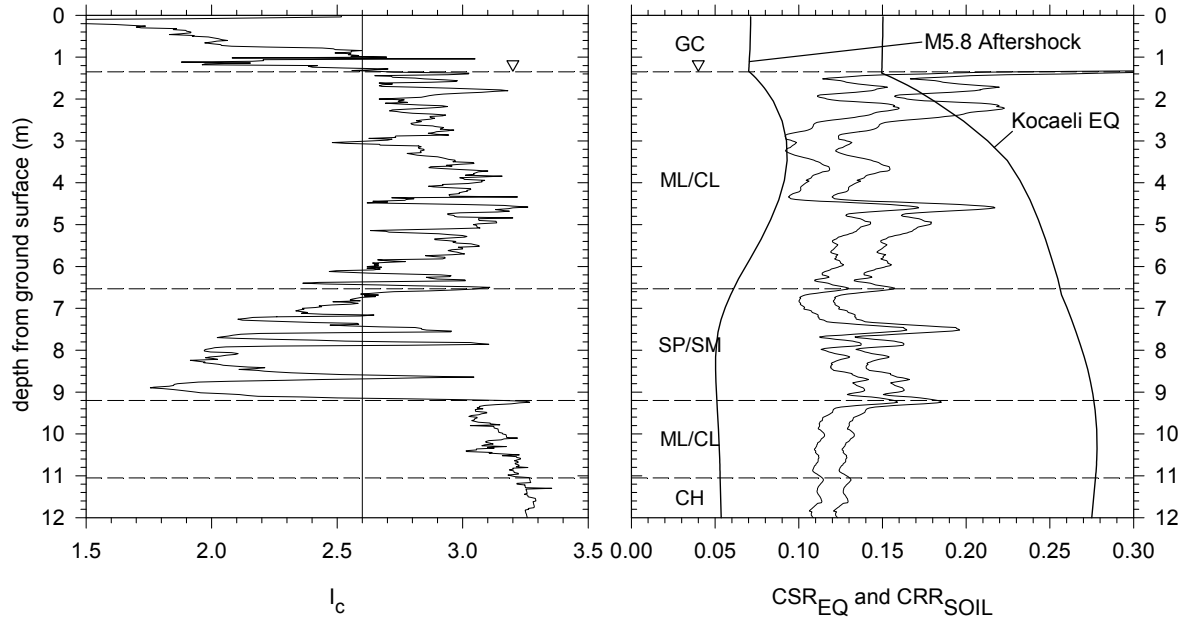

Figure 4-95. Soil behavior type index and cyclic stresses – E16 (Parking Lot)

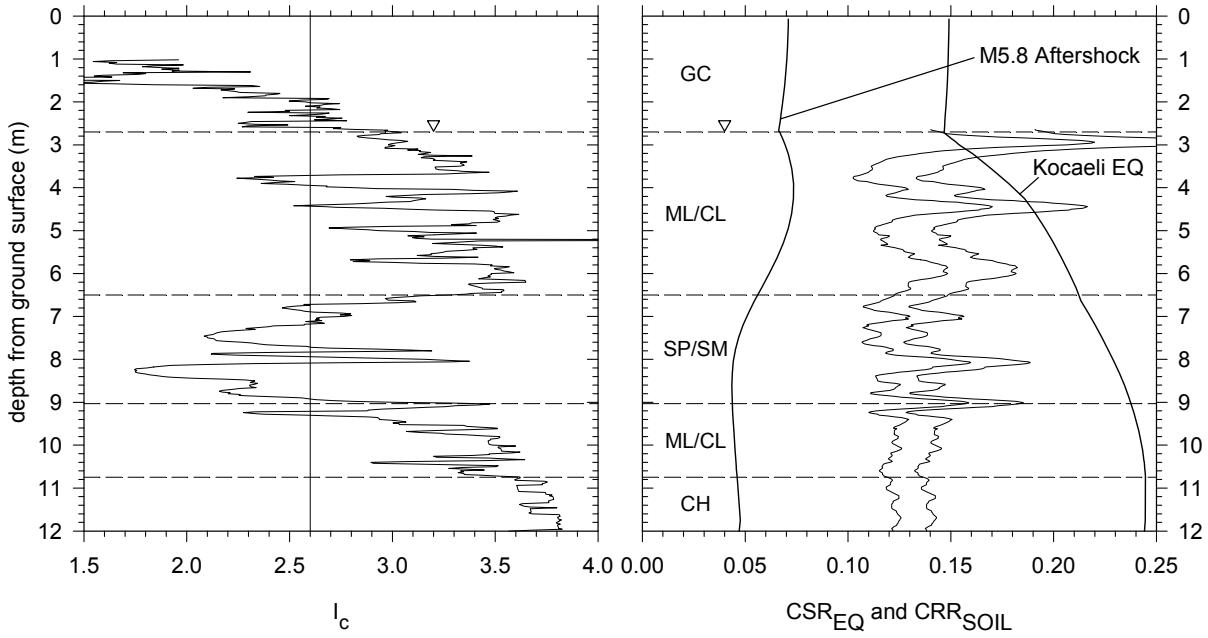

Figure 4-96. Soil behavior type index and cyclic stresses – E19 (Parking Lot)

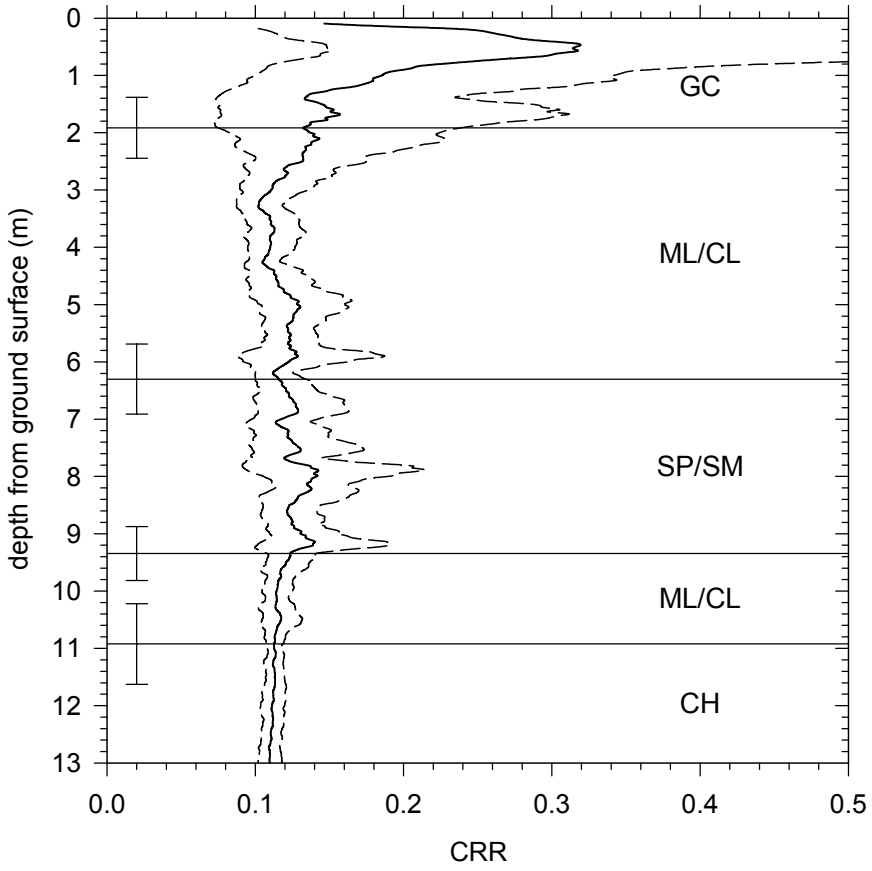

Figure 4-97. Estimated cyclic resistance ratio (CRR) for the Parking Lot area including the overconsolidation effects of the surcharge fill placement and removal. Median values and the 95% confidence interval (based on a log-normal distribution) from the CPT's at this section of the site. Layer boundaries inferred from these CPT's; mean values with plus/minus one standard deviation range.

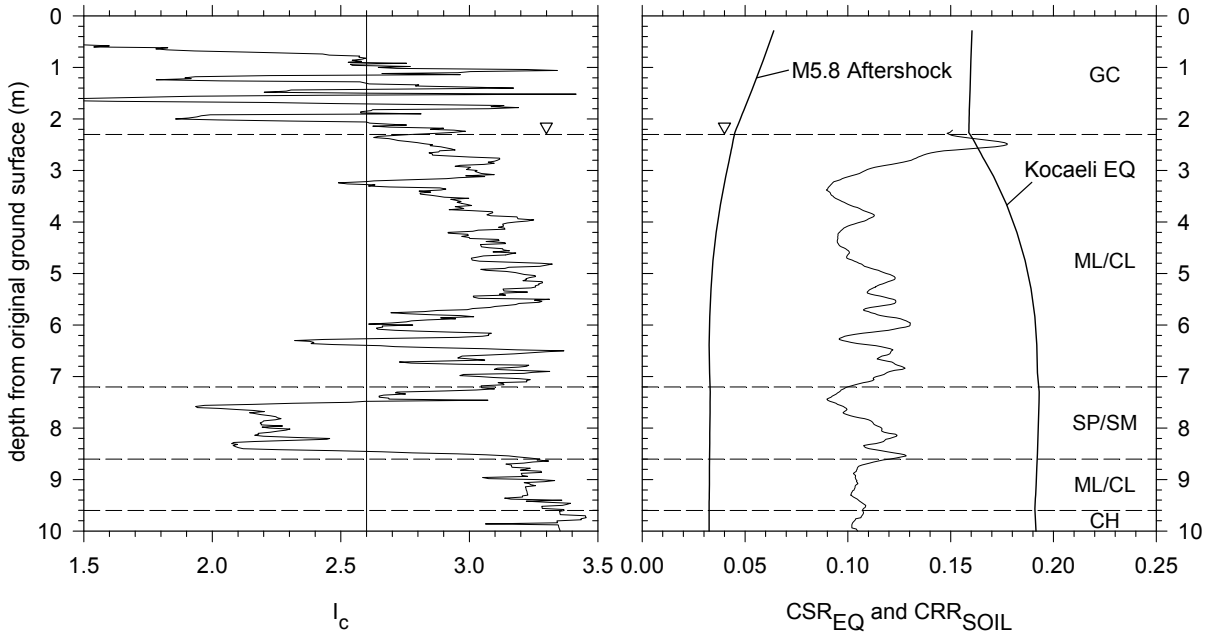

Figure 4-98. Soil behavior type index and cyclic stresses – F5 (Lot C)

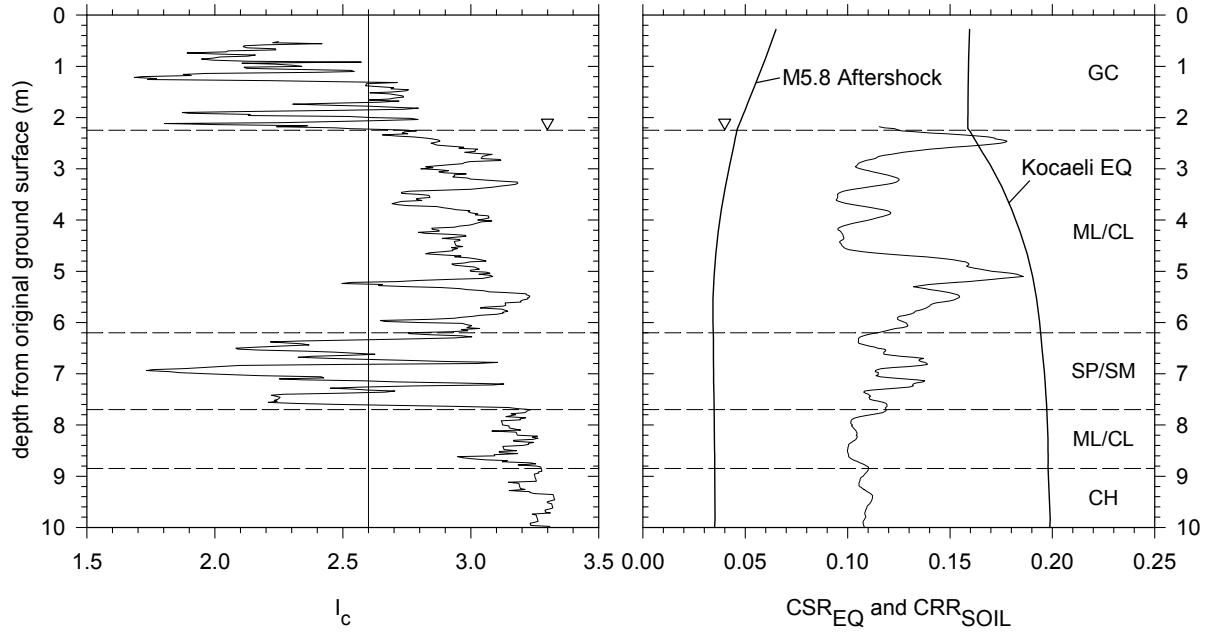

Figure 4-99. Soil behavior type index and cyclic stresses – F7 (Lot C)

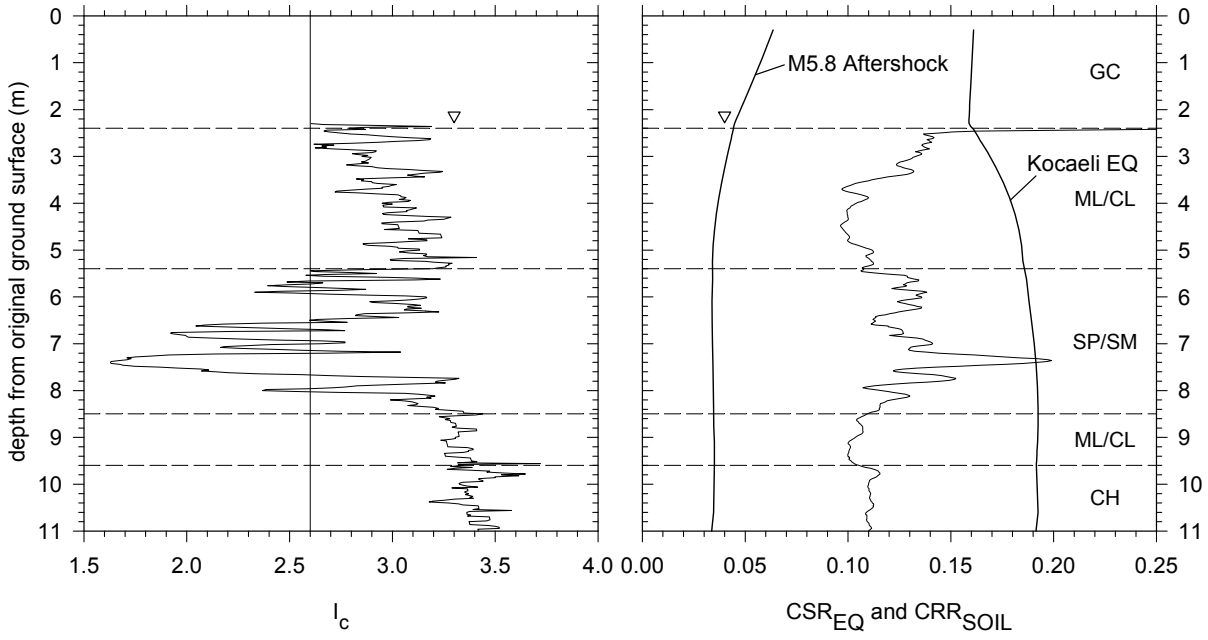

Figure 4-100. Soil behavior type index and cyclic stresses – H1 (Lot C)

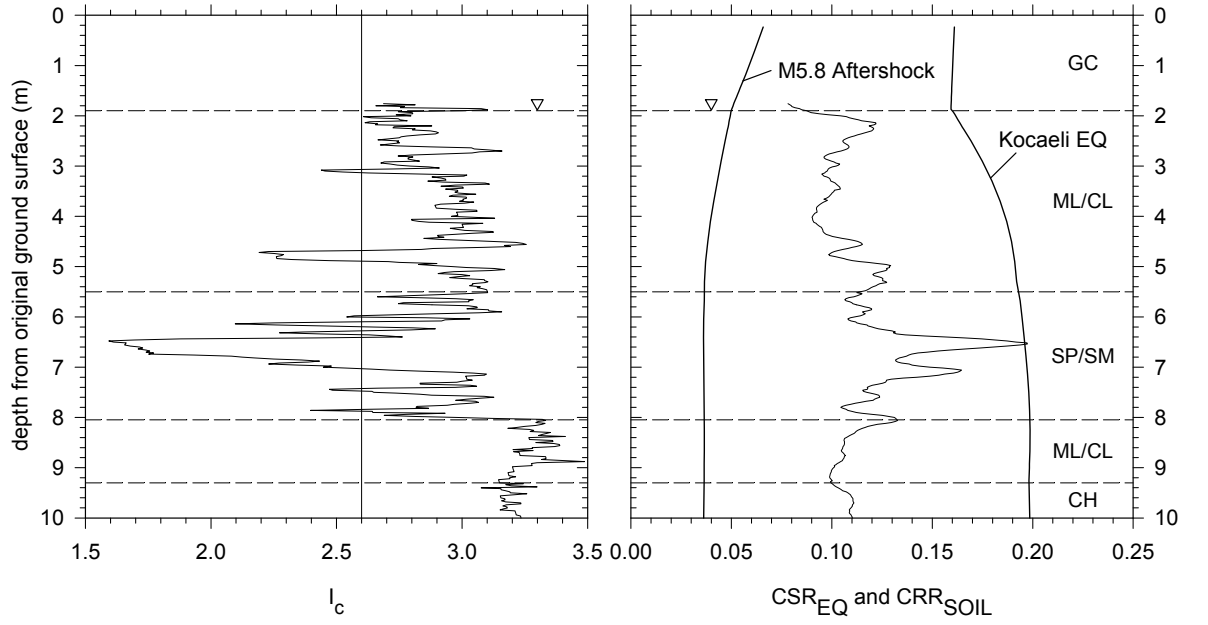

Figure 4-101. Soil behavior type index and cyclic stresses – H4 (Lot C)

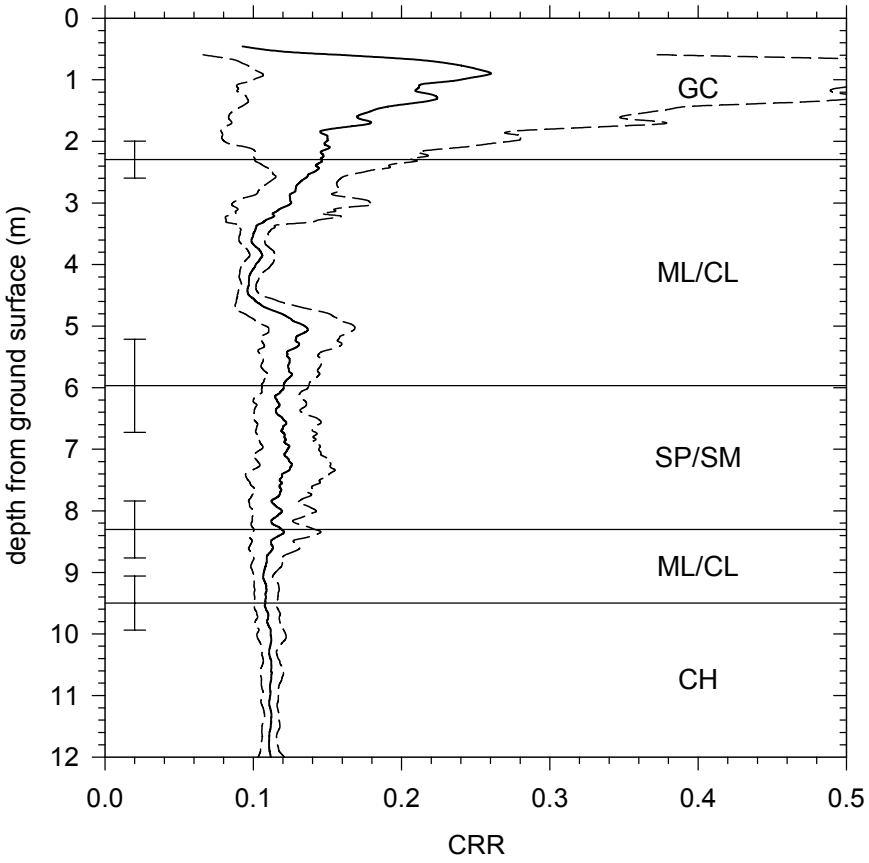

Figure 4-102. Estimated cyclic resistance ratio (CRR) for Lot C. Median values and the 95% confidence interval (based on a log-normal distribution) from the CPT's at this section of the site. Layer boundaries inferred from these CPT's; mean values with plus/minus one standard deviation range.

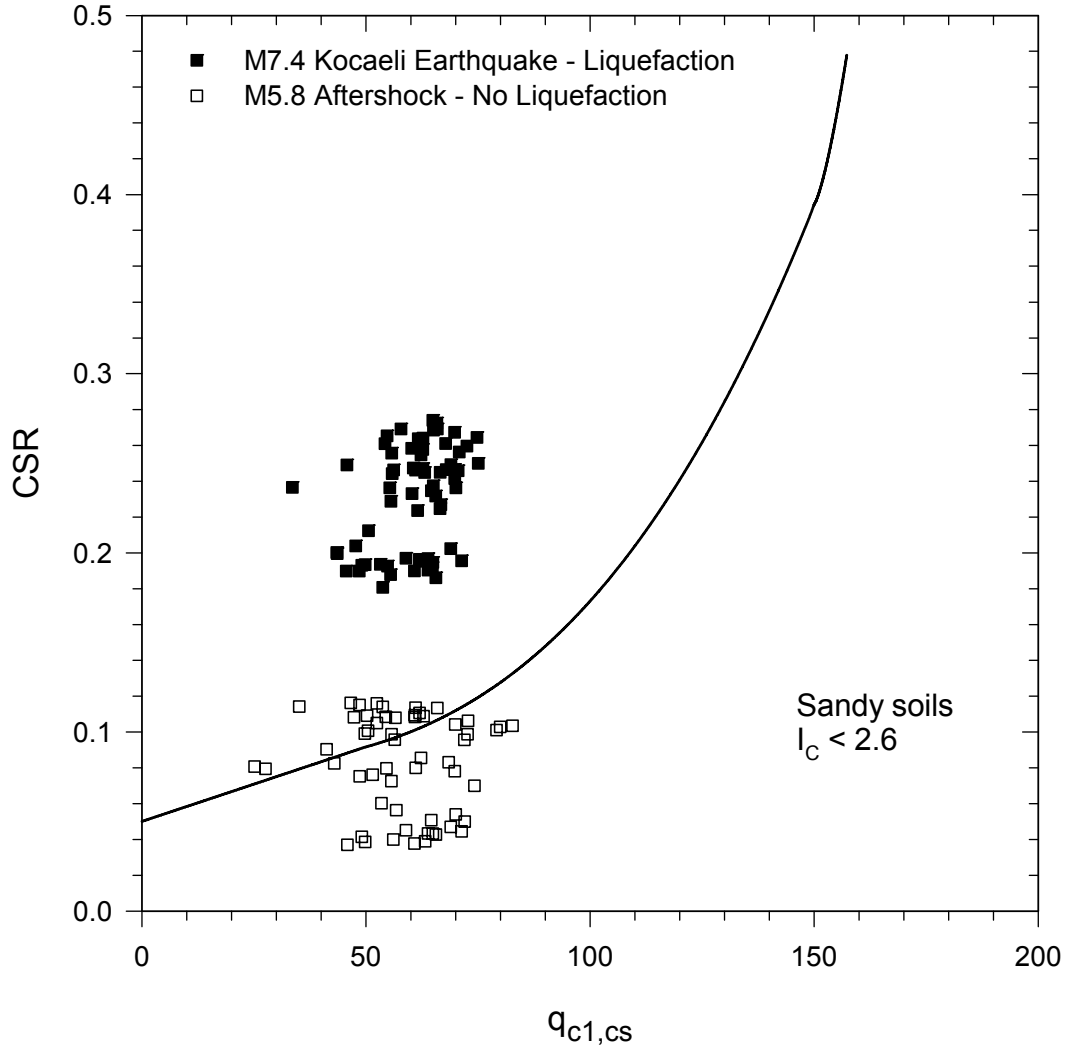

Figure 4-103. Summary of liquefaction/non-liquefaction events at Carrefour site – Sandy soils (I_c <2.6)

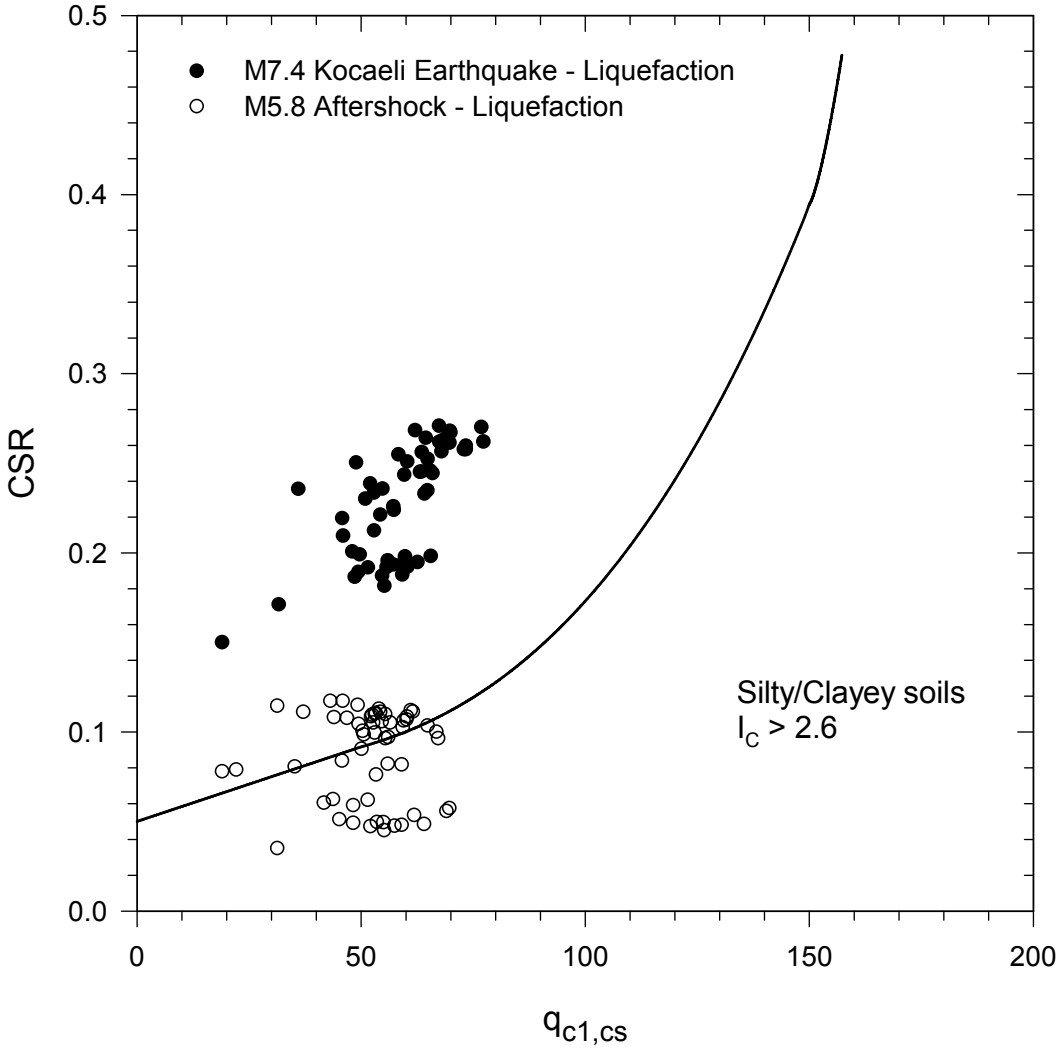

Figure 4-104. Summary of liquefaction/non-liquefaction events at Carrefour site – Soils with fines (Ic >2.6)

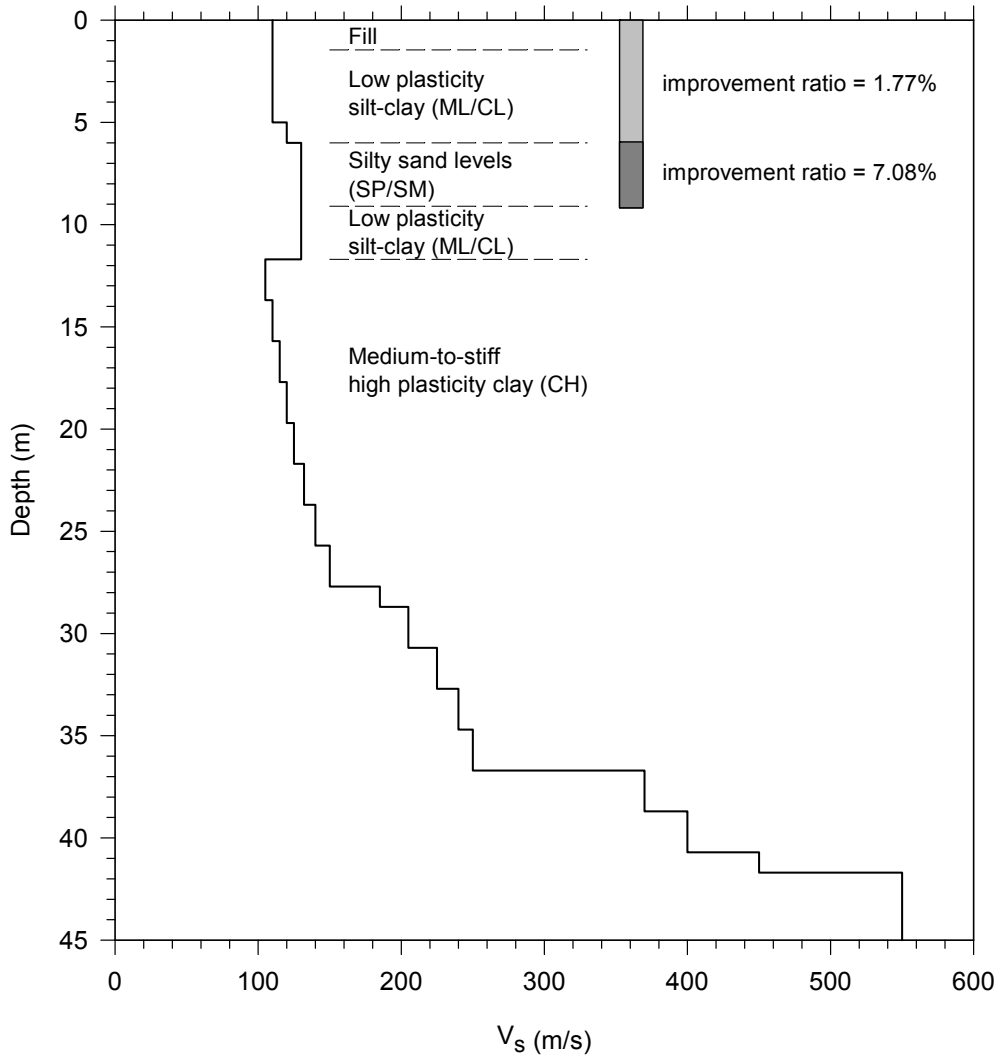

Figure 4-105. Soil layering and shear wave velocity model used in homogenized site response analyses.

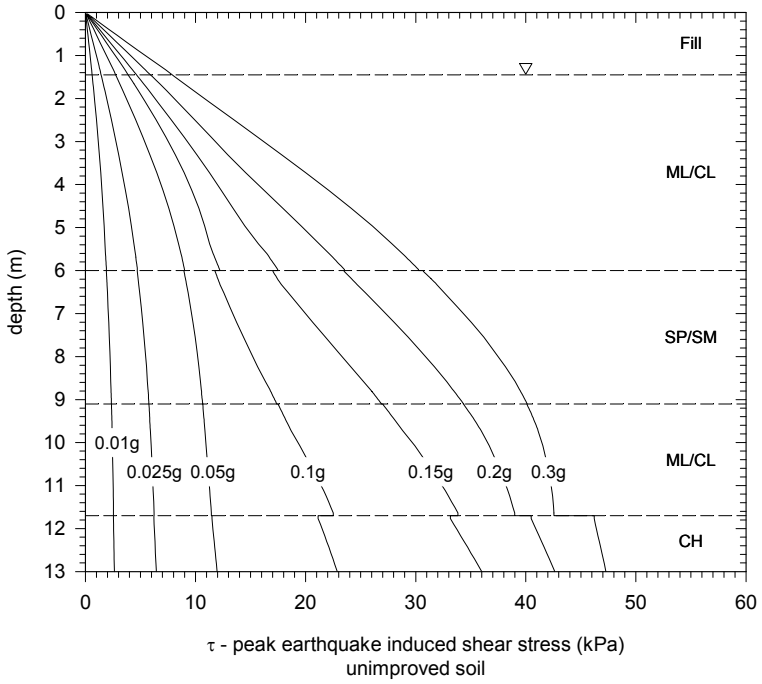

Figure 4-106. Peak shear stress on soil for different levels of shaking – unimproved

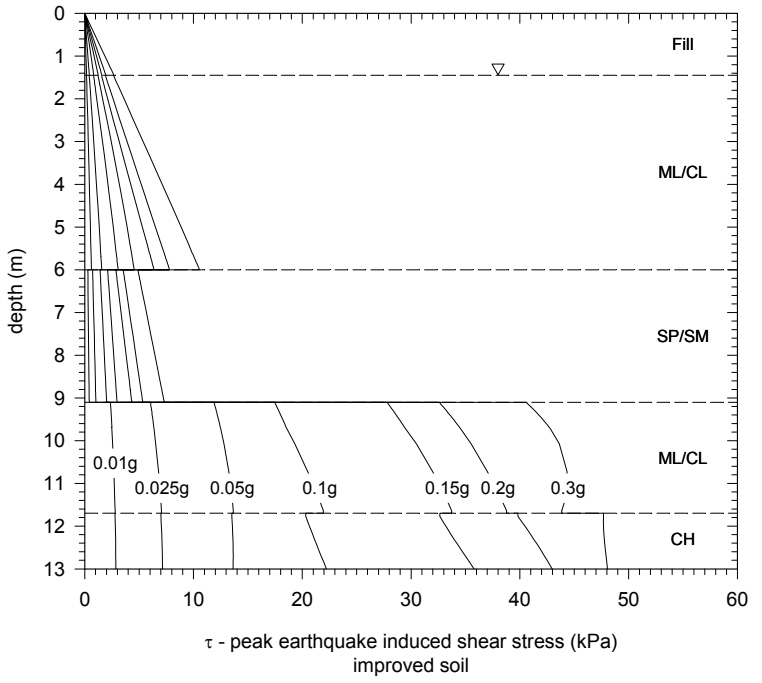

Figure 4-107. Peak shear stress on soil for different levels of shaking – improved

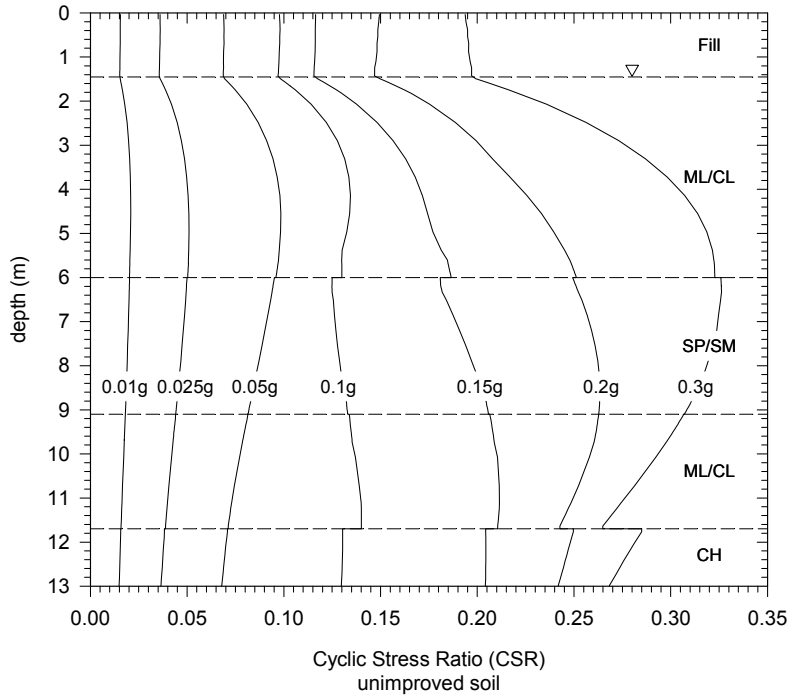

Figure 4-108. Cyclic stress ratio (CSR) for different levels of shaking – unimproved

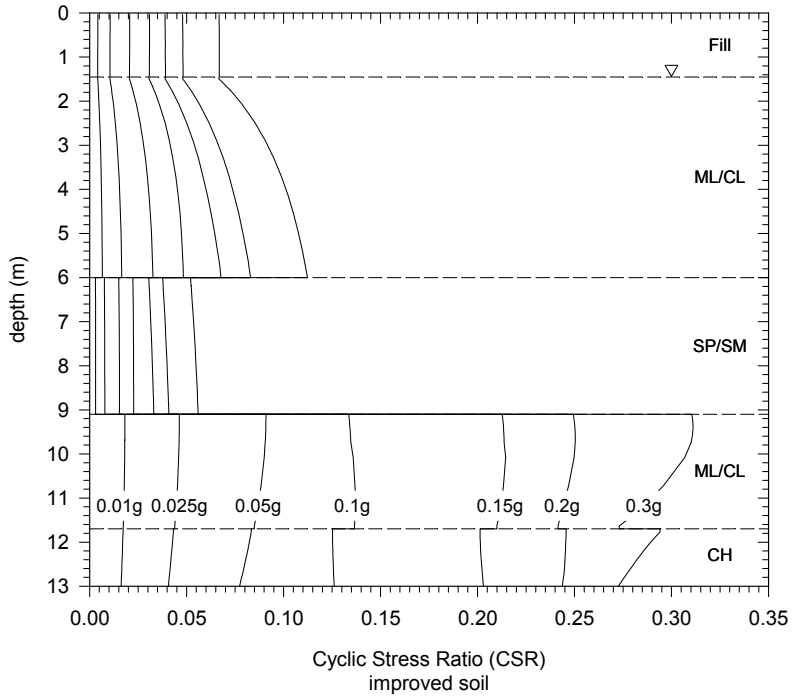

Figure 4-109. Cyclic stress ratio (CSR) for different levels of shaking – improved

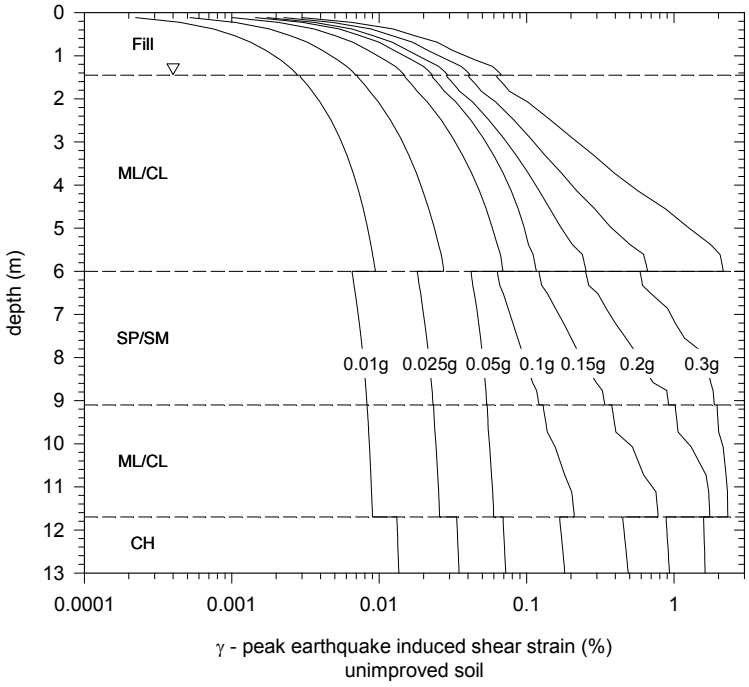

Figure 4-110. Peak shear strain for different levels of shaking – unimproved

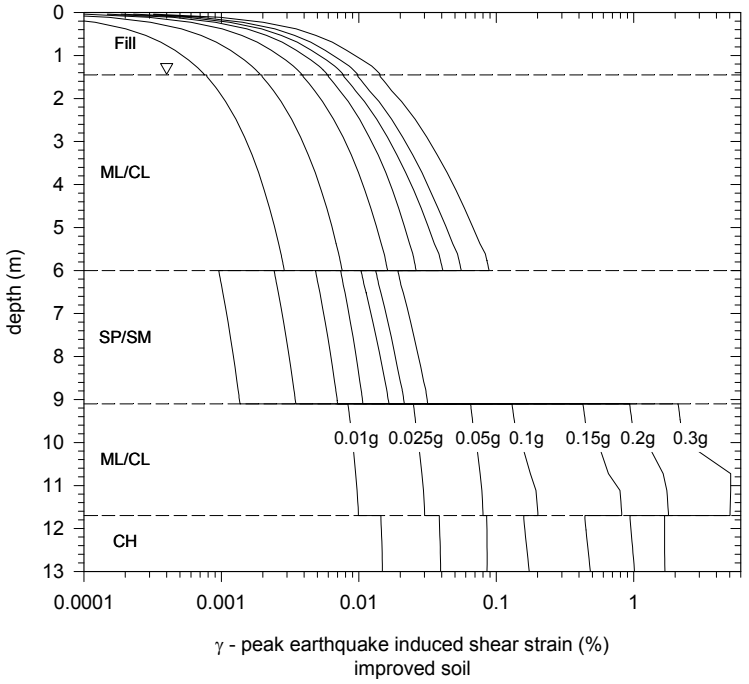

Figure 4-111. Peak shear strain for different levels of shaking – improved

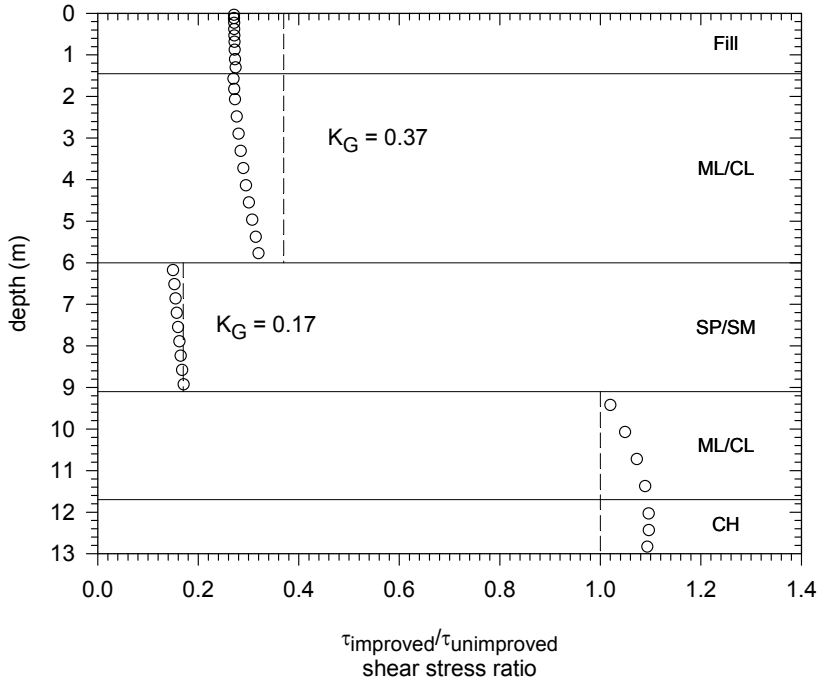

Figure 4-112. Ratio of the peak shear stress on the soil – improved/unimproved (pga = 0.01g)

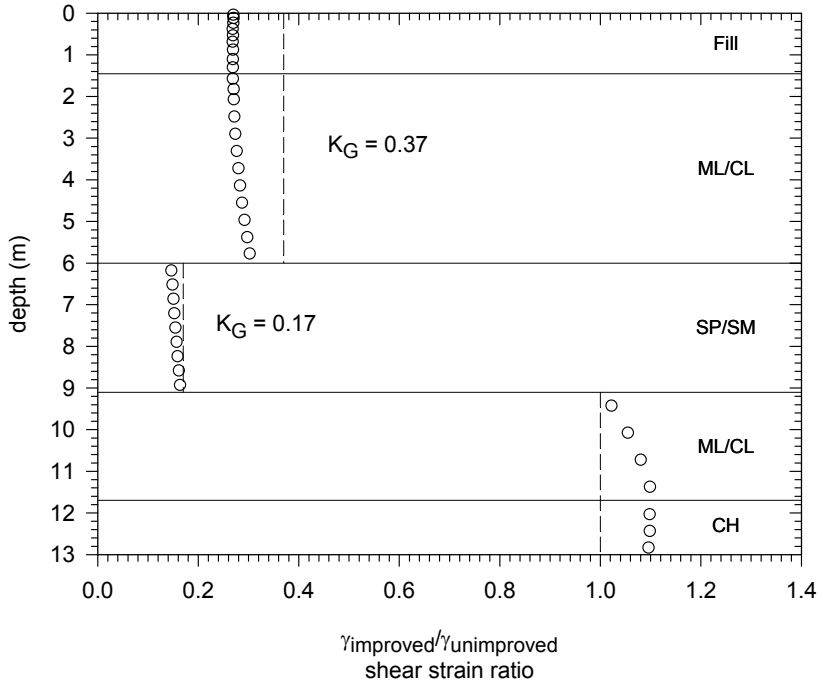

Figure 4-113. Ratio of the peak shear strain – improved/unimproved (pga = 0.01g)

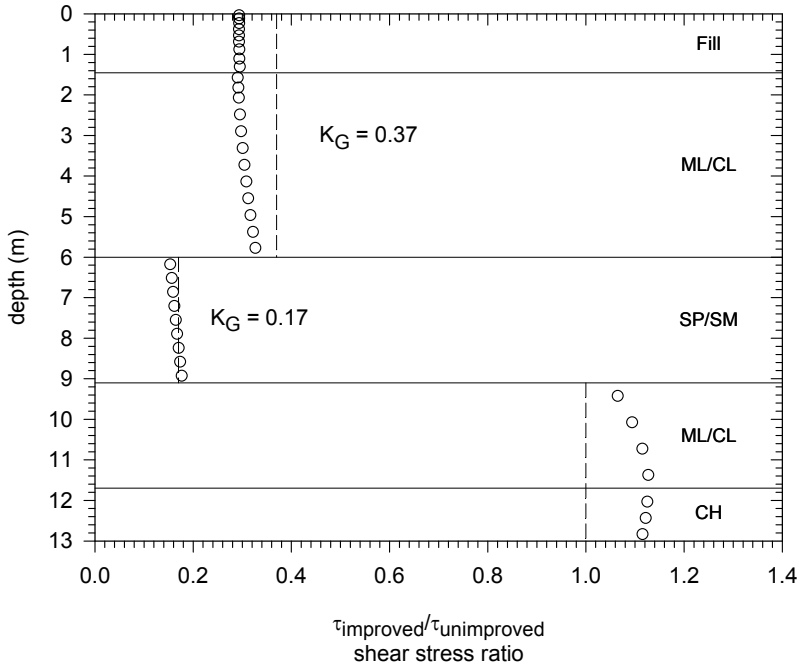

Figure 4-114. Ratio of the peak shear stress on the soil – improved/unimproved (pga = 0.025g)

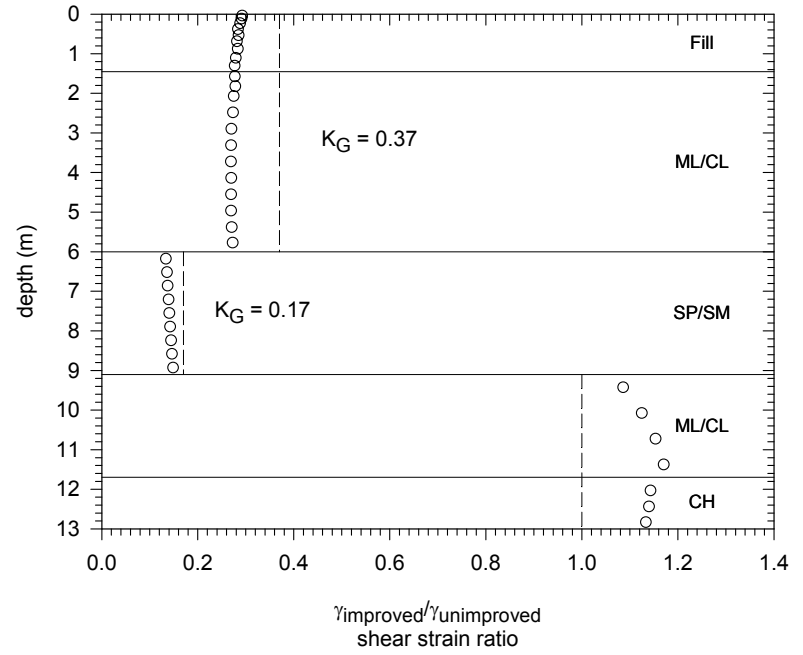

Figure 4-115. Ratio of the peak shear strain – improved/unimproved (pga = 0.025g)

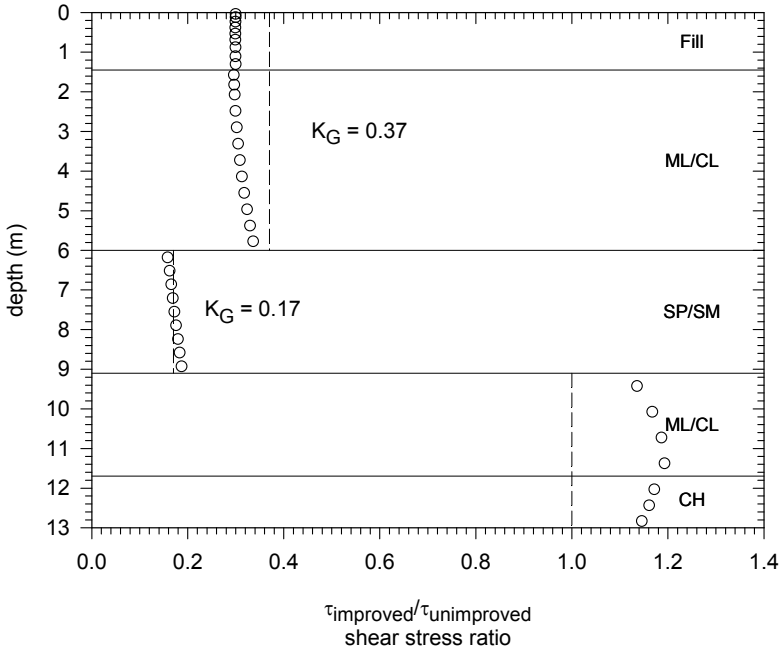

Figure 4-116. Ratio of the peak shear stress on the soil – improved/unimproved (pga = 0.05g)

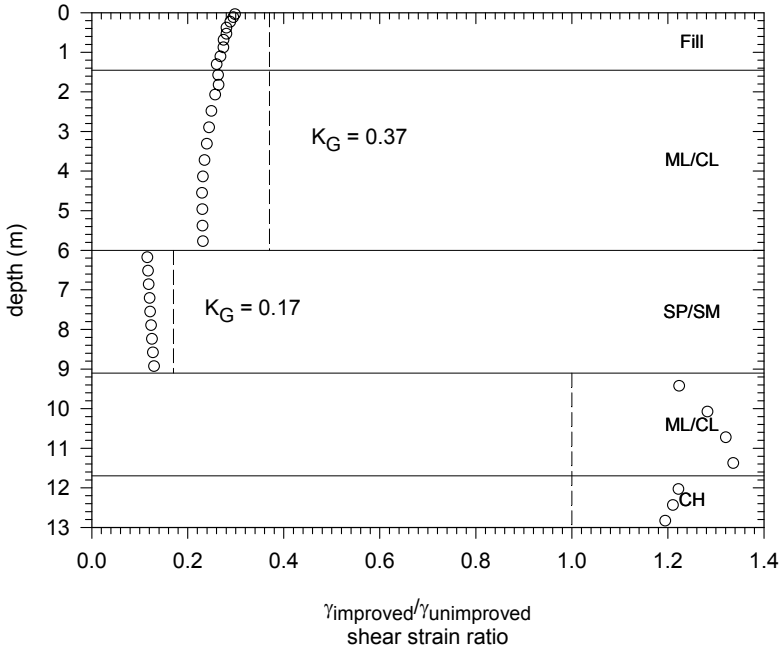

Figure 4-117. Ratio of the peak shear strain – improved/unimproved (pga = 0.05g)

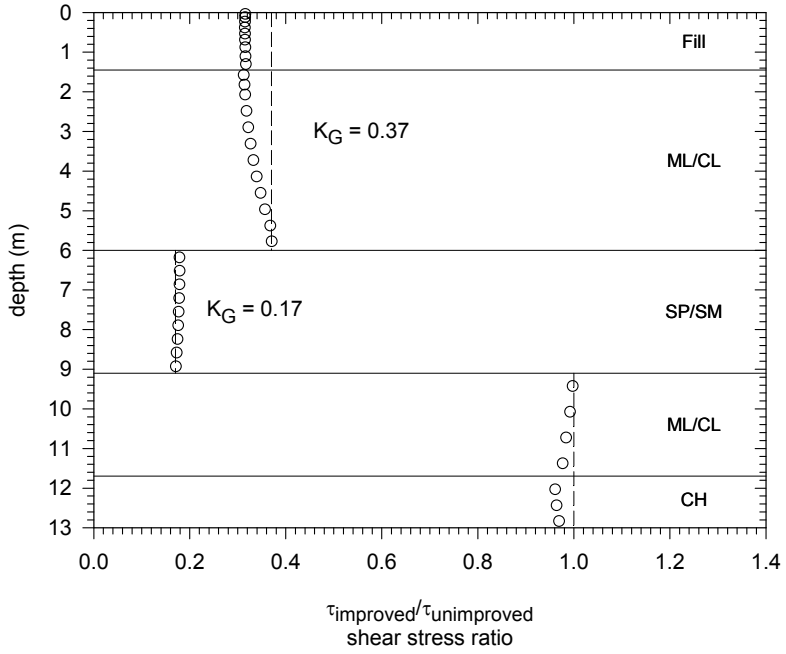

Figure 4-118. Ratio of the peak shear stress on the soil – improved/unimproved (pga = 0.10g)

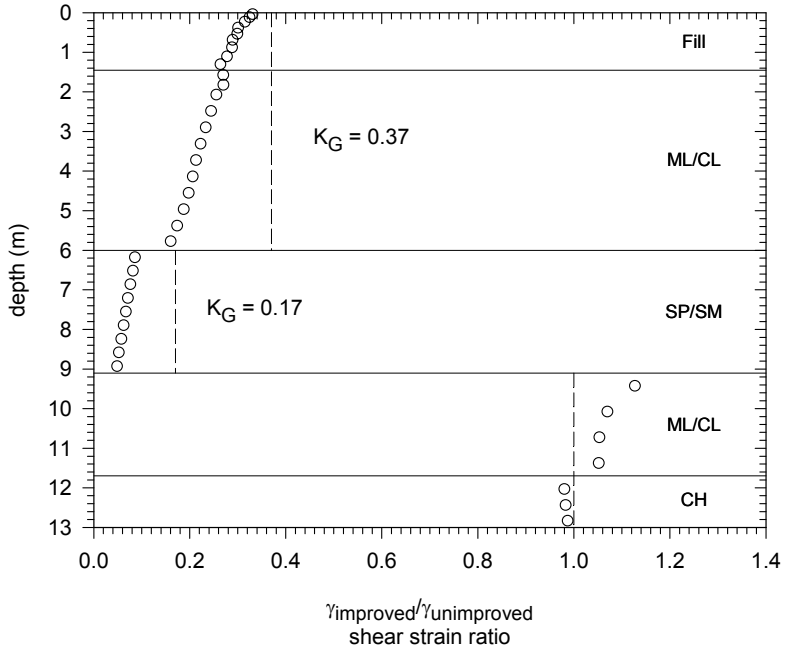

Figure 4-119. Ratio of the peak shear strain – improved/unimproved (pga = 0.10g)

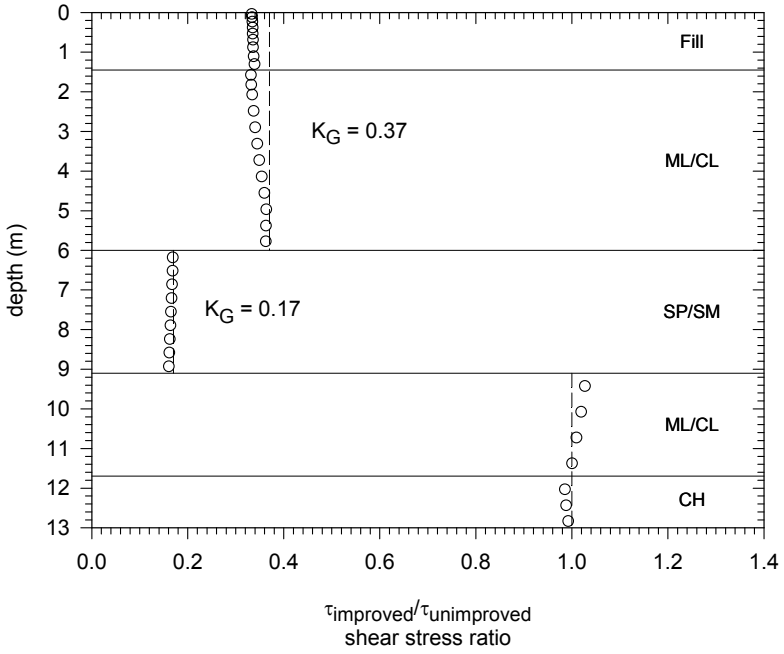

Figure 4-120. Ratio of the peak shear stress on the soil – improved/unimproved (pga = 0.15)

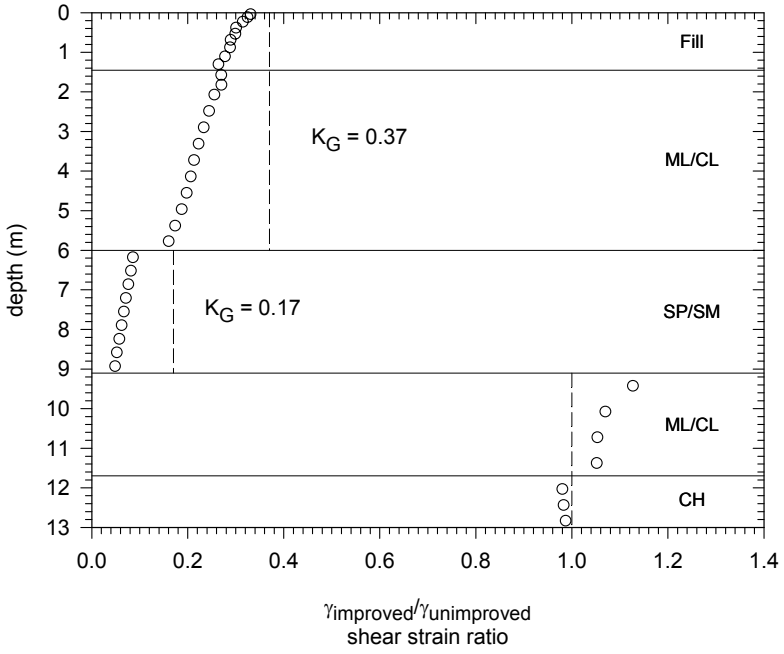

Figure 4-121. Ratio of the peak shear strain – improved/unimproved (pga = 0.15g)

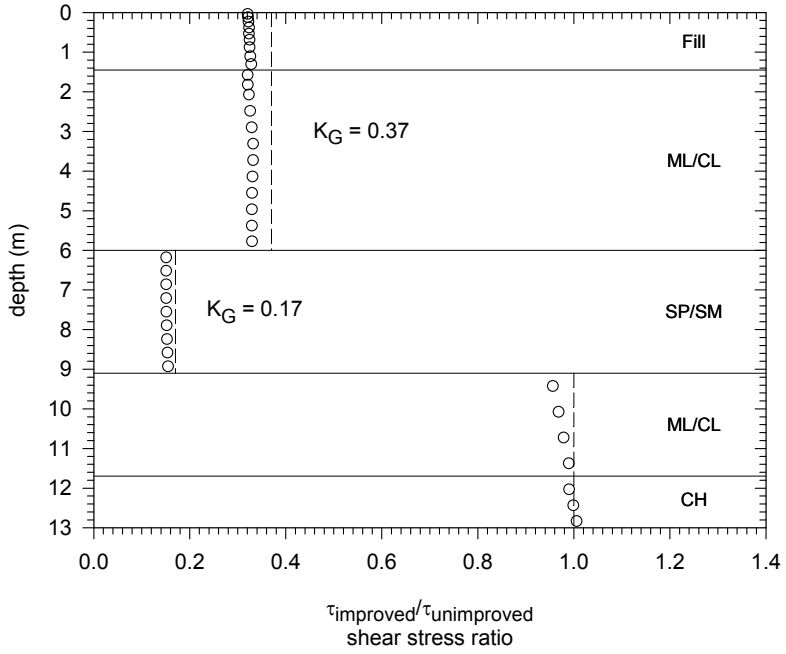

Figure 4-122. Ratio of the peak shear stress on the soil – improved/unimproved (pga = 0.20g)

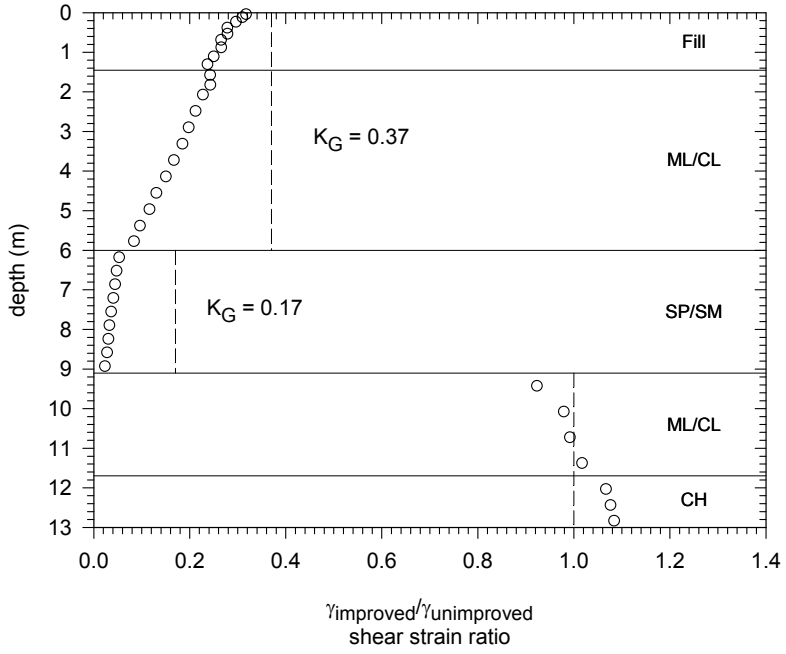

Figure 4-123. Ratio of the peak shear strain – improved/unimproved (pga = 0.20g)

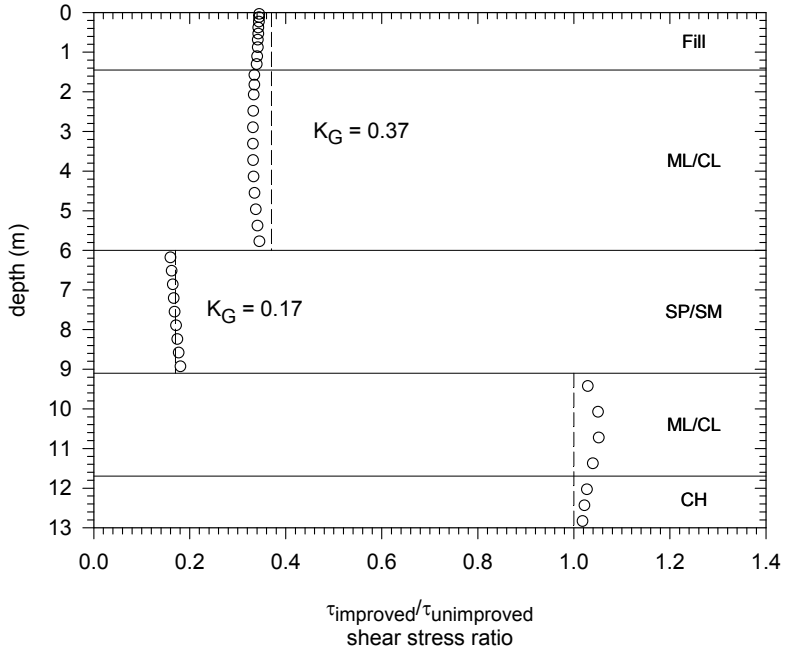

Figure 4-124. Ratio of the peak shear stress on the soil – improved/unimproved (pga = 0.30g)

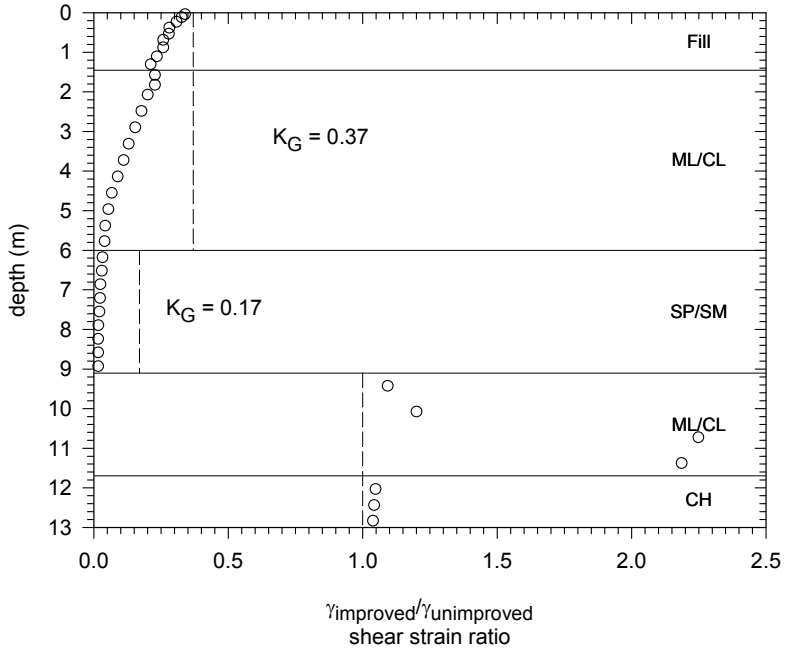

Figure 4-125. Ratio of the peak shear strain – improved/unimproved (pga = 0.30g)

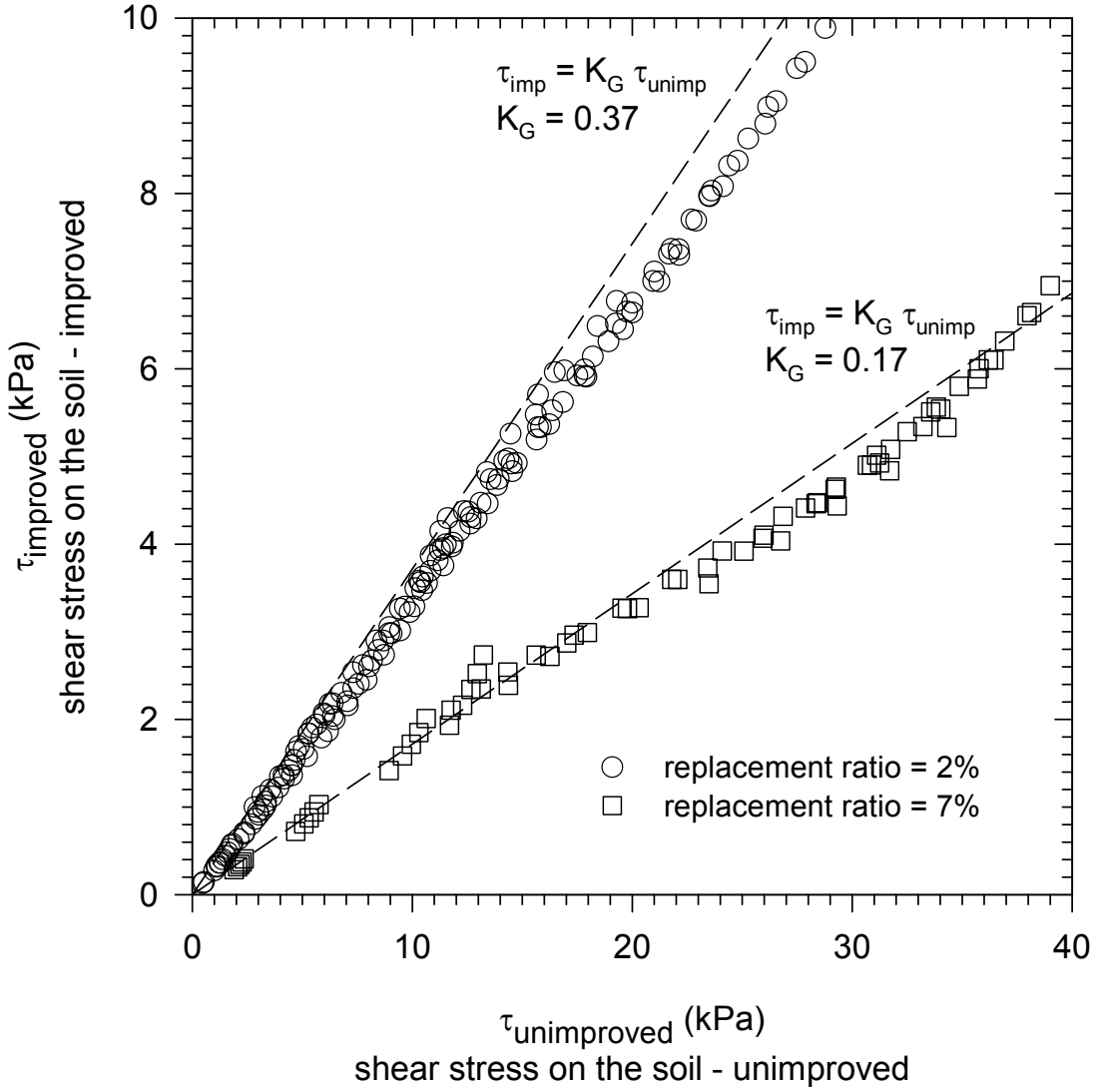

Figure 4-126. Peak shear stress on the soil along the profile for various shaking levels (0.01g, 0.025g, 0.05g, 0.10g, 0.15g, 0.20g and 0.30g) – improved and unimproved cases

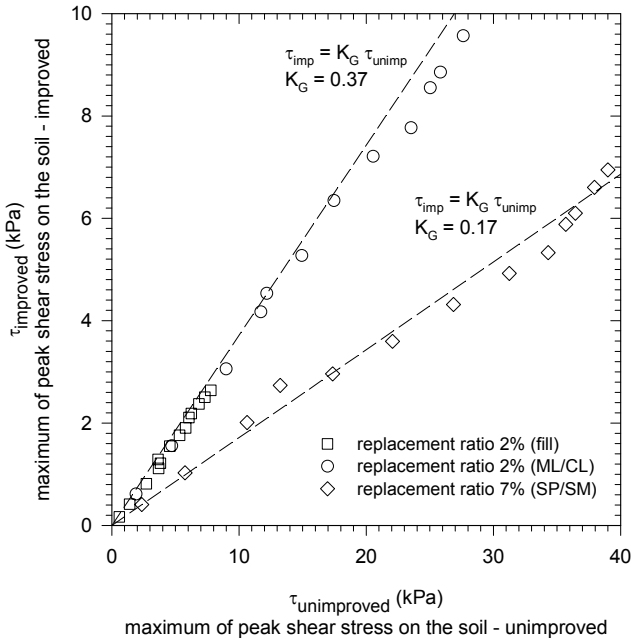

Figure 4-127. Maximum of the peak shear stress of each soil layer for various shaking levels (0.01g, 0.025g, 0.05g, 0.10g, 0.15g, 0.20g and 0.30g) – improved and unimproved cases

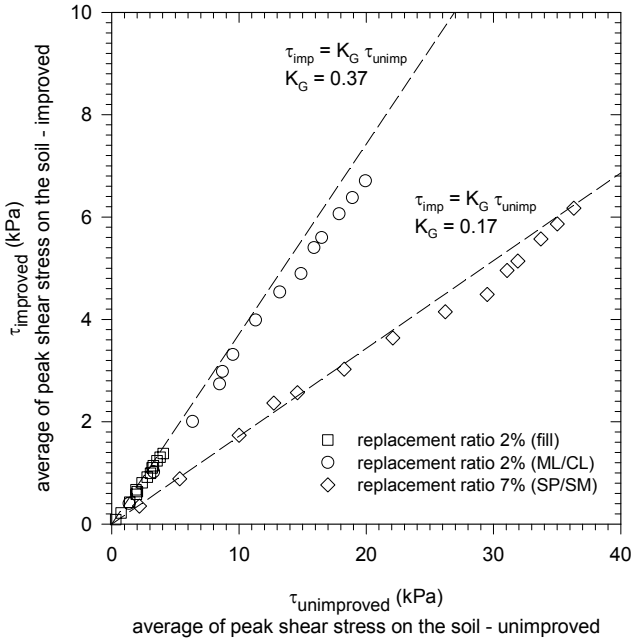

Figure 4-128. Average of the peak shear stress of each soil layer for various shaking levels (0.01g, 0.025g, 0.05g, 0.10g, 0.15g, 0.20g and 0.30g) – improved and unimproved cases

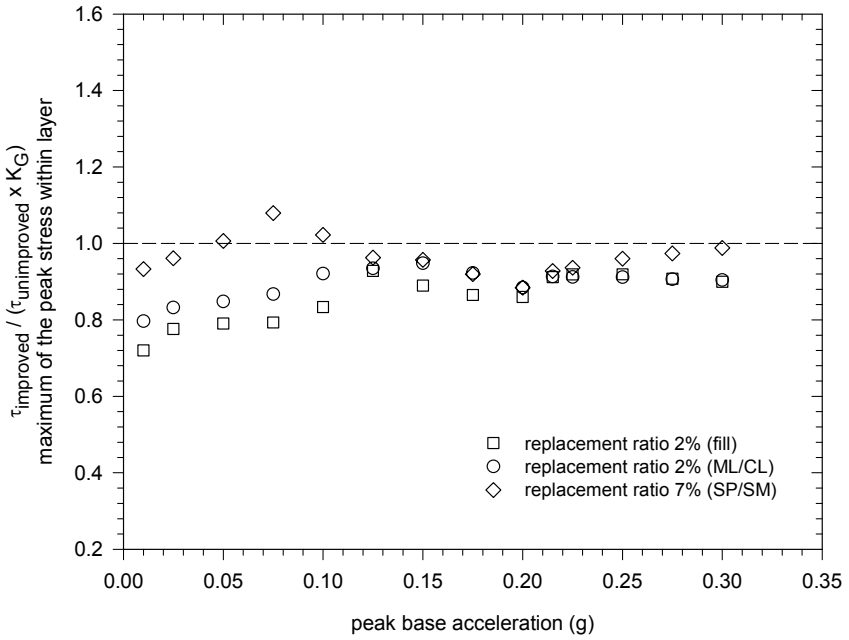

Figure 4-129. Ratio of the calculated shear stress to the reduced shear stress estimated by the shear stress reduction ratio – maximum values of peak shear stress from each layer

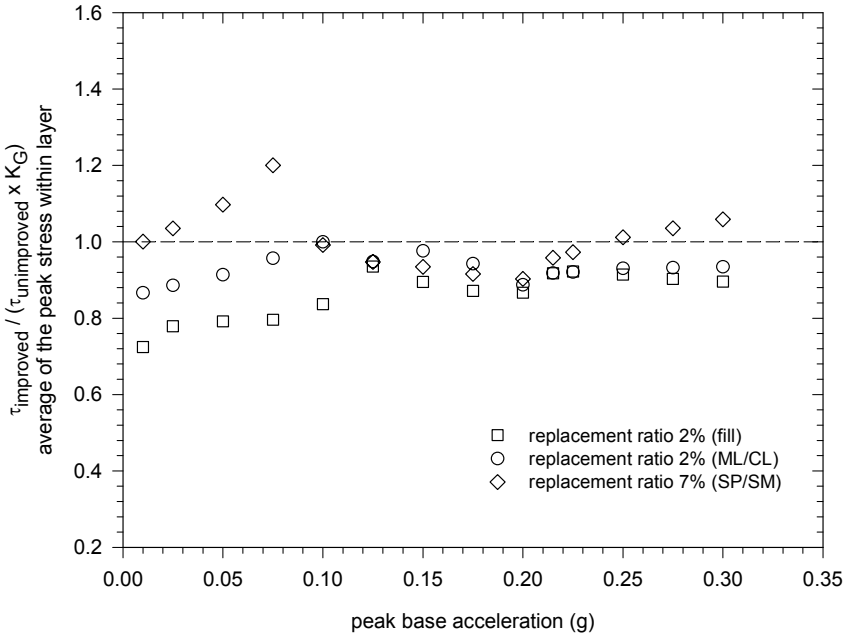

Figure 4-130. Ratio of the calculated shear stress to the reduced shear stress estimated by the shear stress reduction ratio – maximum values of peak shear stress from each layer

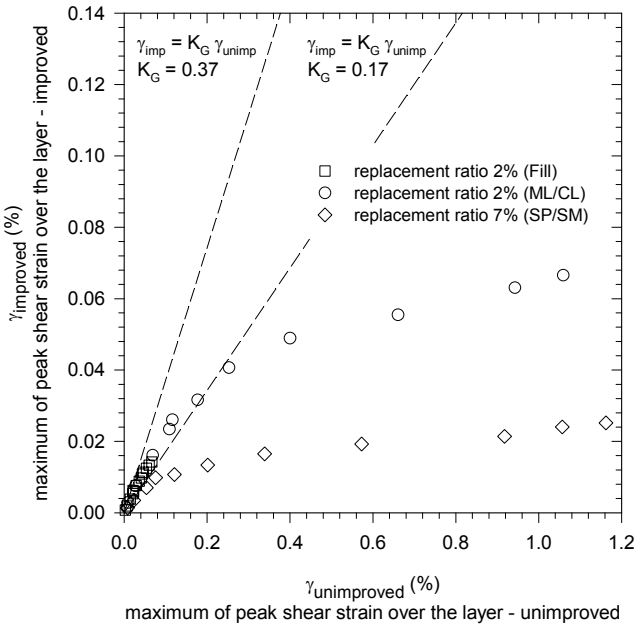

Figure 4-131. Maximum of the peak shear strain of each layer for various shaking levels (0.01g, 0.025g, 0.05g, 0.10g, 0.15g, 0.20g and 0.30g) – improved and unimproved cases

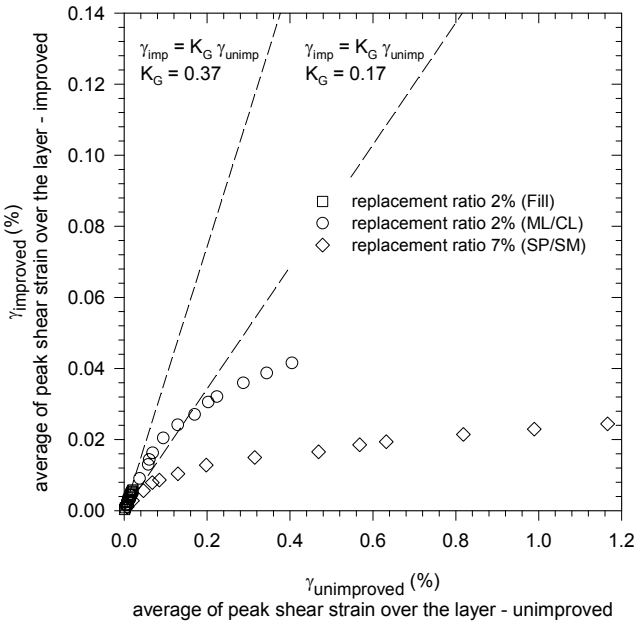

Figure 4-132. Average of the peak shear strain of each layer for various shaking levels (0.01g, 0.025g, 0.05g, 0.10g, 0.15g, 0.20g and 0.30g) – improved and unimproved cases

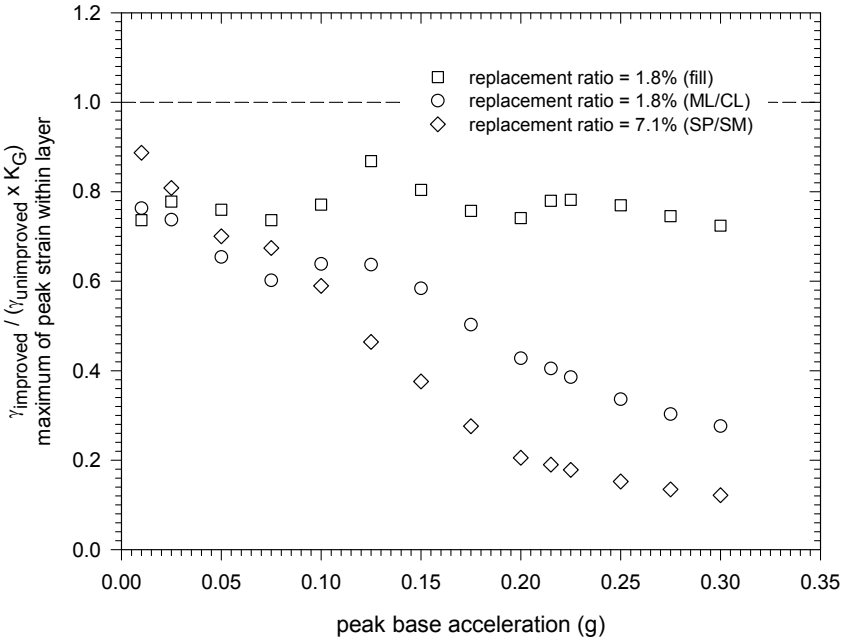

Figure 4-133. Ratio of the calculated shear strain to the reduced shear strain estimated by the shear stress reduction ratio – maximum values of peak shear strain from each layer

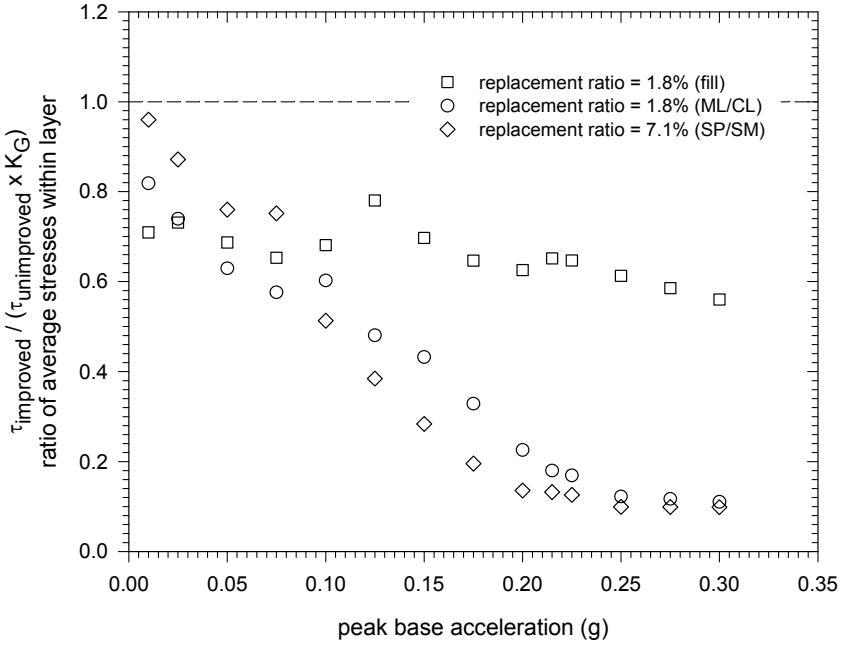

Figure 4-134. Ratio of the calculated shear strain to the reduced shear strain estimated by the shear stress reduction ratio – average values of peak shear strain from each layer

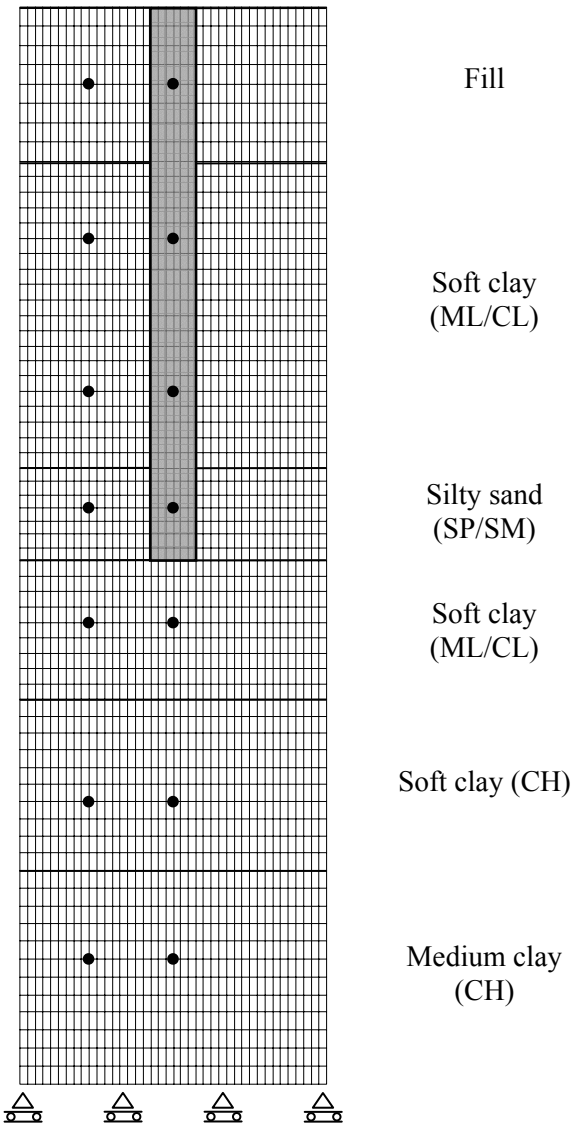

Figure 4-135. Finite elements mesh of one of the models. Case 2 – 0.6m diameter jet grout columns with 4.0 meter center-to-center spacing.

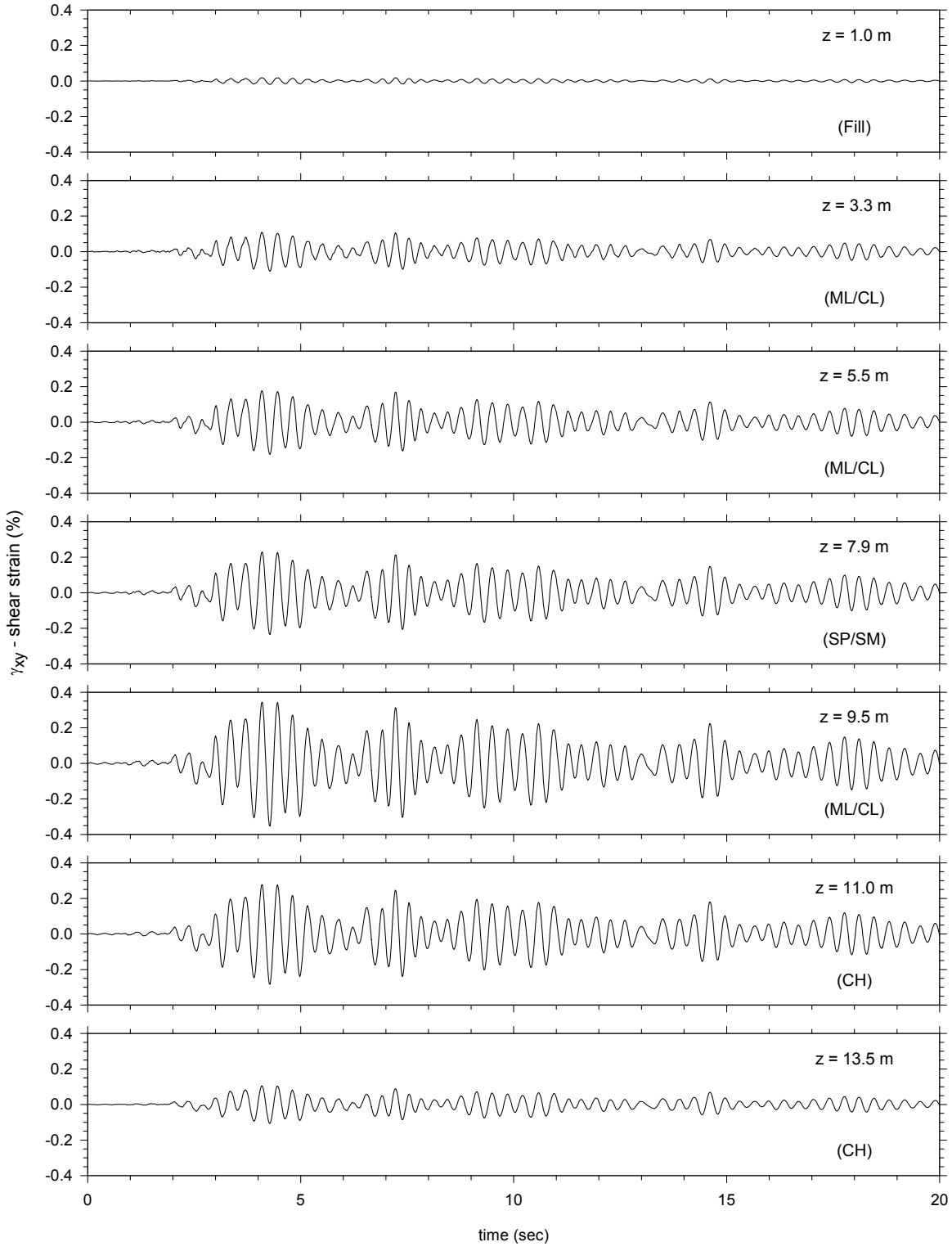

Figure 4-136. Shear strain histories along the unimproved soil profile

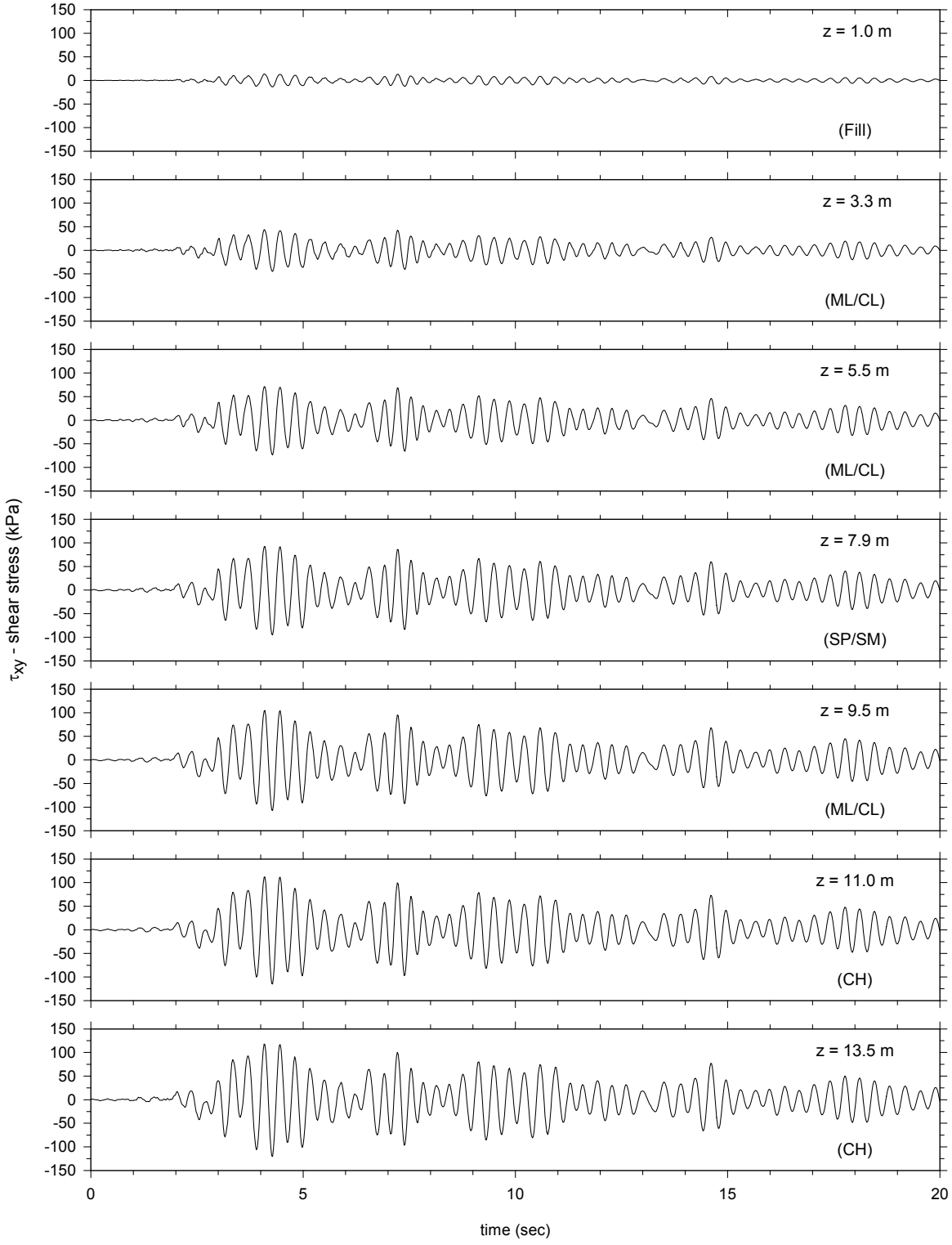

Figure 4-137. Shear stress histories along the unimproved soil profile

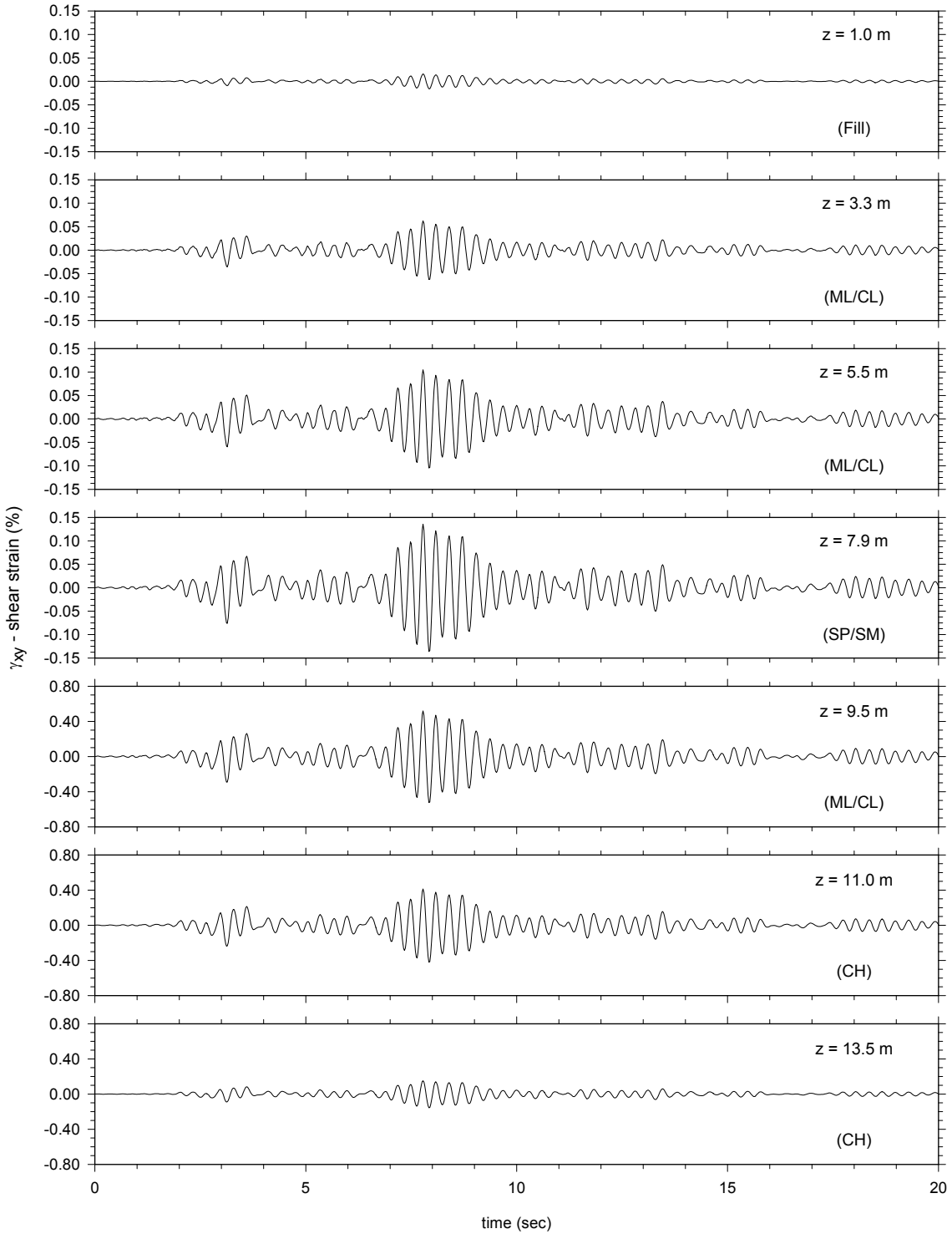

Figure 4-138. Shear strain within the soil – Case 1 – 3 m spaced jet grout columns (0.6 m diameter)

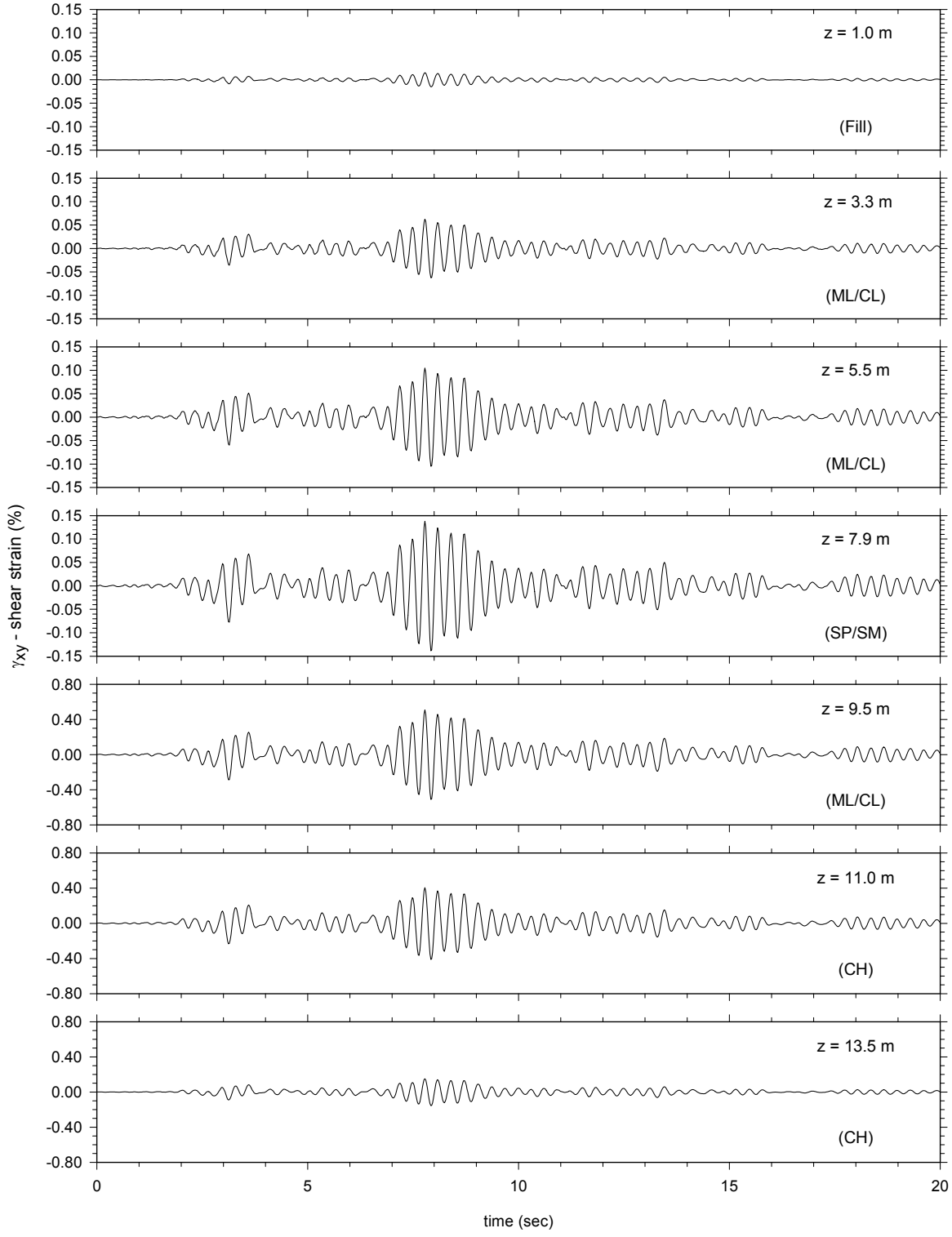

Figure 4-139. Shear strain along the center of the model (along jet grout column centerline and unimproved soils below) – Case 1 – 3 m spaced jet grout columns (0.6 m diameter)

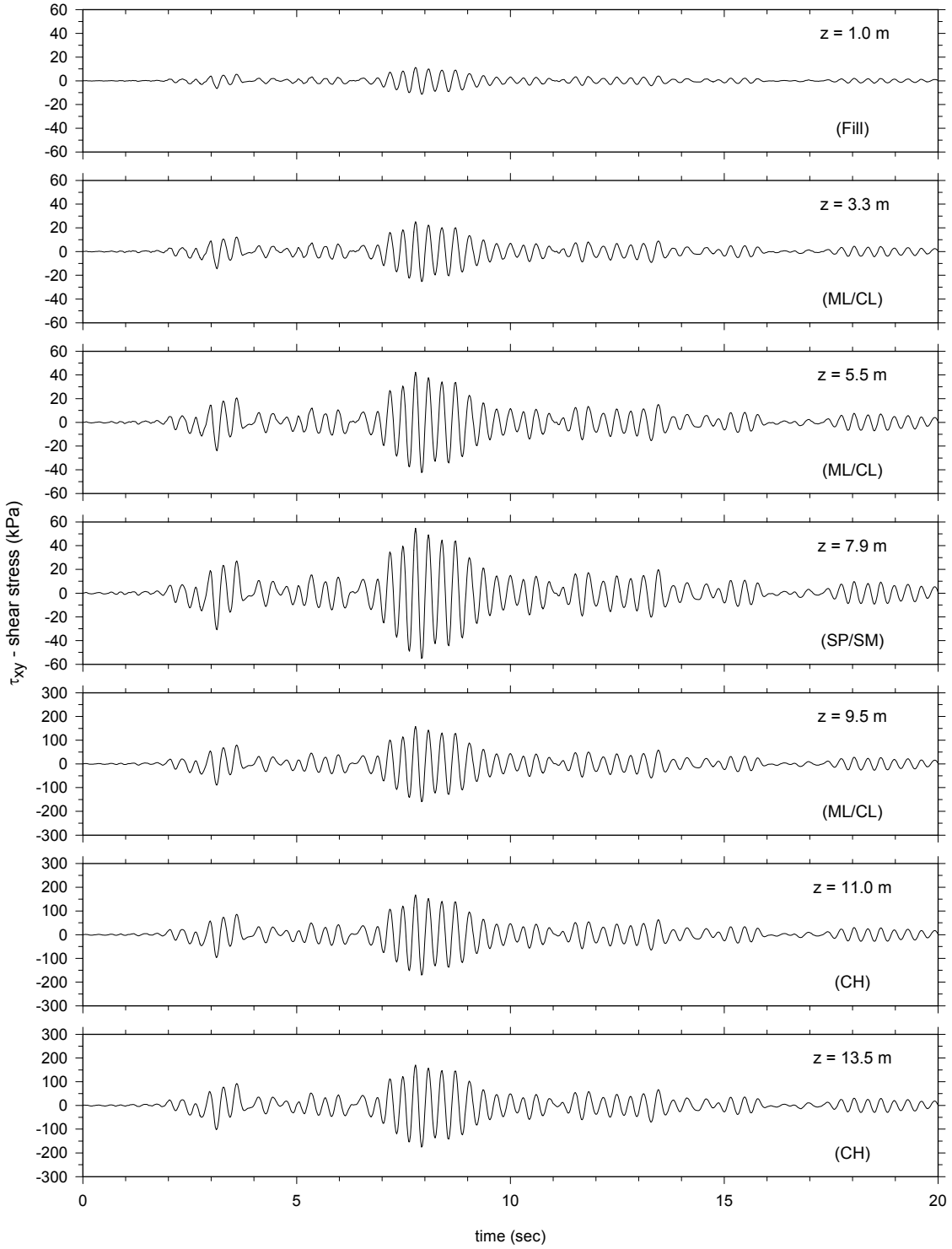

Figure 4-140. Shear stresses within the soil (Case 1) – 3 m spaced jet grout columns (0.6 m diameter)

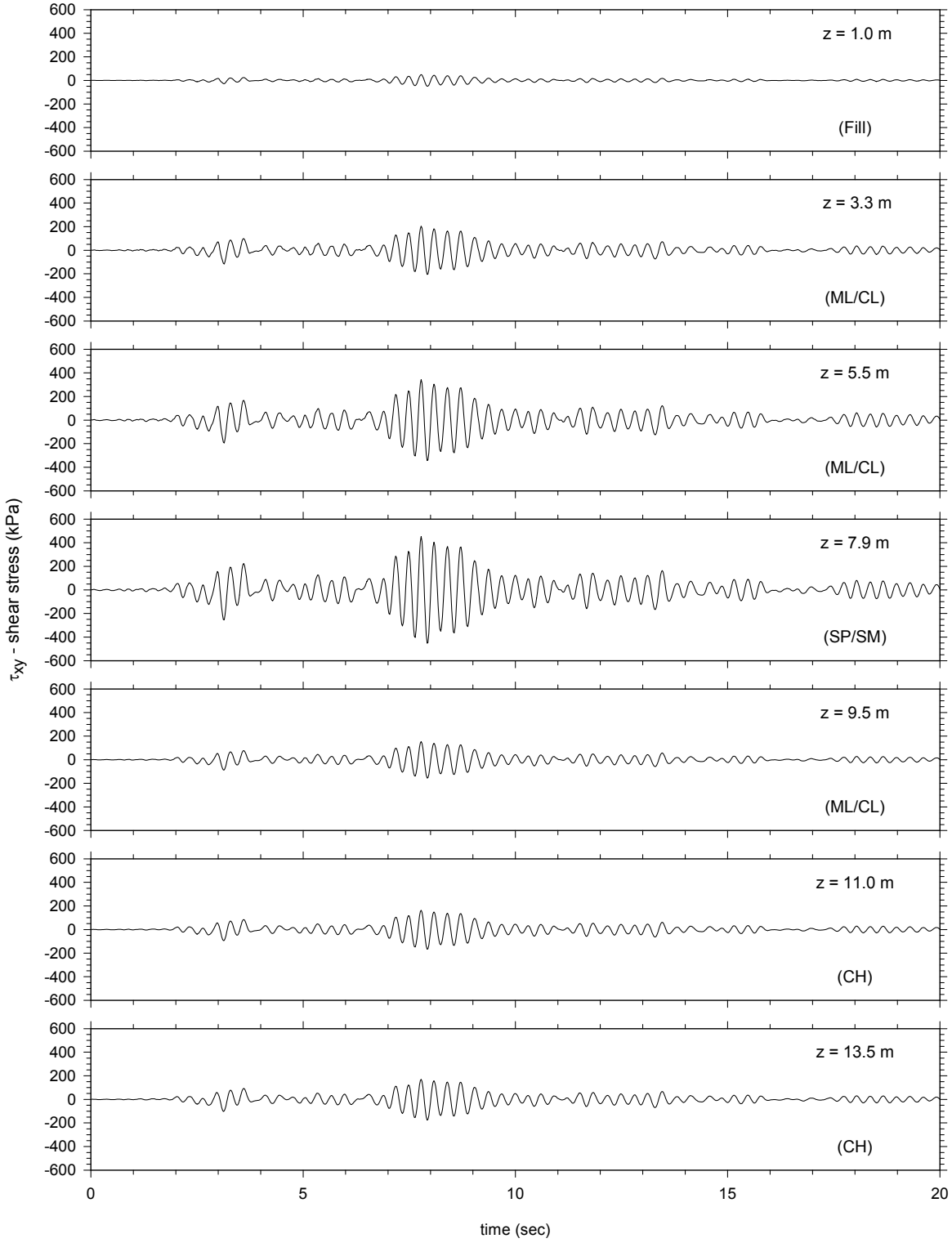

Figure 4-141. Shear stresses within jet grout column centerline (Case 1) – 3 m spaced jet grout columns (0.6 m diameter)

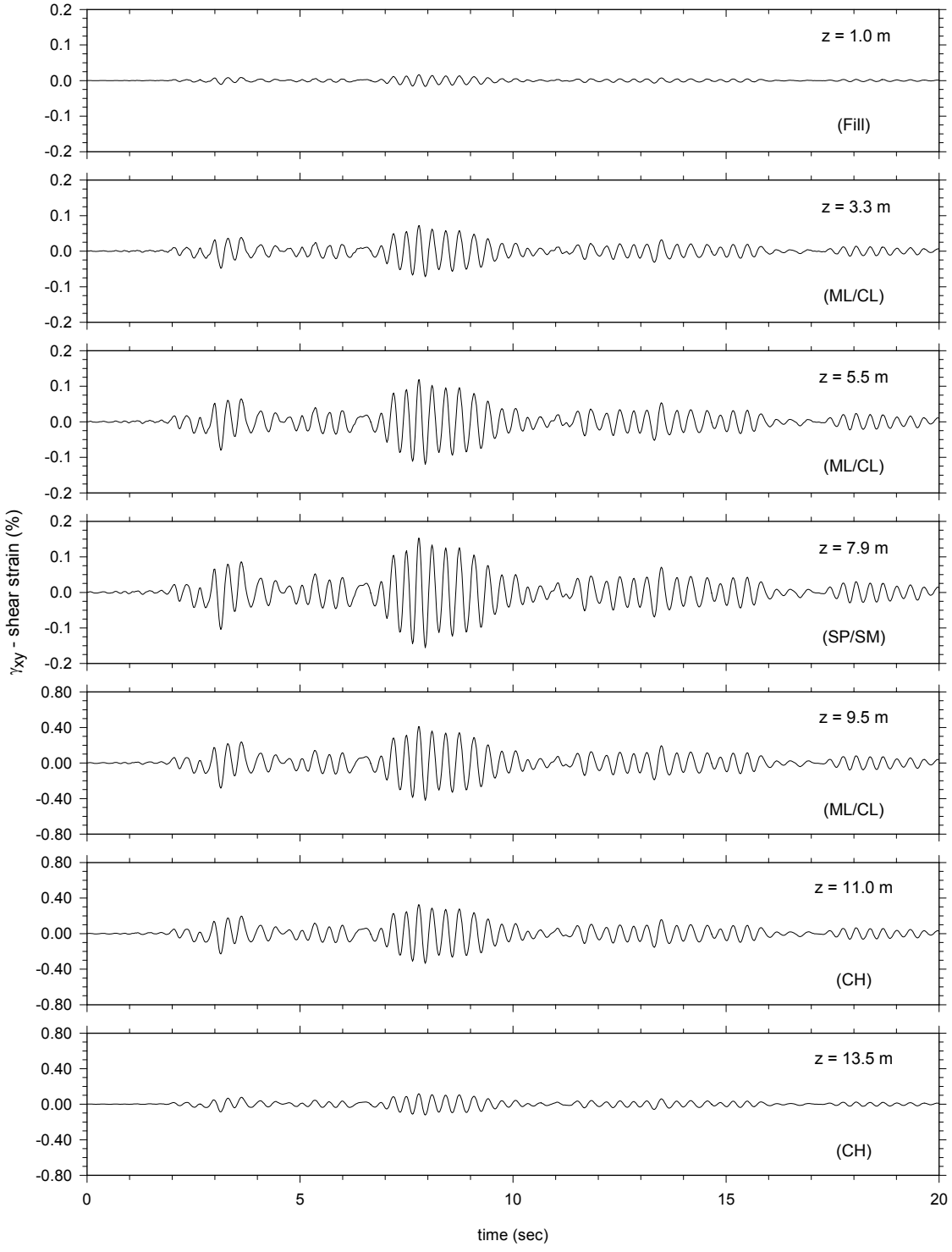

Figure 4-142. Shear strain within the soil (Case 2) – 4 m spaced jet grout columns (0.6 m diameter)

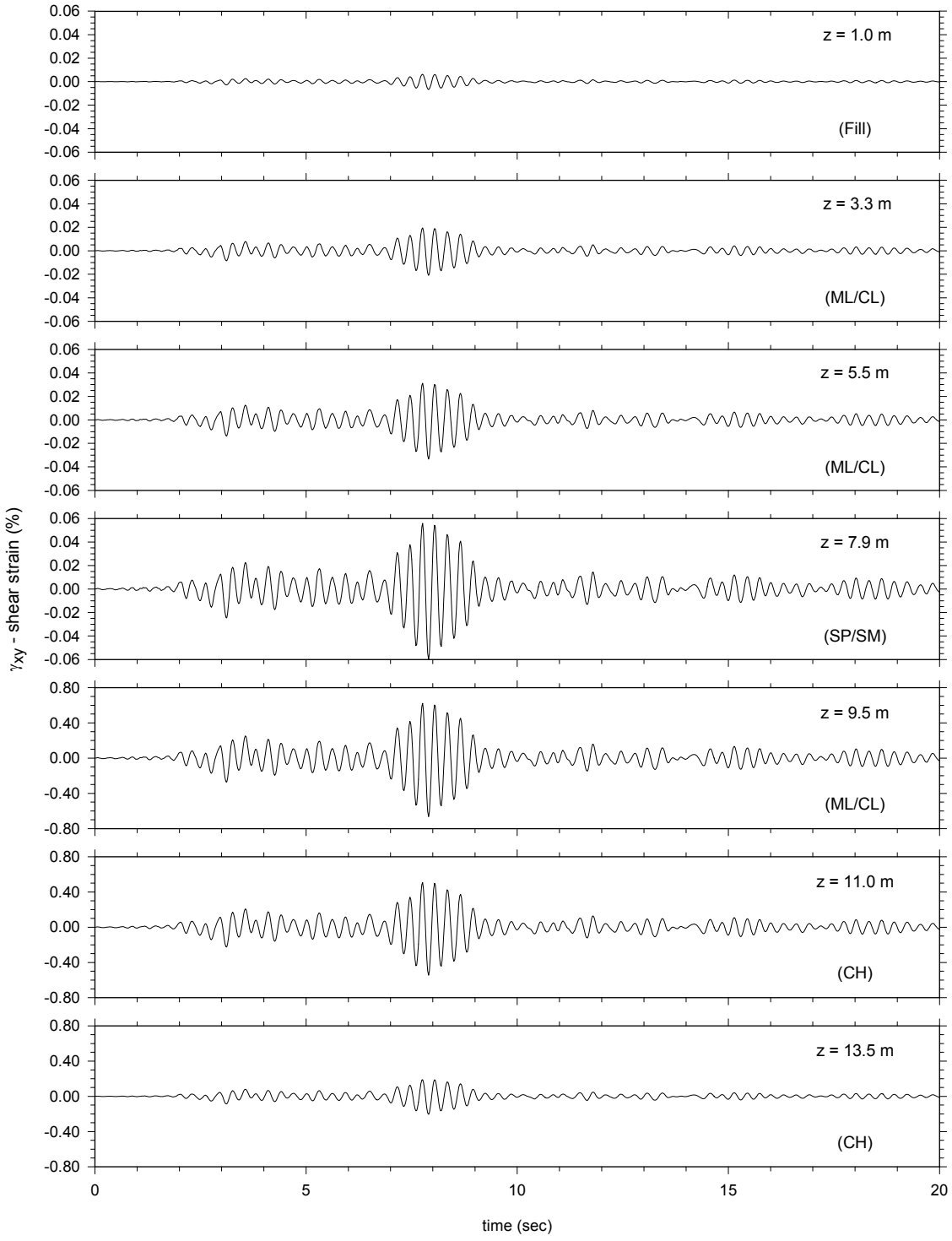

Figure 4-143. Shear strain along the center of the model (along jet grout column centerline and unimproved soils below) (Case 2) – 4 m spaced jet grout columns (0.6 m diameter)

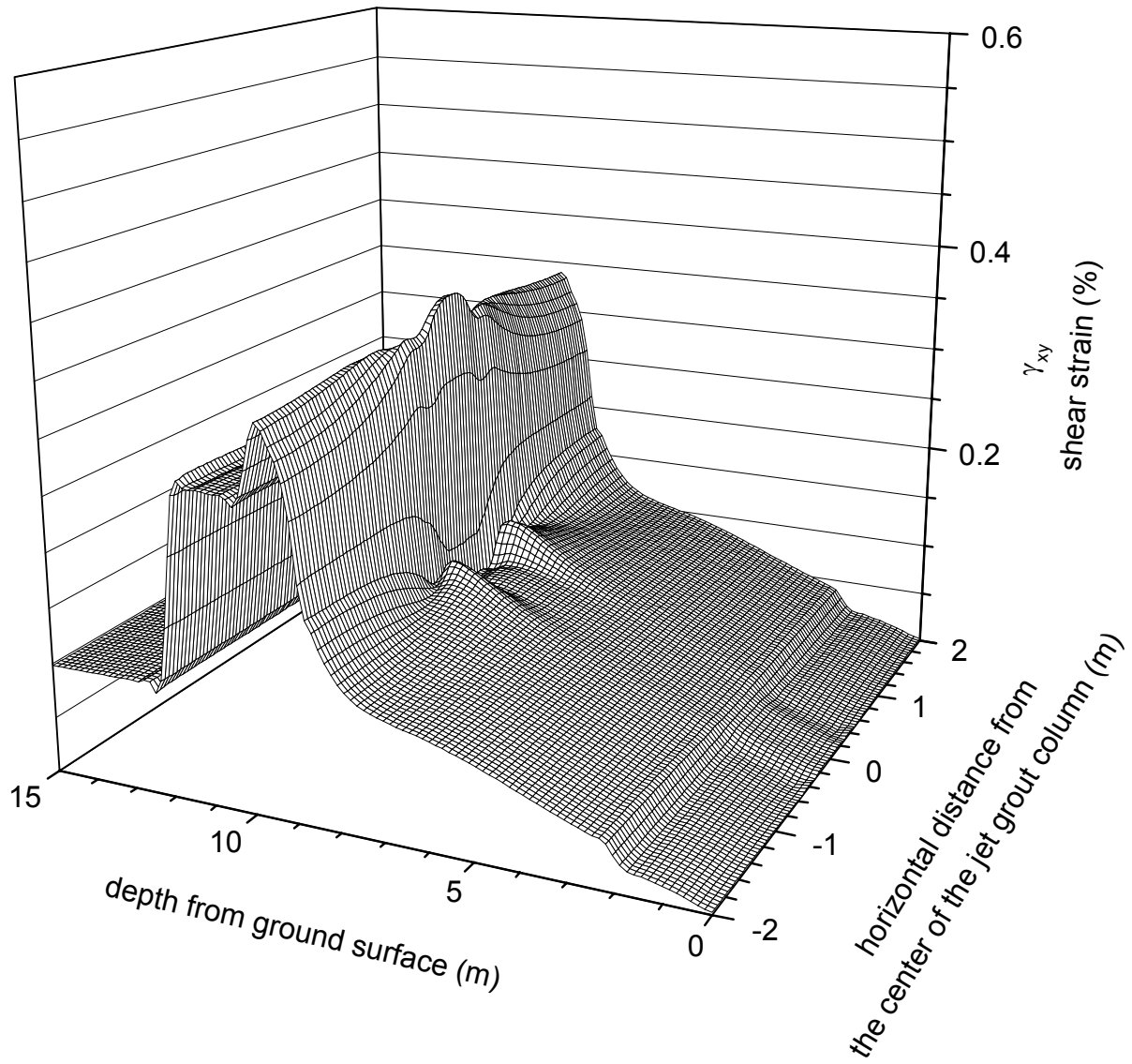

Figure 4-144. Shear strain along the finite element grid – Case 2 – 4 m spaced jet grout columns (0.6 m diameter)

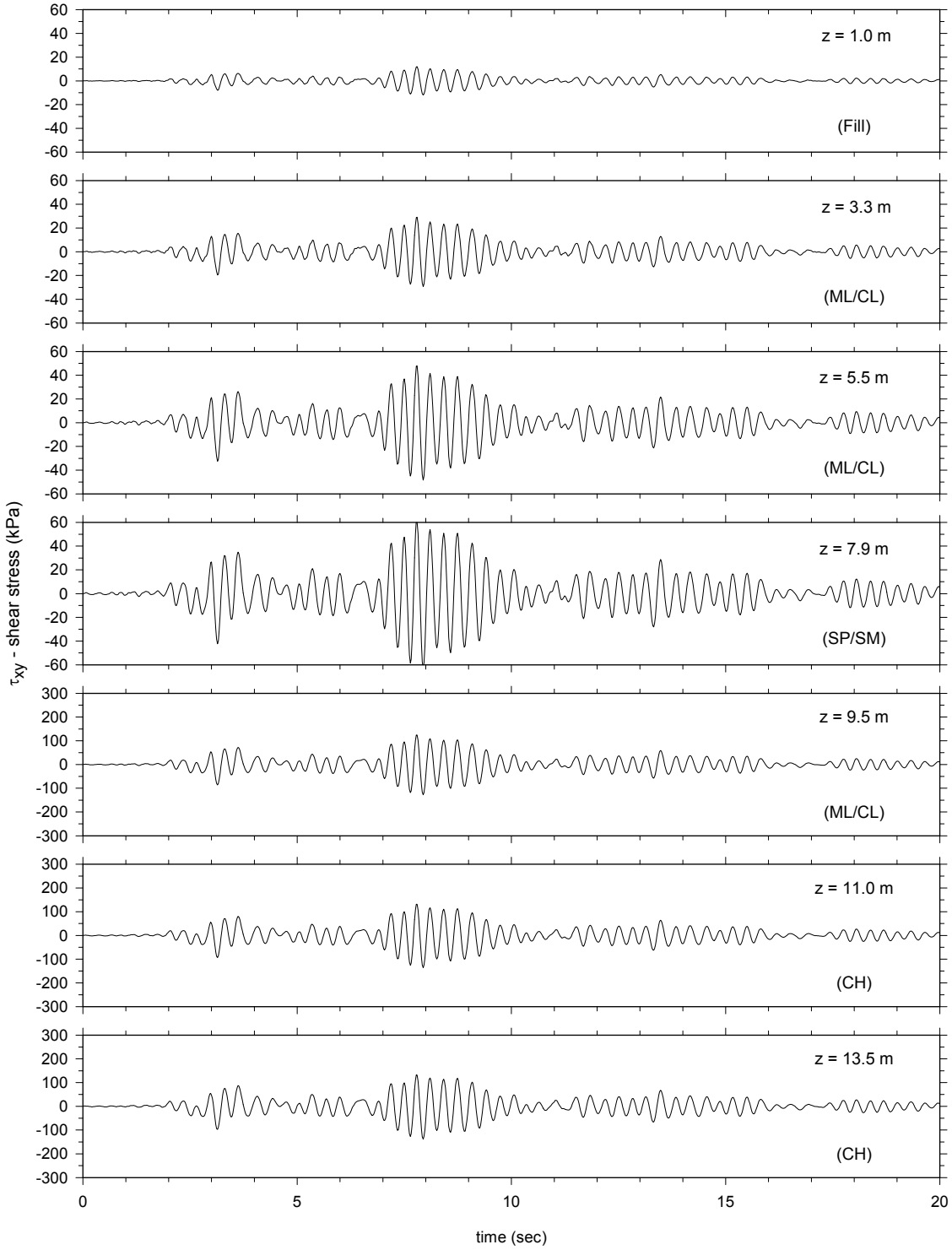

Figure 4-145. Shear stresses within the soil (Case 2) – 4 m spaced jet grout columns (0.6 m diameter)

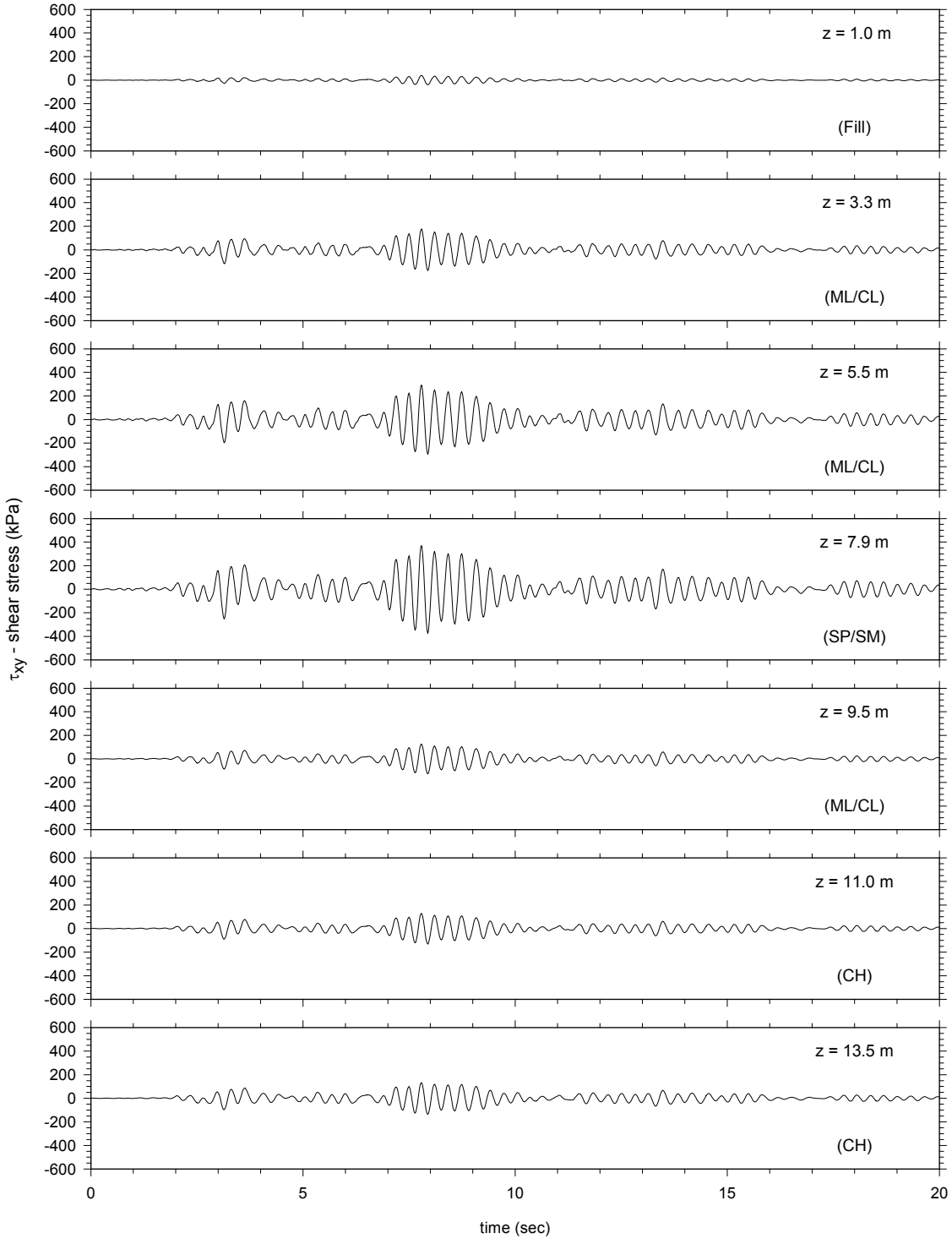

Figure 4-146. Shear stresses along the center of the model (along jet grout column centerline and unimproved soils below) (Case 2) – 4 m spaced jet grout columns (0.6 m diameter)

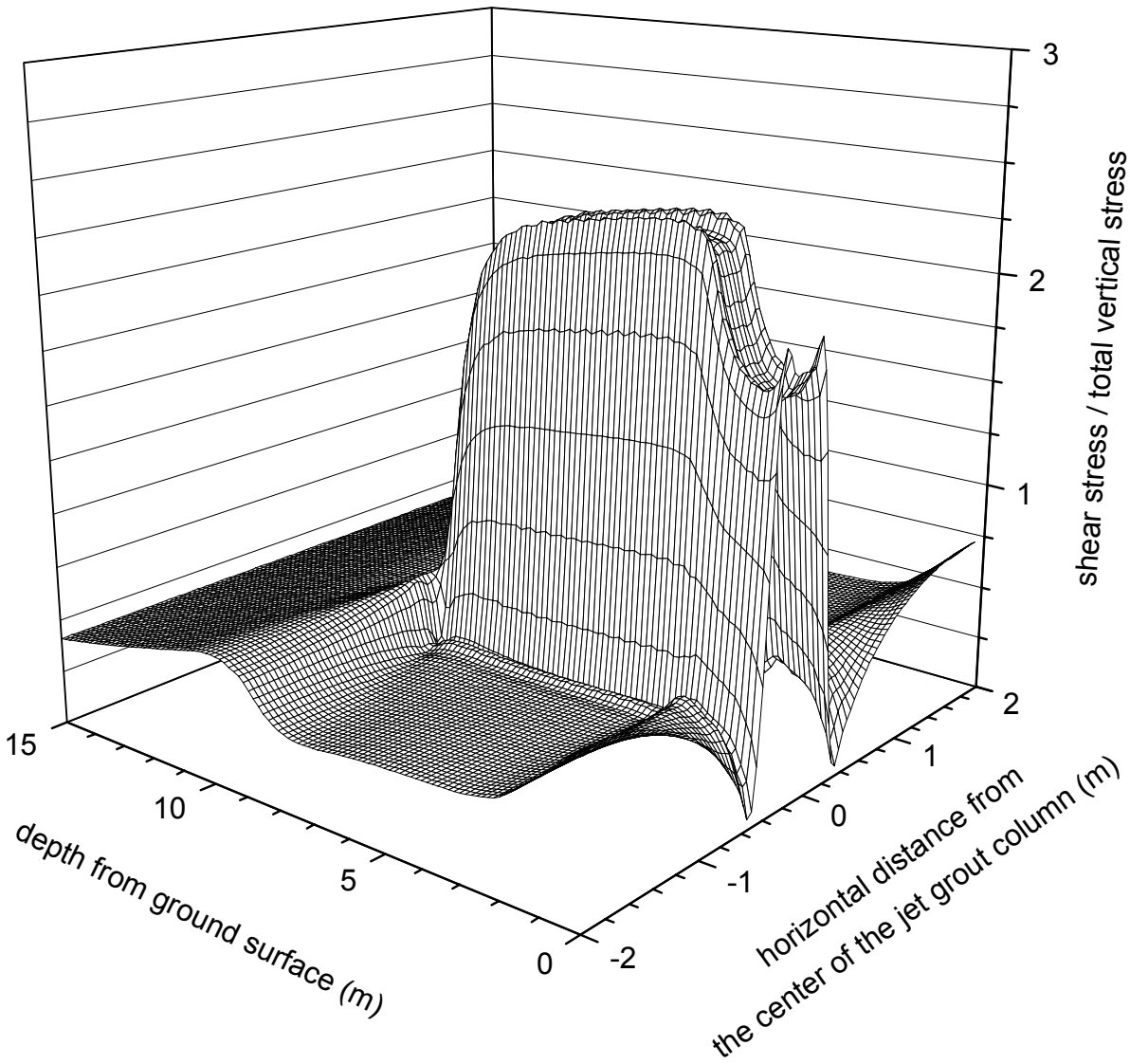

Figure 4-147. Shear stress ratio along the finite element grid – Case 2 – 4 m spaced jet grout columns (0.6 m diameter)

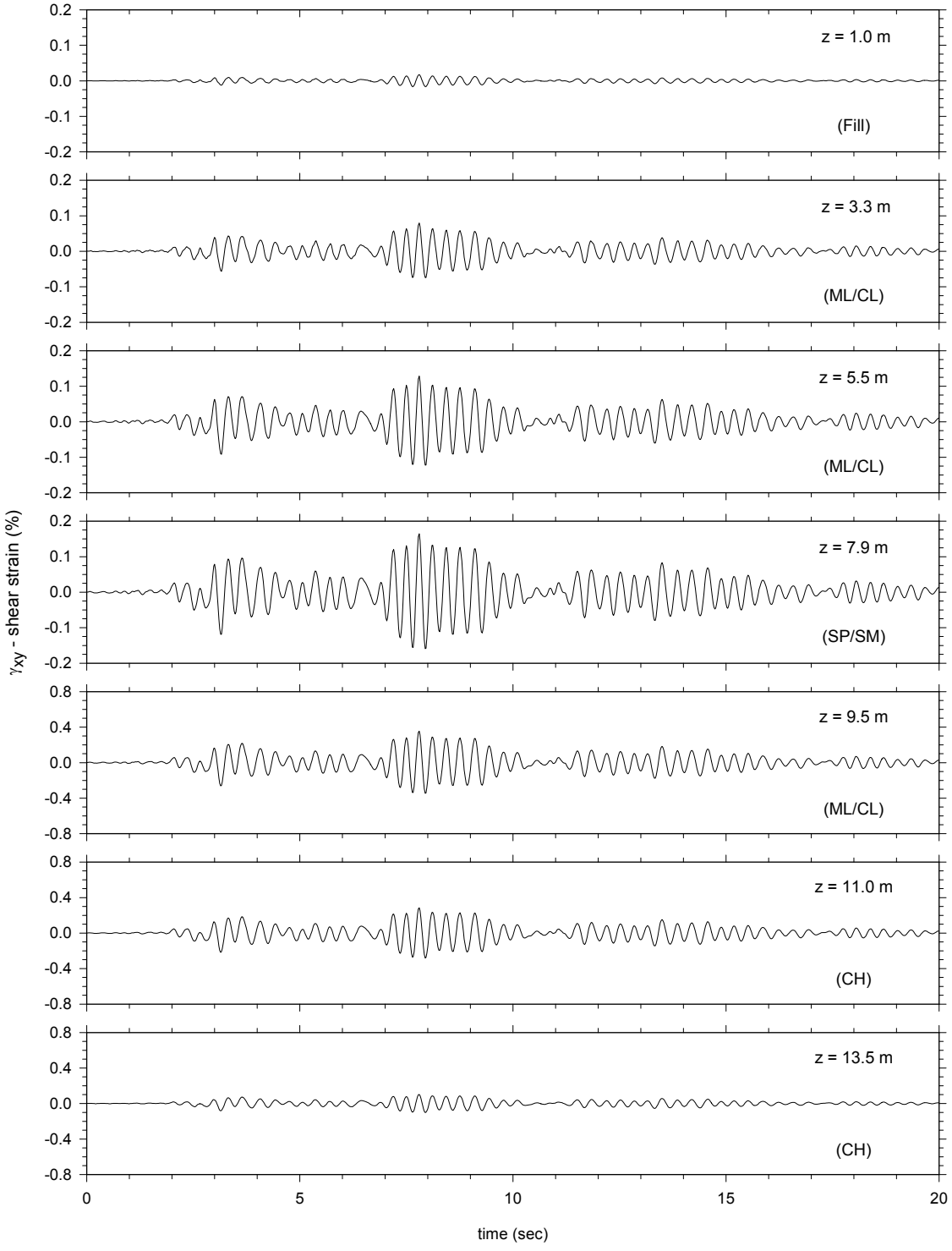

Figure 4-148. Shear strain within the soil – (Case 3) – 5 m spaced jet grout columns (0.6 m diameter)

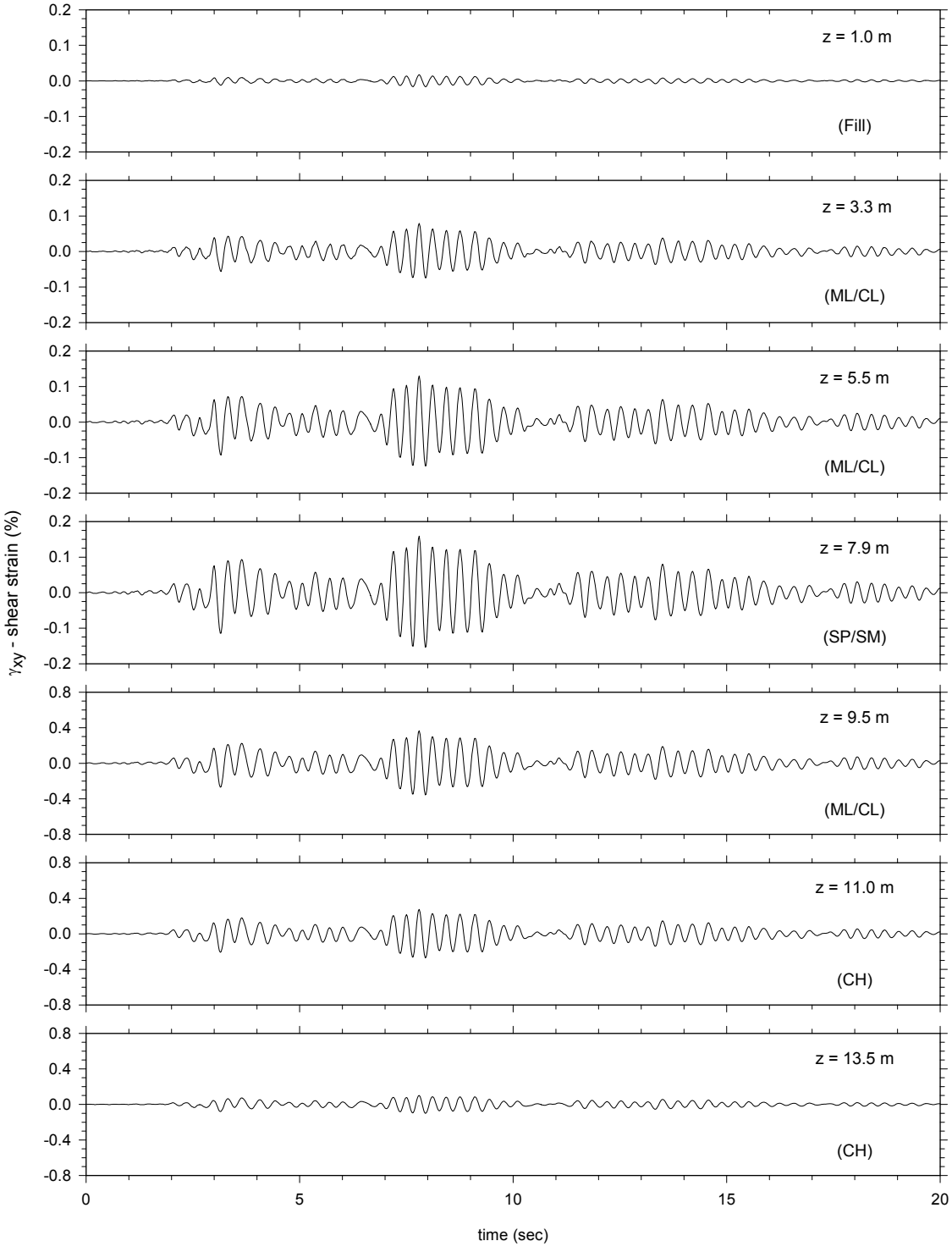

Figure 4-149. Shear strain along the center of the model (along jet grout column centerline and unimproved soils below) – (Case 3) – 5 m spaced jet grout columns (0.6 m diameter)

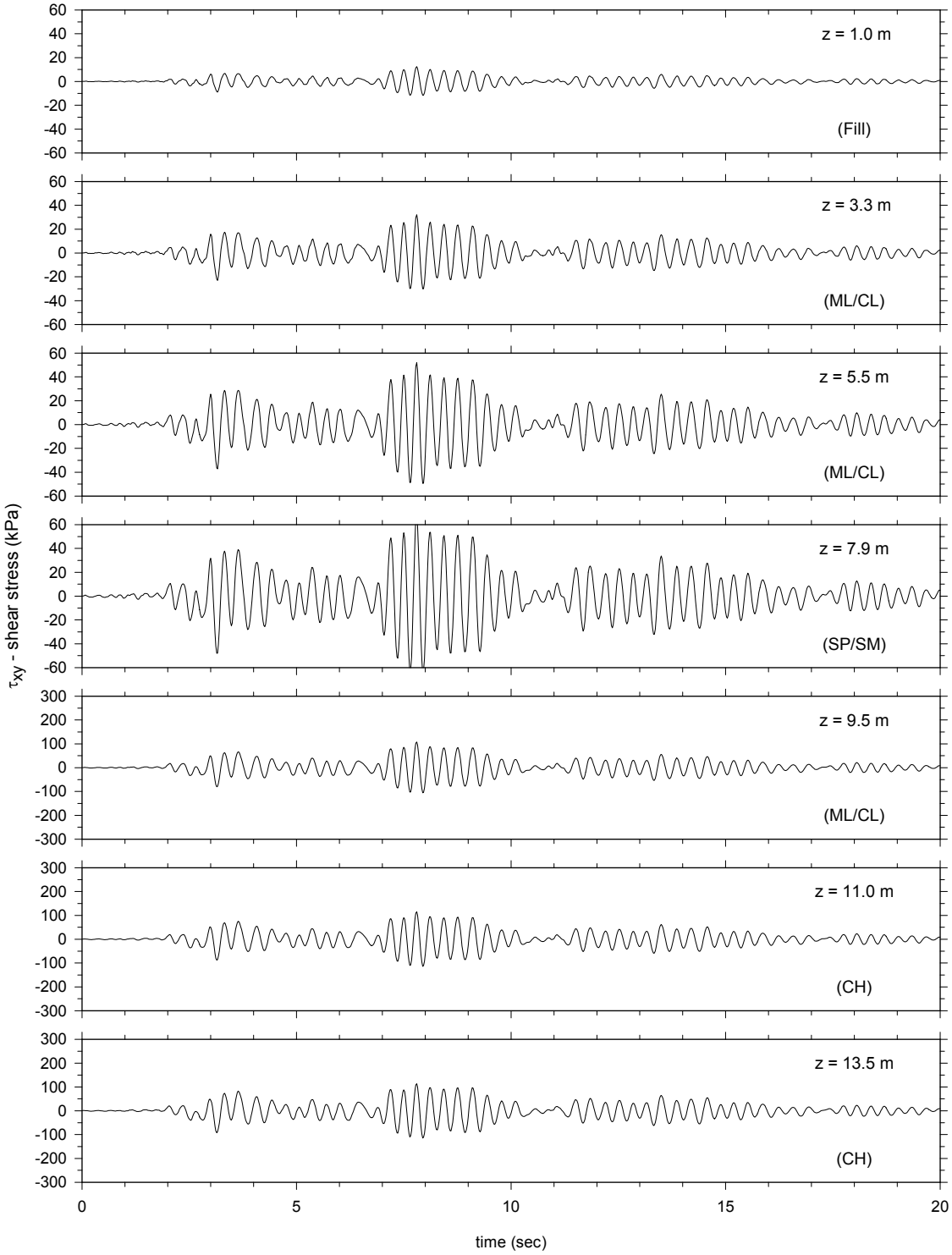

Figure 4-150. Shear stresses within the soil – (Case 3) – 5 m spaced jet grout columns (0.6 m diameter)

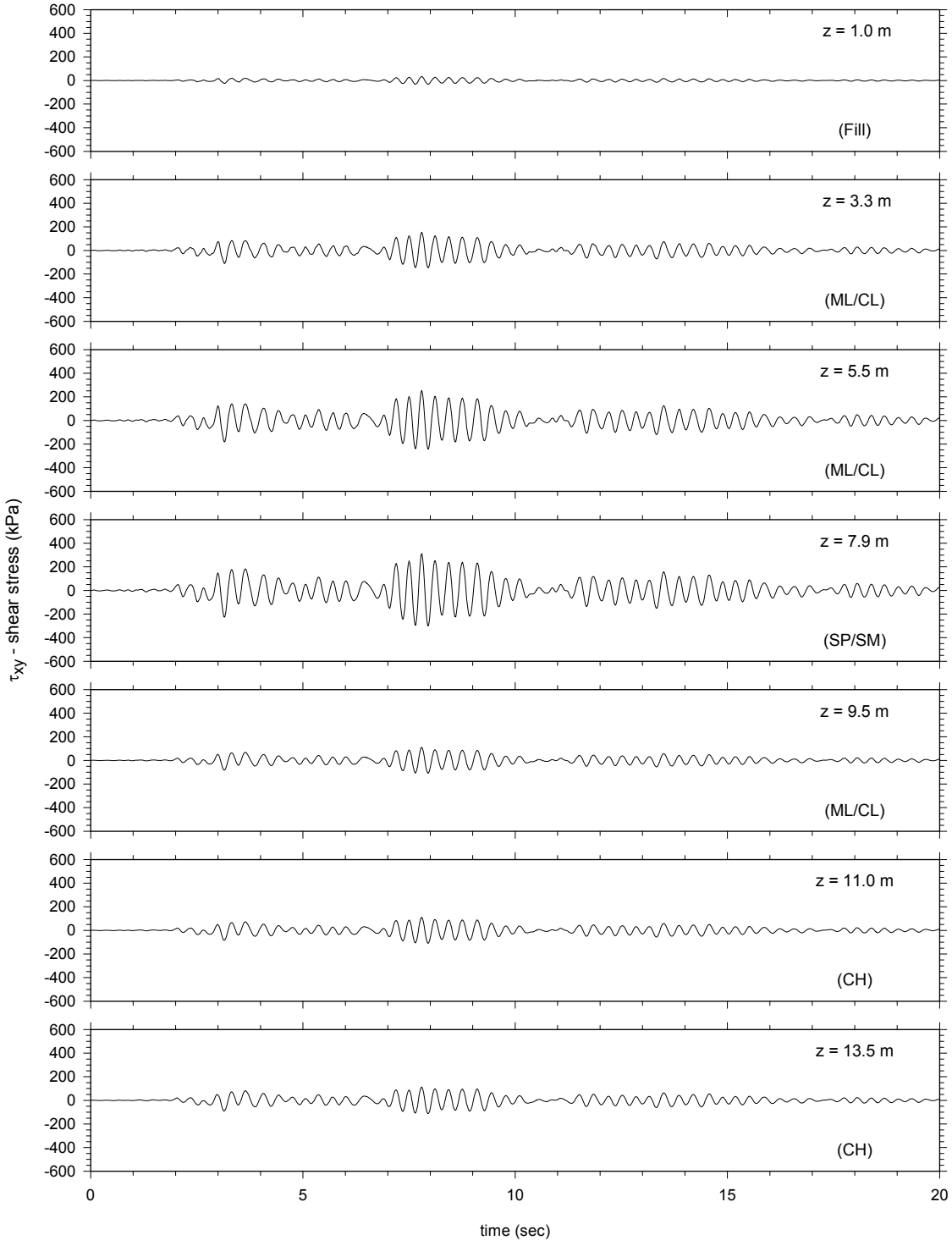

Figure 4-151. Shear stresses along the center of the model (along jet grout column centerline and unimproved soils below) – (Case 3) – 5 m spaced jet grout columns (0.6 m diameter)

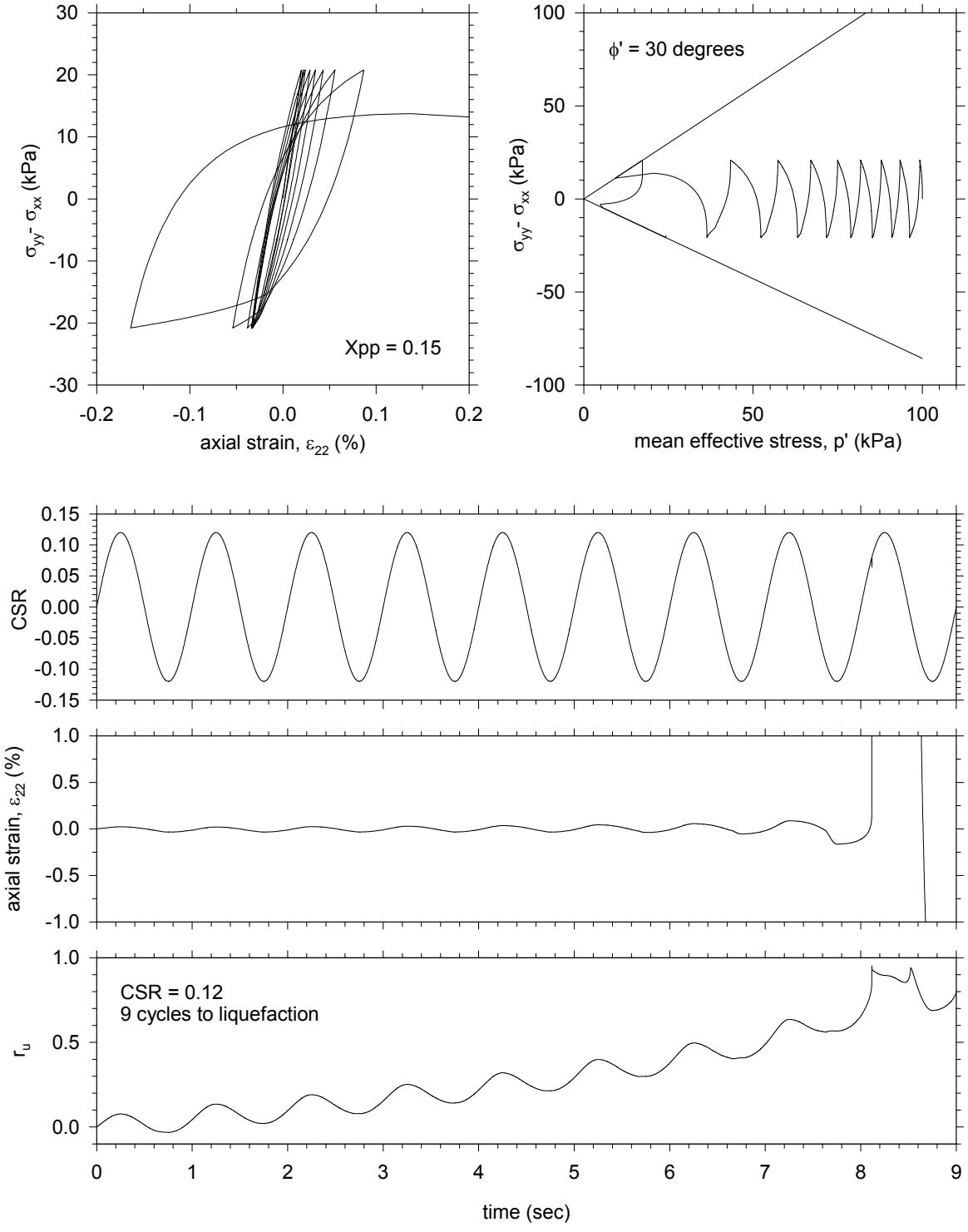

Figure 4-152. Calibration of the multi-yield model – element test with DYNAFLOW – cyclic triaxial test with CSR = 0.12, ϕ' = 30 degrees, X_{pp} = 0.15

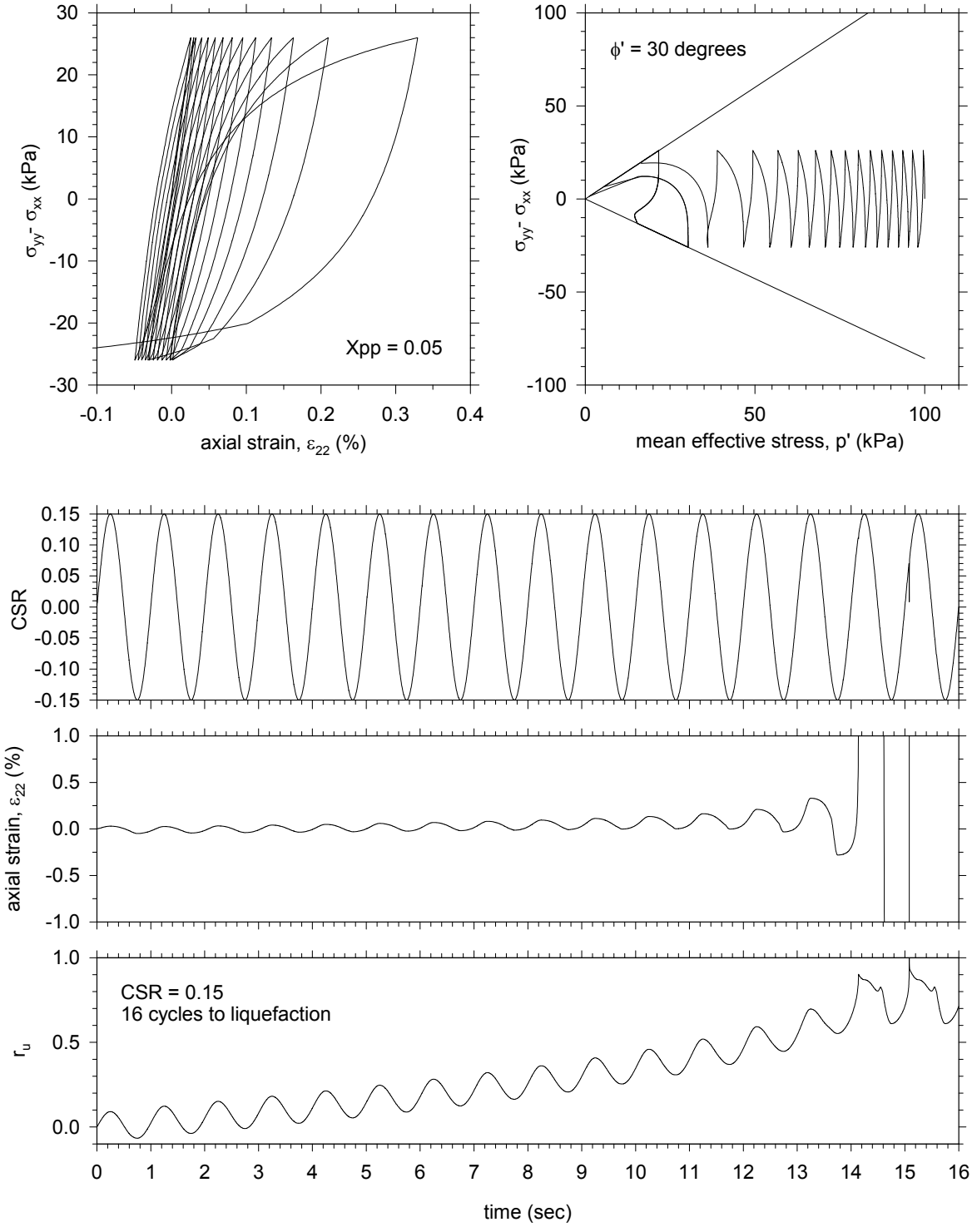

Figure 4-153. Calibration of the multi-yield model – element test with DYNAFLOW – cyclic triaxial test with CSR = 0.15, ϕ' = 30 degrees, X_{pp} = 0.05

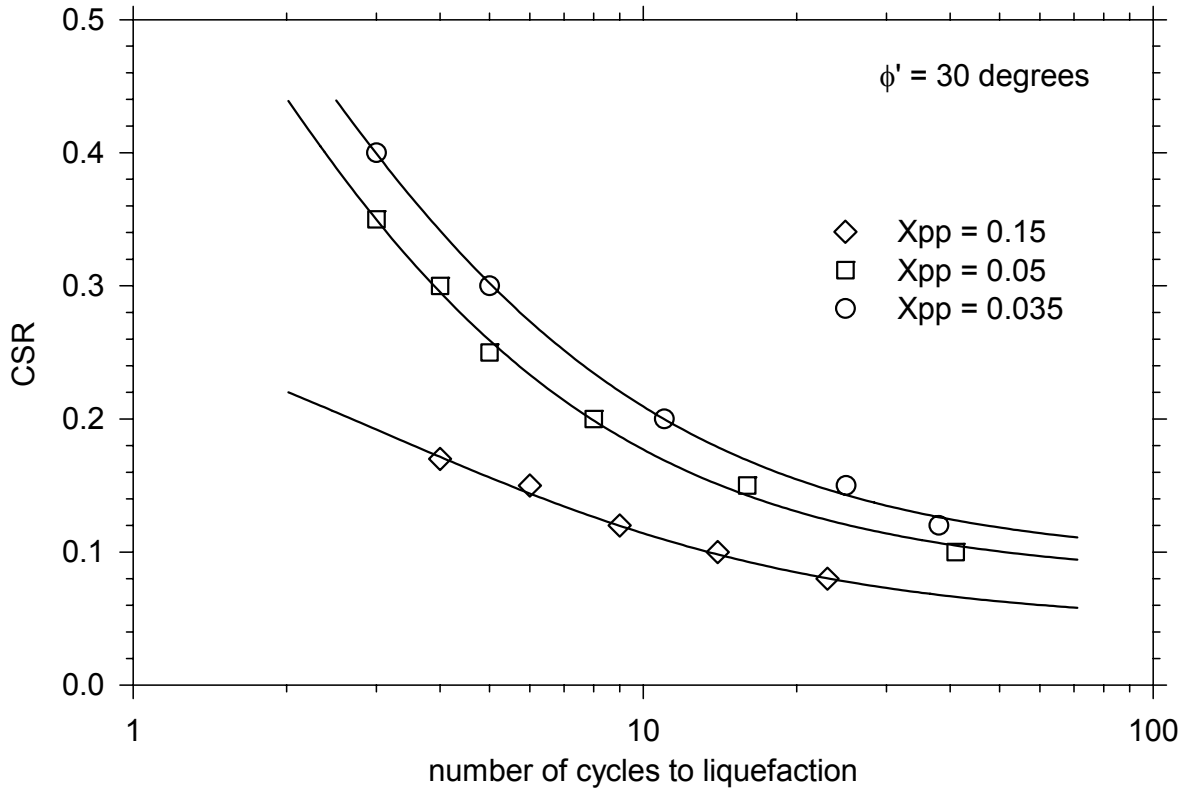

Figure 4-154. Summary of results from element tests for different model parameters

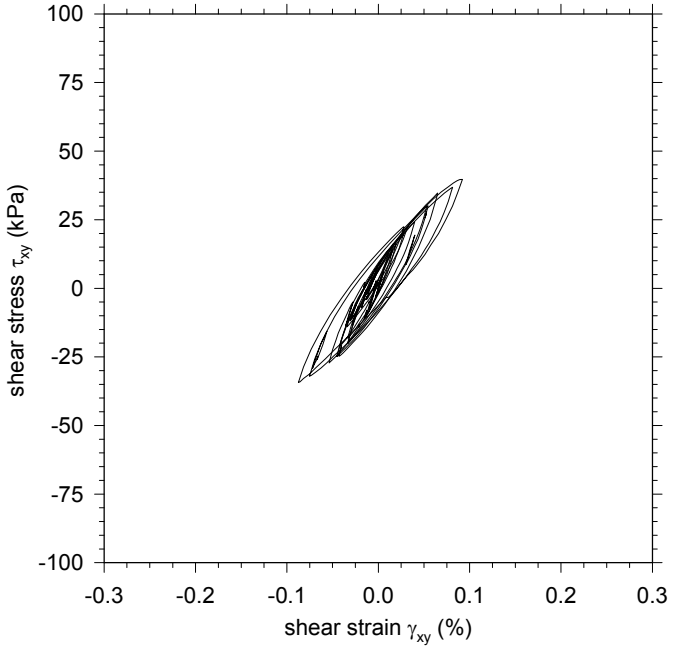

Figure 4-155. Stress strain curve within unimproved soil – z = 3.8 m from ground

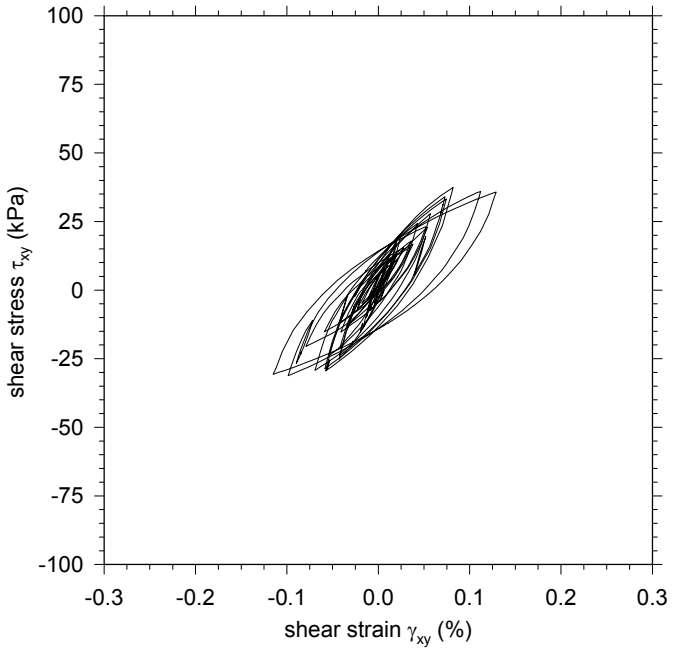

Figure 4-156. Stress strain curve within unimproved soil – z = 4.6 m from ground

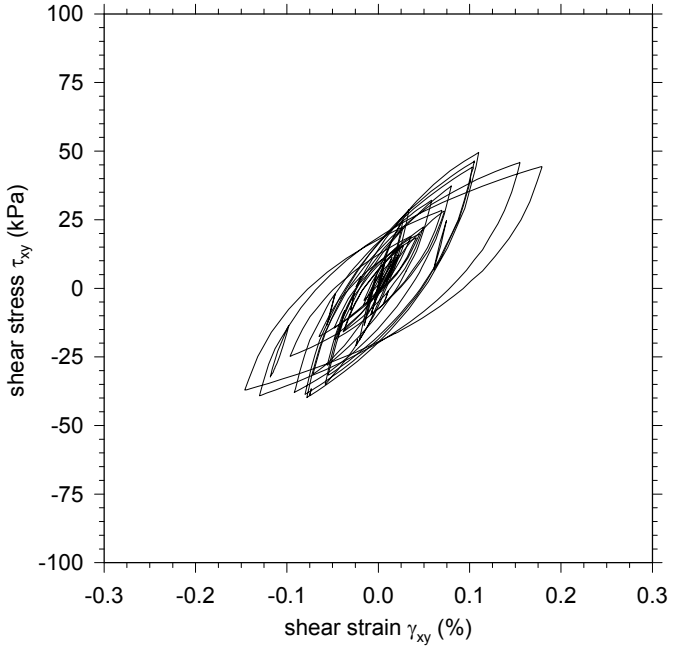

Figure 4-157. Stress strain curve within unimproved soil – z = 5.4 m from ground

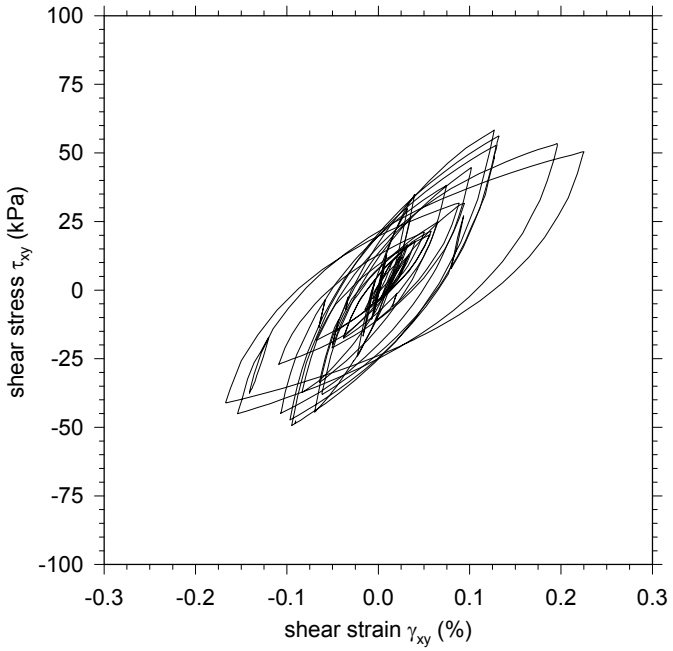

Figure 4-158. Stress strain curve within unimproved soil – z = 6.2 m from ground

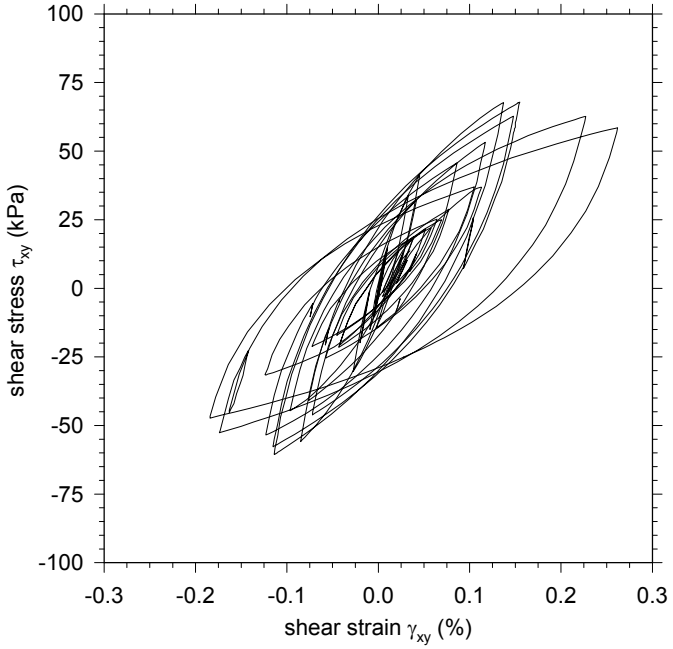

Figure 4-159. Stress strain curve within unimproved soil – z = 7.0 m from ground

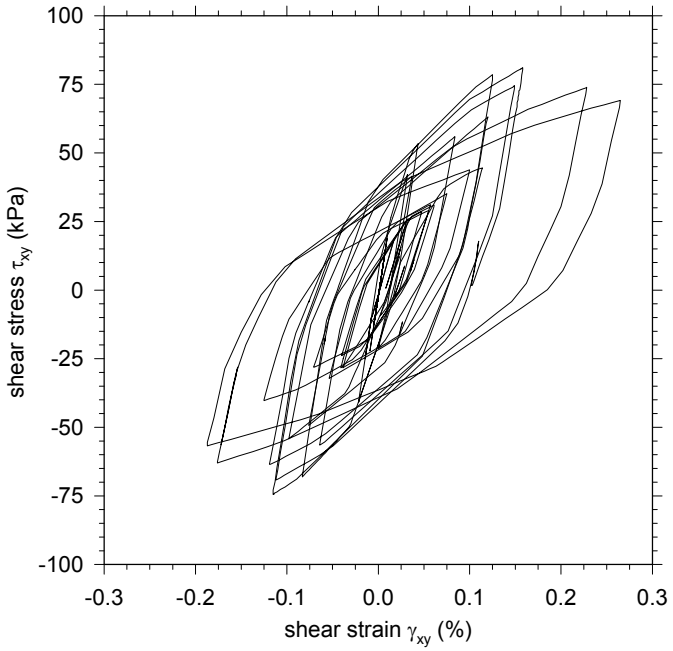

Figure 4-160. Stress strain curve within unimproved soil – z = 7.7 m from ground

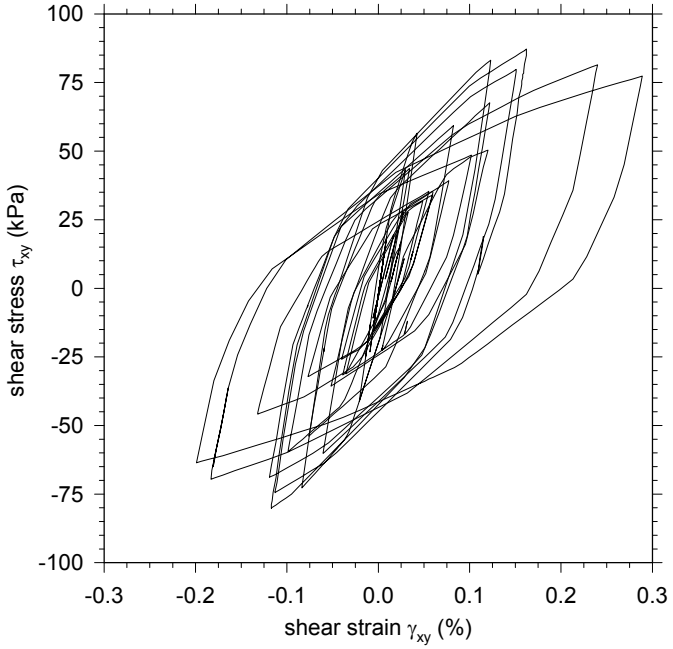

Figure 4-161. Stress strain curve within unimproved soil – z = 8.2 m from ground

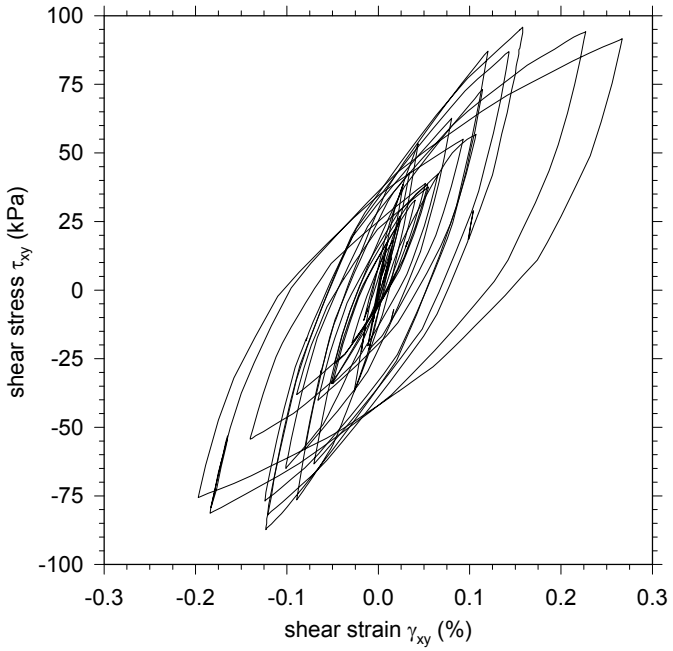

Figure 4-162. Stress strain curve within unimproved soil – z = 8.7 m from ground

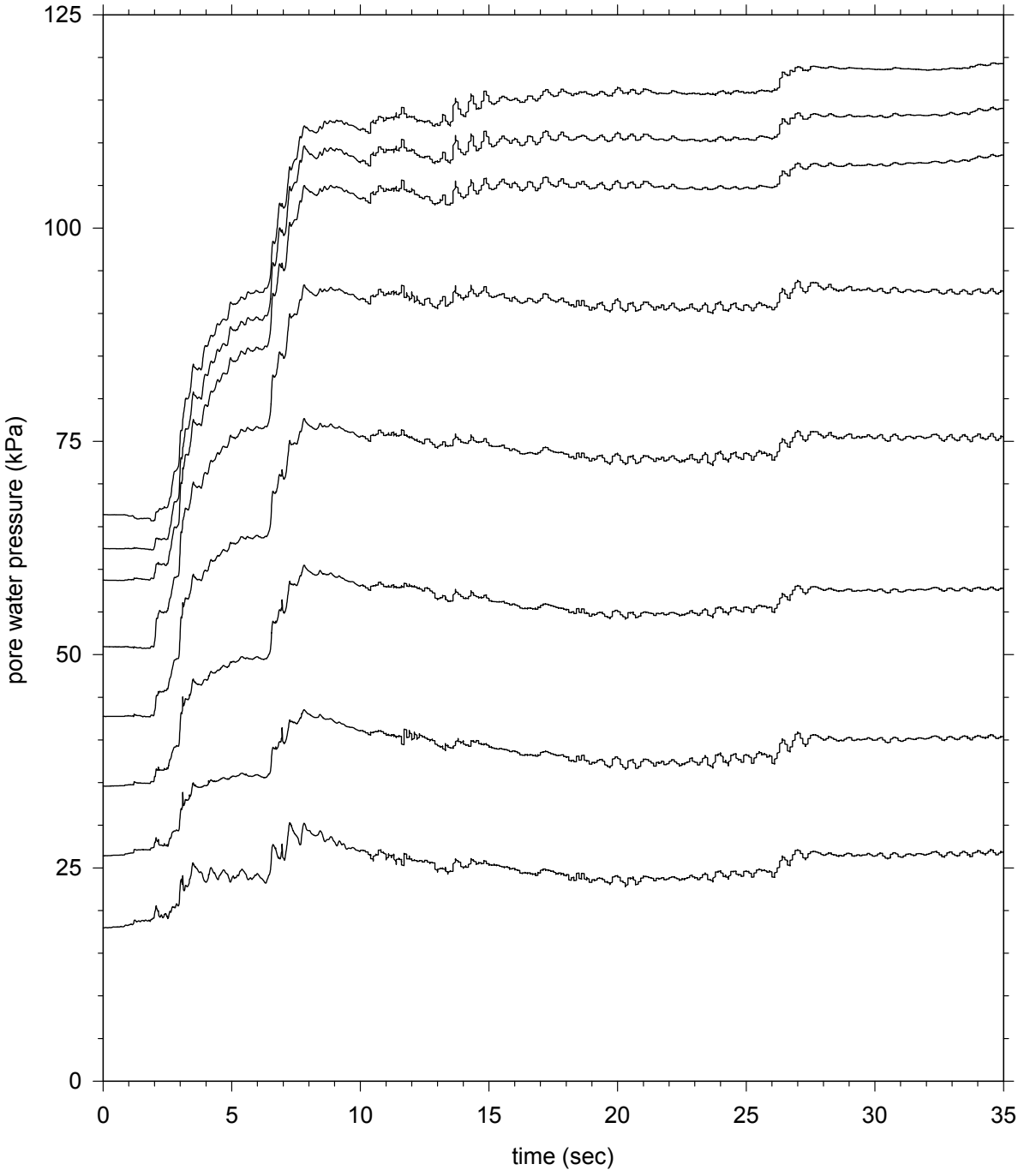

Figure 4-163. Pore pressures within the unimproved ground at depths 3.8 m, 4.6 m, 5.4 m, 6.2 m, 7.0 m, 7.7 m, 8.2 m and 8.7 m from ground surface

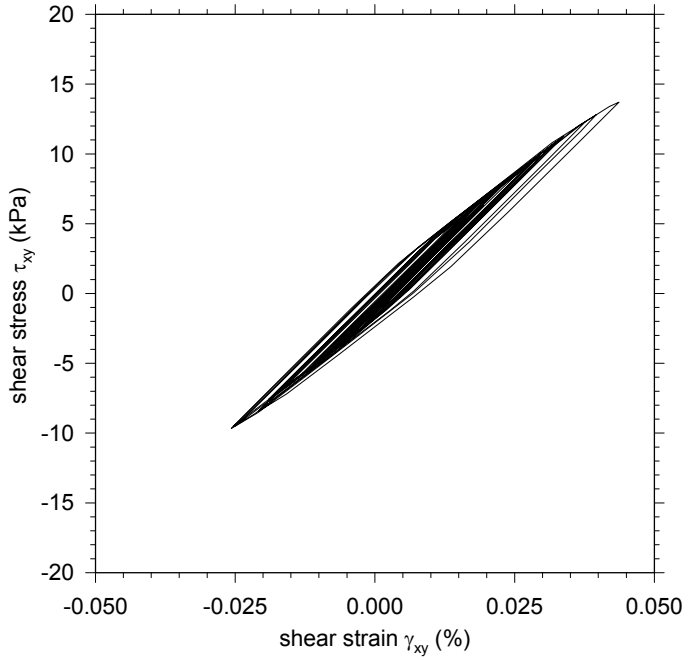

Figure 4-164. Stress strain curve within soil (improved profile) – z = 6.2 m from ground

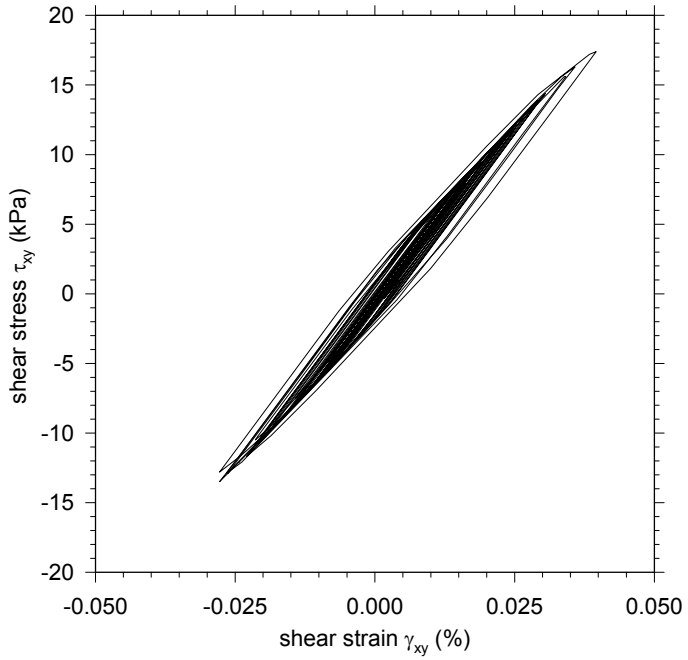

Figure 4-165. Stress strain curve within soil (improved profile) – z = 8.2 m from ground

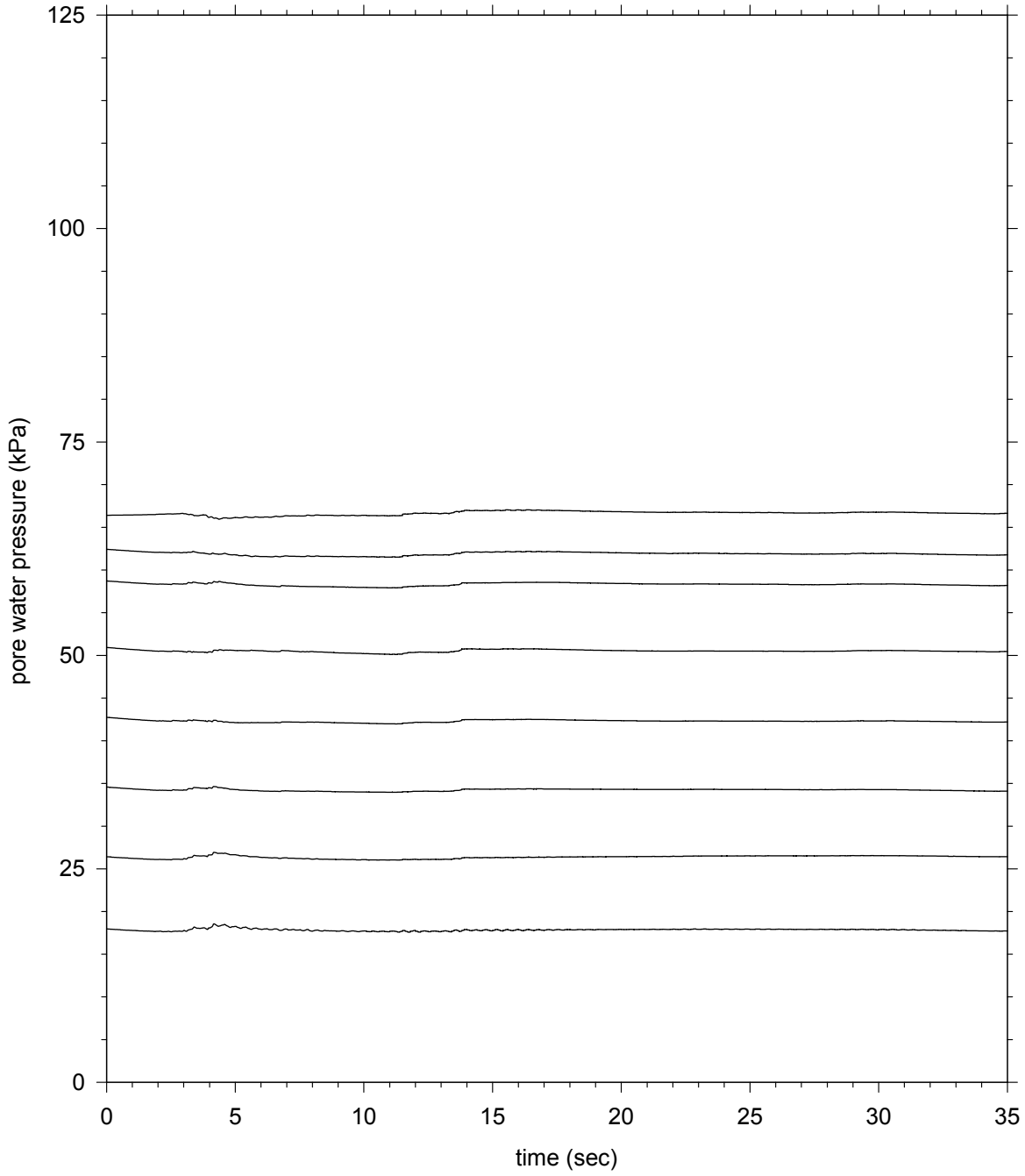

Figure 4-166. Pore pressures within the soil – improved profile – at depths 3.8 m, 4.6 m, 5.4 m, 6.2 m, 7.0 m, 7.7 m, 8.2 m and 8.7 m from ground surface